Universidade de Aveiro Departamento de Biologia
2016

Ana Sofia da Cunha Guimarães

Estudo dos mecanismos de distribuição e motilidade peroxissomal baseados em microtubulos, utilizando o fungo filamentoso U. maydis

Unveiling the mechanisms for microtubule-based peroxisome motility and distribution by exploiting the filamentous fungus U. maydis

Universidade de Aveiro Departamento de Biologia
2016

Ana Sofia da Cunha Guimarães

Estudo dos mecanismos de distribuição e motilidade peroxissomal baseados em microtubulos, utilizando o fungo filamentoso *U. maydis*

Unveiling the mechanisms for microtubule-based peroxisome motility and distribution by exploiting the filamentous fungus U. maydis

Tese apresentada à Universidade de Aveiro para cumprimento dos requisitos necessários à obtenção do grau de Doutor em Biologia, realizada sob a orientação científica do Doutor Michael Schrader, Professor associado do Departamento de Biociências da Universidade de Exeter, Reino Unido, e do Professor Doutor Gero Steinberg, Professor catedrático, Departamento de Biociências da Universidade de Exeter, Reino Unido

Apoio financeiro da FCT, do POCTI e do FSE no âmbito do III Quadro Comunitário de Apoio através da bolsa SFRH / BD / 73532 / 2010

Ao meu pai

o júri

presidente

Doutor Mário Guerreiro Silva Ferreira
professor Catedrático, Departamento de Engenharia de Materiais e Cerâmica, Universidade de Aveiro

Doutor Jorge Eduardo da Silva Azevedo
professor Catedrático, Instituto de Ciências Biomédicas Abel Salazar, Universidade do Porto

Doutor Carlos Jorge Alves Miranda Bandeira Duarte
professor Associado com agregação, Faculdade de Ciências e Tecnologia, Universidade de Coimbra

Doutor Michael Schrader
professor Associado, Departamento de Biociências, Universidade de Exeter, Reino Unido

Doutora Ana Luísa Monteiro de Carvalho
professora Auxiliar, Faculdade de Ciências e Tecnologia, Universidade de Coimbra

Doutora Daniela Maria Oliveira Gandra Ribeiro
professora Auxiliar convidada, Universidade de Aveiro

agradecimentos

First, I would like to thank Gero Steinberg for all his invaluable teachings, and constant challenging and breaking of new boundaries. To Michael Schrader for the opportunity to work in his group and for his continues support, intellectual discussions, and joyful moments.

To all my lab colleagues in Exeter, my deepest appreciation for all the collaborations, intense lab meeting and great moments. To Gulay that started this project and with whom I learned immensely. To Ewa for her genuine attitude and for her experimental help with part of this work. And to Sreedhar and Martin for their support with microscopy and cloning.

To my Exeter family, my words will always be scarce to describe my gratitude for your kindness, friendship, and laughter: Jeremy, Arianna, Tiago, Diana, Joana and Inês. And to my dearest friends: Magdalena, Afsoon and Miriam. Magdalena, you were my support from the very beginning and you made me part of your family from the start, I will always be grateful for your kindness and your inner beauty. My Afy, although we met for a short period in Exeter, our friendship has been strong, your compassion and joyful attitude make you the amazing human being you are. Lastly, to my beloved Miriam! I will never be able to thank you for your support, friendship, and *colacao* in the middle of the night. You are the best housemate/friend anyone can have. You kept me strong and with a smile on my face. Thank you so much for everything.

A todos os membros do laboratório de Aveiro por sempre tão bem me receberem: à Ana, Isabel, Mónica, Sílvia e Rita. À Daniela pela sua imensa disponibilidade e por ser sempre genuína. À João pelo companheirismo e amizade durante todos estes anos. Ao Miguel, o meu grande obrigada por tudo, especialmente durante a fase final da tese. À Fátima por ser sempre uma grande amiga e uma excelente colega e pelo seu terno sorriso.

À Maria pela sua amizade. Pelos telefonemas ao fim do dia, pelas gargalhas e caminhadas, mas muito especialmente pelo grande apoio durante esta tese e por ter tido a paciência para a rever.

A todos os meus amigos que ao longo da minha vida me acompanharam. Ao Rui obrigada pela tua amizade de tantos anos e por todo o apoio, és uma pessoa extraordinária. À Eloísa, grande amiga para todas as ocasiões, o teu apoio incondicional foram fundamentais nestes últimos anos. Obrigada por tudo!!

Ao meu mano mais velho por ser sempre um modelo a seguir. À minha cunhada pela sua serenidade. Aos meus queridos sobrinhos Alice e Francisco. À minha maravilhosa mãe, por toda a sua força, por todo o apoio e carinho que me transmitiu e por me ensinar a acreditar sempre. Por último, ao meu pai, por ter sido uma pessoa extraordinária, gentil e corajosa. Por ter ensinado à sua menina a questionar-se e principalmente a procurar as repostas. Obrigada por todos os ensinamentos e por todo o amor. Até sempre…

palavras-chave

Peroxissomas, *Ustilago maydis*, motilidade, endossomas primários, β-oxidação, distribuição, actina, microtúbulos

resumo

Os peroxissomas são organelos subcelulares ubíquos responsáveis por diversas funções metabólicas, nomeadamente a β-oxidação de ácidos gordos e destoxificação de espécies reativas de oxigénio, sendo por isso essenciais para a saúde e desenvolvimento humanos. O fungo filamentoso *Ustilago maydis* é um organismo biotrófico, do filo basidiomycota, que infesta o milho. Possui características similares às células de mamífero, nomeadamente a mobilidade através dos microtúbulos, o crescimento polar e a mitose aberta. Neste estudo usámos o *U. maydis* como modelo para o estudo de processos fundamentais da biologia dos peroxissomas. A cooperação entre os peroxissomas e a mitocôndrias tem-se revelado de grande interesse dada a existência de colaboração na β-oxidação de ácidos gordos, manutenção do equilíbrio oxidativo e do sistema imunitário inato. As mitocôndrias das plantas e leveduras não realizam β-oxidação, deste modo, é essencial um modelo geneticamente acessível para o estudo da relação entre os organelos. Assim, combinámos técnicas de biologia celular, molecular e de bioinformática gerámos um inventário das proteínas peroxissomais e das suas vias no *U. maydis*. Estudos com um mutante deficiente em peroxissomas, ΔPex3, revelaram a existência de uma cooperação paralela e complexa das vias de β-oxidação nas mitocôndrias e nos peroxissomas, à semelhança do que se observa nos mamíferos. Enquanto em leveduras e plantas os peroxissomas movem-se por filamentos de actina, em mamíferos os peroxissomas interagem e movimentam-se através dos microtúbulos. A mobilidade e dinâmica dos peroxissomas é fundamental para a distribuição intracelular, posicionamento, interações entre organelos e formação de novos organelos. Alterações no tráfico e/ou distribuição citoplasmática dos peroxissomas pode levar à perda de funções essenciais e levar à degeneração e morte celular. Aqui mostrámos que no *U. maydis* os peroxissomas se movem ao longo dos microtúbulos, mas este movimento é dependente dos endossomas primários. Adicionalmente, mostrámos que os corpos lipídicos e o retículo endoplasmático parecem partilhar um mecanismo semelhante. A distribuição uniforme dos peroxissomas é tida como essencial para as suas funções. No entanto, o mecanismo para a distribuição destes organelos é ainda desconhecido. Usando o *U. maydis* podémos verificar que os processos baseados no transporte através dos microtúbulos e distribuição polar, dependente da actina, são essenciais para a posicionamento dos peroxissomas. Os processos baseados no transporte através dos microtúbulos incluem transporte direto e difusão ativa. Estudos nas células de mamífero COS-7 revelaram um mecanismo semelhante na distribuição dos peroxissomas. Em suma, dispomos de novas evidências uso do *U. maydis* como modelo poderá conduzir a um melhor entendimento da dinâmica e biologia dos peroxissomas, o que poder-se-á revelar de grande valor biológico e de importância biomédica

keywords

Peroxisomes, *Ustilago maydis*, motility, early endosomes, β-oxidation, actin, distribution, microtubules

abstract

Peroxisomes are ubiquitous subcellular organelles, which fulfil important metabolic functions, notably the β-oxidation of fatty acids and the metabolism of hydrogen peroxide, and are thus essential for human health and development. The filamentous fungus *Ustilago maydis* is a biotrophic, basidiomycete responsible for corn smut disease. *U. maydis* exhibits several features similar to mammals including polar growth, microtubule-dependent organelle trafficking and open mitosis. In this study, we have exploited *U. maydis* as a new model system for studying fundamental processes in peroxisome biology. An intimate interrelationship between peroxisomes and mitochondria is emerging, where both organelles cooperate in cellular lipid homeostasis, oxidative balance, and innate immune response. As mitochondrial fatty acid β-oxidation is lacking in yeast and plants, suitable genetically accessible model systems to study this interrelationship are scarce. Combined molecular, cell biology and bioinformatics analyses were performed to provide a first comprehensive inventory of *U. maydis* peroxisomal proteins and pathways. Studies with a peroxisome-deficient Δpex3 mutant revealed the existence of parallel and complex, cooperative β-oxidation pathways in peroxisomes and mitochondria, mimicking the mammalian system. In mammalian cells, peroxisomes bind to and move along microtubules. In contrast, peroxisome motility in yeasts and plants requires the actin cytoskeleton. Peroxisome motility and dynamics are important prerequisites for peroxisome inheritance, proper intracellular distribution, positioning, organelle interactions, and biogenesis. A loss of trafficking and disturbed cytoplasmic distribution of peroxisomes can lead to a regional loss of essential peroxisomal activities and thus, to cell damage and degeneration. We revealed that peroxisomes in *U. maydis* move along microtubules, but peroxisome motility is early endosome-dependent. Moreover, lipid droplets and the ER appear to share a similar mechanism. Even distribution of peroxisomes is critical for cellular functions. However, the exact mechanism(s) for uniform peroxisome distribution are elusive. Using *U. maydis,* we demonstrated that the distribution and positioning of peroxisomes is dependent on microtubule-based processes and an actin-based polar drift. Microtubule-based processes include directed transport and active diffusion, which is a result of a constant flow and activity of motor proteins and organelles. These counteracting forces allow the proper distribution of peroxisomes throughout the hyphal cell. Moreover, work in mammalian cells, revealed a similar mechanism for proper distribution of peroxisomes. In summary, we provide novel evidence that the filamentous fungus *U. maydis* represents a suitable model to study fundamental biological processes of mammalian cells. Peroxisome motility and dynamics are important for cellular function and may prevent cell damage and degeneration. The use of *U. maydis* as a model system will lead to a better understanding of peroxisome dynamics and biology and will thus be of great cell biological and biomedical importance.

TABLE OF CONTENTS

PRECEITOS LEGAIS

The author declares that the experimental results, besides being included in this thesis, were also published under the name of Guimarães, S.C.. The author declares that she has participated in the planning and execution of the experimental work and in the data preparation and interpretation.

Camões F*, Islinger M*, **Guimaraes SC***, Kilaru S, Schuster M, Godinho LF, Steinberg G, Schrader M. New insights into the peroxisomal protein inventory: Acyl-CoA oxidases and -dehydrogenases are an ancient feature of peroxisomes. *Biochim Biophys Acta*. 2015 Jan;1853(1):111-25. doi: 10.1016/j.bbamcr.2014.10.005.

Guimaraes, SC; Schuster M; Bielska E; Dagdas, G; Kilaru, S; Meadows BRA; Schrader M; Steinberg G. - Peroxisomes, lipid droplets, and endoplasmic reticulum "hitchhike" on motile early endosomes - *J Cell Biol*. 2015 Dec 7;211(5):945-54.

Lin, C*; Schuster M *; **Guimaraes SC**, Ashwin P.; Schrader, M.; Metz J; Hacker, C., Gurr, S.J. and Steinberg G. Active diffusion and microtubule-based transport oppose myosin forces to position organelles in cells. *Nat Commun.* 2016 Jun 2;7:11814. doi: 10.1038/ncomms11814.

**Shared first author*

LIST OF FIGURES

LIST OF TABLES

ABBREVIATIONS

aa	Amino acid
a, b	Mating type loci
ACAD	Acyl-CoA-Dehydrogenase
ACOX	Acyl-CoA-Oxidase
APH	Aminoglycoside phosphotransferase
ATM	Ataxia telangiectasia mutated
ATP	Adenosine 5’ Triphosphate
BiFC	Bimolecular fluorescence complementation
Ble^R	phleomycin-resistance-cassette
bp	Base pair(s)
BP	Bifunctional Enzyme
cbx-locus	gene locus of the iron-sulphur subunit of the succinate dehydrogenase from *U. maydis*
Cbx^R	carboxin-resistance-cassette
CM	complete medium
CoA	Coenzyme A
crg - promoter	conditional arabinose induced promoter
C-terminal/ C-term	carboxy-terminal
Δ	Deletion
dH_2O	Distilled water
DMEM	Dulbecco's Modified Eagle Medium
DMSO	Dimethyl Sulfoxide
DNA	Desoxyribonucleic acid
dNTP	Desoxynucleotides
Dyn2	Dynein heavy chain
EDTA	Ethylenediamintetraacetic Acid
eGFP	enhanced green fluorescent protein
EM	Electron Microscopy
ERMES	ER-Mitochondria Encounter Structure
ER	Endoplasmic Reticulum
$FADH_2$	Flavin adenine dinucleotide
FRAP	Fluorescence recovery after bleaching
Fw	Forward
GFP	green fluorescent protein
h	hour
hygR	hygromycin-resistance-cassette
KIF	kinesin superfamily proteins
Kin1	kinesin-1
Kin3	kinesin-3
MAVS	Mitochondrial Antiviral Signalling Proteins
mCherry	Monomeric Cherry fluorescent protein
min	minute
mTor	mammalian target of rapamycin

nar	Conditional nitrate reductase promoter
nat^R	nourseothricin-resistance-cassette
NM	Nitrate medium
N-terminal/N-term	amino-terminal
Ori	Origin of replication
Otef	Constitutive otef promoter
P (<, >,=)	P value
P	Promoter
p	Plasmid
PBS	Phosphate buffered saline
PCR	Polymerase Chain Reaction
PEG	Polyethylene glycol
PMPs	Peroxisomal membrane proteins
PPAR	Peroxisomal proliferator activator receptor
PtdINs(3)P	phosphatidylinositol 3-phosphate
PTS	Peroxisomal targeting signal
PX	Phox domain
Rab5	small endosomal Rab5-like GTPase
Reg	Regeneration
Rho	Small GTPase belonging to Ras superfamily proteins
RNA	Ribonucleic acid
RNS	Reactive Nitrogen Species
ROI	Region of interest
ROS	Reactive Oxygen Species
rpm	Revolutions per minute
RT	Room temperature
s	Second
Sc-URA	*S. cerevisiae* medium depleted of uracil
SD	Synthetically defined medium for culturing *S. cerevisiae*
SDS	Sodium Dodecyl Sulfate
SEM	Standard error of the mean
SNARE	soluble NSF attachment protein receptor
SEM	Scanning Electron Microscopy
SCPx	Sterol Carrier Protein X
TEM	Transmission electron microscopy
TFE	Trifunctional Enzyme
Tm	Melting temperature
ts	temperature-sensitive allele
t-SNARE	Target soluble *N*-ethylmaleimide attachment protein receptor
Tub1	α-tubulin from *U. maydis*
URA3	*S. cerevisiae* gene involved in *de novo* synthesis of uracil
v/v	Volume per volume
w/v	Weight per volume
UV	Ultraviolet
Yup1	Early endosomal t-SNARE1 of *U. maydis*

1. INTRODUCTION

1.1 Peroxisomes

1.1.1 The Peroxisome – General features

Peroxisomes are single bilayer membrane organelles virtually present in all eukaryotic cells. Their number and metabolic functions can vary between cell types and developmental stages as they adapt to physiological conditions by changing the number, shape, size, and enzymatic content (Schrader et al., 2012; Smith and Aitchison, 2013). Peroxisomes are part of the microbody family which comprises peroxisomes, and other specialized structures with adapted metabolic functions (Figure 1A-D). The family includes Woronin bodies in fungal cells; glyoxisomes in plants seeds; and glycosomes in *Trypanosomatidae* family (Figure 1A). Peroxisomes are usually found in spherical or rod-shape (0.1-0.5 µm in diameter), however they can also exhibit elongated structures. Peroxisomes are devoided of DNA, thus all peroxisomal proteins are encoded from nuclear DNA (Lazarow and Fujiki, 1985). They can be categorized in: membrane proteins, such as peroxins; and matrix proteins, mainly enzymes for metabolic and detoxification purposes. Matrix proteins are post-translationally imported from the cytosol into the peroxisomal matrix, crossing the membrane as mono- or oligomers. Peroxisomes in rats (Volkl et al., 1988), plants (Kleff et al., 1997), and fungi (Liu et al., 2011; Veenhuis et al., 1981) may present a crystalline electron-dense core which is thought to result from urate oxidase and/or catalase aggregation (Fig. 1B). However, their exact function is unknown.

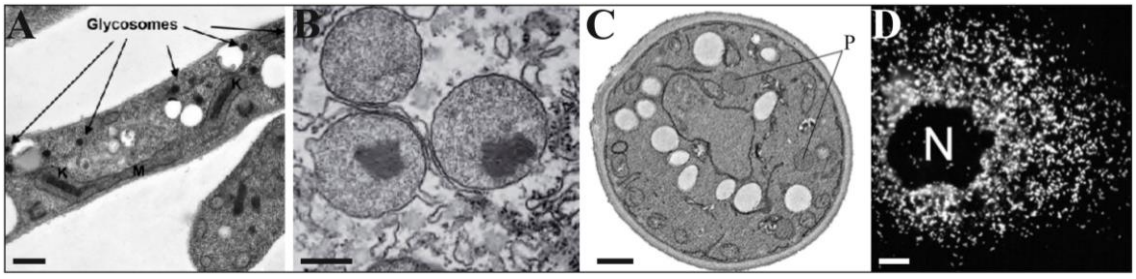

Figure 1 - Morphology of peroxisomes and peroxisome-related structures in different organisms. A) Transmission electron microscopy (TEM) of *Trypanosoma brucei*. Arrows indicate glycosomal structures. Bar 0.5 µm. (*adapted from* Bauer et al., 2013) B) Electron micrograph (EM) of rat liver peroxisomes exhibiting crystalline core inclusions of urate oxidase. Bar 200 nm. *Adapted from* Alberts, 2014. C) EM (electron microscopy) of wild type *Saccharomyces cerevisiae* with labeled peroxisomes (P). Bar 0.5 µm. *Adapted from* Vizeacoumar et al., 2003. D) Immunostaining of peroxisomes with an antibody against the membrane protein Pex11β-myc in COS-7 cells. N- Nucleus. Bar 10 µm. *Adapted from* Koch et al., 2003.

Mammalian peroxisomes are of crucial importance in health and development as they participate in a panoply of functions such as the β-oxidation and α-oxidation of fatty acids; detoxification of reactive oxygen species (ROS); biosynthesis of docosahexaenoic, bile acids and ether phospholipids. Hence, impaired peroxisomal activity or alterations in peroxisomal proteins result in clinically heterogeneous peroxisomal disorders (Braverman et al., 2013) (Figure 2). Over the past years the existence of cross talk between peroxisomes and different organelles has become increasingly evident (Schrader and Yoon, 2007; Camoes et al., 2009; Delille et al., 2009; Schrader et al., 2015b;). The role of potential membrane contact sites in metabolism, signalling, dynamics and lipid biosynthesis might be of key importance towards the understanding of peroxisomal diseases and therapeutics (Schrader et al., 2015a).

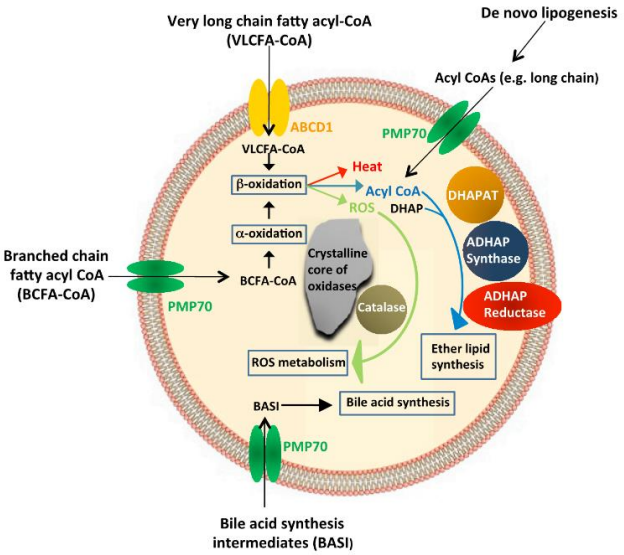

Figure 2 - Peroxisomal structure and functions The peroxisome is a single bilipidic membrane organelle with different functions in metabolism. Peroxisomes harbour β-oxidation and hydrogen peroxide detoxification throughout species, however holding specific function in a species-specific manner. In mammalian cells, peroxisomes are important for β-oxidation of long- and very long- chain fatty acids, α-oxidation of branched chain fatty acids, bile acids and ether-linked phospholipids, and removal of reactive oxygen species. Some peroxisomes contain a dense crystalline core of oxidative enzymes with unknown function. *Adapted from* Lodhi and Semenkovich (2014)

1.1.2 Peroxisomal functions

Peroxisomes are versatile organelles involved in several metabolic functions. Although peroxisomal roles can vary according to cell type, development and/or environmental conditions (see Table 1 for a general description of peroxisomal functions), hydrogen peroxide homeostasis and fatty acid metabolism is conserved across species. Below, a more detailed view of lipid metabolism, oxidative balance and a synthesis of other functions is presented.

Table 1: Peroxisomal functions in different species. Functions harboured partially or exclusively in the peroxisomes of plants, fungi and animals. * - present. *Adapted from* Smith and Aitchison, 2013

Partially or exclusively peroxisomal pathways	Plants	Fungi	Animals
Biosynthesis			
Bile acids			*
Hormonal signalling molecules	*		*
Polyunsaturated fatty system			*
Ether phospholipids (plasmogens)			*
Pyrimidines			*
Purines			*
Antibiotics (penicillin)		*	
Toxins for plant pathogenesis		*	
Biotin	*	*	
Secondary metabolites	*	*	
Isoprenoid and cholesterol	*		*
Degradation			
Prostaglandin			*
Amino Acids		*	*
Polyamine	*	*	*
H_2O_2 degradation by catalase	*	*	*
Oxidation of fatty acids	*	*	*
Purine	*		*
Superoxide radical destruction by superoxide dismutase	*		*
Methanol degradation		*	
Glyoxylate cycle	*	*	
Photorespiration	*		
Other			
Maintenance of cellular integrity		*	
Bioluminescence of firefly luciferase			*
Signalling platforms in viral innate immune defence			*
H_2O_2 signalling in hypothalamic neurons			*

Lipid metabolism

Fatty acids play multiple important roles in the living cell. They are the building blocks of the cell membrane, regulate enzymes and membrane channels, and serve as signalling molecules and precursors for hormones. Importantly, they store and provide energy to the cell (Poirier et al., 2006). Fatty acids can be utilized as a sole carbon source by numerous species. The principal pathway for fatty acid degradation is β-oxidation, by which molecules are broken down in a repetitive spiral of four steps. Each reaction removes two carbons from the fatty acid-chain in the form of acetyl-CoA. While taxonomic virtually ubiquitous throughout eukaryotes, β-oxidation displays a startling diversity of substrate specificity, enzyme architecture, and subcellular localization across kingdoms (Wanders and Waterham, 2006b). In mammals and fungi, fatty acids are degraded in two subcellular compartments:

mitochondria and peroxisomes. Conversely, in yeast and plants, although not consensual (Masterson and Wood, 2001; Masterson and Wood, 2009), fatty acid degradation relies solely on peroxisomes. Peroxisomal α- and β-oxidation initializes the oxidation of saturated- and unsaturated- long- (C16-C20), very long-chain fatty acids (>20), and 3-methyl-branched fatty acids, which are chain-shortened and subsequently routed to the mitochondria to be further oxidize. Shorter fatty acids can be metabolized in both organelles (Wanders 2010), comprising the four steps of the β-oxidation (dehydrogenation, hydration, second dehydrogenation, and thiolytic cleavage). However, each reaction, in each organelle, is catalysed by different set of enzymes, encoded by different genes (Figure 3).

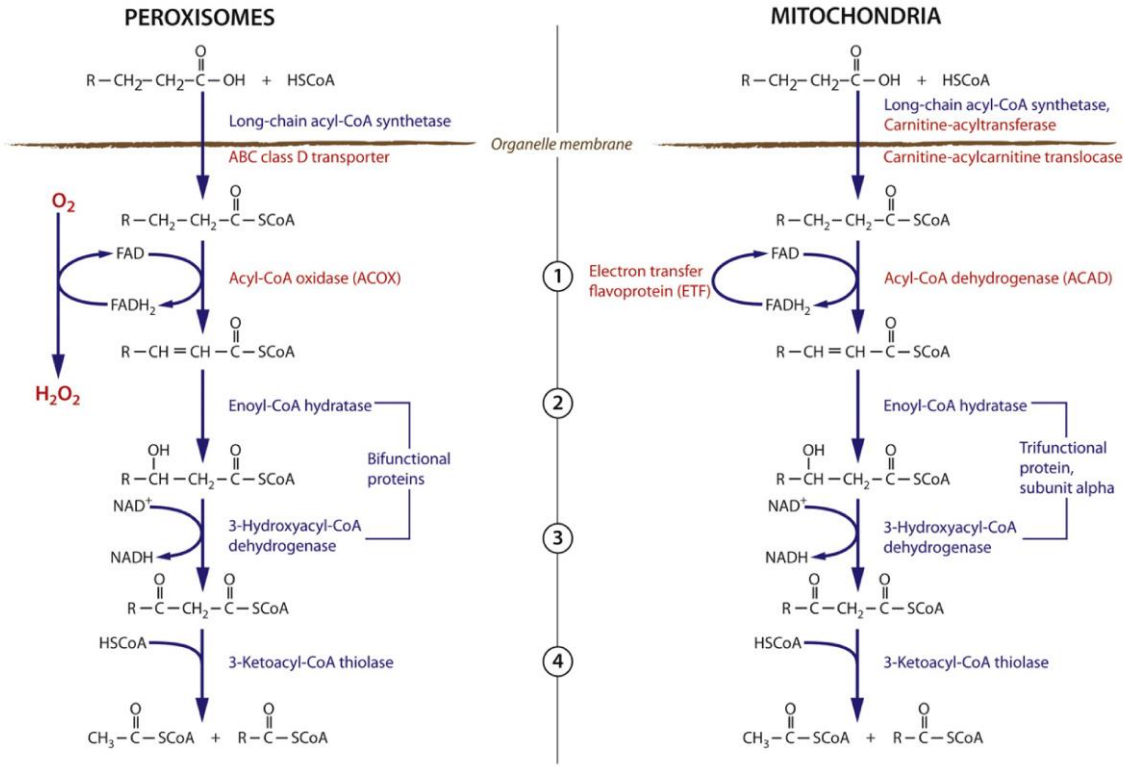

Figure 3 - Comparison of peroxisomal and mitochondrial fatty acid β-oxidation pathways. β-oxidation of fatty acids in mammals is carried out in peroxisomes and mitochondria in four subsequent reactions (1-4), which are preceded by an activation step of coupling the free fatty acids to coenzyme A. Fatty acids are unable to diffuse freely through the organelle membrane, therefore, membrane-bound long-chain acyl-CoA synthetases activates the fatty acids outside the organelle. The activated long-chain fatty acids enter the organelle through specific import systems. Short- and medium-chain fatty acids are supposed to enter freely into the mitochondria, prior to activation. Peroxisomes degrade long- and very long-chain fatty acids down to 8 carbons length. The octanoic acid is then exported from the peroxisome lumen to be targeted to the mitochondria. Peroxisomes and mitochondria differences in the import system and catabolic reactions are marked in red. The two organelles, although sharing the same steps for fatty acid degradation, possess different sets of enzymes with substrate specificity towards the different length of fatty acid-chains. *Adapted from* Camoes et al., 2015.

Mammalian mitochondria host two β-oxidation pathways. The type I β-oxidation pathway degrades medium- and short-chain fatty acids through four basic reactions involving the enzymes acyl-CoA dehydrogenase (ACAD), enoyl-CoA hydratase, 3-hydroxyacyl-CoA dehydrogenase, and 3-ketoacyl-CoA thiolase. The type II pathway, breaks down long-chain substrates, includes only ACAD and the trifunctional enzyme (TFE; Uchida et al. 1992) which catalyses the final three steps. In mammalian peroxisomes, acyl-CoA oxidase (ACOX) substitutes dehydrogenase in the first step of β-oxidation. The activities of enoyl-CoA-hydratases and 3-hydroxyacyl-CoA-dehydrogenases are combined in the peroxisomal bifunctional enzyme (BP) to catalyse reaction two and three. There are two phylogenetically unrelated peroxisomal bifunctional enzymes (L-BP and D-BP). L-BP catalyses the dehydrogenation of most peroxisomal β-oxidation substrates, with the exception of dicarboxylic enoyl-CoA esters which are D-BP-specific (*reviewed in* Wanders et al., 2015). Finally, the last step is coordinated by two thiolases: 3-ketoacyl-CoA-thiolase and Sterol Carrier Protein X (SCPx), with redundant function in oxidation of very long-chain fatty acids. However, cleavage of 3-ketoacyl-CoA esters of pristanic acid, and di- and trihydroxycholestanoic acid is solely catalysed by SCPx (*reviewed in* Wanders et al., 2015). The medium-chain fatty acids and acetyl group are routed to the mitochondria to enter the tricarboxylic acid cycle, however the precise mechanism is still unclear. Shuttle mechanism as membrane pore system (Antonenkov and Hiltunen, 2012a; Mindthoff et al., 2016) has been described. The degradation of fatty acids in mitochondria supplies the cell with ATP. Peroxisomes lack a respiratory chain. Therefore, electrons released by $FADH_2$ are transferred directly to O_2 - generating H_2O_2, thus the energy is released as heat (contributing to thermogenesis, Lazarow, 1987).

Substrate import is also distinct between the two organelles. Mitochondria relay on a carnitine exchange system. Briefly, fatty acyl-CoA, when in the outer mitochondrial membrane, exchanges CoA for carnitine, resulting in fatty acid-carnitine. The latter can then cross through facilitated diffusion from the inner membrane into the mitochondrial matrix. Once in the matrix, fatty acyl-carnitine is converted back to fatty acyl-CoA. As peroxisomal membrane is impermeable to fatty acids, hence the exact transport into the lumen is not fully elucidated. However, different lines of evidences indicate that fatty acid transport into peroxisomes can be mediated via ATP-binding cassette (ABC) transporters (Wanders 2007),

a Pex11 non-selective channel (in *S. cerevisiae*) (Mindthoff et al., 2016), a channel pore formed by the integral membrane protein, Pxmp2 (Rokka et al., 2009), and/or the carnitine shuttle system, since peroxisomes possess the carnitine acyltransferase protein (van Roermund et al., 1999; Antonenkov and Hiltunen, 2012b).

In mammals and fungi, peroxisomes are the sole site of α-oxidation, which is fundamental for metabolizing 3-methyl-branched-chain fatty acids. These fatty acids can alternatively be metabolised by ω-oxidation. Branched-chain fatty acids are characterised by the presence of a methyl group at the 3-position, unable to be removed by β-oxidation. Therefore, conversion from a 3-methyl- to a 2-methyl fatty acid is required for subsequent β-oxidation (Wanders et al., 2011a). The most prominent branched-chain fatty acid is phytanic acid that after a single cycle of α-oxidation results in pristanic acid. Phytanic acid solely derives from dietary uptake and cannot be synthesised *de novo*. Pristanic acid, on the other hand, can either arise from dietary uptake or from phytanic acid metabolism. The enzymatic reactions of α-oxidation involve five steps: 1) fatty acid activation to acyl-CoA; 2) hydroxylation of the acyl-CoA to 2-hydroxyacyl-CoA; 3) cleavage of the 2-hydroxyacyl-CoA in an aldehyde and formyl-CoA; 4) oxidation of the aldehyde to the corresponding acid and 5) formation of an acyl-CoA ester. It is well known that step 2) is catalysed by phytanoyl-CoA 2-hydroxylase (Jansen et al., 1997; Mihalik et al., 1997). A deficiency in this enzyme results in a peroxisomal disorder, Refsum's disease (*reviewed in* Wanders et al., 2015). Clinical alterations of this pathology include phytanic acid accumulation in tissues and body fluids of the patients. Although Refsum's disease elucidates the importance of α-oxidation in mammals, in fungal species it is still a mystery.

Redox Balance and Cell Signalling

In addition to their important role in lipid metabolism, peroxisome play an essential part in the maintenance of cellular oxidative balance. A shift in the cellular redox equilibrium results in an increase in oxidative stress, which ultimately damages biomolecules and can lead to autophagy. High levels of oxidative stress have been related to several diseases such as atherosclerosis, cancer, diabetes, and neurodegeneration. Notably, peroxisomes possess both oxidative and antioxidant mechanisms. As such, peroxisomes harbour numerous enzymes that produce or degrade ROS/RNS (Reactive Nitrogen Species) as part of their

catalytic cycles (Schrader and Fahimi, 2006). The most prominent ROS-producing enzymes are the flavin-containing oxidases, which reduce O_2 to H_2O_2 (Antonenkov et al., 2010). Peroxisomes are also thought to contain xanthine dehydrogenases that generate superoxide (O^-_2) or nitric oxide (NO^-) (Angermuller et al., 1987; Stolz et al., 2002). To be noted, that recent studies have not been able to identify this latter enzyme (Kikuchi et al., 2004). These by-products can rapidly combine and form new ROS/RNS species. For instance, NO^- combines with O^-_2 to form peroxynitrite ($ONOO^-$) (Pacher et al., 2007), and H_2O_2, through the Fenton reaction, may give rise to hydroxyl radicals (OH^-) (Powers and Jackson, 2008). ROS/RNS can be metabolized in the peroxisomal matrix or diffuse across peroxisome membrane pores (Fransen et al., 2012). To neutralise their hazardous effect, peroxisomes comprise several antioxidant enzymes such as catalase, peroxiredoxin and Cu/Zn-superoxide dismutase (Bonekamp et al., 2009; Antonenkov et al., 2010). Although peroxisomes are emerging as platforms for redox balance much is, yet, to be unravel. However, it has been shown that alteration in peroxisomal H_2O_2 causes different cellular processes (e.g. neuronal activity, autophagy, and secretion of matrix metalloproteinases) (*reviewed in* Lismont et al., 2015).

Peroxisomes are involved in the biosynthesis of docosahexaenoic acid (DHA) and plasmalogens (Van Veldhoven, 2010). These lipophilic molecules are essential to maintain membrane lipid composition, fluidity, and function which ultimately protects cells from oxidative stress (Fransen et al., 2013). Interestingly, plasmalogens function as scavengers for free radicals (Wallner and Schmitz, 2011; Nordgren and Fransen, 2014). Antioxidant properties of peroxisomes were recently revealed in a pejvakin knockout mouse which shows hypervulnerability of auditory cells and neurons to sound exposure (Delmaghani et al., 2015). It was shown that pejvakin localises to peroxisomes, and is likely a peroxisomal membrane or membrane-associated protein. Peroxisomal antioxidant defence also protects the cochlea from noise-induced oxidative stress (Delmaghani et al., 2015).

Dixit and co-workers (2010) showed that peroxisomes cooperate in the anti-viral immune response, with mitochondrial antiviral signalling proteins (MAVSs) present at the peroxisomal membrane. The peroxisomal role in the innate immune response was later confirmed by alteration in type III interferon expression in response to pathogenic stimuli

(Odendall et al., 2014) (see 1.1.5.2 for details). The mammalian target of rapamycin (mTOR) pathway has also been related with peroxisomes (Zhang et al., 2013; Zhang et al., 2015). mTOR nucleates two multi-protein complexes, mTORC1 and mTORC2. mTORC1 regulates cell growth and proliferation both by promoting anabolic and catabolic, such as autophagy, processes. One of the core sensors for regulation of mTORC1 activity is TSC (Tuberous Sclerosis Complex) complex (TSC1, TSC2, TBC1D7, and Rheb), in which TSC2 functions as negative signalling regulator. ATM (Ataxia telangiectasia mutated), a DNA repair kinase is activated in response to oxidative stress, by activating AMPK and TSC2 (Alexander et al., 2010; Tripathi et al., 2013). Recent studies showed that TSC2 was localized at peroxisomes and upregulated when cells were exposed to fibrates (peroxisome-proliferator agent). This stimulation resulted on an augment of peroxisomal ROS production. Upregulation of TSC2 by peroxisomal ROS repressed mTORC1 signalling, hence, increasing autophagy (Zhang et al., 2013). Moreover, it was shown that ATM mediates the activation of TSC and targets peroxisomes for selective autophagy in response to ROS (Zhang et al., 2015). Additionally, ATM has been found at peroxisomal membranes (Watters et al., 1999; Zhang et al., 2015). Also, it was observed that phosphorylates Pex5 at Ser141 resulting in ubiquitination of Lys209, thus generating the binding site for the autophagy adaptor p62, leading to an increase in pexophagy (Zhang et al., 2015). However, these results are controversial since Menon and co-workers (2014) could not confirm the localization of TSC2 at the peroxisomes, so additional information and confirmation of such observations should be undertaken.

Other functions

Peroxisomes harbour several other pivotal roles that are, in some cases, species-specific. In the parasite *Trypanosomatidae*, specialized peroxisomes, glycosomes, harbour the glycolytic cycle for energy production (Michels et al., 2006). In fungi, the (partial) synthesis of secondary metabolites such as antibiotics (e.g. *Penicillium chrysogenum*, *Aspergillus nidulans*, *Acremonium chrysogenum*) (Martin et al., 2010), toxins (e.g. aflatoxin by *Aspergillus flavus* and *Aspergillus parasiticus*; sterigmatocystin by *A. nidulans;* paxilline from *Penicillium paxilli*, and AK-toxin from *Alternaria alternata*) (Saikia and Scott, 2009; Imazaki et al., 2010; Bhetariya et al., 2011), and D-biotin (e.g. *Aspergillus oryzae, A. nidulans*) are compartmentalised in the peroxisomes (Bartoszewska et al., 2011; Islinger et

al., 2012). Furthermore, they also contribute to melanin production in *Colletotrichum orbiculare*, which is essential for the formation of the infection melanised tube, the appressorium (Asakura et al., 2012). Melanization of the appressorium is known to be essential for pathogenicity of the fungus *M. oryzae* and *Colletotrichum* family. Ascomycetes filamentous fungi possess peroxisomal specialised structures, so called Woronin bodies (Jedd and Chua, 2000). These structures act by sealing wounding-induced septal pores, thus preventing cytoplasmic bleeding of the damaged hyphae. In summary, peroxisomes are essential for fungal development and pathogenicity (van der Klei, 2013). In plants, peroxisomes are involved in photorespiration; photo morphogenesis; biosynthesis of biotin, phytohormones and isoprenoid; pathogen and herbivore defence mechanisms; senescence-associated processes, and metabolism of urate, polyamines, sulphite, phyloquinone, volatile benzenoids, and branched-chain amino acids (Corpas et al., 2001; Baker A, 2002; del Rio et al., 2006; Nyathi and Baker, 2006; Hu et al., 2012). They house the production of signalling molecules such as indole-3-acetic and jasmonic acid. These molecules are essential for auxin and jasmonic acid signalling pathways, known to be involved in critical stages of plant development. In higher eukaryotes, peroxisomes are partially responsible, for ether phospholipid (e.g. plasmalogens) biosynthesis, glyoxylate detoxification (Wanders and Waterham, 2006a; Waterham and Ebberink, 2012), antiviral innate immunity (Dixit et al., 2010) (described in more detail in 1.1.5.2), peptide hormone metabolism (Hoftberger et al., 2010), brain aging and Alzheimer's disease (Kou et al., 2011), and age-related diseases (Fransen et al., 2012; Manivannan et al., 2012; Lismont et al., 2015). Plasmalogens are of particular interest as they are located in the inner leaflet of the myelin bilayer. They seem to play a role as antioxidants, either by ROS scavenging (Broniec et al., 2011) or by prevention of PUFAs (polyunsaturated fatty acids) from oxidative damage (Sindelar et al., 1999). Moreover, peroxisomes are of major importance for the degradation of prostaglandins, amino acids and polyamines.

1.1.3 Peroxisome biogenesis

The peroxisomal biogenesis mechanism is still a matter of debate. Generally it is thought that peroxisomes are a semi-autonomous organelles that form by growth and division from pre-existing peroxisomes. However, evidences have been presented that peroxisomes can form *de novo* in association with the endoplasmic reticulum (ER) (Tabak et al., 2003;

Hoepfner et al., 2005; Tabak et al., 2006; van der Zand et al., 2006; Tabak et al., 2008; van der Zand et al., 2010; van der Zand et al., 2012; Kim and Hettema, 2015; Yuan et al., 2016). The proteins involved in peroxisome biogenesis and maintenance are denominated peroxins and are encoded by PEX genes. Peroxins are either membrane proteins or peripheral proteins. Peroxisome membrane biogenesis requires three peroxins, Pex3, Pex16 (not essential in yeast) and Pex19. The absence of any of these proteins leads to a loss of mature peroxisomes in the cell (Hohfeld et al., 1991; Matsuzono et al., 1999). Studies performed in *S.* cerevisiae suggest that *de novo* biogenesis requires the formation of a Pex3 and Pex19 pre-peroxisomal vesicle and subsequent budding off from the ER (Kragt et al., 2005; van der Zand et al., 2010; Agrawal et al., 2011; van der Zand et al., 2012). Peroxisomes become import competent when two heterotypic preperoxisomal vesicles, each containing half of the translocon complex [Ring finger complex (PEX2, PEX10 and PEX12) and docking complex (PEX13 and PEX14)], fuse. Therefore, resulting in the formation of the translocon at the peroxisomal membrane, allowing the import of matrix proteins (van der Zand et al., 2012).

Peroxisomal growth and division is a multi-step mechanism (involving elongation, constriction/segmentation and fission of the peroxisomal membrane) present throughout different organisms (yeast, plants and animals) (Figure 4) (Schrader et al., 2012). Initial elongation is mediated by Pex11, a family of proteins known to deform and elongate the peroxisomal membrane (Figure 4 A) (Thoms and Erdmann, 2005; Koch and Brocard, 2011; Schrader et al., 2012). The constriction step is still elusive. However, recently, pejvakin, a protein linked to human deafness, was shown at the constriction sites. Its depletion resulted in enlarged peroxisomal clusters (Delmaghani et al., 2015). Peroxisomal fission relies on dynamin-like mechano-enzymes (Drp1 in mammals) (Praefcke and McMahon, 2004). Drp1 is recruited from the cytosol by tail-anchored membrane adaptors, Mff and/or Fis1 (Figure 4 B). Dynamin-like proteins are self-assembling GTPase which form a spiral like structure around the constricted sites in order to mediate scission through GTP hydrolysis (Figure 4 C) (Praefcke and McMahon, 2004). Fis1 has been identified as an adaptor for Drp1 at mitochondria and peroxisomes (Koch et al., 2005; Yoon et al., 2003). However, its exact function is unclear, as Mff appears to be the major receptor for Drp1, at peroxisomes and mitochondria (Gandre-Babbe et al., 2008; Otera et al., 2010). Regardless of the biogenesis mechanism, it is consensual that peroxisomes and the ER are closely interconnected. The

ER provides lipids and proteins, such as peroxisomal membrane proteins, to peroxisomes, which they are unable to synthesise (*reviewed in* Schrader et al., 2016). Moreover, the close proximity of peroxisomes and the ER is supposed to facilitate the exchange of metabolites between both compartments (Geuze et al., 2003; Tabak et al., 2008). Therefore, it is likely that the two mechanisms are not mutual exclusive but instead, they might function as a cooperative system. The fact that peroxisome biogenesis relies on two different mechanisms, ER-based and an autonomous system, is intriguingly uncommon and it is unclear if both mechanism are cooperative or species-/condition-specific.

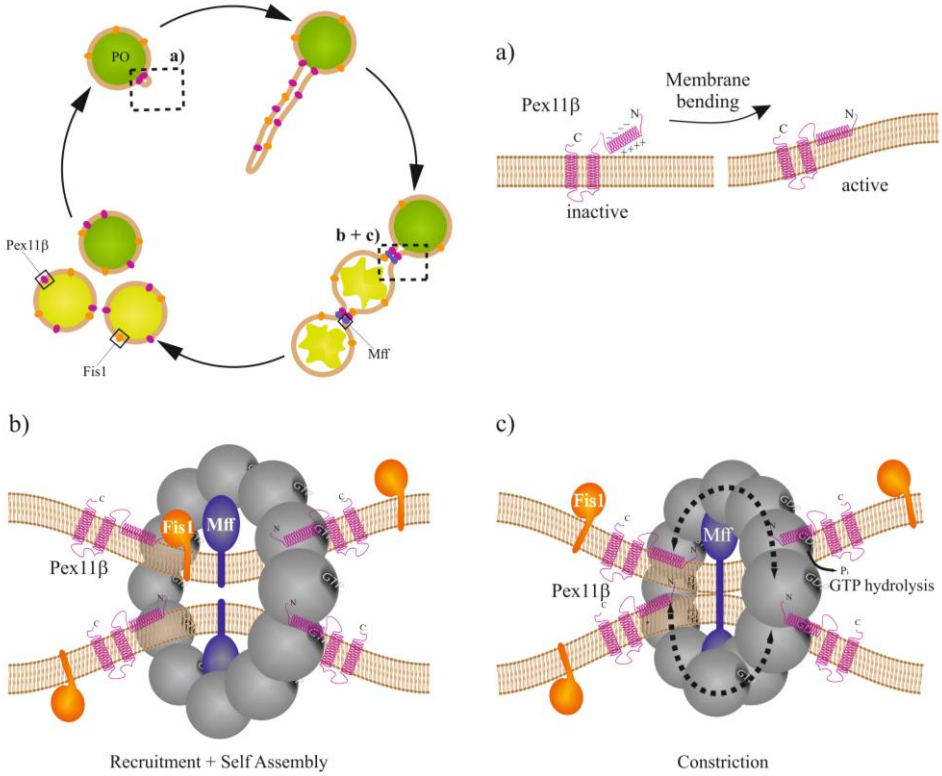

Figure 4 - Peroxisome biogenesis growth and division model. In the mammalian system this model is well defined in three steps according to peroxisomal morphological alterations: elongation, constriction and fission. a) Pex11β mediates peroxisomal membrane extension from pre-existing peroxisomes. Insertion of docosahexaenoic acid at the peroxisomal membrane induces Pex11β oligomerization. Active oligomers insert into the leaflet of the lipid bilayer via Pex11β amphipathic helices, hence inducing membrane bending/deformation (Opalinski et al., 2011, Yoshida et al., 2015). b) Membrane deformation subsequently induces the recruitment of the fission machinery (e.g. DLP1, Mff and Fis1). Mff recruits cytosolic DLP1 that assembles into ring-like structures. c) Pex11β binds to DLP1 and stimulates DLP1 GTPase activity (Williams et al., 2015). GTP hydrolysis leads to constriction of the DLP1 ring structure culminating in final membrane scission. *Adapted from* Schrader et al., 2015a.

1.1.3.1 Peroxisomal membrane protein insertion

Peroxisomal membrane protein insertion and matrix protein import are two distinct mechanisms. In fact, if peroxisomal matrix import is impaired, peroxisomal membrane

remnants are still present, the so-called “ghosts” (Santos et al., 1988; Brown and Baker, 2003; Schrader and Fahimi, 2008). Peroxisome membrane biogenesis requires three peroxins, Pex3, Pex16 and Pex19, and the lack of any of those leads to the absence of peroxisomes (Hohfeld et al., 1991; Baerends et al., 1996; Eitzen et al., 1997). Peroxisome membrane proteins (PMPs) can be grouped in two classes: I, directly targeted to the peroxisomes; II, targeted via the ER. The underlying mechanism of membrane formation is not fully elucidated, however, a membrane peroxisomal targeting sequence (mPTS) has been identified that varies depending on protein length, but generally comprises one transmembrane domain, and a cluster of basic amino acids (Van Ael and Fransen, 2006). Class I PMPs contain this sequence and are targeted to peroxisomes through Pex19 (Sacksteder and Gould, 2000; Fransen et al., 2001; Fujiki et al., 2014). Pex19 is predominantly cytosolic but is also found at the peroxisomal membrane, acting as chaperone and import receptor, and has further been described as insertion and assembly/disassembly factor (Fransen et al., 2001; Fransen et al., 2004; Jones et al., 2004; Shibata et al., 2004). Upon binding of Pex19 to the newly synthetized PMPs, the cargo-receptor complex is recruited to the peroxisomal membrane via the docking factor Pex3, an integral membrane protein (Muntau et al., 2003; Fang et al., 2004; Fransen et al., 2005; Pinto et al., 2006). Pex3 binds to the N-terminal domain of Pex19, and the C-terminus of Pex19 is reserved for PMP binding (Fang et al., 2004;Shibata et al., 2004; Matsuzono et al., 2006).

1.1.3.2 Peroxisomal matrix import proteins

Matrix proteins targeted to the peroxisome require a PTS. PTS are short amino acids sequences with two major PTSs known, PTS1 and PTS2. The PTS1 is the most predominant in mammals, and PTS2 the less common. PTS1 is commonly defined as a C-terminal tri-peptide, serine-lysine-leucine (SKL), or conserved variants (S/A/C)-(K/R/H)-(L/M) (Gould et al., 1989). However, PTS1 was redefined as a dodecamer, as the additional amino acids might influence receptor-cargo affinity in a species-specific manner (Brocard and Hartig, 2006). The PTS2 motif comprises an N-terminal degenerated nonapeptide (R-(L/V/I/Q)-xx-(L/V/I/H)-(L/S/G/A)-x-(H/Q)-(L/A) and is present in a few matrix proteins (Swinkels et al., 1991; Kunze et al., 2015). Both PTS1 and PTS2 cargo proteins are translocated into the organelle through Pex5. Pex5 is the cytosolic receptor for PTS1 that mediates the binding to the cargo through its tetratricopeptide (TPR) repeats (Gatto et al., 2000). The knowledge on

PTS2 protein import is still limited. However, it is thought that PTS2 signals bind to Pex7 and Pex5. The PTS2-cargo is recognized by Pex7 via its tryptophan-aspartic acid (WD) repeats. Nonetheless, unlike the PTS1-receptor, Pex7 requires auxiliary proteins for the import process. These PTS2-co-receptors are the redundant Pex18 and Pex21 (*S. cerevisiae*), Pex20 (most other fungi) and Pex5L (the longer of two splice isoforms of Pex5p) (Rodrigues 2015) in plants and mammals (Schliebs and Kunau, 2006). Non-consensual-PTS proteins that show neither PTS1 nor PTS2 motifs are rare but are supposed to be imported by a different region of Pex5 (van der Klei and Veenhuis, 2006) or "piggyback" by formation of a complex with PTS-containing proteins (McNew and Goodman, 1994; Titorenko and Rachubinski, 2001; Islinger et al., 2009;). Pex5 and Pex7 possess a dual localisation: in the cytosol and the peroxisomal membrane. Although not fully understood, the import process can be summarized in five steps: i) the cargo is recognised in the cytosol; ii) the cargo-receptor docks to the peroxisomal membrane; iii) Pex5p is integrated into the membrane forming a transport channel, allowing the translocation to occur; iv) release of the cargo into the peroxisomal matrix; v) receptor ubiquitination and export in an energy-dependent manner mediated by the exportomer complex. Import and recycling of Pex5p are fundamental for the recycling-driven import (*reviewed in* Dias et al., 2016).

1.1.4 Peroxisome proliferation

Peroxisomes are sensitive to external signals and are able to proliferate. In yeast, where β-oxidation occurs solely in peroxisomes, many peroxisomal enzymes and *pex* genes are induced by fatty acids, such as oleic acid, and are repressed by glucose. In *S. cerevisiae*, genes that respond to oleic acid induction possess an oleate response element (ORE) within the promoter that binds the transcription factor Oaf1/Oaf2 (Karpichev et al., 1997). In mammals, the expression of certain genes involved in lipid homeostasis, including all the β-oxidation genes, is controlled by peroxisome proliferator activator receptor α (PPARα), which binds to the peroxisome proliferator response element (PPRE) in the promoter region of these gene (Lemberger et al., 1996). PPRAα has a diverse set of ligands such as a medium and long chain fatty acids, as well as other compounds including clofibrate (acts as hypolipidemic drug) (Issemann and Green, 1990).

1.1.5 Peroxisome inter-organelle cooperation

Organelle interactions are of utterly importance for the coordination of cellular functions and exchange of metabolites. Mechanisms such as signal transduction and vesicular trafficking enable cross-talk between different membrane-bound organelles. It has become evident that organelles communicate through membrane contact sites, hence facilitating close-range interactions and transport of small molecules (English and Voeltz, 2013; Helle et al., 2013; Shai et al., 2016). Proximity does not *per se* imply contact sites, instead tethering of the organelles is required for proper exchange of metabolites (Prinz, 2014; Shai et al., 2016). Peroxisomes have long been visualised in close contact with other cellular compartments such as mitochondria, the ER, lipid droplets and lysosomes. An interplay of peroxisomes with other organelles is thought to be essential to accomplish their different functions (reviewed in Shai et al., 2016) (Figure 5).

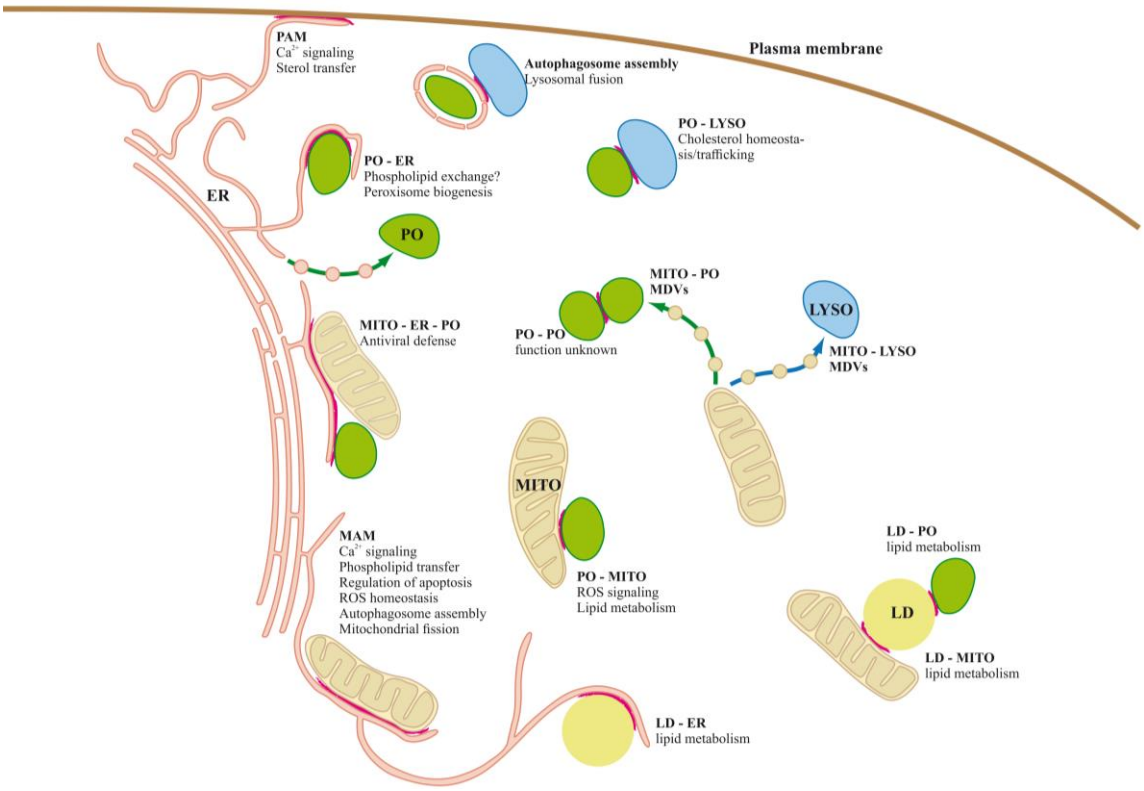

Figure 5 - Overview of inter-organelle connections in mammals. The membrane contacts are highlighted in pink. Peroxisomes and lysosomes were shown to tether through the transient interaction of synaptotagmin VII (lysosomal integral membrane) and the binding lipid PI(4,5)P2 (peroxisomal membrane) (Chu et al., 2015). This contact site is supposed to regulate the transport of cholesterol from the lysosome to the peroxisome. Abbreviations:; LD – lipid droplets; LYSO – lysosome; MITO – mitochondria, PAM – plasma membrane associated membrane; PO – peroxisomes *Adapted from* Schrader et al., 2015b.

1.1.5.1 Peroxisomes and lipid droplets

Lipid droplets are ubiquitous subcellular organelles responsible for lipid storage (Chapman et al., 2012; Mak, 2012; Walther and Farese, 2012). Their size varies within a cell, ranging from 1 – 100 μm in diameter (Herms et al., 2013) with a core of neutral lipids, triacylglycerol, and sterol esters, surrounded by a phospholipid monolayer (Murphy, 2001; Martin and Parton, 2006; Wilfling et al., 2014). Lipid droplets are known to arise from the ER, although the mechanism is not fully understood (Murphy and Vance, 1999; Ohsaki et al., 2009; Pol et al., 2014). They are dynamic organelles that move directionally along microtubules. Close association of lipid droplets with other subcellular structures such as peroxisomes, mitochondria, lysosomes and the ER (Ploegh, 2007; Helle et al., 2013; Kohlwein et al., 2013; Gao and Goodman, 2015) has been observed. Peroxisomes and lipid droplets control lipid homeostasis, therefore the close association between the two organelles suggests the regulation of metabolism and lipid trafficking across membranes. The ER and lipid droplets are the exclusive membrane lipids suppliers (Shai et al., 2016). BiFC (bimolecular fluorescence complementation) studies, in *S. cerevisiae*, showed that lipid droplets interact with peroxisomal membrane proteins (e.g. Pex1, Pex3, Pex5, Inp1, Pex30, etc), that might act as a tether for the organelle (Pu et al., 2011). Moreover, protrusion-like structures, pexopodia, have been described as peroxisomal membrane extension that enter into the core of the lipid droplets. This interaction would facilitate the transfer of metabolites between both organelles (Binns et al., 2006). Accordingly, changes in morphology and number of lipid droplets were observed in peroxisome-deficient knockout mice (Dirkx et al., 2005), and under peroxisomal malfunction or stress conditions in the nematode *Caenorhabditis elegans* (Zhang et al., 2010). In conclusion, lipid droplets and peroxisomes show an interplay through physical proximity to the control of lipid homeostasis.

1.1.5.2 Peroxisomes and mitochondria

Mitochondria are of key importance for ATP production, β-oxidation of fatty acids, stress response, homeostatic regulation, lipid and amino acid metabolism. Interestingly, it has become increasingly evident that mitochondria share metabolic functions and proteins with peroxisomes (Schrader et al., 2015b). In recent years a cooperation in the regulation of lipid homeostasis (Wanders et al., 2015); ROS homeostasis and redox signalling (Lismont et al.,

2015) membrane fission (Delille et al., 2009); and anti-viral signalling and defence (Dixit et al., 2010; Odendall et al., 2014) (Figure 6) became evident.

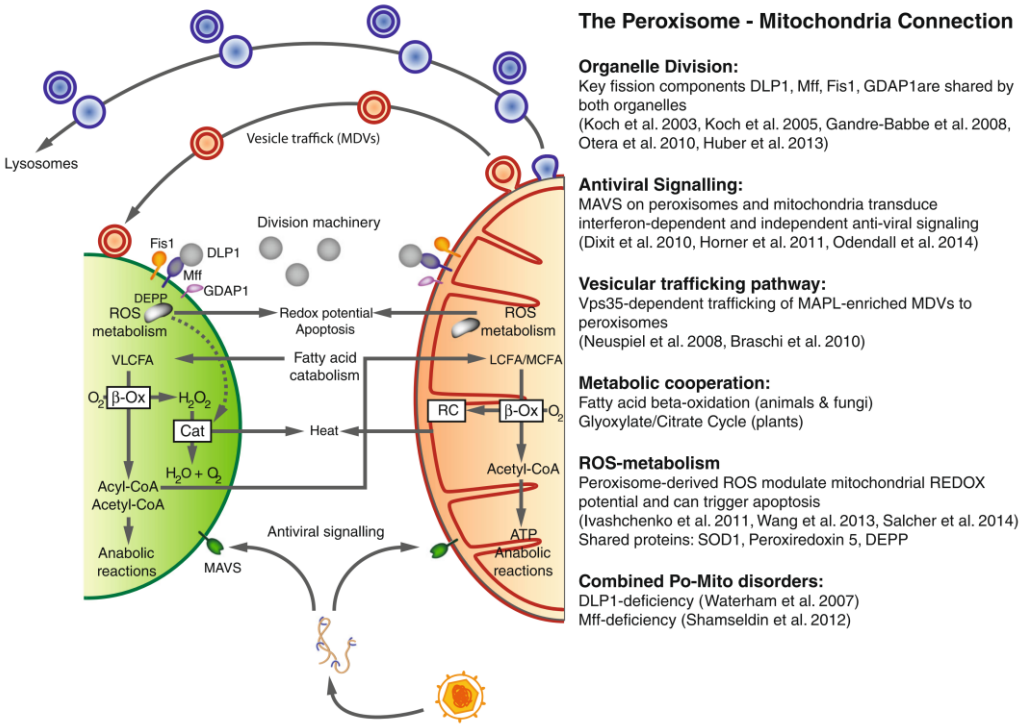

Figure 6 - Mitochondria – peroxisome interplay. Overview of the different shared functions between mitochondria and peroxisomes in mammals. A*dapted from* Schrader et al., 2015a.

Inter-organelle cooperation is supported by mitochondrial alterations which are observed in peroxisome-related disorders (Thoms et al., 2009). In fact Zellweger models show impaired mitochondrial respiration, DNA depletion and altered carbohydrate metabolism (Peeters et al., 2011; Peeters et al., 2015).

Although a peroxisome-mitochondria cooperation is evident, the exact mechanisms of communication are elusive. It has been suggested an interplay through membrane contact sites (Horner et al., 2011), mitochondria-derived vesicles (Neuspiel et al., 2008) or diffusion across membranes (Antonenkov and Hiltunen, 2012a). In yeast, a subpopulation of mitochondria-ER contact sites has been described. The tether between the two structures is mediated by the ERMES complex (ER-Mitochondria Encounter Structure) (Kornmann et al., 2009), a four protein complex. The complex consists of two mitochondria outer membrane proteins (mdm10 and mdm34), an integral ER protein (mmm1) and a peripheral mitochondrial membrane protein (Mdm12) that tethers the ER to the mitochondria outer membrane (Kornmann et al., 2009). Recently, it was shown that peroxisomes are possibly

in close proximity with the ERMES (Cohen et al., 2014). Interestingly, in *S. cerevisiae,* peroxisomes are close to pyruvate decarboxylation sites of complex region, at the mitochondria matrix, potentiating the metabolic transfers over short distances (Cohen et al., 2014). Moreover, Pex11 was shown to interact with mdm34 (Mattiazzi Usaj et al., 2015) in *S. cerevisiae*. This three way interaction might be of crucial importance for transfer of metabolites and peroxisome/mitochondria division.

Antiviral signalling

An antiviral immune response is initiated when viral components (such as genome) are detected (Takeuchi and Akira, 2009). Pathogenic RNA binds to either RIG-I (RNA helicases retinoic acid-inducible gene I) or MDA-5 (melanoma differentiation-associated gene 5) receptors. Following the activation of RIG-I or MDA-5 they bind to their co-factor MAVS (mitochondrial antiviral signalling), triggering the innate immune response. MAVS is localized at the membrane of the mitochondria, peroxisomes, and at a distinct membrane compartment that links the ER to the mitochondria (MAM). The reason for such diverse localization is not yet understood. During viral infection, RIG-I is recruited to MAM to activate the MAVS response. NF-kB and interferon regulatory factor 3 (IRF3) are activated, which induces downstream signalling of the antiviral pathway. Gene expression of encoding inflammatory cytokines and type I interferons is initiated. MAM functions as a platform to link peroxisomes and mitochondria during antiviral response (Horner et al., 2011). Moreover, peroxisomal MAVS fail to produce type I interferon (Dixit et al., 2010). However, peroxisomal MAVS can induce the JAK-STAT1 pathway and therefore generate an antiviral state (Odendall et al., 2014). Proteomic studies showed increasing levels of peroxisomal proteins at the MAM during RNA virus infection, suggesting a close interaction of peroxisomes with mitochondria and/or MAM during anti-viral response (Horner et al., 2015).

Organelle division

Mitochondria and peroxisomes share key proteins of their division machinery (Schrader et al., 2012). This mechanism is essential for organelle maintenance. It is not surprising, that mutations in key proteins of the division machinery (DLP1, Mff, and GDAP1) lead to severe diseases/pathologies in humans (Waterham et al., 2007; Ribeiro et al., 2012; Shamseldin et

al., 2012). Membrane fission also enables organelle turnover through degradation (pexophagy and mitophagy). Autophagic events are dependent on the size of the organelles, which may present steric challenges. Thus, peroxisomal and mitochondrial fission is pivotal for subsequent engulfment by the phagophore (Gomes and Scorrano, 2013; Mao et al., 2014). In *S. cerevisiae* it was shown that peroxisomes recruit Dnm1 and Vps1 fission proteins. Dnm1 and Vps1 interact with a scaffold protein, Atg11 (Autophagy-related protein 11), promoting organelle segregation followed by degradation. Moreover, pexophagy occurs at the peroxisome-mitochondria contact sites (Mao et al., 2014), and mitochondria require the ER for degradation purpose (Friedman et al., 2011). Thus, the interaction ER-mitochondria-peroxisomes may be required for appropriate organelle degradation (Mao et al., 2014).

1.1.5.3 Peroxisomes and the ER

The ER is known to interact with several organelles, such as mitochondria, plasma membrane and peroxisomes (Friedman and Voeltz, 2011). Peroxisome-ER interactions have long been described by electron microscopy (EM) by close juxtaposition (Novikoff and Shin, 1964; Novikoff and Novikoff, 1972; Reddy and Svoboda, 1973). Furthermore, a cooperation between peroxisomes and the ER is required for the biosynthesis of ether phospholipids, formation of GPI anchored proteins, and production of polyunsaturated fatty acids, cholesterol, bile acids, and isoprenoids. As described (see 1.1.3), the ER is important for peroxisome biogenesis. A role for the ER in peroxisome formation is undeniable, as it provides the phospholipids required for peroxisomal membrane formation in addition to some PMP. It is thought that PMPs are inserted into the ER and then delivered to the peroxisomes. However, tail-anchored proteins seem to follow a different path, since they are translated at cytoplasmic ribosomes (Borgese and Fasana, 2011) and subsequently inserted directly into the peroxisomal membrane, in mammals (Chen et al., 2014; Kim and Hettema, 2015), or via the ER using the GET pathway (Guided Entry of Tail-anchored Proteins) (Mariappan et al., 2011), in *S. cerevisiae*.

1.1.6 Peroxisome motility

Peroxisome motility and dynamics are important prerequisites for peroxisome inheritance, proper intracellular distribution, positioning, organelle interactions and biogenesis. Peroxisomal motile events have been visualized across species, although relying on different transport mechanisms. In yeast and plants, peroxisome motility and inheritance is governed by actin (Hoepfner et al., 2001; Jedd and Chua, 2002; Mathur et al., 2002; Muench and Mullen, 2003; Fagarasanu et al., 2006; Chang et al., 2007; Chang et al., 2009;) Whereas in fungi and mammals it is mediated by microtubules.

Peroxisome motility in yeast

S. cerevisiae divides asymmetrically by forming a bud from the mother cell. Each division process double peroxisome number and subsequently evenly distributes them between the mother cell and the bud (Hoepfner et al., 2001; Motley and Hettema, 2007). In *S. cerevisiae* peroxisomes exist in short number, therefore, it is pivotal that the distribution between the mother and daughter cell is finely regulated. Peroxisomes can either be static or show directed motility. Peroxisome inheritance factors, Inp 1 and 2 play antagonistic, yet crucial roles in peroxisomal motility in yeast. Inp1 tethers peroxisomes to the cortical ER immobilizing them (Fagarasanu et al., 2005), acting as a molecular hinge between ER-bound Pex3 and peroxisomal Pex3 (Knoblach et al., 2013). Inp2, localized at the peroxisomal membrane, is recognized by the myosin motor, Myo2, which moves along actin cables (Fagarasanu et al., 2006; Chang et al., 2009). However, peroxisomal partitioning is not fully blocked in Inp2 deleted strains (Fagarasanu et al., 2006). Pex19 was shown to bind to Myo2 in an Inp2-independent manner (Otzen et al., 2012) Altogether, peroxisomal segregation is regulated through Myo2 binding to Pex19 and Inp2 in *S. cerevisiae*.

In heterothallic yeast, *Yarrowia lipolytica,* peroxisomes are highly mobile and move dynamically from the mother cell to the bud and inversely, contrarily to *S. cerevisiae* (Chang et al., 2007; Chang et al., 2009). Their motility is governed by the actin cytoskeleton (Chang et al., 2007; Chang et al., 2009). YlInp1 (Inp1 homologue) has an opposing effect in *Y. lipolytica* compared to *S. cerevisiae*, as its deletion segregates peroxisomes into the bud (Chang et al., 2007). In this model, no homologue of Inp2 is expressed, instead pex3 and its paralogue, pex3b are required for peroxisomal membrane attachment to the myosin motor

(Chang et al., 2009). Fission yeast *Saccharomyces pombe* exhibits different motility mechanisms, as peroxisomes move along microtubules (Jourdain et al., 2008) without direct binding to a motor protein. Instead, it was observed that disruption of microtubules or the mitochondria fission/fusion machinery resulted in the inhibition of peroxisome motility. Peroxisomes remained located juxtaposed to mitochondria. Hence, it was suggested that peroxisomes anchor to mitochondria, which then directly bind to microtubules.

Peroxisomal motility in mammals and fungi

In mammalian cells and filamentous fungi, peroxisomes bind to and move bidirectional along microtubules (Rapp et al., 1996; Wiemer et al., 1997; Kural et al., 2005; Egan et al., 2012b). Peroxisomes show three types of motions: a) Resting or pausing; b) short range motility/oscillating; and c) saltatory, long range motility (Huber et al., 1997; Schrader et al., 2000; Ishikawa et al., 2001; Mathur et al., 2002; Jourdain et al., 2008). In mammalian cells, peroxisomal motility is thought to be coordinated via the motor proteins (dynein and kinesins) (Schrader et al., 1996; Schrader et al., 2000; Thiemann et al., 2000; Hoogenraad et al., 2000; Kural et al., 2005; Kulic et al., 2008; Kapitein et al., 2010; Dietrich et al., 2013). In an elegant study, it was shown that dynein or kinesins attach alternatively to peroxisomes, implying a “tug of war” mechanism (Kural et al., 2005). Interestingly, abolishing one motor protein results in the absence of peroxisomal bidirectional motility, suggesting cooperation between motors (Kural et al., 2005; Kim et al., 2007; Ally et al., 2009). So far, the precise mechanism of peroxisome binding to the molecular motors is not fully understood. However, it was suggested that Pex14 mediates long-range transport by binding directly to tubulin (Bharti et al., 2011). In fact, in Pex14-defficient fibroblasts directed motility is abolished. In contrast to yeast, peroxisome motility is not acto-myosin dependent. Though, actin regulators such as NMM IIA (non-muscle myosin IIA), RhoA and Rho kinase II (ROCKII) bind to the peroxisomal membrane in human fibroblasts (Schollenberger et al., 2010). Noteworthy, actin is not directly involved in peroxisomal motility, instead it might generate force that supports short range motility and/or tethering to other organelles or motor proteins.

Peroxisomal motility is thought to be important to maintain distribution, biogenesis, degradation, and organelle-organelle interaction. In cells from Zellweger patients and patients suffering from D-BF protein deficiency, peroxisomes are enlarged, less abundant,

clustered and lose their alignment along microtubules (Nguyen et al., 2006). Together this might implicate a role of peroxisomal motility in peroxisomal disorders. Moreover, in an Alzheimer-like model, peroxisome number was reduced and distribution altered, with peroxisomes locating predominantly at the cell body and absent at the neurites (Stamer et al., 2002). Interestingly, in cells treated with microtubule-depolymerising drugs, peroxisomes cluster and elongate (Schrader et al., 1996; Schrader et al., 1998) but the reason is still unknown. However, cytoskeleton integrity seems to be crucial for *de novo* biogenesis. Pex16 reintroduction in Pex16-depleted cells failed to induce the formation of new peroxisomes when microtubules were depolymerized (Brocard et al., 2005).

Peroxisome motility was also suggested to be essential for peroxisome degradation (Hara-Kuge and Fujiki, 2008). Pexophagy is defined by the formation of autophagosomal membranes that sequester peroxisomes, fusing them with vacuoles. One essential protein for autophagosomal membranes is LC3 (Atg8 human homologue), which interacts with Pex14 via microtubules (Hara-Kuge and Fujiki, 2008). Recently, it was shown, that Pex5 and LC3II compete for the interaction with Pex14, *in vitro*, implying that proteins that lose their import capacity are targeted for degradation (Jiang et al., 2015).The regulation of peroxisomal motility is not well understood. However, in mammals directed motility along microtubules is regulated by the co-stimulation of the ATP-lysophosphatidic acid (LPA) receptor. The LPA receptor activates Rho pathway via G12/13, arresting peroxisomal long-range motility (Huber et al., 1997; Huber et al., 1999). Peroxisome motility is abolished when the GTPase RhoA is constitutively inactive. RhoA localizes at the peroxisomal membrane. Therefore, RhoA cycling states of GDP- and GTP-binding controls peroxisome binding to the microtubules. Moreover, it was suggested that RhoA might enable peroxisomal attachment to actin (Schollenberger et al., 2010).

1.2. The filamentous fungus *Ustilago maydis*

Fungi are simple eukaryotic organisms surrounded by a cell wall, extended by polar tip growth. There are two morphological forms of fungi: yeast and hyphae (or filamentous) (Figure 7). Yeast cells are unicellular organisms that reproduce asexually by budding or

fission. Filamentous fungi are multicellular organisms with polar tip growth. Several species of filamentous fungi have emerged as powerful model organisms to study cellular mechanisms. Dimorphic fungi are rare, and they can exist in yeast-like and filamentous forms (Figure 7 A-B). One example is the corn-smut fungus *Ustilago maydis*. The *U. maydis* life cycle includes a yeast-like unicellular, saprotrophic and non-pathogenic (sporidia) stage (Figure 7 A); and a dikaryotic, invasive, and pathogenic stage (hyphal cells) (Figure 7 B). *U. maydis* is a biotrophic, basidiomycete fungus and the causative agent of maize (*Zea mays*) smut disease (Brefeld, 1883; Banuett, 1995). It has been rated as one of the top 10-plant pathogens for scientific and/or economical focus (Dean et al., 2012). However, *U. maydis* has not a major economically impact, as corn yield is only reduced by 2% through fungal infection. In fact, *U. maydis* core importance relies on its scientific use, as it is a model system for the investigation of the molecular basis of plant pathogenicity and fundamental cellular mechanisms (Bolker, 2001; Feldbrugge et al., 2004; Steinberg and Perez-Martin, 2008). Curiously, it is a well know *delicatessen* in Mexico, where farmers artificially infect the corncobs for the preparation of *Huitlacoche*, a plant gall formed by the fungus in the infected corn (Figure 7 D).

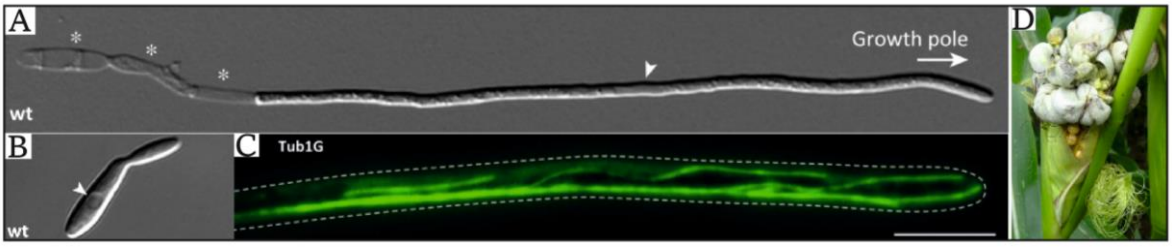

Figure 7 - The dimorphic fungus *U. maydis*. A) Filamentous hyphal cell with polarized growth and a single nucleus in the middle of the cell (arrow). Vacuolated structures are formed at the basal pole with the formation of retraction septa, leaving behind the sections devoided of cytoplasm (asterisks). B) *U. maydis* in its yeast-like form. C) Strain expressing α-tubulin-GFP (Tub1G) exhibiting microtubule bending. Bars, 10 μm. D) A maize cob infected with *U. maydis*, showing the characteristic plant gall. *Adapted from* Jansen et al., 2014.

In its filamentous form, *U. maydis* grows apically. This process requires a constant flow of membranes and proteins to the growing hyphal tip. The "Spitzenkörper" is the structure located at the hyphal tip which is crucial for hyphal growth (Bartnicki-Garcia et al., 1995), its position defines the growth directionality (Girbardt, 1969; Rida et al., 2006). The "Spitzenkörper" was first visualized by light microscopy as a dark region (Brunswik, 1924) at the hyphal apex and later by EM (Howard, 1981). Further studies showed that it can be found in a broad range of fungi (Girbardt, 1969).

1.2.1 Pathogenicity of *U. maydis*

U. maydis dimorphism is present in nature and it can be reproducible under laboratory conditions. The yeast-like form (sporidia) lives on dead organic matter and colonizes the soil, where it proliferates by polar budding. The infection process starts with the mating of two compatible haploid cells on the surface of the plant. The pheromone receptor system is key for recognition of compatible sporidia. This system is encoded by the biallelic *a* mating-type locus: lipopeptide pheromone precursor (mating factor; *mfa1* or *mfa2*) and a transmembrane pheromone receptor (*pra1* or *pra2*) which controls the fusion of the sporidia by recognition of the opposite mating type (*a1* fuse to *a2*) (Spellig et al., 1994b; Bolker, 2001; Szabo et al., 2002). A pheromone signalling cascade is triggered enabling the formation of the conjugation tube that will orient its growth along the pheromone gradient of the mating partner (Snetselaar et al., 1996). The response to pheromone signalling induces G2 cell cycle arrest (Garcia-Muse et al., 2003). In their quest for its mating partner, each hypha can reach up to 150-160 μm (Steinberg et al., 1998). Thus, mating partners approach each other and fuse at their tips initiating plasmogamy (Banuett and Herskowitz, 1994; Spellig et al., 1994a; Spellig et al., 1994b) (Figure 8).

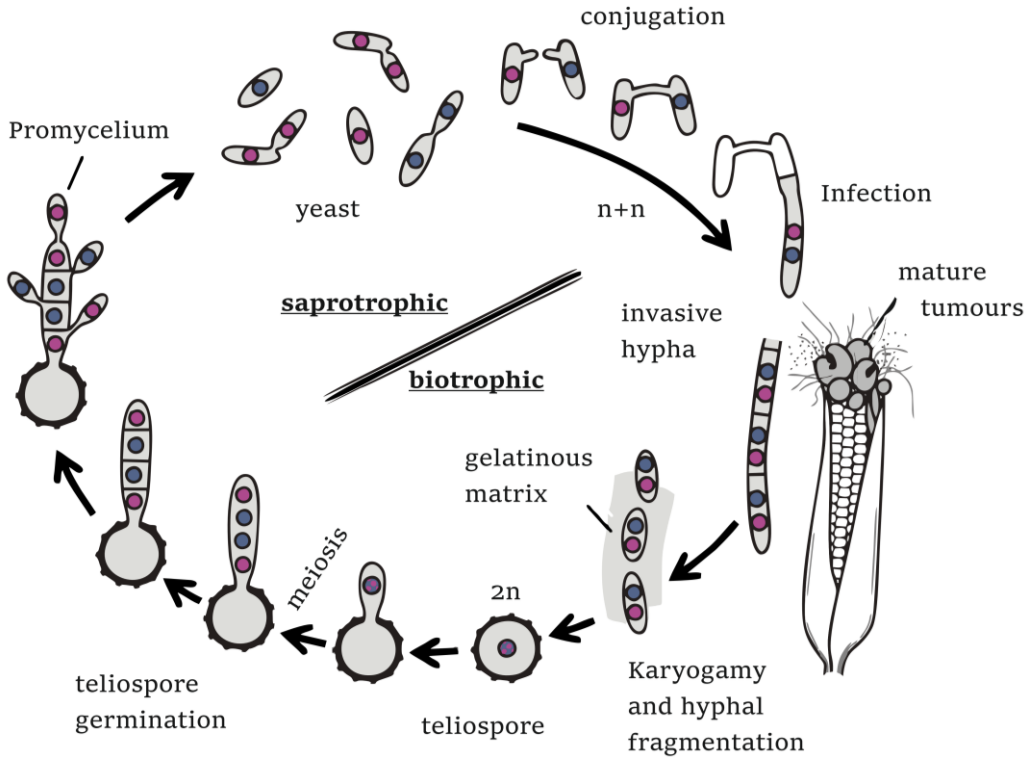

Figure 8 - The *U. maydis* life cycle. Sporidia, under stress conditions will switch for polar growth and hence form a conjugation tube. On the surface of the plant leaf, two compatible sporidia are able to recognize compatible partners through an exchange of pheromone signals. The two compatible haploid cells (different color nuclei) fuse their conjugation hyphae resulting in dikaryotic hyphae, which are able to penetrate the plant

(*Zea mays*). Once inside the plant, the elongated hyphae colonize the plant, giving rise to large tumors. After proliferation, nuclear fusion occurs and hyphae fall apart, forming teliospores. Teliospores germinate to form a promycelium, which will form sporidia after meiosis, and the cycle reinitiates.

The multiallelic *b* locus (approximately 25 alleles) is responsible for hyphal growth, encoding a pair of homeodomain transcription factors: bE and bW (Rowell, 1955 Day et al., 1971; Kronstad and Leong, 1990; Froeliger and Leong, 1991). bE and bW dimerize and control sexual and pathogenic development. The dikaryotic filament grows in close contact with the plant epidermis. The distal end of the hypha contains vacuolated sections devoid of cytoplasm which are thought to be essential for cytoplasmic migration during hyphal growth (Steinberg et al., 1998). The empty compartments are left behind and isolated from the remaining hyphae through retraction septa. These phenomena enable rapid growth of the infectious hypha (Snetselaar et al., 1996; Lanver et al., 2010). Once the hypha perceives the plant signalling defence, a slightly swollen appressorium is formed (Snetselaar, 1992). This specialized infection structure allows the pathogen to enter the plant. *U. maydis* appressorium is different from dome-shaped structures with high turgor pressure formed in other fungi such as *M. grisea*. Instead, the *U. maydis* appressorium is unmelanized and morphologically undifferentiated, and it is supposed to enter the plant tissue by secreting plant cell wall degrading enzymes (Schirawski et al., 2005). Within the plant tissue, the cell cycle arrest is released and the hyphae colonises the host. The colonization will lead to an irregular division of host cells, resulting in the formation of tumours in the plant. Within the tumours, the fungus proliferates, the karyogamy occurs and black diploid teliospores develop. Tumour rupture will allow the spores to be spread by the wind. Teliospores rest until suitable conditions to form promycelium occur. After meiosis, the promycelium generates sporidia and the cycle restarts.

1.2.2 *U. maydis* as a model system for cell biology

U. maydis possesses remarkable features that make it a powerful tool for cell biology studies. It has a fully sequenced genome (Kamper et al., 2006), which comprises 20.5 Mb contained in 23 chromosomes. The 6902 genes are listed in the MIPS *U. maydis* database (http://pedant.helmholtz-muenchen.de/pedant3htmlview/pedant3view?Method=analysis&Db=p3_t237631_Ust_maydi_v2GB). Interestingly, the genome is characterized by a small number of introns and,

when present, they are short in length. As it has long been described (and although fungi possess a cell wall), phylogenetically, fungi are closer to animals than to plants (Whittaker, 1969). Remarkable, the *U. maydis* genome shows that in some biological processes it exhibits more similarities to humans than to the baker's yeast. Namely: a) DNA repair mechanisms (Kojic et al., 2002); b) microtubule organization (Fink and Steinberg, 2006); c) long-distance transport (Wedlich-Soldner et al., 2002b; Schuchardt et al., 2005;); d) polarized growth (Castillo-Lluva et al., 2007) and e) open mitosis (Straube et al., 2005; Fink and Steinberg, 2006) (for details see Table 2).

Table 2: Processes found in U. maydis and humans but not in *S. cerevisiae* model systems. *Adapted from* Steinberg and Pérez, 2008.

DNA repair	The breast cancer susceptibility protein BRCA2 participates in DNA repair
Microtubule organization	Dynein transports assembled microtubules and polarizes the tubulin array Microtubules grow slowly but depolymerize rapidly
Long-distance transport	Kinesin-1 and myosin-5 cooperate in order to deliver material to the tip Kinesin-3 mediates traffic of early endosomes Microtubules support transport of RNA-binding proteins
Polarized growth	Cdk5 controls polarity, most likely by affecting Rac1
Mitosis	Dynein removes the nuclear envelope in prophase Dynein supports spindle elongation in anaphase B The nuclear pores disassemble and Nup107-complex components are recruited to the chromosomes
Predicted proteins	Numerous proteins shared between *U. maydis* and humans that are mainly without predicted function

Indeed it seems that fungi are evolutionary related to animal cells and therefore some cellular processes are conserved. *U. maydis* is even more appealing due to its genetic amenability and easy handling of the fungal cells. Over the years, *U. maydis* has become a model system for cell and molecular biology, and suitable molecular tools have been established (Steinberg and Perez-Martin, 2008) (Table 3).

Table 3: Molecular tools for *U. maydis.* *Adapted from* Steinberg and Pérez-Martin, 2008.

Tool	**Description**
Strains	
FB1, FB2, FB6a, FB6b	Haploid strains that differ in their mating loci a1, a2, b1, b2
SG200	Haploid strain, in which the a1 allele was replaced by a composite a allele containing mfa1, pra1, and mfa2; due to this genotype the strain is solopathogenic and does not need to fuse with a mating partner
AB33	Haploid strain that carries two compatible b-alleles under the control of the inducible nar1-promoter (see below); shift to inductive medium triggers filamentous growth.

AB31	Haploid strain that carries two compatible b-alleles under the control of the inducible crg1-promoter (see below); shift to inductive medium triggers filamentous growth.
FBD11	Diploid strain that is solopathogenic and is often used to check lethality of genes.
Promoters	
Ptef	Constitutively active promoter that controls transcription of the gene for the translation elongation factor
Potef	Modified *tef* promoter in which two direct repeats of the synthetic fragment containing seven tetracycline – responsive elements
mfa	Regulates the expression of pheromone gene. It has a low basal activity, is strongly induced after pheromone stimulation
Pcrg1	Carbon-regulated promoter. Repressed when cells are growing in glucose as carbon source and induced when cells are using arabinose as carbon source.
Pnar1	Nitrogen-regulated promoter. Repressed when cells are growing with ammonium as nitrogen source and induced when cells are using nitrate as nitrogen source.
Tet-system	Tetracycline-regulated system for gene expression
Sfi-integration system	Method that allows generating constructs for gene replacement without the need of cloning.
Genomic libraries	There are several genomic libraries constructed in self-replicating plasmids suitable for cloning by complementation
Self-replicating UARS plasmids	Set of plasmids that carry various antibiotic resistance and that replicate autonomously in *U. maydis*
Fluorescent proteins	Various fluorescent proteins have been used in *U. maydis*, including variants of the green fluorescent protein and monomeric red fluorescent protein and derivatives
Mating assays	Cell -cell fusion and filamentous growth can be induced by growing compatible strains on solid charcoal medium
Synthetic pheromone	Short peptide that, when applied in liquid culture, induces the dimorphic switch in compatible yeast-like cells
Bioinformatics	The MIPS *U. maydis* Genome Database provides profound information on the predicted proteins (http://mips.gsf.de/genre/proj/ustilago/). This information is based on the high quality draft genomic sequence of the Broad Institute.

Furthermore, filamentous fungi have been suggested as a model for neurological diseases. Like neuronal cells, *U. maydis* hyphal cells possesses different polarities. An antipolar region in the central area and a unipolar segment of 10-12 µm behind the tip and the septa. Both neurons and *U. maydis* present polarized growth and intracellular long-distance organelle trafficking mediated by kinesins and dyneins along the microtubule array. Moreover, short distance and tip delivery depends on actin filaments (Schuster et al., 2012). The work performed in *A. nidulans* showed the underlie mechanism in the human developmental disorder lissencephaly (Morris et al., 1998). In *U. maydis* and neurons, microtubule network is form by long arrays that assist in the directed intracellular long-distance transport along the hypha or axon. This process of long-distance transport plays a key role in brain development and it is associated with several neurodegenerative diseases (Hirokawa and Takemura, 2005; Hirokawa and Tanaka, 2015). In the three models (*U. maydis, A. nidulans*

and neurons), plus-end transport (anterograde) is mediated by kinesins and minus-end (retrograde) transport by dynein, and some minus-end kinesins (in neurons).

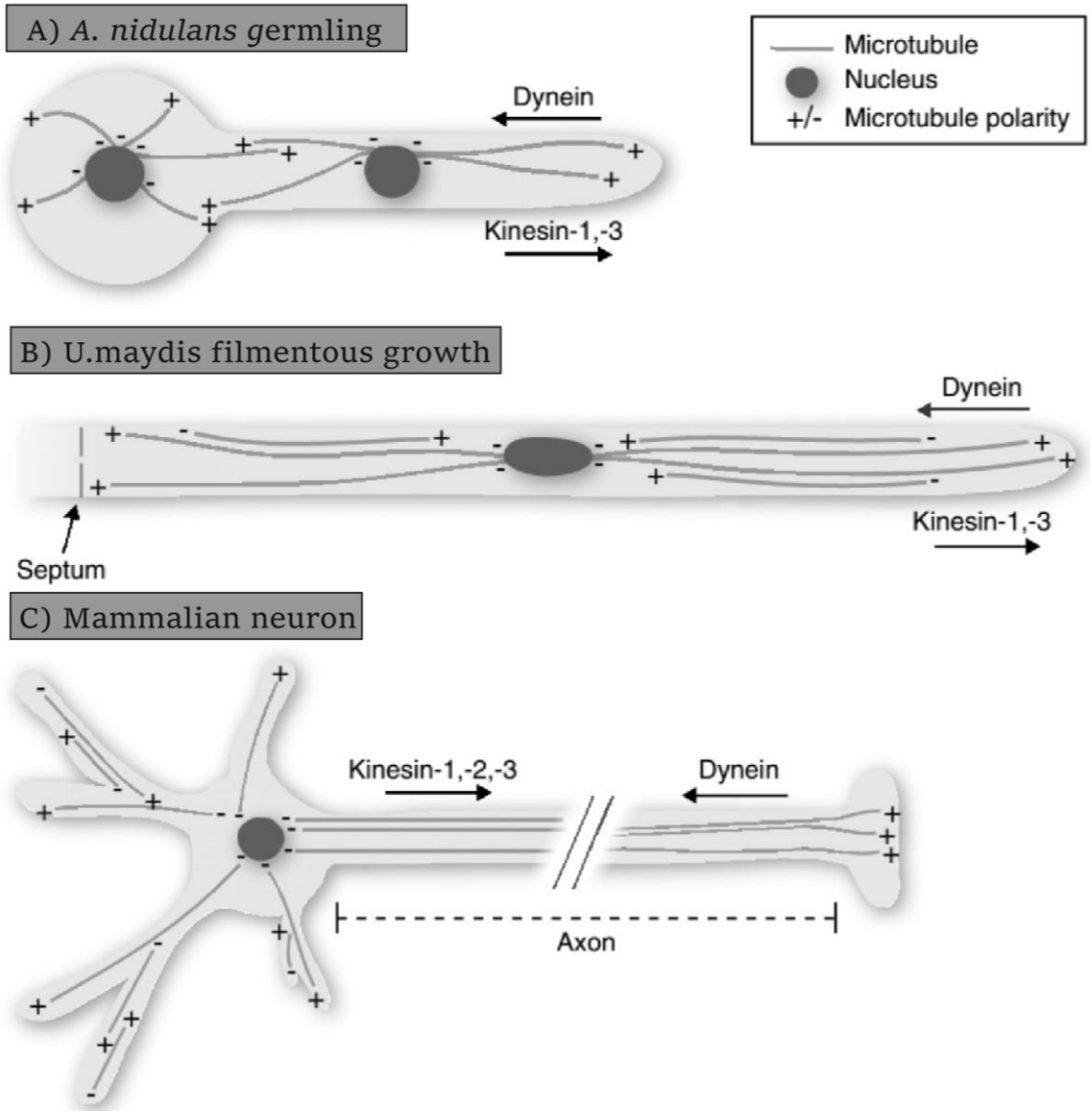

Figure 9 - Comparative microtubule organization in neurons, *U. maydis* and *A. nidulans.* A) *A. nidulans* grows by rapid polar extension forming polarized and multinucleated hyphae. The region from the closest nucleus to the tip forms oriented microtubule arrays with the plus-end directed to the polar extension and the minus-end anchored at the spindle pole body. Kinesin-1 and -3 motors regulate plus-end motility, whereas dynein mediates minus-end directed motility. Between nuclei the microtubules possess antipolar polarity. B) *U. maydis* hyphal cells represent a uninucleated filamentous structure with polar growth. Regions 10 – 12 µm behind the tip or septa are unipolar oriented with the microtubule plus end at the apical region. Kinesin-1 and -3 mediate plus-end directed motion and dynein is involved in minus-end directed motility. C) Neurons in mammals contain unipolar microtubules within the axon with the microtubule plus end located at the synaptic terminal. In the dendrites, microtubule orientation is anti-parallel. Anterograde transport is regulated by kinesin-1, -2 and -3 while retrograde motility is mainly mediated by dynein. *Adapted from* Egan et al., 2012a.

1.2.3 The importance of endocytosis in *U. maydis*

The early endosomes act as the major sorting station within the endocytic pathway, hence endosomes have emerged as crucial regulatory signaling machineries. They are responsible for cargo regulation, either recycled to the plasma membrane, retro-transported to the Golgi, or further trafficked to late endosomes for degradation (Hsu and Prekeris, 2010; Jovic et al., 2010). Rab GTPase and SNARE proteins (Huotari and Helenius, 2011; Jean and Kiger, 2012) regulate endosome trafficking and fusion. Rab proteins are fundamental for fusion events but also for the functional organization of endosomal compartments (Zerial and McBride, 2001; Stenmark, 2009; Huotari and Helenius, 2011; Jean and Kiger, 2012). Motility of early endosomes over long-distance has been described in animals (Nielsen et al., 1999) and filamentous fungi (Wedlich-Soldner et al., 2000; Steinberg, 2014). In *U. maydis*, early endosomes long-distance motion supports polar growth and retrograde signalling triggers effector expression which suppresses plant immunity during cell invasion (Bielska et al., 2014a).

U. maydis has 10 described kinesins, although only kinesin-1 (conventional kinesin) and kinesin-3 (KIF1A/Unc-104 homologue) mediate cargo transport. These kinesins were shown to be up-regulated in hyphal cells and are fundamental for extended hyphal growth (Schuchardt et al., 2005; Lenz et al., 2006). Retrograde transport in *U. maydis* is mediated by dynein. Dynein is responsible for nuclear migration (Fuchs et al., 2005) and the transport of diverse organelles (e.g. vacuoles, endosomes, the ER) (Wedlich-Soldner et al., 2002a; Wedlich-Soldner et al., 2002b). Moreover, dynein is essential for fungal survival and growth. Rapid bidirectional movement of early endosomes is mediated by kinesin-3 and dynein (Wedlich-Soldner et al., 2002a; Lenz et al., 2006; Egan et al., 2012b), which frequently turn direction, thereby distributing the moving organelles throughout the hyphal cell (Schuster et al., 2011c). Hook1, described in *U. maydis* and mammals, is an adaptor protein for early endosome attachment to the molecular motors. It is suggested to be required for cargo recycling for early endosomes (Maldonado-Baez et al., 2013; Bielska et al., 2014b). In Alzheimer's disease, the endocytic pathway is disturbed. Recently, it was shown that Hook is reduced in the brains of Alzheimer' patients, and depletion of Hook3 enhances β-amyloid production (Herrmann et al., 2015). Early endosomes have been suggested to function as multipurpose platforms (Gould and Lippincott-Schwartz, 2009). In fact, in filamentous fungi

different roles are arising. It was shown that polysomes hitchhike on early endosomes for distribution of the translation machinery (Higuchi et al., 2014). Moreover, it was suggested that septin translation occurs on early endosomes and hence septin formation might occur on early endosomes (Baumann et al., 2014). Altogether, these recent findings emphasize the importance of early endosomes in filamentous fungi.

2. OBJECTIVES

Peroxisomes are essential, multifunctional organelles, and highly dynamic. One of the common features of peroxisomes is their role in fatty acid degradation. The importance of peroxisomes for cellular lipid metabolism is reflected by genetic defects that affect peroxisomal β-oxidation resulting in severe metabolic diseases (Waterham et al., 2016) (Wanders 2016). In yeast, fatty acid β-oxidation is thought to occur solely in peroxisomes. In contrast, in animals this process is shared with mitochondria. The model organism *S. cerevisiae*, is of great use for the study of peroxisome biology, but it displays some fundamental differences when compared to mammals. The latter show cooperation of peroxisomes and mitochondria in fatty acid β-oxidation and microtubule-based organelle transport. In mammalian cells, peroxisomes move along microtubules, whereas in yeast cells peroxisome motility and inheritance is actin-dependent. In mammals, the knowledge on microtubule-based motility and positioning of peroxisomes is still incomplete. In peroxisome-related diseases, phenotypical alterations of peroxisome motility and distribution suggest the importance of these processes for human health.

Over the past decade, the filamentous fungus *U. maydis* has been introduced as a model system for studying fundamental cell biological processes. *U. maydis* shares many important features (microtubule organization, long-distance microtubule transport, involvement of kinesins, polarized growth, and open mitosis) with human cells and provides the technical advantages of yeast cells (genetic accessibility, short generation time, simple cultivation methods, sophisticated molecular tools). Therefore, we have exploited *U. maydis* to reveal the potentials of this model for studying peroxisome biology and dynamics. The specific aims were as follows:

1. Perform a bioinformatics analysis to decipher the peroxisomal "proteome" in *U. maydis*. Moreover, combine fungal genetics and molecular cell biology to characterise fatty acid β-oxidation in *U. maydis* (Chapter 4);
2. Use *U. maydis* as a model to elucidate the microtubule-dependent transport mechanisms of peroxisomes and other organelles (Chapter 5).
3. Use *U. maydis* as a model to understand the fundamental mechanisms determining peroxisomal distribution (Chapter 6).

3. GENERAL METHODS

Standard molecular biology methods and protocols from Sambrook (2001) were followed. Methods described here were routinely used and most of the *U. maydis* strains presented in this thesis were obtained in three major steps, overview in Figure 10:

1. Plasmid generation using yeast-*E.coli* shuttle vector by *in vivo* recombination in *S. cerevisiae (Raymond et al., 1999)*
2. *E. coli* transformation and plasmid DNA extraction followed by restriction enzyme digestion
3. *U. maydis* transformation (Schulz et al., 1990) and selection of appropriate transformants by antibiotic resistance.

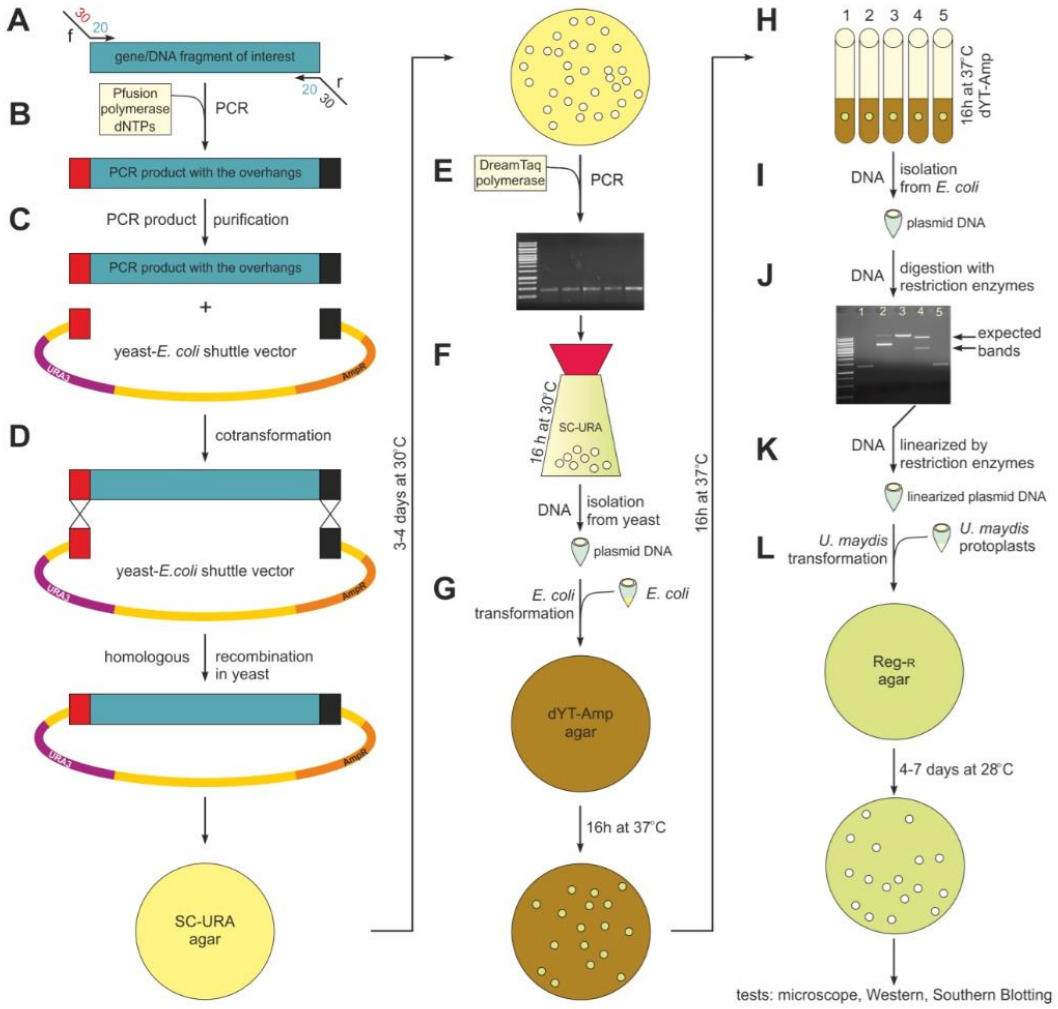

Figure 10 - Schematic overview of the procedures to obtain *U. maydis* strains. Abbreviations: URA3, yeast selectable marker; AmpR *E. coli* ampicillin resistance; Reg-R, *U. maydis* regeneration agar with selectable antibiotic.

In addition to the described methods below, each chapter contains a section with methods used specifically in that part of the study.

3.1 Media and buffers

All buffers and media used in this study are described below in alphabetical order (Table 4).

Table 4: Description of buffers and media used in this study.

Buffers/Media	Final Concentration
Alkaline lysis solution	1% (w/v) SDS, 0.2 M NaOH
CM (complete) medium, pH 7.0	0.25% (w/v) casamino acids, 0.1% (w/v) yeast extract, 1% (v/v) vitamin solution (Holliday, 1974), 6.25% (v/v) salt solution (Holliday, 1974), 0.05% (w/v) DNA from herring sperm, 0.15% (w/v) NH_4NO_3
DNA wash buffer	50 mM NaCl, 10 mM Tris-HCl pH 7.5, 2.5 mM EDTA, 50% (v/v) ethanol
dYT-glycerol	1.6% (w/v) tryptone, 1% (w/v) yeast extract, 0.5% (w/v) NaCl, 69.6% (v/v) glycerol
dYT medium	1.6% (w/v) tryptone, 1% (w/v) yeast extract, 0.5% (w/v) NaCl
Neutralization solution	0.9 M sodium acetate pH 4.8, 0.5 M NaCl
NM (nitrate minimal) medium, pH 7.0	0.3% (w/v) KNO_3, 6.25% 8v/v) salt solution (Holliday, 1974)
NSY-glycerol	0.8% (w/v) nutrient broth, 0.1% (w/v) yeast extract, 0.5% (w/v) sucrose, 69.6% (v/v) glycerol
PBS buffer	137 mM NaCl, 2.7 mM KCl, 4.3 mM $Na_2HPO_4*7H_2O$, 1.4 mM KH_2PO_4
Reg (regeneration) Agar	1% (w/v) yeast extract, 2% (w/v) peptone, 2% (w/v) sucrose, 18.22% (w/v) sorbitol, 1.5% (w/v) agar
Salt Solution (Holliday, 1974)	16% (w/v) KH_2PO_4, 4% (w/v) Na_2SO_4, 8% (w/v) KCl, 4.08% (w/v) $MgSO_4*7H_2O$, 1.32% (w/v) $CaCl_22H_2O$, 8% (v/v) Trace elements
SCS buffer	20 mM $Na_3C_6H_5O_7$ pH 5.8, 1M sorbitol
Sc-Ura medium	0.17% (w/v) yeast nitrogen base without amino acids, 0.5% (w/v) $(NH_4)_2SO_4$, 0.5% (w/v) casein hydrolysate, 0.002% (w/v) adenine, 2% (w/v) glucose
STC buffer	10 mM Tris-HCl pH 7.5, 100 mM $CaCl_2$, 1 M sorbitol
TE buffer pH 8.0	10 mM Tris, 1 mM EDTA
Trace elements (Holliday, 1974)	0.06% (w/v) H_3BO_3, 0.14% (w/v) $MnCl*4H_2O$, 0.4% (w/v) $ZnCl_2$, 0.4% (w/v) $Na_2MoO_4*2H_2O$, 0.1% (w/v) $FeCl_3*6H_2O$, 0.04% (w/v) $CuSO_4*5H_2O$
U. maydis lysis buffer	5.85% (w/v) NaCl; 10% (v/v) 1M tris-HCl (pH8.0); 20% (w/v) triton X; 50% (v/v) 20% SDS; 2% (v/v) 0.5 M EDTA
Vitamin solution (Holliday, 1974)	0.1% (w/v) thiamine HCl, 0.05% (w/v) riboflavin, 0.05% (w/v) pyridoxine HCl, 0.2% (w/v) D-pantothenic acid hemicalcium salt, 0.05% (w/v) 4-aminobenzoic acid, 0.2% (w/v) nicotinic acid, 0.2% (w/v) choline chloride, 1% (w/v) myo-inositol
Yeast lysis buffer	2% (v/v) Triton X-100, 1% (w/v) SDS, 100 mM NaCl, 1 mM EDTA, 10 mM Tris
YEPS medium	1% (w/v) yeast extract, 0.4% (w/v) peptone, 0.4% (w/v) sucrose
YPD medium	1% (w/v) yeast extract, 2% (w/v) peptone, 2% (w/v) sucrose

NOTE: Agar plates were obtained by adding agar at 2% (final concentration in CM or Sc-Ura) or 1.3% (final concentration in dYT).

3.2 General methods

3.2.1 Plasmid generation - Yeast Recombinational Cloning

Molecular cloning is a recurring technique for plasmids generation. Commonly it comprises the amplification of a region of interest by polymerase chain reaction (PCR), followed by digestion of the target vector, ligation and *E. coli* transformation. Nevertheless, in this study we have mostly used yeast recombination cloning (YRC). YRC is a simple, cheap, and highly efficient technique. This method (Ma et al., 1987) allows the use of homologous recombination in yeast to generate DNA fragments from overlapping independent parts. Briefly, segments are generated with homology to integrate into the linearized backbone vector. Primers were designed with 20-40 bp homology of the C- and N- terminus of the gene of interest plus 30 bp overhang within the yeast - *E. coli* shuttle vector (Figure .11)

The Yeast *E. coli* shuttle vector contains the yeast *URA3* selectable marker which encodes orotidine-5'-phosphate decarboxylase, an enzyme required for *de novo* synthesis of pyrimidine ribonucleotides such as uracil. The vector also contains: 2μ *ori* (origin of replication) amplified from plasmid pEYA2 (Invitrogen, Paisley, UK); the ampicillin resistance cassette (amp^R); *E. coli* origin of replication (oriC), and *U. maydis* resistance cassette of interest [carboxin (cbx^R), hygromycin (hyg^R) or nourseothricin (nat^R)].

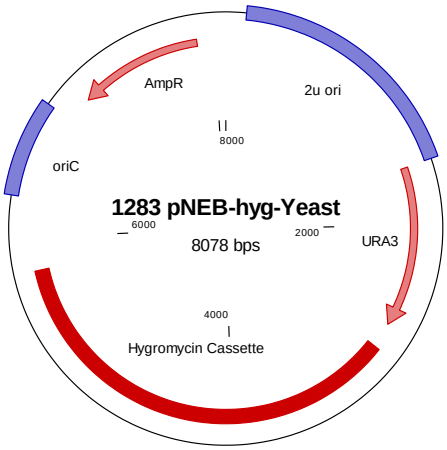

Figure 11 - Yeast E. coli shuttle vector pNEBhyg. Plasmid containing three selectable markers for: yeast (*URA3*), *E. coli* (*Amp*^{R}) and *U. maydis* (*hyg*^{R}). Graphic was generated in Clone Manager 9 Professional Edition (Scientific & Educational Software).

3.2.2 Plasmid Generation

3.2.2.1 PCR

To obtain plasmids by *in vivo* recombination in *S. cerevisiae* (Raymond et al., 1999), DNA fragments were amplified by Phusion® High-Fidelity DNA Polymerase (New England Biolabs #M0530L) in a PCR reaction (using 34 cycles). Fragments with 30 bp homology overhangs to the appropriate regions within the yeast - *E. coli* shuttle vector were generated. The components of the PCR reaction mix and PCR steps are shown below (fw- forward; rv- reverse; Tm-annealing temperature).

Template DNA	1 µl
10 µM fw primer	2 µl
10 µM rv primer	2 µl
5x Phusion HF buffer	10 µl
10 mM dNTPs	4 µl
dH_2O	30.5 µl
Phusion polymerase	0.5 µl
V_T	50 µl

Temp (ºC)	**Time**	
98ºC	30 s	
98ºC	10 s	34 Cycles
Tm-4ºC	20 s	
72ºC	30 s/ 1 kb	
72ºC	10 min	
10ºC	∞	

3.2.2.2 Purification of PCR products

DNA fragments obtained from PCR were purified as follow (Boyle and Lew, 1995). Briefly, PCR products were ran on an agarose gel and the corresponding fragment size was cut out and incubated with approximately 900 µl of 6 M sodium iodide at 55ºC, to allow the agarose to dissolve. To the solution 40 µl of 10% silica glass beads (Sigma #S-5631; in 3 M sodium iodide) were added and incubated at 55ºC for 5 min to allow the binding of the DNA to the beads. The mixture was then centrifuged for 1 min at 13300 rpm. Then, 500 µl of DNA wash buffer were added, incubated for 5 min at RT and centrifuged at maximum speed for 15 s. The washing step was repeated 3 times. After the last wash the supernatant was thoroughly and carefully discarded and 10-20 µl of distilled water (dH_2O) were added and incubated at 55ºC for 5-8 min for a proper DNA elution. The supernatant was collected after spinning down and later used as purified fragment for homologous recombination in yeast.

3.2.2.3 *S. cerevisiae* transformation

Yeast *S. cerevisiae* strain DS94 (MATα, ura3-52, trp1-1, his3-111, and lys2-801, Raymond *et al,* 1999) were grown overnight in 3 ml culture of YPD medium at 28ºC, 200 rpm. The next day, 2 ml of the latter were added to a 50 ml culture of YPD and let shaking (200 rpm) for around 5 hours at 28ºC. Cells were then harvested by spinning down at 2200 rpm for 5 min at room temperature. The supernatant was discarded and the pellet washed in 10 ml of sterile distilled water and spun down at 2200 rpm for 5 min. The supernatant was carefully removed and the resulting pellet resuspended in 300 µl of dH_2O. 50 µl of yeast cells were combined with: 50 µl of denatured solution of salmon sperm DNA (2 µg/µl, w/v in dH_2O; Sigma, Cat No: D1626); 2 µl (around 1 µg/µl) of linearized shuttle vector; and 2-4 µl of purified PCR fragments. To the transformation mixture 32 µl of 1 M lithium acetate (in dH_2O) and 240 µl 50% PEG 4000 (w/v in dH_2O) were added homogenized by pipetting repetitively. After, the mixture was incubated at 28ºC for 30 min ollowed by 15 min heat shock (45ºC). Cells were then spun down at 2200 rpm for 2 min and resuspended in 200 µl of dH_2O and then spread onto Sc-Ura plates and incubated at 28ºC for 2-4 days.

3.2.2.4 *S. cerevisiae* colony PCR screening

To screen for positive transformants, individual colonies were picked with a tip and (part) spread onto a Sc-Ura plates, and the remaining was submerge into the PCR reaction. PCR reaction comprised DreamTaq Green PCR Master mix polymerase (Fermentas #K1081) and the appropriate primers. The primers would bind within the gene of interest and the shuttle vector. The PCR conditions were the follow:

Yeast Colony	--
10 µM f primer	1 µl
10 µM r primer	1 µl
dH_2O	8 µl
2xDream Taq Green PCR Master Mix	10 µl
V_T	20 µl

Temp (ºC)	Time	
95ºC	5 min	
95ºC	30 s	34 Cycles
Tm-4ºC	20 s	
72ºC	1min / 1 kb	
72ºC	10 min	
10ºC	∞	

3.2.2.5 Plasmid DNA isolation from *S. cerevisiae*

Positive colonies from colony PCR, were grown overnight in 15 ml of Sc-Ura medium at 30ºC, 200 rpm. The following day, the cells were harvested by spinning down at 1500 rpm for 5 min and the pellet resuspended in 0.5 ml of sterile distilled water. Cells were transferred into 1.5 ml Eppendorf tube and spun down for 5 s at 13300 rpm. After discarding the supernatant, the cell pellet was vortexed in the residual water. 200 µl of yeast lysis buffer and 200 µl of phenol:chloroform:isoamyalcohol (25:24:1) was added together with 0.3g of glass beads (size 425-600 µm), for cell disruption. The suspension put into IKA Vibrax VXR (IKA-Werke, Staurfem Germany) for 10 min on vibration. After, 200 µl of TE buffer (pH 8.0) were added and cell debris and organelles were removed by centrifugation for 5 min at 13300 rpm. The aqueous phase was then transferred to a new tube and separated from the lower organic phase containing proteins, polysaccharides and lipids. To the aqueous phase, containing nucleic acids, $1/10^{th}$ volume of 3M sodium acetate (pH 5.5) and 1 ml of 96% ethanol were added and the obtained mixture was incubated at -20ºC for 15 min. The mixture was spun down at 13.300 rpm for 20 min. The supernatant was discarded and the pellet was resuspended in 400 µl of TE buffer (pH 8.0) and 4 µl of RNase A (10mg/ml). The incubation at 37ºC allowed the pellet to dissolve. 10µl of 4 M ammonium acetate and 1 ml of 96% ethanol were added to the solution and spun down for 2 min at 13300 rpm. After discarding the supernatant, the pellet was washed twice with 500µl of 70% ethanol. Finally, the air dried pellet was resuspended in 20 µl of dH_2O.

3.2.2.6 *E. coli* transformation

E. coli strain DH5α (Hanahan, 1985) was routinely used for cloning purposes. Briefly 4-6 µl of isolated yeast DNA was added to 50 µl aliquot of chemically competent *E. coli* cells and kept on ice for 10 min. Heat shock was performed at 42ºC for 45-60 s followed by 10 min on ice. After which, 900 µl of dYT were added and incubated for 1 h at 37ºC, 200 rpm. Cells were plated onto dYT agar plates containing 100 µg/ml ampicillin and were grown ON at 37ºC.

3.2.2.7 Plasmid DNA isolation from *E. coli* by alkaline lysis

Single bacterial colony was transferred into 3 ml of dYT/ampicillin (100µg/ml) media and grown overnight, 220 rpm. The culture was transferred into a microtube and centrifuged at 13300 rpm for 1 min and the supernatant discarded. The cell pellet was resuspended in 150 µl of TE (pH 8.0) with 5 µl of RNase A (10 mg/ml) by vigorous vortexing. Then, 150 µl of lysis solution was added to the solution that was mixed by inverting 5-10 times. 500 µl of neutralization solution were added and the microtube was inverted several times for proper mixing. The solution was left on ice for 5 min, and subsequently centrifuged at 14,000 rpm for 12 min at 0ºC. The supernatant was transferred to a clean microtube. DNA precipitation was done as follow, 2 volumes of ice-cold 100% ethanol were added, vortexed and left at -20ºC for 30 min. Then, a centrifugation at 14,000 rpm for 20 min at 0ºC was performed. The supernatant was thoroughly removed and the pellet washed with 70% ethanol. A centrifugation at 14,000 rpm for 7 min at 0ºC was performed and the supernatant completely discarded. The pellet was allowed to air-dry and resuspended in 50-100 µl of distilled water.

3.2.2.8 Plasmid DNA digestion

To search for positive clones, appropriate digestion with restriction endonuclease were performed. The enzyme was chosen considering the digestions of interest for both vector and insert.

For typical DNA digestion, the components were added at the following concentrations:

100 µg/ml DNA
1X reaction Buffer
1U/µg DNA of restriction enzyme

Digestions were usually performed at 37ºC for 2 hours unless otherwise determined by the restriction enzyme chosen. The digestion was run in an agarose gel. Positive clones were linearized using adequate restriction enzyme, or a combination of enzymes, purified and used for *U. maydis* transformation. Correct *E.coli* strain holding plasmid DNA was stored at -80ºC in dYT -25% glycerol.

3.2.3 *U. maydis* transformation

The transformation procedure follows the protocol described by Schulz et al, 1990. Briefly, 50 µl of *U. maydis* protoplasts (see 3.2.2.1 - Protoplast generation) were incubated for 30 min on ice with 4 µl of linearized plasmid DNA (1-5 µg) in the presence of 1 µl of heparin (1 mg/ml). After, 500 µl of PEG (40% w/v in STC, filter sterilised) was added on top of the protoplast and carefully mixed by pipetting up and down, and left on ice for another 15 min. After which the transformation mixture was spread onto 2 (one with 80% and the other with 20% of the transformation mixture) Reg-agar (regeneration agar) plates containing two layers: bottom layer contained selective antibiotic and top layer no antibiotic was added. Plates were usually incubated for 4-7 days at 28ºC. Transformants were singularised and grown on CM-agar plates containing the appropriate antibiotic. After confirmed by microscopy and/or southern blotting, strains were stocked at -80ºC in NSY-glycerol at 1:1 ration.

3.2.3.1 Protoplasts generation

The protoplast generation protocol was described by Schulz et al 1990. In brief, *U. maydis* strain of interest was grown overnight in 50 ml YEPS culture at 28ºC, 200 rpm. When OD600nm was at 0.4-0.8 range, the culture was spun down for 10 min at 3000 rpm. The resulting cell pellet was resuspended in 25 ml SCS and centrifuged again for 10 min at 3000 rpm. For cell wall digestion, the pellet was resuspended in 2 ml SCS containing 7 mg/ml of lysing enzymes from Trichoderma harzianum (containing β-glucanase, cellulase, protease and chitinase activities; Sigma #1412) and left at room temperature for 10-15 min. When 30-40% of the cells became rounded (protoplast formation was monitored under the microscope), 10 ml of cold SCS were added, followed by centrifugation at 2200 rpm for 7 min at 4ºC after which the supernatant was removed, this step was repeated twice. Finally, the pellet was resuspended in 10 ml of cold STC and centrifuged at 2100 rpm for 12 min. The obtained pellet was resuspended in 500 µl of cold STC and stored in 50 µl aliquots that were immediately used for transformation or stored at -80ºC

4. EXPLOITING THE FILAMENTOUS FUNGUS *U. MAYDIS* AS A NEW MODEL FOR PEROXISOME RESEARCH: COOPERATIVE PEROXISOME-MITOCHONDRIA β-OXIDATION

4.1 Introduction

Over the past years, new roles for peroxisomes have emerge: cellular signalling and innate immune response (see chapter 1.1.5.2). In this respect the close inter-relationship between mitochondria and peroxisomes became more evident. The two organelles cooperate in β-oxidation in animals, whereas in plants and yeast is thought to be exclusively peroxisomal. As highlighted in chapter 1.1.2, both organelles possess their set of enzymes to catalyse the similar reaction of the degradation pathway. Once inside the peroxisomal lumen, oxidation of acyl-CoA is initiated by ACOX transferring electrons in the form of H^- from their prothetic group, $FADH_2$ to O_2, thus generating H_2O_2. Contrarily, in mitochondria, ACADs transfer electrons to FAD, generating $FADH_2$ which will be then used for ATP production within the respiratory chain. Peroxisomes and mitochondria β-oxidation also diverge in their substrates. Peroxisomes preferably oxidise saturated- and unsaturated- very long-, and long fatty acids, whereas mitochondria oxidises long-, medium- and short-chain fatty acids. In peroxisomes, fatty acids are shortened to eight carbons and subsequently conjugated to carnitine and routed to the mitochondria for final oxidation. This close interconnection between peroxisomes and mitochondria for adequate fatty acid degradation requires a coordinated regulation of lipid metabolism in both organelles and transfer of metabolites among them, process which is still poorly understood.

Peroxisome and mitochondria cooperation goes beyond fatty acids breakdown purposes. In fact, both organelles contribute to cellular ROS homeostasis and redox-sensitive relationship (see 1.1.2). Moreover, they also share the key components of their division machinery, which might imply the existence of a coordinated biogenesis, under certain conditions. Strikingly, peroxisomes and mitochondria cooperate in anti-viral signalling and defence. Furthermore, vesicular trafficking between the two compartments has been described (see 1.1.5.2).

Overall, this interplay might be of medical relevance, since it has been suggested that alteration in peroxisome metabolism, biogenesis and/or dynamics potentially influences mitochondria functions, and *vice versa* (Camoes et al., 2009; Schrader et al., 2015a). Therefore, such close relationship might improve our understanding in inter-organelle cooperation and interplay, and hence their relevance on cell physiology and disease (Thoms et al., 2009).

S. cerevisiae has been a valuable model to understand different aspects of cellular and disease-related processes in mammals. However, studies on organelle cooperation, shared β-oxidation and microtubule-based motility are not conceivable in the budding yeast. The use of basidiomycete *U. maydis* as a novel model for the study of such processes has been proposed (Steinberg and Perez-Martin, 2008). This fungal system possesses the technical advantages of yeast but shares mechanisms with humans (e.g. long distance transport, polarizes growth). Genome-wide analysis predicted that *U. maydis* shares a higher number of proteins with *H. sapiens* than with *S. cerevisiae* (Munsterkotter and Steinberg, 2007). We have combined molecular and cell biology, bioinformatics, and phylogenetic analyses for a comprehensive inventory of *U. maydis* peroxisomal proteome and pathways (Camoes et al., 2015). A genomic comparison with other fungi, such as *S. cerevisiae*, and *H. sapiens* revealed that *U. maydis* possesses a complex and complete enzymatic inventory for peroxisomal and mitochondrial β-oxidation, rendering *U. maydis* as a suitable model for the study of metabolic cooperation between the two organelles. Here, I will mainly focus on the studies to characterize fatty acid β- and α-oxidation in *U. maydis*

4.2 Materials and methods

4.2.1 Plasmids and strains

U. maydis strains and plasmids used in this study are described in Table 5. More detailed information described below.

Table 5: List of strain and plasmids used in this study.

Strain/ Plasmid	Genotype	Reference
Sg200	*a*1 *mfa2 b*W2 *b*E, *ble*^{R}	(Bolker et al., 1995)
Sg200Δpex3	*a1 mfa2 bW2 b*E, *ble*^{R} *Δpex3, hyg*^{R}	This study
Sg200Δpex3_GFP-SKL	*a1 mfa2 bW2 b*E, *ble*^{R} *pΔpex3, hyg*^{R} / po^{C} GSKL	This study
AB33Δpex3_pex3crg	*a2 PnarbW2 PnarbE1, bleR Δpex3, hyg*^{R} / pex3crg	This study
FB2_GFP-SKL	*a2b2/* po^{C}GFP-SKL	This study
AB33_GFP-SKL_mCherry-Catalase	*a2 PnarbW2 PnarbE1, bleR /* po^{C}GSKL / pomCh-Catalase	This study
po^{C}GSKL	P*otef-egfp-skl, cbx*^{R}	(Steinberg and Schuster, 2011)
mChCatalase	P*otef-mCherry-Catalase, hyg*^{R}	This study
pex3crg	P*crg-pex3-egfp, cbx*^{R}	This study

a, *b*: mating type loci; P: promoter; -: fusion; Δ: deletion; *hyg*^{R}: hygromycin resistance; *ble*^{R}: phleomycin resistance; *nat*^{R}: nourseothricin resistance; *cbx*^{R}: carboxin resistance; *G418*^{R}: geneticin resistance; *otef*: constitutive promoter; /: ectopically integrated; *E1, W2*: genes of the *b* mating type loci; *egfp*: enhanced green fluorescent protein; *mcherry*: monomeric cherry; SKL, peroxisomal targeting sequence

Plasmid po^{H}mCherry-Catalase (carboxin)

po^{H}mChCatalase. To visualise catalase in *U. maydis*, the gene um11067 was amplified from gDNA of 521 strain, *U. maydis* annotated strain, by using primers sg53 and sg54. These primers contain 20 bp of homologous sequence at the N-term and C-term of the gene of interest. The 2250 bp of the catalase gene were amplified, with the 30bp overhangs to the backbone vector, by PCR. After it was inserted into cloning vector pNEBhyg-yeast (Schuster et al., 2011b) which contains: 878 bp *Otef* promoter; 711 bp *mCherry;* and 307 bp of *Tnos*, through yeast recombination cloning, resulting in po^{H}mCherry-Catalase. The plasmid was

subsequently inserted ectopically into *U. maydis* (AB33GFP-SKL, Steinberg and Schuster, 2011) by digestion with *Ssp*I, resulting in AB33GFP-SKL_mCherry-Catalase strain. Correct insertion was confirmed by microscopy and PCR.

Plasmid Δpex3

For deletion of *Pex3* in *U. maydis*, plasmid p*Δpex3* was generated through *in vivo* recombination. The 1847 bp *pex3* (um06200) gene was amplified, through PCR, with 20 bp overhangs of upstream and downstream the gene. Was then recombined with the cloning vector pNEBhyg-yeast (Schuster et al., 2011a) carrying 1030 bp *NudE* promoter and 1158 bp *pex3* terminator resulting in p*Δpex3.* The plasmid p*Δpex3* was digested with *Dra*I and integrated homologously into the *pex3* locus of the strain Sg200 or AB33, resulting in Sg200Δpex3 or AB33Δpex3.Correct insertion was confirmed by southern blot. To the strain AB33Δpex3, crg-pex3-GFP plasmid (unpublished) was ectopically integrated after digestion with *Kpn*I. The strains was grown on CM (complete medium)-glucose overnight and shifted to arabinose in the following day. After confirmation of peroxisomal-like fluorescence structures we integrate mCherry-SKL, G418 (see more details in 5.2.1).

Table 6: Primers used in this study.

Primer	**Sequence 5' -> 3'**
sg9	AACTGTTGGGAAGGGCGATCGGTGCGGGCC TTTGCGCGGCCGAGCATGTC
sg10	GCTTGGCACTGGCCGTCGTTTTACAACGTCAGTTGTGACAAGGGGCCAAGA
sg11	TACGAACGCTTTCGACTCAGCCGTCAATCCAGTAGGGTCCAACGTCTACGT
sg12	TGTTGTGTGGAATTGTGAGCGGATAACAAAGAATCCGCTCTCAGGATACG
sg53	TCCACCGGCGGCATGGACGAGCTGTACAAGATGGGAGAGTGTCCATTTGC
sg54	CATTAAAGTCGTCCAAATCAAGCGCCCTCCTTAGAACCTGGCACGGGCAA

4.2.2 Southern Blot

First, we isolated genomic DNA from the *U. maydis* strain (Sg200 or AB33; and Sg200_Δpex3 or AB33_Δpex3). The method used was adapted from Hoffman and Winston, (1987). 2 ml of *U. maydis* strains were grown overnight in YEPS, and centrifuged at 13000 rpm for 1 min. The supernatant was discarded, and 0.3 g glass beads were added to the pellet, together with 400 µl of lysis buffer and 500 µl phenol-chloroform. The samples were incubated for 10 min on a Vibrax-VXR shaker (IKA; Sigma Aldrich, Dorset, UK). After, were centrifuge for 15 min at 13000 rpm, from which the aqueous phase was transferred to

a new tube with. 1 ml of ethanol, and centrifuged for 5 min at 13000 rpm. After which the pellet was resuspended in 50 µl TE/RNAseA and incubated at 55 °C. DNA was either immediately used or stored at –20 °C .

For southern blotting, we digested the genomic DNA of wild type and deletion strains with *Ecor*RI and *Xho*I. Endonucleases were chosen so they would cut in the insert and not in the wild type locus. Probes were generated using DIG probe labelling mix (Roche, West Sussex, UK) as per the manufacturer's instruction. The following parameters were used as a guide for probe amplification; initial denaturation at 98 °C for 45 s, followed by 30 cycles of 98 °C for 10 s, 60 °C for 10 s, and 72 °C for 60 s, and then a final extension at 72 °C for 60 s. The probe was then purified by gel extraction and precipitation (see 3.2.2.2.). Following isolation and digestion of genomic DNA, DNA fragments were separated on an agarose gel. The gel was depurinated in 0.25 M hydrogen chloride for 15 mins and subsequently neutralised in 0.4 M sodium hydroxide. DNA was transfer from the agarose gel to the membrane, for at least 4 h, through capillarity. Then, the membrane was UV cross-linked to ensure covalent bound of the DNA to the membrane. The membrane was incubated with hybridization buffer and probe at 68 °C overnight. The following day, the membrane was washed, blocked and then detected using streptavidin-IRDye 800CW conjugate (LiCOR; GE Healthcare)

4.2.3 Laser-based epifluorescence microscopy

Microscopy of *U. maydis* was performed as previously described (Schuster et al., 2011a). Briefly, cells were placed on a thin layer of 2% agarose, covered with a cover slip, and immediately observed using a IX81 motorized inverted microscope (Olympus, Hamburg, Germany) and a VS-LMS4 Laser-Merge-System equipped with 488 and 561 nm, 75mW solid-state lasers using Dual-View Microimager (Optical Insights, Tucson, USA) and appropriate filters. GFP-SKL was visualized at 150ms exposure time at 4% of the 488 nm laser and mCherry-Catalase or mCherry-SKL were visualises at 15%-50% of the 561 nm lases. Images were captured using a charge-coupled device camera (Photometric CoolSNAP HQ2, Roper Scientific, Germany). All parts of the system were under the control of the software package MetaMorph (Molecular Devices, Downingtown), which was also used for image processing and overlay.

4.2.4 Scanning electron microscopy.

For scanning electron microscopy, either Sg200_GFP-SKL or Sg200_Δpex3 0.22 micron polycarbonate membrane, and air dried for 2 min. Then, the samples were attached to a cryosledge and rapidly frozen in liquid nitrogen, followed by water sublimation at −95°C for 3 min using the Alto 2100 chamber (Gatan Ltd., Oxfordshire, UK). This was followed by gold sputtering and observation in Jeol JSM-6390LV scanning electron microscope (JEOL, Ltd., Welwyn Garden City, UK).

4.2.5 Induction of peroxisome proliferation with oleic acid

FB2_GFPSKL cells were grown overnight in complete medium (CM) (Holliday, 1974) containing 1% (w/v) glucose at 28°C and 200 rpm, until an OD_{600} of 0.8. Cells were centrifuged at 3000 rpm for 10 min and washed twice with nitrogen minimal medium (NM) to remove all carbon sources. The pellet was resuspended in NM medium and equal volumes were transferred into flasks with NM medium containing 1% (w/v) glucose (control) or 0.2% (v/v) oleic acid (Merck) (final concentration) and incubated for 1hr at 28ºC and 200 rpm. Peroxisome numbers were determined by laser-based epifluorescence microscopy. Z-stacks were taken at 300 nm step size with 150 ms exposure time using a Piezo drive (Piezosystem Jena GmbH, Jena, Germany) and analysed as maximum projection using MetaMorph.

4.2.6 Growth assays on fatty acids

To examine growth on different fatty acids, wild type cells (Sg200) and those lacking peroxisomes (Sg200Δpex3) were grown overnight in CM containing 1% glucose at 28ºC and 200 rpm until an OD of 0.6-0.8. Cells were washed 3 times and resuspended in 5 ml of sterile NM. A 5% dilution was plated on NM-Agar plates supplemented with different fatty acids, acetate or glucose. The following fatty acids (from Sigma-Aldrich, St. Louis, MO if not stated otherwise) were used in a concentration range between 0.1 – 0.001%: butyric acid (4:0), valeric acid (5:0), hexanoic acid (6:0), decanoic acid (10:0), myristic acid (14:0), myristoleic acid (14:1(n-5)), palmitic acid (16:0), palmitoleic acid (16:1(n-7)), oleic acid (18:1(n-9)) (Merck, Darmstadt, Germany), pristanic acid (2,6,10,14-tetramethyl 15:0), phytanic acid (3,7,11,15-tetramethyl 16:0), erucic acid (22:1(n-9)) and lignoceric acid (24:0). Fatty acids were dissolved in ethanol. Glucose and acetate were used at 1%. Plates

were incubated for 2-3 days at 28ºC and images acquired using stereomicroscope Nikon SM2 800, camera control pro 2.7.1 (Nikon®).

4.3 Results

4.3.1. *U. maydis* encodes a complex set of peroxisomal and mitochondrial fatty acid β-oxidation proteins

For a comprehensive characterisation of peroxisomes in *U. maydis* we screened the *U. maydis* (strain 521) (work performed in collaboration with Dr Fátima Camões and Dr Markus Islinger, University of Aveiro, Portugal) fully sequence genome database for proteins with a PTS1 or a PTS2. As we observed non-canonical C-terminal PTS1 sequences (e.g. ACADs), we initially searched with the broader consensus sequence, (ASCNPHTG)–(RKHQNS)–(LMIVF) (Neuberger et al., 2003). All candidate proteins were analysed and validated for PTS1 by using PTS1 predictor algorithms. Mitochondria and ER targeting, and transmembrane domains were also screened (for more details see Camoes et al. 2015). As a result, 124 candidates beared a PTS1 or PTS2 which were further categorized according to their homology to known proteins from other species and organizes into specific metabolic pathways. Peroxins and others peroxisomal membrane proteins were identified by key word search and BLAST analysis.

We have focused on the key proteins involved in the fatty acid breakdown, both from peroxisome and mitochondria. Candidate genes coding for the β-oxidation enzymes were identified and a phylogenetic analysis was performed to validate their conservation across species (Table 7). As described, fatty acids require an initial step before the import into the peroxisomal matrix. Fatty acids must be conjugated to CoA to be subsequently imported into the peroxisome via ABC class transporters (Antonenkov and Hiltunen, 2012). In *U. maydis* we identified two transporter homologues to the ABC half transporters PXA1 (um03945) and PXA2 (um01105) (Table 7). The two membrane proteins are related to the mammalian peroxisomal transporters ABCD1 and ABCD2, although no homologue of ABCD3 was found in *U. maydis*. For ACOX, enzyme that catalyses the first step of peroxisomal β-oxidation, four candidates were found (um01966, um02028, um02208, um04324) With the exception of um04324 – the homologue of *S. cerevisiae* POX1, all other putative proteins possess a PTS1. The lack of a PTS1 in this ACOX group is a characteristic shared among the fungi analysed, suggesting a PTS-independent import mechanism.

The second and third step are catalysed by two phylogenetically unrelated multifunctional enzymes: L- (LBP) and the D-bifunctional protein (DBP). In *U. maydis*, unlike mammals, only D-BP is expressed. However, other putative peroxisomal proteins might fulfil their enzymatic reaction. These include several enoyl-CoA hydratases (um01747, um02097, um11001) and a 3-hydroxyacyl-CoA dehydrogenase of the SDR-family (um10825) which all possess a putative PTS1 (Table 7). The last enzymatic reaction is catalysed by a 3-ketoacyl-CoA thiolase, and SCPx (in mammals). For 3-ketoacy-CoA thiolase two homologues were identified (um01090, with a predicted PTS2, and um02715 without a PTS). Lastly, two homologue genes to SCPx were identified (um11938 with AKL as the PTS1, and um01986 without a PTS), however they lack the SCP domain. Interestingly, we identified SCPs (um11938, um01850) with a PTS1, feature observed in different fungal species (Table 7).

The mitochondrial fatty acid β-oxidation comprises a first step of dehydrogenation catalysed by ACADs. In *U. maydis*, we found seven potential candidates: um00694, um01049, um06185, um10665, um01466, um06400 and um00122 (Table 7). um01049 and um06185 genes relate to the mammalian enzymes ACADM and ACDSB, while um00694 resembles the prokaryotic ACAD family (encoded by FadE genes). um10665, um01466, um06400 and um00122 contain a predicted C-terminal PTS1. Interestingly, only um06400, a homologue of the mammalian ACAD11, was found throughout species (Shen and Burger, 2009a; Camões et al., 2015). This enzyme subfamily is characterized by a C-terminal PTS1, and their existence across species suggest that it is evolutionary conserved. The fungal version of ACAD11 (ACAD11n – um 06400) lack the N-terminal region, the aminoglycoside phosphotransferase (APH) domain, that is found among animals (Shen and Burger, 2009b). However, in *U. maydis*, and other fungi, individual proteins with the homology to the APH domain were found (um06422-ACAD11c). This suggests an evolution where ACAD and APH were combined in one protein, ACAD11, to better fulfil their function.

Previously, through *in silico* studies it was suggested that ACAD11 family proteins are imported into peroxisomes (Shen and Burger, 2009b; Kikuchi et al., 2004). In fact, by expressing UmACAD11n and UmACAD11c in *U. maydis*, and in mammalians cells, we observed a correct targeting to the peroxisomal compartment (data not shown, Camoes et

al., 2015). To further confirm this localization, we have expressed rat ACAD11 in mammalian cells which showed a clear localization on the peroxisomes. Together these findings show that ACADs are *bona fide* peroxisomal proteins in fungi and mammals.

The second step of mitochondrial β-oxidation is performed by enoyl-CoA hydratase. In *U. maydis* three candidates were identified (um01433, um02762, um11556). Um11556 represents a homologue of medium-chain enoyl-CoA hydratase. In *M. oryzae*, deletion of its homologue severely affected mitochondrial β-oxidation (Patkar et al., 2012). For the two last reactions, third and fourth, two homologues were found to 3-hydroxyacyl-CoA dehydrogenase (um01099 and um02105) and 3-ketoacyl-CoA thiolase (um03571 and um03298) (Table 7)

To gain further insight into the parallel fatty acid β-oxidation, we determined the subcellular localization of ACAD and ACOX in *U. maydis.* um02208 (ACOX) was tagged with GFP and shown co-localization with the peroxisomal marker mCherry-SKL (more detail on chapter 5) (data not shown, see Camoes 2015). Similarly, we generated a mCherry fusion of the catalase homologue (um11067) and co-localize it with GFP-SKL (more detail in 5.3.1). Catalase is a routinely used as a marker for peroxisomes. In both cases, peroxisomal presented morphology similar to the mammalian cells, rod and spherical shaped organelles (fig 12). Overall, our approach demonstrated that *U. maydis* possesses a complete and complex set of enzymes to perform a cooperative peroxisomal and mitochondria β-oxidation.

Table 7: Mitochondrial and peroxisomal β-oxidation enzymes in *U. maydis, S. cerevisiae and H. sapiens*.

	Step	**Enzyme**	***U. maydis***	***S. cerevisiae***	***H. sapiens***
Peroxisomal β-oxidation	Import	ABC-half-transporters	um01105	PXA2	ABCD1
			um03945	PXA1	ABCD2
					ABCD3
	Step 1	Acyl-CoA oxidases (ACOX)	um01966	POX1	ACOX1
			um02028		ACOX2
			um02208		ACOX3
		Acyl-CoA dehydrogenases (ACAD)	um04324 um06400 um01466		ACAD11
	Step 2	Enoyl-CoA hydratases	um00122 um01747 um02097		
	Step 3	3-Hydroxyacyl-CoA dehydrogenases	um11001 um10825		HCD2 HCDL2
	Step 2/3	MFE2	um10038	FOX2	DHB4

		MFE1			ECHP
	Step 4	3-Ketoacyl-CoA thiolases	um01090	POT1	THIK
		SCPX	um01986		SCPX
	Accessory	SCP	um11938		
			um01850		
		Dienoyl-CoA isomerases	um10273		ECH1
		3,2-Trans-enoyl-CoA isomerases	um01599		ECI2
			um03158		
Mitochondria β-oxidation	Step 1	Acyl-CoA dehydrogenases (ACAD)	um00694		
			um01049		ACADM
			um06185		ACADSB
					ACADVL
					ACAD9
					ACAD10
					ACADS
					ACADL
	Step 2	Enoyl-CoA hydratases	um11556		ECHM
			um02762		ECHD1
			um01433		ECHD2
					ECHD3
	Step 3	3-Hydroxyacyl-CoA dehydrogenases	um01099		HCDH
			um02105		
					HCDL2
	Step 2/3	Trifunctional enzyme			ECHA
	Step 4	3-Ketoacyl-CoA thiolases	um01843		
			um02715		
			um3298		
			um03751		THIM
					THIL
	Accessory	Dienoyl-CoA isomerases			ECH1
		Trans-enoyl-CoA isomerases			ECI1
					ECI2

4.3.2 *U. maydis* peroxisomes respond to fatty acid treatment

Peroxisomes show a remarkable plasticity and response to stimuli. In mammalian and yeast cells peroxisomal proliferation can be induced by dietary fatty acids. Exposure to peroxisome proliferators alters peroxisomal number and protein content within the cell. In this line, fatty acid degradation enhanced due to an increase in both the amount and activity of β-oxidation enzymes (Schrader et al., 2012). As seen in Table 3, *U. maydis* presents a vast repertoire of different strains. In this study we have used the FB1-GFP-SKL strain (Steinberg and Schuster, 2011), a haploid strain unable to form hyphae, with peroxisomes labelled in green to study in more detail the peroxisomal population in *U. maydis*. *U. maydis* cultures were grown and observed under the microscope. To access the complete pool of peroxisomes within the cell, maximum projections were acquired from 200 nm z-axis step streams. Contrarily to the yeast *S. cerevisiae*, *U. maydis* possesses a high number of peroxisomes, implying proximity to the mammalian system. In control conditions, where glucose is used as the sole carbon source, *U. maydis* cells display an average number of 40.2 ± 1.805 (n = 44) peroxisomes/cell (Figure 12 A-B). To investigate if peroxisomal proliferation can be induced by fatty acids, similar to mammals and yeast, we incubated the strain with minimal

media supplemented with 0.2% of oleic acid, as the sole carbon source, for 1 h. A range of concentrations (0.2-2%) were tested but higher amounts of oleic acid showed an augmented degree of toxicity with highly vacuolated cells after short periods of time (data not shown). After exposure to oleic acid, peroxisome number increased 1.6 fold (65.9 ± 2.98, n = 41) (Figure 12 A-B), confirming that in *U. maydis* peroxisomes respond to external fatty acid stimulation. Morphologically, clear alterations in the peroxisomal phenotype were also visualised. Interestingly, a wide variety of phenotypes were evident as also seen in mammalian cells. Although not exclusively, but more prominent, treated cells showed elongated and constricted, "beads-on-a-string"-like peroxisomes contrasting with the spherical or rod-shaped peroxisomes in control cells (Figure 12 A, ROI). Those morphological alterations are reminiscent of peroxisomal growth and division processes, as observed in mammals.

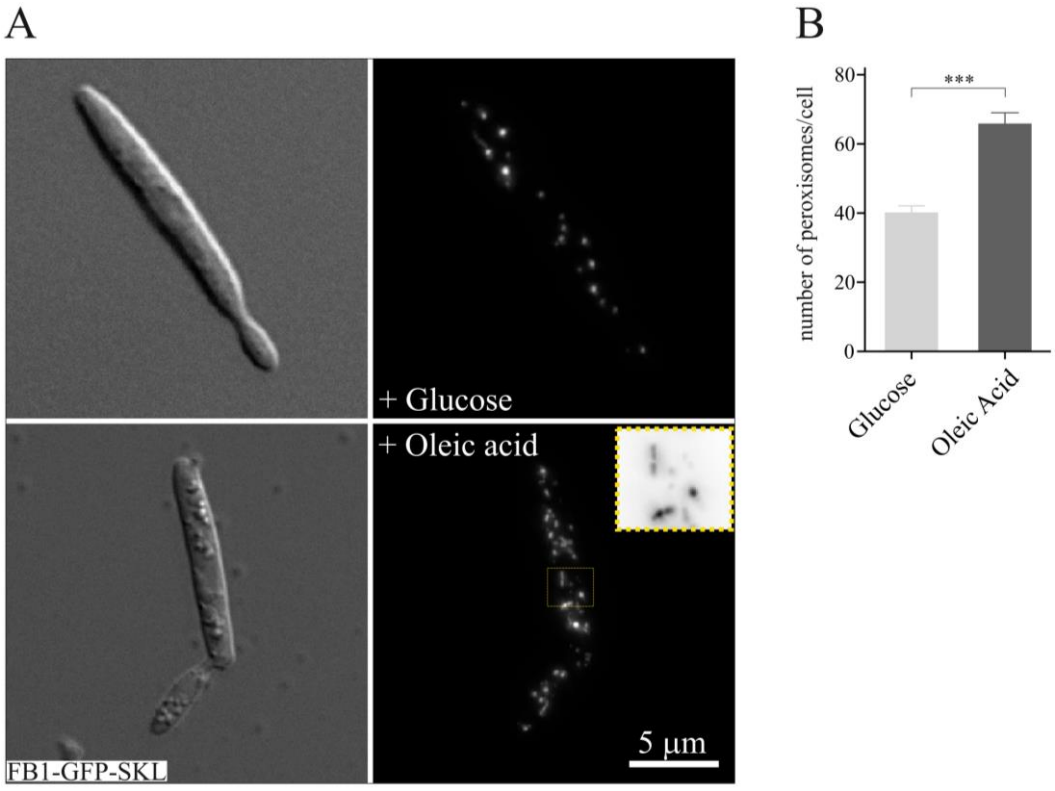

Figure 12 - *U. maydis* peroxisomes proliferate when exposed to fatty acids. FB1GFP-SKL cells were treated for 1 hour with minimal medium supplemented with 0.2% of oleic acid as the sole carbon source. A) Control cells showed an average number of 40.2 peroxisomes per cell, which increased when cells were treated with oleic acid (66%). Changes in morphology could be observed in the treated cells. Amplified ROI (yellow dashed) show changes in peroxisome morphology. Scale bar 5 µm. B) Peroxisome number/per cell in cells incubated with oleic acid is statistically different from the control. All bars are given as mean ± SEM (error bars) from at least 2 experiments. n = 41-44. ***: different to control at P<0.0001 (Student-t-test).

4.3.3 Characterization of a *U. maydis Pex3* null mutant

Peroxin 3 is a peroxisomal membrane biogenesis factor. Depletion of Pex3 results in the inability to use oleic acid as a sole carbon source; the accumulation of peroxisomal matrix proteins in the cytosol; and the absence of morphologically detectable peroxisomes (Erdmann et al., 1989). *Pex3* null mutants show a similar phenotype across species (Barnett et al., 2000;; Hettema et al., 2000; Fang et al., 2004; Hoepfner et al., 2005; Opalinski et al., 2012). In *U.* maydis, Um06200 represents a homologue of the *Pex3* gene. We have deleted Pex3 from the two distinct *U. maydis* strains: Sg200 (Bolker et al., 1995) and AB33. Sg200 is a haploid FB1 (a1b1) strain (Banuett and Herskowitz, 1989), harbours an active b mating type complex. Therefore, it grows in the yeast-like form in liquid medium and forms hyphae at the water–air interface, without mating required. The Pex3 deletion was confirmed by Southern blot (data not shown). To visualise if peroxisomes were absent, a peroxisomal marker (GFP-SKL) was introduced into the Sg200-Δpex3 strain. A disperse, cytosolic fluorescence signal confirmed the absence of peroxisomes in the deletion mutant (Figure 13 A).

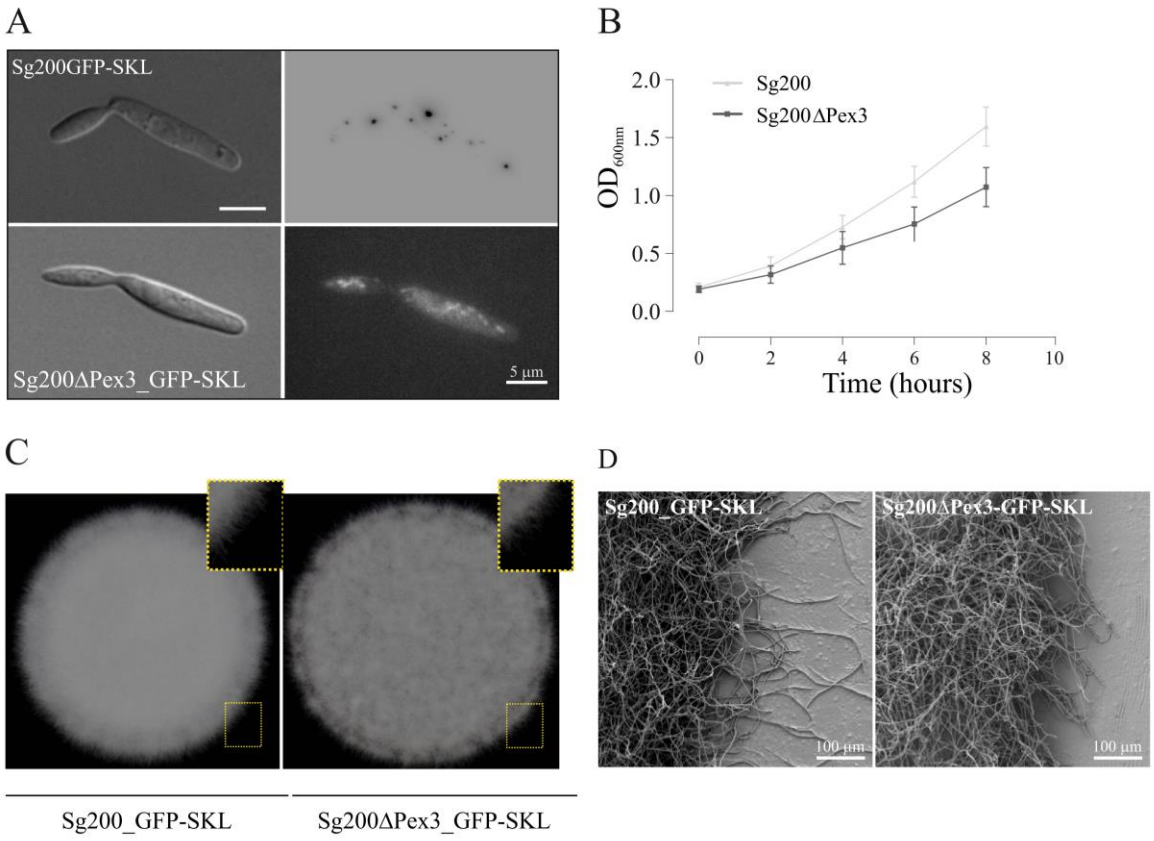

Figure 13 - Characterization of peroxisome-deficient strain.A) Upper panel shows peroxisomal wild type morphology in yeast-like cells in *U. maydis*. However, when *pex3* is depleted no punctuated structures were observed but instead a mislocalization of GFP-SKL to the cytosol. Bar 5 µm. B) Growth curve comparing wild

type and Δpex3 cells. Cells were grown overnight, washed and diluted into fresh media to the same volume and OD_{600nm}. OD_{600nm} was then measured every hour for 8 hours. No statistical differences between the two curves were found. C) 2Sg200 strain grown in complete media with glucose and 1% charcoal, in agar, is able to form hyphae. Cells were dotted in this solid medium and hyphae were visible in both wild type and deleted cells. D) For SEM analysis, cells were grown under the same conditions and scanned by SEM. Elongated hyphae can be observed in both conditions. Scale bar 100 μm.

Kretschmer et al. (2012) have shown that deletion of specific enzymes of the peroxisomal β-oxidation pathway (D-BP and hydroxyacyl-CoA dehydrogenase), impairs filamentous growth in different carbon sources. To elucidate whether peroxisomes are essential for fungal filamentation, we have used the solopathogenic Sg200 strain. Sg200 filamentation is induced in complete media (CM) supplemented with glucose and 1% charcoal. Hence, we have grown Sg200 (control) and Sg200ΔPex3 (deletion) in CM and spotted in a CM/Glucose agar charcoal plate and grown for 48 h. The growing colonies were visualised under a stereo microscope. For a more detailed visualization, colonies were cryo-sledged and rapidly frozen for Scanning Electron Microscopy (SEM) observation. In both approaches, colony formation showed filamentous cells (Figure 13 C-D). Moreover, previously, it was suggested that strain deficient in peroxisomal enzymes, had lower growth rates when compared to wild type conditions (Kretschmer et al., 2012). We compared growth rates between the control and deletion strain. Cultures had the same starting OD_{600nm} and were grown over an 8 hours period until the stationary phase. We have observed a slightly slower growth rate in the deletion strain when compared to the control. Curve fitting showed no statistical significance between the two curves.

The absence of peroxisomes in yeast cells with a single gene mutation (Pex3 or Pex19) is restored by complementation with the wild-type version of the gene (Hohfeld et al., 1991; Baerends et al., 1996). To confirm it in *U. maydis*, an AB33Δpex3_pex3-crg-GFP_mChSKL was generated. For that, we have used pex3-crg-GFP plasmid where *crg* is a carbon-regulated promoter, repressed when cells grow on glucose as carbon source, and induced when it is changed to arabinose. This inducible gene allowed a tight control of peroxisome formation over a 24 hours' time-course. Furthermore, by introducing mCherry-SKL, we were able to confirm the correct peroxisomal targeting and if/when peroxisomes became import-competent (Figure 14). Briefly, cells were grown overnight in CM-Glucose media, washed and shifted to CM-Arabinose media and subsequently observed over 24 hours period. After 1 hour, we observed a bright dot-like structure (positive for GFP fluorescence

signal) that most likely represents a peroxisome although not import-competent (negative for mCherry fluorescence signal). However, after 2 hours at least two peroxisomes presented a visible mCherry-SKL signal. In the following hours an increasing peroxisomal number was registered.

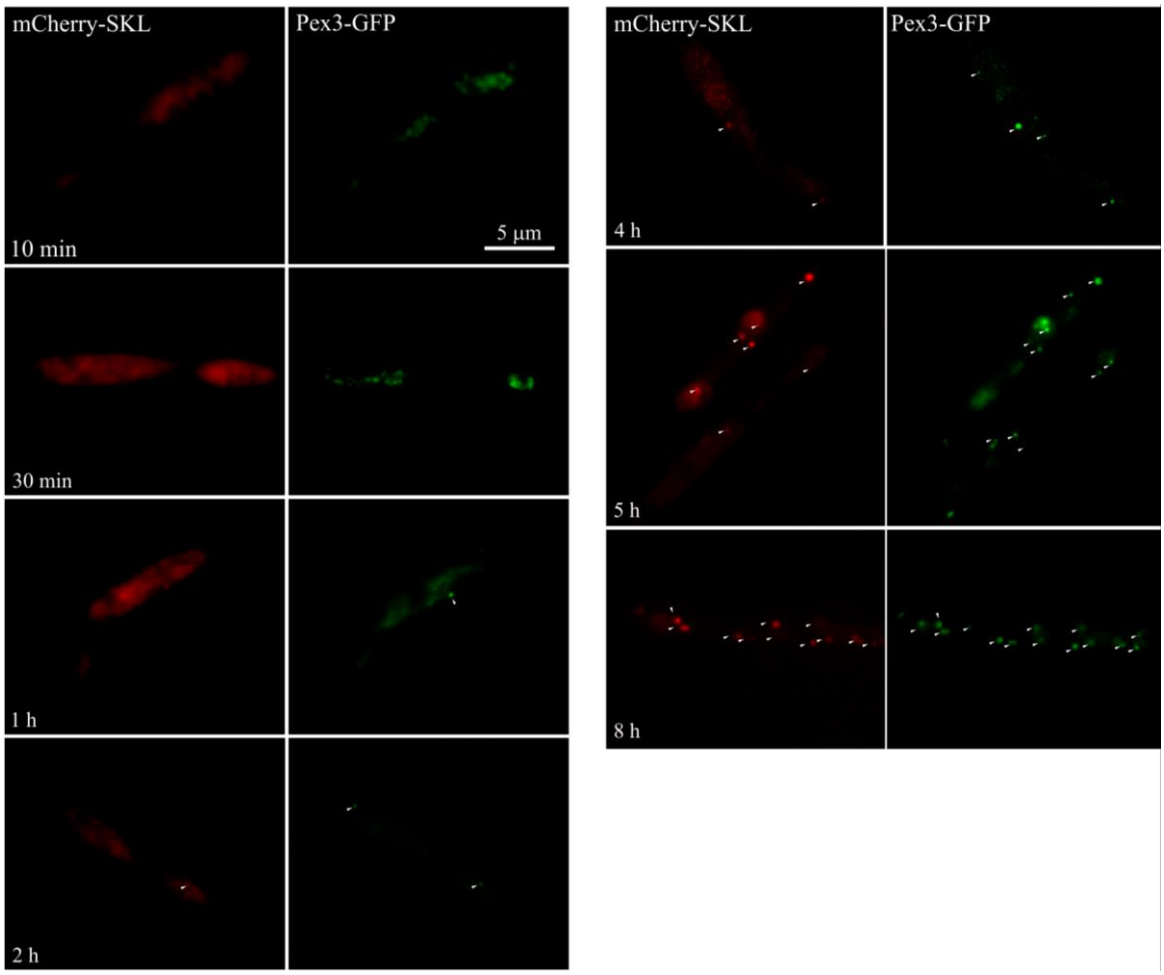

Figure 14 - Peroxisome population is re-established after reintroduction of Pex3. AB33ΔPex3-Pex3-crg-GFP-mCherry-SKL allowed us to visualize the formation of peroxisomes after reintroduction of Pex3 over a 24h time course. Immediately after shifting, the cells presented unspecific fluorescence as can be seen in the 10 min panel. After 10 min in arabinose media no spherical-shaped peroxisomes were present. However, after 30 min peroxisomes appear to start forming, which becomes obvious after 1 hour of media shifting. Peroxisomes become import competent after approximately 2 hours where mCherry-SKL can be seen co-localizing with Pex3-GFP. Increased numbers of peroxisomes are seen in a time dependent manner, reaching a stable plateau after 8 hours. Representative images of time courses performed 3 times.

4.3.4 *U. maydis* peroxisomes sequester a spectrum of fatty acids overlapping with mitochondrial β-oxidation

To understand the existence of a cooperative β-oxidation system between peroxisomes and mitochondria in *U. maydis*, we have tested a wide spectrum of fatty acids as energy source. In order to gain more insight on the spectrum of fatty acids degraded in peroxisomes, we

cultivated wild-type and Δpex3 strains in a glucose-free medium supplemented with a fatty acid of interest at a final concentration of 0.001%. For comprehensive studies, analysis of size and density of each individual colony were performed. To be noted that in control conditions, the deletion mutant present a slightly less dense colony when compared to the control (Figure 15 – Glucose). Fatty acids can cause a high degree of toxicity therefore, to discriminate between inability to break down fatty acids for energy generation, or a toxic effect of over accumulation on the fungal cells, we have performed control studies with the fatty acid supplemented with 1% glucose, as a complementary carbon source. Overall, reduction in the growth of the deletion mutant was observed with all fatty acids tested, with the exception for acetate. Growth in short- and medium- fatty acids (C4-C10) was still significant, suggesting that the breakdown of those fatty acid does not occur primarily at the peroxisomes (Figure 15 – SCFA, MCFA). However, growth on saturated long-chain fatty acids (myristic and palmitic acid) was profoundly reduced in the Δpex3 mutant (Figure 15 – LCFA). Notably, the loss of peroxisomal β-oxidation massively repressed the growth on very long-chain (lignoceric acid) (Figure 15 – VLCFA) and most unsaturated fatty acids (e.g., myristoleic, palmitoleic, oleic acid) (Figure 15 – Unsaturated FA). Noteworthy, accumulation of unsaturated fatty acids, *per se*, i.e. when supplemented with glucose, already cause significant toxicity (Figure 15). With palmitoleic acid exhibiting the most severe toxicity phenotype. Overall, these findings suggest that unsaturated fatty acids acid can only be degraded in certain amounts in the peroxisomes of *U. maydis*.

Our genomic screen revealed the existence of an incomplete enzyme inventory for α-oxidation of C3-branched-chain fatty acids. By providing pristanic acid to the system, the deletion strain grew poorly. Growth impairment was even more noticeable with phytanic acid. In mammalian cells, ω-oxidation, via the ER through the use of P450 enzymes, is able to metabolize branched-chain fatty acids (Wanders et al., 2001). The resulting pristanic acid is subsequently degraded in the peroxisome via β-oxidation. In concordance to our observations it is likely that *U. maydis* utilise a similar combined ER/peroxisomal mechanism. Most of the fatty acids were diluted in ethanol, thus we have tested different concentrations of ethanol (0.001-1%). No differences were observed between the two strains.

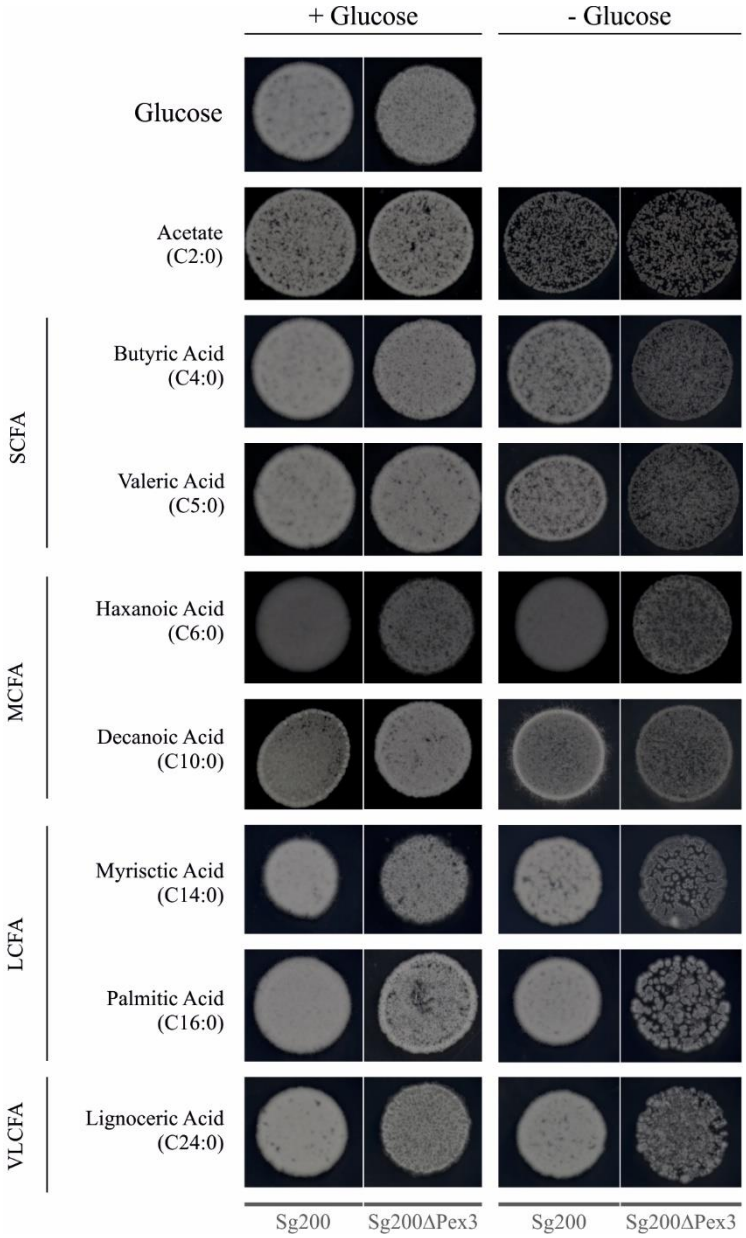

Figure 15 A - Growth of control and ΔPex3 strains on different fatty acids. The wild type strain Sg200 and the Sg200 Δpex3 strain were spotted on agar plates containing different fatty acids (0.001%) or acetate (1%) in the absence or presence of glucose (1%). Photographs were taken after 48 h at 28 °C. SCFA, short-chain fatty acids; MCFA, medium-chain fatty acids; LCFA, long-chain fatty acids; VLCFA, very long-chain fatty acids.

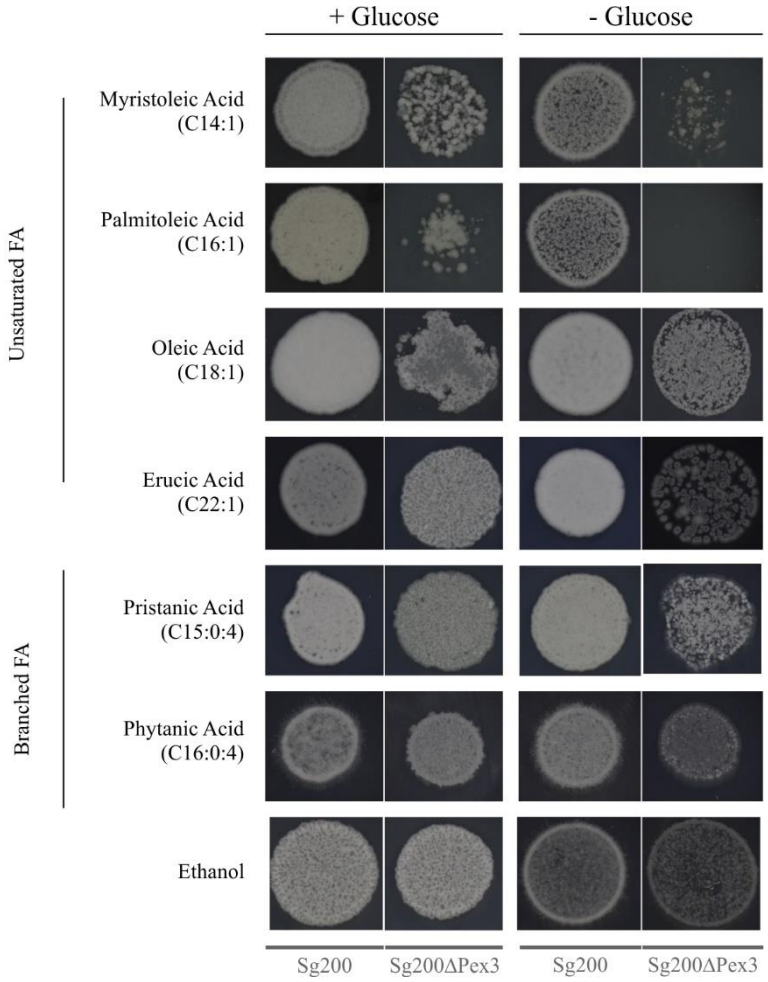

Figure 15 B - Growth of control and ΔPex3 strains on different fatty acids (continued). The wild type strain Sg200 and the Sg200 Δpex3 strain were spotted on agar plates containing unsaturated fatty acids (0.001%), branched fatty acids, or ethanol (1%) in the absence or presence of glucose (1%). Photographs were taken after 48 h at 28 °C. FA – fatty acid

In summary, *U. maydis* seems to share both peroxisomal and mitochondrial β-oxidation, as observed in mammalian cells. Moreover, peroxisomes in *U. maydis* preferably degrade unsaturated-long chain fatty acids, very-long chain fatty acids and branched-chain fatty acids. Short- and medium-chain fatty acids are oxidize in the mitochondria.

4.4 Discussion

Peroxisomes are pivotal organelles in the maintenance of lipid of homeostasis that harbour β-oxidation across species. In mammals, the degradation pathway is shared with mitochondria which differs from yeast and plants. This mutual pathway may exhibit a more energy efficient system. In humans, the genetic defects on the enzymes of the β-oxidation processes cause severe peroxisomal-related diseases. Our bioinformatics study revealed that *U. maydis*, contrarily to other fungi (Shen and Burger, 2009), comprises a complete enzymatic set of peroxisomal and mitochondrial fatty acid degradation. Therefore, it resembles to mammals, rending *U. maydis* as suitable model to study such processes.

In yeast cells, the use of fatty acids as energy source is only activated in specific conditions, since glucose, alcohol and organic acids are preferred. Therefore, the existence of β-oxidation solely on peroxisomes is likely more efficient. In support, yeast cells in basal conditions, harbour 1-5 peroxisomes per cell. Nonetheless, their number increases dramatically when fatty acid degradation is required. In *U. maydis* peroxisomes are constitutively in higher number, in agreement with mammals, therefore, revealing the importance of peroxisomes in the filamentous fungus. Significance that has been previously confirmed on the roles for cell survival and/or pathogenicity (Klose and Kronstad, 2006; Kretschmer et al., 2012).

Peroxisomes require two minimal biogenesis factors, Pex3 and Pex19 proteins. In Pex3 or Pex19 depleted cells peroxisomes are absent. Nevertheless, by reintroducing the deleted gene, peroxisomes are newly formed and the peroxisomal population is re-stablished (Hohfeld et al., 1991; Baerends et al., 1996). In our system, by deleting *pex3* no peroxisomes were visible. This was further confirmed by introducing the peroxisomal marker, GFP-SKL, which resulted in a cytosolic localisation. Interestingly, the absence of peroxisomes does not seem to influence the filamentous growth of *U. maydis*. Hence, contradicting previous work in filamentous fungi, where the hyphal cell has impaired polar growth when β-oxidation proteins are absent (Kretschmer et al., 2012). To confirm our observation we deleted *pex3* in two different strains, Sg200 and AB33. Sg200 is a solopathogenic strain, which harbours an active *b* mating type complex, and consequently grows as yeast-like cell in liquid medium

and as filaments in water-air surface. On the other hand, AB33 is a haploid strain that carries two compatible *b* alleles and shifts to filamentous growth when grown in inducible media. Curiously, no impaired hyphal growth was observed. Previous study (Kretschmer et al., 2012) have used a FB1 strain, which is unable to form hyphal cells without the mating partner (FB2) and therefore it is expected that hyphal cells are absent. We now know that peroxisomes are essential for sexual development of *U. maydis*, more accurately, peroxisomal β-oxidation of fatty acid is essential for mating (*reviewed in* Peraza-Reyes and Berteaux-Lecellier, 2013). In our observation, by overcoming mating with the use of AB33 and/or Sg200 strains we were able to visualize filamentous growth. *Pex3* null cells showed a slight decrease in the growth rate when compared to the control, in liquid medium. The same slight discrepancy was observed in solid media. In several fungal species, it was shown that core enzymes of glycolysis are dual targeted to the peroxisomes and cytoplasm (Freitag et al., 2012). Therefore, by depleting peroxisomes glucose catabolism could be impaired resulting in the subtle growth defect observed.

To investigate if peroxisome biogenesis is similar to other organisms, we also reintroduced Pex3 in ΔPex3, in combination with a peroxisomal matrix marker. We used the *crg* promoter, which induces protein expression when cells are grown in arabinose supplemented medium. We fused the Pex3-GFP construct to the promoter and integrated intothe ΔPex3 strain. The peroxisome population recovered after 8 hours. Notably, after 30 min the first peroxisome appears; such rapid formation is likely due to the availability of peroxisomal proteins in the cytosol. In line with our results, we can confirm that 1) peroxisomes in the *Pex3* null strain are absent; 2) the peroxisome population is re-established after reintroducing Pex3 and 3) *Pex3* null strains exhibit normal growth on basal conditions, which is not significantly different from the wild type cells

In order to gain more insight in the peroxisomal contribution to fatty acid β-oxidation, we used ΔPex3 strain. Our results suggest that mitochondria β-oxidation is pivotal for saturated short- and medium-chain fatty acids, whereas peroxisomes harbour the breakdown of saturated and unsaturated long- and very long-chain fatty acids. Previous studies on single peroxisomal or mitochondria β-oxidation enzyme led to similar results (Klose and Kronstad, 2006).

Peroxisomes are also of core importance for detoxification purposes. ΔPex3 only grew poorly on saturated and unsaturated fatty acid media even when supplemented with glucose. Similar toxicity has been reported in *U. maydis* for deletion of the Pex6 or D-PBE genes. Previously, it has been proposed that peroxisomes degrades fatty acids that have been removed from phospholipidic membrane (Lockshon et al., 2007). Therefore, the toxicity caused by unsaturated and saturated fatty acids could disturb the biophysical properties of the endomembrane system. Moreover, a newly proposed cell death mechanism, liponecrosis (Richard et al., 2014; Sheibani et al., 2014), was shown to occur in response to external stimuli such as exogenous exposure to palmitoleic acid. This mechanism could also explain the toxicity of the fatty acids. Finally, peroxisomes were given acetate as carbon source, however, no effect on colony growth was observed. Suggesting that glyoxylate cycle does not rely on peroxisomes alone, as observed previously in *A. nidulans* (Hynes et al., 2008). This results contradict Kretschmer et al. (2012) that showed impairment growth in acetate when hydroxyacyl-CoA dehydrogenase was deleted. However, it might imply that mitochondria plays a more important role than anticipated. In fact, studies performed in *Eu glena gracilis* visualise the presence of glyoxylate cycle enzymes in the mitochondria (Ono et al., 2003)

We have shown that peroxisomal β-oxidation is responsive to fatty acids induction. Both by morphological alterations and through RNA expression levels (data not shown, Camões et al 2015). In fact, fatty acid treatments, oleic acid, activate both peroxisomal (ACOX) and mitochondrial (ACADM and ACDSB) β-oxidation enzymes. These results further demonstrate that shared β-oxidation is present in a distant species such as the basidiomycetes. Why such energy efficient mechanism exist is not known. However, it was recently hypothesised that during eukaryotic evolution, mitochondrial β-oxidation of unsaturated fatty acids may have been transferred to peroxisomes to quench the formation of ROS production by the electron transfer from FADH through oxidative phosphorylation (Speijer, 2011). Therefore, evolutionary, bimodal β-oxidations seems to fulfil a balance between efficiency and toxicity of the by-products generated.

In conclusion, we have demonstrated that *U. maydis* presents an adequate model to study peroxisomes. *U. maydis* offers the potential to study complex interrelationships such as the peroxisome-mitochondria connection in a model organism which is easy to cultivate and genetically accessible, but maintains the principle of organelle cooperation found in higher eukaryotes.

5. PEROXISOMES, LIPID DROPLETS AND THE ER HITCHHIKE ON EARLY ENDOSOMES

5.1 Introduction

Intracellular trafficking of different vesicles, organelles, proteins and RNA is essential for cellular maintenance (Vale, 2003). In mammals and fungi it is coordinated by microtubules and actin. Microtubules are dynamic and polarized structures, with the minus-end normally located at the perinuclear region, and the plus-end at the cell periphery. Cargo transport along microtubules is mediated by motor proteins through ATP hydrolysis, converting energy into movement. Kinesins are responsible (generally) for the transport towards the plus end, whereas dynein mediates the transport to the minus-end.

In mammalian cells, peroxisomes are dynamic organelles that are scattered throughout the cell. They can either exhibit short range or long-distance motions. It is thought that peroxisome motility is essential for the maintenance of lipid homeostasis, biogenesis, and for anti-viral immune response (Neuhaus et al., 2016). Directed motility is not well defined neither mechanistically nor functionally. It is known that peroxisomes move along microtubules and bind (directly or indirectly) to dynein and/or kinesins (Huber et al., 1997; Huber et al., 1999; Kural et al., 2005; Kulic et al., 2008). However, the precise role of direct transport is still unclear. It was suggested that active transport might direct peroxisomes, at least a subpopulation, for pexophagy (Bharti et al., 2011; Jiang et al., 2015). In the previous chapter (Chapter 4) we have shown that *U. maydis* is a suitable model for the study of peroxisomal metabolism. Moreover, *U. maydis*, as described (1.2.2), possesses intracellular long-distance organelle trafficking along microtubules and short distance- and tip delivery transport, which is actin dependent. Thus, it presents the technical advantages of genetically accessible organisms but with the intracellular trafficking more closely related to mammals. In filamentous fungi, little is known about peroxisome trafficking. In *A. nidulans* peroxisomes require kinesin-3 and dynein for long-range motility (Egan et al., 2012b). Interestingly, the deletion of kinesin or the motor adapter of dynein and kinesin, HookA, results in the clustering of peroxisomes at the plus-end (Egan et al., 2012b; Zhang et al., 2014). How peroxisomes cluster at the plus-end when anterograde motor is absent, is elusive.

In this study we set out to study the peroxisomal transport mechanism in *U. maydis*. Surprisingly, peroxisomes hitchhike on early endosomes to move over long distances. Moreover, as observed in *A. nidulans*, peroxisomes cluster at the polar region. To reveal if this mechanism was exclusively peroxisomal, we have considered the motile behaviour of other organelles. In fact, early endosomes also support motility of the ER and lipid droplets but not of mitochondria. Overall, we show that early endosomes are fundamental for peroxisome and lipid droplet distribution and motility in the fungal cell.

5.2 Materials and methods

5.2.1 Strains and plasmids

U. maydis strains and plasmids used in the present study are described in Table 8. Strains AB33_GFP-SKL, AB33_HDEL-GFP, AB33ΔMyo5 and AB33GFP-Rab5_Δhok1 were previously described (Wedlich-Soldner et al., 2002a; Steinberg and Schuster, 2011; Bielska et al., 2014b). The primers used in the course of this chapter are described in Table 8.

Table 8: Strain and plasmids used in the current study.

Strain name	Genotype	Reference
AB33_GFP-SKL	*a2* P*narbW2* P*narbE1*, *ble*^{R} / po^{C}GSKL	This study
AB33GFP-Tub1_GFP-SKL	*a2* P*narb*W2 P*narb*E1, *ble*^{R} / poGTub1^{C} /po^{H}GSKL	This study
AB33ΔKin3_GFP-SKL	*a2* P*narbW2* P*narbE1*, *ble*^{R}, *Δkin3*, *nat*^{R} / po^{H}GSKL	This study
AB5Dyn2^{ts}_GFP-SKL	*a2* P*narbW2* P*narbE1*, *dyn2ts*, *hyg*^{R}/ po^{C}GSKL	This study
AB33Kin3-GFP_mCherry-SKL	*a2* P*narbW2* P*narbE1*, *ble*^{R} , P*kin3-kin3-egfp*, *hyg*^{R}/ po$^{G}{}_{m}$ChSKL	This study
AB33GFP-Hok1_mCherry-SKL	*a2* P*narbW2* P*narbE1*, *ble*^{R}, P*hok1-hok1-egfp*, *hyg*^{R}/ po$^{C}{}_{m}$ChSKL	This study
AB33_GFPRab5a_mCherrySKL	*a2* P*narbW2* P*narbE1*, *ble*^{R} / poGRab5 /po$^{C}{}_{m}$ChSKL	This study
AB33GFP-Rab5a_ΔHok1_mCherrySKL	*a2* P*narbW2* P*narbE1*,*ble*^{R} , poGRab5,Δ*hok1*, *hyg*^{R} / po$^{G}{}_{m}$ChSKL	This study
AB33ΔRab5a_Yup1-GFP_mCherrySKL	*a2* P*narbW2* P*narbE1*, *ble*^{R}, *Δrab5a*, *nat*^{R}/ poYup1G / po$^{G}{}_{m}$ChSKL	This study
AB33Yup1^{ts}_GFP-SKL	*a2* P*narbW2* P*narbE1*, *ble*^{R} *yup1ts*, *hyg*^{R} / po$^{C}{}_{m}$ChSKL	This study
AB33GFP-Rab5a_ΔHok1_mCherry-SKL_ΔC	*a2* P*narbW2* P*narbE1*,*ble*^{R}/poGRab5, Δ*hok1*, *hyg*^{R} / po$_{m}$ChSKL / pHok1$^{1-624}$	This study
AB33GFP-Rab5a_ΔHok1_mCherry-SKL_ΔC-PX	*a2* P*narbW2* P*narbE1*,*ble*^{R}/poGRab5, Δ*hok1*, *hyg*^{R} / po$_{m}$ChSK / pHok1$^{1-624}$-PX	This study
AB33mCherry-Rab5a_Erg6-GFP	*a2* P*narbW2* P*narbE1*,*ble*^{R} / poChRab5 / poErg6G	This study
AB33ΔHok1_mCherry-Rab5a_Erg6-GFP	*a2* P*narbW2* P*narbE1*, *ble*^{R}, *Δhok1*, *nat*^{R} / pomChRab5a / poErg6G	This study
AB33_HDEL-GFP	*a2* P*narbW2* P*narbE1*,*ble*^{R} / poERGFP	(Wedlich-Soldner et al., 2002a)
AB33ΔHok1_HDEL-GFP	*a2* P*narbW2* P*narbE1*, *ble*^{R}, *Δhok1*, *nat*^{R} / poERGFP	This study
AB33HDEL-GFP-mCherryRab5a	*a2* P*narbW2* P*narbE1*, *ble*^{R} /poERGFP / poChRab5	This study
AB33GFP-Rab5_ΔHok1	*a2* P*narbW2* P*narbE1*, *ble*^{R} / poGRab5, *Δhok1*, *nat*^{R}	(Bielska et al., 2014b)

AB33ΔHok1_GFP-SKL	*a2* P*narbW2* P*narbE1*, *ble*^{R}, *Δhok1*, *nat*^{R} / po^{C}GSKL	This study
AB33_Lga2-GFP_mCherry-SKL_ΔHok1	*a2* P*narbW2* P*narbE1*, *ble*^{R} / poLgaG / po^{H}mChSKL, *Δhok1*, *nat*^{R}	This study
AB33Erg6-GFP_mCherry-SKL	*a2* P*narbW2* P*narbE1*,*ble*^{R} / poErg6G / po^{G}mChSKL	This study
AB33Pex3-GFP_mCherry-SKL	*a2* P*narbW2* P*narbE1*, *ble*^{R}, *pex3-egfp*, *hyg*^{R} / po$^{C}{}_{m}$ChSKL	This study
Sg200_Erg6-GFP	*a1 mfa2 bW2 b*E, *ble*^{R} / poErg6G	This study
AB33Δrrm4_GFP-Rab5a_mCherry-SKL	*a2* P*narbW2* P*narbE1*, *ble*^{R}, Δ*rrm4*, *hyg*^{R} / poGRab5 / po$^{G}{}_{m}$ChSKL	This study
AB33_Lga2-GFP	*a2* P*narbW2* P*narbE1*, *ble*^{R} /	(Steinberg and Schuster, 2011)
po^{C}GSKL	P*otef-egfp-skl*, *cbx*^{R}	(Steinberg and Schuster, 2011)
poGTub1	P*otef-egfp-tub1*, *cbx*^{R}	(Steinberg et al., 1998)
po$^{H}{}_{m}$ChSKL	P*otef-mcherry-skl*, *hyg*^{R}	This study
po$^{C}{}_{m}$ChSKL	P*otef-mcherry-skl*, *cbx*^{R}	This study
pHok1$^{1\text{-}624}$	P*hok-Hok1(1-624)-HA*, *cbx*^{R}	This study
pHok1$^{1\text{-}624}$-PX	P*hok1-Hok1(1-624)-PX-HA*, *cbx*^{R}	This study
po^{H}GSKL	P*otef-egfp-skl*, *hyg*^{R}	This study
po$^{G}{}_{m}$ChSKL	P*otef-mcherry-skl*, *G418*^{R}	This study
poYup1G	P*otef-yup1-egfp*, *cbx*^{R}	(Wedlich-Soldner et al., 2000)
poGRab5	P*otef-egfp-rab5a*, *nat*^{R}	(Schuster et al., 2011a)
poLgaG	P*otef-lga2-gfp*, *cbx*^{R}	(Steinberg and Schuster, 2011)
poErg6G	P*otef-erg6-egfp*, *cbx*^{R}	This study
poChRab5	P*otef-mcherry-rab5a*, *nat*^{R}	(Wedlich-Soldner et al., 2000)
poERGFP	P*otef-cal*^{S}*-egfp-HDEL*, *cbx*^{R}	(Wedlich-Soldner et al., 2002a)
Po^{C}mChEca1	P*otef-mcherry-eca1*, *Eca1*^{R}	This study
po^{N}mChEca1	P*otef-mcherry-eca1*, *nat*^{R}	This study

a and *b*, mating type loci; P, promoter; -, fusion; Δ, deletion; *hyg*^{R}, hygromycin resistance; *ble*^{R}, phleomycin resistance; *nat*^{R}, nourseothricin resistance; *cbx*^{R}, carboxin resistance; *G418*^{R},neomycin resistance; *otef*, constitutive promoter; /, ectopically integrated; *E1*, *W2*, genes of the b mating type locus; *egfp*, enhanced GFP; *mcherry*, monomeric cherry; *kin3*, kinesin-3; *dyn2*, C-terminal half of the dynein heavy chain; *hok1*, Hook1 protein in *U. maydis*, *rrm4*, RNA-binding protein; rab5a, small endosomal GTPases; rho3, small GTPase; *yup1*, endosomal t-SNARE; *PX*, PX domain from the putative endosomal t-SNARE protein yup1; *pex3*, peroxisonal biogenesis factor 3;*SKL*, peroxisomal targeting sequence; *tub1*, α-tubulin;*cal*^{S} , signal sequence of calreticulin from rabbit (nt1-51);HDEL, ER retention signal; Erg6, lipid droplets Δ24 sterol methyltransferase; *lga2*, putative mitochondrial matrix protein; Eca1, gene that encodes a sarcoplasmic/endoplasmic calcium ATPase.

Plasmid GFP-SKL (carboxin)

po^{C}GFP-SKL and AB33_GFP-SKL were previously described in Steinberg and Schuster (2011). po^{C}GFP-SKL was linearized with *Age*I and transformed into AB33Yup1^{ts} (Fuchs et al., 2006) resulting in AB33Yup1^{ts}_GFP-SKL. For integration of the plasmid into AB33ΔHok1 po^{C}GFP-SKL was digested with *Eco*RV, resulting in AB33ΔHok1_GFP-SKL. AB33_Dyn2^{ts}_GFP-SKL was obtained through linearization of po^{C}GFP-SKL with *Bgl*I to ectopically integrate into AB33_Dyn2^{ts} (made and provided by Feldbrugge but already used and cited in (Higuchi et al., 2014; Schuster et al., 2011a). For visualization of peroxisomes distribution in the absence of Myo5, po^{C}GFP-SKL was digested with *Age*I and ecoptically transformed into AB33ΔMyo5 (Schuchardt et al., 2005).

Plasmid GFP-SKL (hygromycin)

po^{H}GFP-SKL was obtained by replacing carboxin resistance cassette of po^{C}GFP-SKL with hygromycin resistance cassette. po^{C}GFP-SKL was digested with *Sph*I and *Nde*I to remove carboxin fragment. pSL-Hyg was cut by the same enzymes to obtain hygromycin fragment with sticky ends. 2642 bp hygromycin fragment and 4338bp vector backbone were ligated to produce po^{H}GFP-SKL. Plasmid was confirmed by PCR and restriction enzyme digestion. po^{H}GFP-SKL was linearised with *Kpn*I and ectopically integrated in AB33Δkin3 (Higuchi et al., 2014) resulting in the strain AB33Δkin3_GFP-SKL. AB33GFP-Tubulin_GFP-SKL allowed co-visualization of peroxisomes and MTs. It was generated by digestion of po^{H}GFP-SKL with *Bgl*I and integrated ectopically into AB33-GFP-Tubulin.

Plasmid mCherry-SKL (carboxin)

The *gfp* and the carboxin resistance cassette of plasmid po^{C}GFP-SKL (Steinberg and Schuster, 2011) were replaced with mCherry and a hygromycin resistance cassette resulting in plasmid po^{C}mCherry-SKL. The plasmid was linearized with *Eco*RV and integrated ectopically into the strain AB33 resulting in AB33mCherry-SKL. To obtain AB33Hok1-GFP_mCherry-SKL strain, the plasmid Hok1-GFP$_3$ (Bielska et al., 2014) was digested with *Psi*I and *BamH*I and homologously integrated into the *hok1* locus of AB33 strain, resulting in AB33Hok1-GFP. Integration of a single eGFP into the *hok1* locus was confirmed by PCR and Southern blotting. Next, po^{C}mCherry-SKL was linearized with *Ssp*I and inserted into

AB33Hok1-GFP resulting in the AB33GFP-Hok1_mCherry-SKL strain. po^{C}mCherry-SKL was linearized with *EcoR*V and transformed into AB33GFP-rab5a which resulted in AB33GFP-Rab5a_mCherry-SKL strain. To obtain AB33_Lga2-GFP_mCherrySKL strain, po^{C}mCherry-SKL was digested with *EcoR*V and transformed into AB33_Lga2-GFP (Steinberg and Schuster, 2011) resulting in AB33_Lga2-GFP_mCherry-SKL. Furthermore, p^{N}ΔHok1 plasmid (Bielska et al, 2014) was linearized with *AlwN*I and *Hpa*I and integrated into AB33_Lga2-GFP_mCherry-SKL resulting in AB33_Lga2-GFP_mCherry-SKL_ΔHok1. Deletion of the gene was confirmed by Southern blot.

Plasmid ΔRab5a

The plasmid contains nourseothricin resistance gene flanked by native promoter of rab5a and 940bp downstream of Rab5a ORF in pCRIITOPO background (Kudla et al.,1999). In order to obtain AB33_ΔRab5a, p^{N}ΔRab5a was linearized with *Psi*I and integrated into rab5a locus of AB33. Deletion of rab5a gene was confirmed with PCR and southern blotting. pYup1-GFP (Wedlich-Soldner et al., 2000) was linearized with *EcoR*V and integrated into AB33ΔRab5a cells to generate AB33ΔRab5a_Yup1-GFP.

Plasmid mCherry-SKL (G418)

In order to replace carboxin (*cbx*^{R}) for neomycin resistance (G418), plasmid po^{C}mCherry-SKL was digested with *Kpn*I and *Psh*AI and neomycin resistance was introduced by ligation. po^{G}mCherry-SKL was linearized with *Sca*I and integrated ectopically into AB33-GFP-Rab5a_ΔHok1 (Bielska et al., 2014) and into AB33ΔRab5a_Yup1-GFP resulting in the AB33-GFP-Rab5a_ΔHok1_mCherry-SKL and AB33ΔRab5a_Yup1-GFP_mCherry-SKL, respectively. po^{G}mCherry-SKL was digested with *Ssp*I and integrated ectopically into AB33Kin3-GFP (Schuster et al., 2011b) and AB33ΔRrm4_GFP-Rab5 (Higuchi et al., 2014) resulting in the strains AB33Kin3-GFP_mCherry-SKL and AB33ΔRrm4_GFP-Rab5_mCherry-SKL, respectively. For colocalization studies of lipid droplets or endoplasmic reticulum and peroxisomes, strain AB33Erg6-GFP_mCherry-SKL and AB33-HDEL-GFP_mCherry-SKL were generated by introducing ectopically the *Dra*I digested plasmid po^{G}mCherry-SKL into to the strain AB33Erg6-GFP and AB33-HDEL-GFP.

Plasmid Hok1$^{1-624}$-HA

This plasmid contains a region encoding the first 624 aa of Hok1, fused to human influenza (HA) tag. To obtain the plasmid, a 2,970-bp region, encoding the *hok1*promoter (1,002 bp) and the first 624 aa of Hok1, was amplified from genomic DNA of *U. maydis* strain 521, using primers $_{f}$EB408-$_{r}$EB410. A 391-bp region encoding the HA sequence (MVYPYDVPDYA), *Tnos* terminator, and a fragment of the carboxin resistance cassette was amplified from the plasmid pHok1$^{1-624}$G (Bielska et al., 2014), using primers fEB412-rEB14, and was cloned into the pNEBcbx-yeast-SspI plasmid (Bielska et al., 2014), digested with *Eco*RI and *Sac*I, by *in vivo* recombination in the yeast *S. cerevisiae* FY834. The plasmid was linearized with *Age*I an integrated into the succinate dehydrogenase locus of AB33GFP-Rab5a_ΔHok1_mCherySKL resulting in the AB33GFP-Rab5a_ΔHok1_mCherry-SKL_Hok1$^{\Delta C}$.

Plasmid Hok1$^{1-624}$PX-HA

This plasmid contains a region encoding first 624 aa from Hok1 and the PX domain from Yup1 (Wedlich-Söldner et al., 2000), fused to the HA tag. To obtain the plasmid, a 2,935-bp region encoding the *hok1*promoter (1,002 bp) and the first 624 aa of Hok1, was amplified from the genomic DNA of *U. maydis* strain 521, using primers $_{f}$EB408-$_{r}$EB402. A 546-bp region, encoding the PX domain from the endosomal t-SNARE Yup1 (aa 4–148) and flanking overhangs including the HA sequence, was amplified from the pHok1$^{1-624}$PXG (Bielska et al., 2014) using primers $_{f}$EB403-$_{r}$EB404. A region encoding the *nos* terminator, and a fragment of the carboxin resistance cassette was amplified from the pHok1$^{1-624}$PXG (Bielska et al., 2014), using primers $_{f}$EB409-$_{r}$EB14, and cloned into the pNEBcbx-yeast-SspI plasmid (Bielska et al., 2014), digested with *Eco*RI and *Sac*I, by in vivo recombination. The plasmid was linearized with *Age*I an integrated into the succinate dehydrogenase locus of AB33GFP-Rab5a_ΔHok1_mCherry-SKL resulting in the AB33GFP-Rab5a_ΔHok1_mCherry-SKL_Hok1$^{\Delta C}$PX.

Plasmid mCherry-Eca1 (nourseothricin)

po^{N}mCherry-Eca1 was generated by replacing carboxin cassette to nourseothricin. It was digested with *Bsi*WI and *Sph*I to remove cbx cassette. The nourseothricin resistance cassette was obtained through amplification by PCR with 30-bp homology sequences (SG22-SG24)

of the vector pNEB-Nat and recombined by yeast resulting in po^{N}mCherry-Eca1. For colocalization studies of lipid droplets and endoplasmic reticulum, strain AB33-Erg6-GFP_Eca1-mCherry was generated by introducing ectopically the *Dra*I digested plasmid po^{N}mCherry-Eca1 into to the strain AB33Erg6-GFP.

Plasmid Pex3-GFP (hygromycin)

To obtain Pex3-GFP (um6200), a 936-bp fragment near 3' end of *pex3* gene followed by *egfp* and *nos* terminator, the hygromycin resistance cassette, and 1024-bp fragment downstream of the gene. For generation of the plasmid, *in vivo* yeast recombination was used. The flanks were amplified by PCR with 30-bp overhangs from *U. maydis* genomic DNA (strain 521) using the set of primers GD92-GD93 and GD94-GD95 and cloned into a cloning vector resulting in pex3-egfp. For homologous integration into AB33 strain, the plasmid was digested with *Dra*I which resulted in AB33_Pex3-GFP strain that the correct insertion was confirmed by southern blot. Next, po^{C}mCherry-SKL was digested with *Eco*RV and ectopically inserted into AB33_Pex3-GFP originating AB33Pex3-GFP_mCherry-SKL.

5.2.2 Growth conditions

All cultures of *U. maydis* were grown at 28ºC with shacking at 200rpm for 8hr to overnight in complete medium (CM), supplemented with 1% glucose. To achieve hyphal formation, induction of nitrate reductase was achieved by transferring CM$_{gluc}$ grown cultures to nitrate minimal medium (NM) containing 1% glucose and incubate them for 8-14 h at 28ºC and shacking at 200 rpm. For temperature sensitive mutants, strains were grown and hyphal induced at a permissive temperature of 22ºC. Inactivation of Dyn2 and Yup1 was achieved by shifting the cultures to a restrictive temperature (Dyn2^{ts} at 32ºC; Yup1^{ts} at 34ºC) for 2 h and 5 h, respectively.

5.2.3 Laser-based epifluorescence microscopy

U. maydis microscopy was performed as previously described (Schuster et al., 2011a). Briefly, cells from a liquid culture were placed on a 2% agarose cushion, covered with a coverslip, and immediately observed using a motorized inverted microscope (IX81;

Olympus) with Plan-Apochromat 100×/1.45 NA oil total internal reflection fluorescence microscopy or UPlan-SApochromat 60×/1.35 NA oil objective lenses (Olympus) and a VS-LMS4 Laser Merge System (Visitron) with 70-mW observation solid-state lasers at 488 and 561 nm. Photobleaching experiments were performed using a 405-nm/60-mW diode laser, which was decreased by a neutral density 0.6 filter, resulting in 15-mW output power, coupled into the light path by an adaptor (OSI-IX 71; Visitron Systems). The 405-nm laser was controlled by a controller (UGA-40; Rapp OptoElectronic) and VisiFRAP 2D FRAP control software for Meta Series 7.5.x (Visitron Systems). Synchronised observation of mCherry and GFP fluorescence was performed using an imager (Dual-View Micro; Photometrics) equipped with a dual-line beam splitter (z491/561; Chroma Technology Corp.) with an emission beam splitter (565 DCXR; Chroma Technology Corp.), an ET-Band pass 525/50 (Chroma Technology Corp.), and a single band pass filter (BrightLine HC 617/73; Semrock). Images were acquired using a camera (CoolSNAP HQ^2; Photometrics/Roper Scientific). All parts of the system were under the control of the software package MetaMorph (Molecular Devices), which was also used for fluorescence measurements and image processing. For temperature-dependent experiments, the objective lenses were cooled or heated using a metal hull connected to a water bath (Huber). For bleaching analyses, a region of variable length was photobleached by a 100-ms light pulse using a solid-state 405-nm laser at 100% laser power with a beam diameter of 10 pixels. Subsequently, 100 frames were taken using the 488-nm and/or 561-nm lasers at exposure times of 150ms. Statistical analysis was performed accordingly, and all values given in the text are means ± SEM of at least two experiments. All statistical analysis was performed using Prism 5.03 (GraphPad Software).

5.2.4 Organelle motility analysis

For organelle flux measurements, image series of 300 (peroxisomes) or 150 frames (ER and lipid droplets) were acquired at 150 ms exposure time. Peroxisomes motility parameters (velocity, run length and frequency) were measured in kymographs generated by MetaMorph, anterograde and retrograde signals were determined by counting the unipolar region, 10 μm behind the tip. Frequency analysis of the ER and lipid droplets was performed

in a similar manner. For ER events were measure as follow: 2 μm in a 5 μm region within the unipolar region. All experiments were done at least twice.

To determine the flux of the different organelles in the deletion mutants (AB33Δkin3_GFP-SKL, AB33Dyn2^{ts}_GFP-SKL, AB33ΔRab5a_Yup1-GFP, AB33Yup1^{ts}_GFP-SKL, AB33GFP-Rab5a_ΔHok1_mCherry-SKL_Hok1$^{\Delta C}$PX, AB33GFP-Rab5a_ΔHok1_mCherry-SKL_Hok1$^{\Delta C}$ and AB33ΔRrm4_GFP-Rab5_mCherry-SKL, AB33_ΔHok1_Erg6-GFP, AB33_ΔHok1_HDEL-GFP) and their respective control, (AB33_GFP-SKL, AB33_Erg6-GFP_mCherry-Rab5a, AB33_HEDL-GFP), the same analysis was performed . Briefly, 100 frames series were acquire at a exposure time of 150 ms and flux was established by kymograph analysis either accounting all the cell (peroxisomes and lipid droplets) or by measuring 2 μm in a 5 μm region within the unipolar region (ER). Temperature sensitive mutants were measure using proper temperature control, namely, AB33_GFP-SKL at 32ºC for 2 hours (Control of AB33Dyn2^{ts}) and at 34ºC for 5 hours (control for AB33Yup1^{ts}).

5.2.5 Protein colocalization experiments

Regarding peroxisomal colocalization studies AB33_Kin3-GFP_mCherry-SKL, AB33_GFP-Hok1_mCherry-SKL and AB33_GFP-Rab5_mCherry-SKL strains were used for co visualisation of peroxisomes with Kin3, Hok1 and early endosomes was performed by photobleaching a region of 10-20 μm in length 5 μm behind the hyphal tip by a 100-ms light pulse of the 405-nm laser (60 mW) at 80% laser power. Subsequently, 100 frames were taken using a Dual-View Micro imager, with the 488-nm laser (80% output for Kin3 and Hok1GFP and 20% output for GFP-Rab5A) and the 561-nm laser (25% output power) at a 150-ms exposure time. To visualise microtubule-based peroxisome motility AB33_GFP-αTubulin_GFP-SKL strain was used to acquire 300 frames stream at 150 ms exposure. Colocalization was observed in the image series using the MetaMorph software.

Co-localization of the ER and lipid droplets, with early endosome was performed in a similar manner, shortly, a region of 15-20 μm5 μm behind the tip was photobleached by a 150 ms pulse of the 405 nm laser (80% power). After, 100 frames were acquired using Dual-View Micro Imager, with 488 nm laser (10% output power for EG and 20% output power for Erg6G) and the 561 nm (30% output). For co-localization of Erg6-GFP and mCherry-SKL,

Eca1-mCherry with Erg6-GFP, and HDEL-GFP with mCherry-SKL 100 planes at 150 ms were acquired with a 488 nm laser f 40% output and 561 nm laser with 50% output. For an accurate alignment of different cell components, data acquisition was performed after calibration of the system. TetraSteck fluorescent microspheres (Thermo Fisher Scientific) of 0.2 µm size were diluted 1:10 in water. 1 µl of this suspension was placed on an agar pad and two or three images were taken, using the dual imager (10% output power of 488- and 561-nm lasers, at 150 ms). Both channels were aligned using the "Split View" function in MetaMorph using the defined parameters to align the acquired data. All Kymographs were generated from the acquired image series using the MetaMorph software.

5.2.6 Measurement of organelle distribution

To measure peroxisomes, early endosomes, ER, mitochondria and lipid droplets distribution in ΔHok1 background image of hyphal cells were acquired. For HDEL-GFP and Lga2-GFP, GFP-Rab5, Erg6-GFP and GFP-SKL, z-axis image stacks were acquired at an exposure time of 150 ms and 200nm steps in z-direction. From these stacks, maximum projections were generated using MetaMorph 7.5.x and the average fluorescent intensity over 20-30 µm behind the hyphal cell and 5 µm outside was measured using the linescan function in MetaMorph 7.5.x (Molecular Devices, Downingtown, PA). The measurements of each hyphal cell were transferred into the software Excel (Microsoft, Redmond, USA) and the average intensity of each pixel was calculated.

5.2.7 Inhibitor experiments

For inhibitor experiments, 500-µl cultures were incubated at 200 rpm in a 2-ml tube at 28°C with either benomyl at 30 µM (stock: 30 mM in DMSO; Fluka; Sigma-Aldrich) or latrunculinA at 20 µm (stock: 20mM in DMSO, Life Technologies) Control cells were treated equivalent amounts of solvent DMSO. Cells were placed onto a 2% agar cushion supplemented with the inhibitor or DMSO and immediately microscope. Image series of 100 frames at 150ms were acquired. All experiments were performed at least twice.

Table 9: Primers used in this study.

Primer	Sequence 5' → 3'
EB14	GTACGAAAGCGAGACGAGTTGAGCGAAGATCTCATGTTTGACAGCTTATCATCG
EB402	GTGGTATTGAGATTCCTTGGAGTGGCTGTGTGACCAACTGATTCAGTCGTAATC
EB403	GCATTGCGATTACGACTGAATCAGTTGGTCACACAGCCACTCCAAGGAATC
EB404	GTTTGAACGATCTGCAGCCGGGCGGCCGCTTCACGCATAGTCAGGAACATCGTATGGGTAAACCATGGC TGCTGCTGCCGGCCATTC
EB408	AACTGTTGGGAAGGGCGATCGGTGCGGGCCGTCCTCTACGAGAGACCATAG
EB409	ATGGTTTACCCATACGATGTTCCTGACTATGCGTGAAGCGGCCGCCCGGCTGCAGATC
EB410	GTTTGAACGATCTGCAGCCGGGCGGCCGCTTCACGCATAGTCAGGAACATCGTATGGGTAAACCATGAC CAACTGATTCAGTCGTAATC
EB412	GCATTGCGATTACGACTGAATCAGTTGGTCATGGTTTACCCATACGATGTTCCTGACTATGCGTGAAGC GGCCGCCCGGCTGCAGATC
GD92	AACTGTTGGGAAGGGCGATCGGTGCGGGCCGCAAGTCAAGCTCAAGCTCTG
GD93	GGTGAACAGCTCCTCGCCCTTGCTCACCATCAAAGAAGACCAGGCAGCATAG
GD94	TACGAACGCTTTCGACTCAGCCGTCAATCGTAGGGTCCAACGTCTACGTG
GD95	ATGTTGTGTGGAATTGTGAGCGGATAACAAGTGACGTCATCTACATCGAGG
SG22	GAATTCGAGCTCGGTACCCGGGGGCGCGCCGCGGCCGCTCTAGAACTAGT
SG24	TACCGAGCTCGAATTTCGACCTGCAGGCATGCCCCATATGCATCCTACAG

5.3 Results

5.3.1. Peroxisome long-distance motility is microtubule dependent in *U. maydis* hyphal cells

We have set to study peroxisome motility in the *U. maydis* model system. To visualize peroxisomes, a SKL tripeptide (PTS1) (Gould et al., 1989) was fused to the C-terminus of the green fluorescent protein (GFP) and to the red fluorescent protein (mCherry). GFP-SKL or mCherry-SKL was ectopically integrated into *U. maydis* strain AB33 resulting in strain AB33_GFP-SKL or AB33_mCherry-SKL. Growth in liquid medium with nitrate as nitrogen source induces the formation of b-dependent filaments, so called hyphae (Figure 16 A). Expression of GFP-SKL resulted in a punctate staining pattern scattered throughout the cell. To confirm peroxisome localization in *U. maydis* (Figure16 B), an endogenous construct of Pex3 (Um6200) fused C-terminally with GFP was generated. Co-transforming mCherry-SKL with Pex3-GFP resulted in high co-localization of the two proteins (Figure 16 C) demonstrating the correct subcellular localization to the peroxisomes. We have used live cell techniques to comprehend peroxisomal motility in *U. maydis*, allowing *in vivo* analysis of peroxisome motility through streams and kymographs. Kymographs are graphical representations of a dynamic process of spatial translocation (x-axis) over time (y-axis). In this graphs diagonal lines represent directed long range movements. To understand organelle motion in the fungus we defined general peroxisomal motility parameters. Z-stack streams were acquired, from which maximum projections were generated, from where we could determine that on average the hyphal cell has 110.74 peroxisomes (n=30 cells).

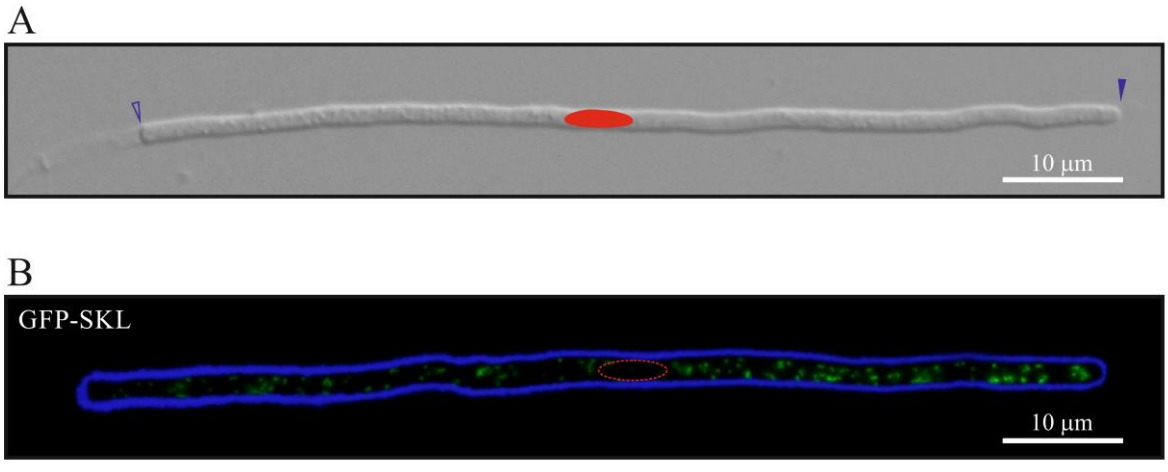

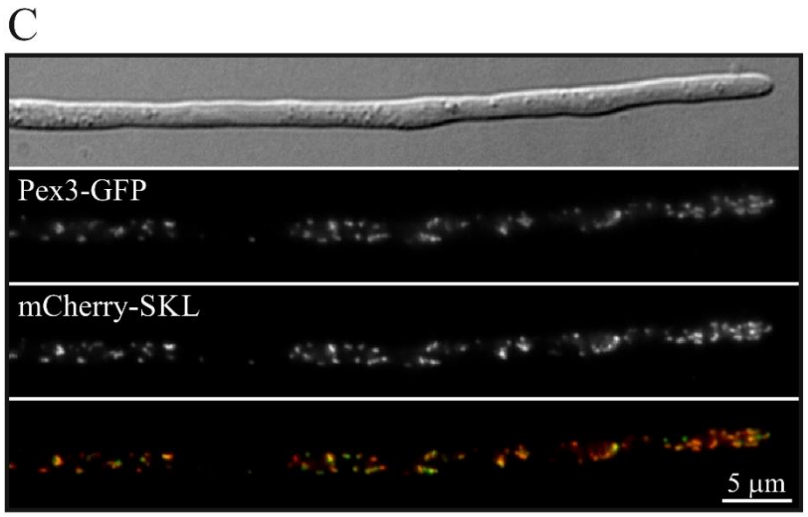

Figure 16 - Peroxisome distribution in *U. maydis*. A) *U. maydis* hyphal organization. The hyphal tip (full blue arrow) grows apically, and vacuolated sections are left behind separated by retraction septa (empty blue arrow). The nucleus is located at the middle of the cell (orange). Bar 10 µm. B) Peroxisome distribution in the hyphal cell. Maximum projection of Z-axis stack. Cell edge indicated in blue. Bar 10 µm C) Hyphal cell expressing mCherry-SKL, and peroxisomal biogenesis factor 3 (Pex3-GFP). Merge image shows co-localization at the peroxisomes. All images were adjusted in brightness, contrast and gamma settings. Bar 5 µm.

The number of peroxisomes in *U. maydis* is more closely related to mammalian cells (many peroxisomes) than with yeast cells (less than 10). By analysing peroxisomal dynamics (streams and kymographs), we could classify three types of motions: long-distance transport, short-range or flickering, and stationary (Figure 17 A), reminiscent with observations in mammalian cells (Huber et al., 1997; Schrader et al., 2000;Ishikawa et al., 2001). A small population of peroxisomes showed directed motility (12.25% ± 1.924) (n=1793 peroxisomes, 25 cells) which is in concordance with mammals (Rapp et al., 1996; Wiemer et al., 1997). Directed motility was considered as an event that occurred with constant velocity, with spatial displacement and with pausing times below 1 s. Therefore, the cut-off for a motile event was of 1.2 µm. In hyphae, peroxisomal mean velocity was calculated as 2.168 ± 0.046 µm/s (n=172 peroxisomes) with an average run length of 6.335 ± 0.29 µm (ranging from 1.255 µm to 56.3084 µm) (Figure 17 B). Peroxisomal motility has been identified as microtubule and/or actin dependent, depending on species. In *U. maydis*, membrane-bound trafficking is regulated by microtubules and F-actin (Wedlich-Soldner et al., 2002a; Lenz et al., 2006; Schuster et al., 2012; Treitschke et al., 2010). In this regard, to identify the cytoskeletal component underlying peroxisomal motility in *U. maydis*, cells were treated with the microtubule depolymerizing drug, benomyl (Davidse and Flach, 1977; Jung et al., 1992), or the actin depolymerizing compound, latrunculin A (Ayscough et al., 1997; Spector et al., 1983). With these reversible drugs, microtubules and actin are fully

depolymerized after 15 minutes (data not shown). Peroxisomal directed motility was not affected when cells were treated with latrunculin A or with the solvent DMSO (control), however, with benomyl this direct motions were completely abolished (Figure 17 C). This implies that peroxisomes move along microtubules *in U. maydis*. To verify this, GFP-SKL was co-labelled with GFP-αTubulin, a microtubule marker. Although microtubules and peroxisomes are both in green (GFP), their distinct morphology clearly allows to distinguish between both. Peroxisomal long-range motility along microtubules could then be confirmed through live cell imaging (Figure 17 D). In conclusion, peroxisomal motility is microtubule-dependent in *U. maydis*, which is reminiscent of animal cells, but distinct from budding yeast and plants where peroxisome motility is actin-based. Thus, *U. maydis* promises to be a valuable model to study the mechanistic and fundamental principles of MT-dependent peroxisome motility

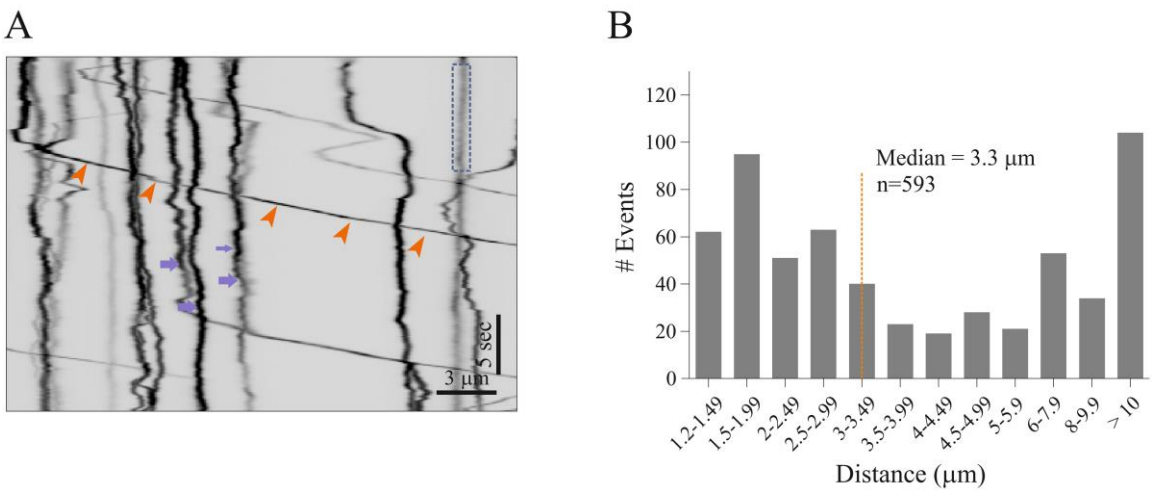

Figure 17 A - Characterization of peroxisome motility in *U. maydis*. A) AB33_GSKL dynamics. Kymograph showing long-distance (orange head arrows), short range (purple arrow) and pausing (grey dashed box) peroxisomes. Image was contrast inverted. Bars, 3 µm, 5 s. B) Analysis of peroxisomal run length in which an event was considered to be over 1.2 µm. 593 events were evaluated exhibiting a median = 3.289 µm and a mean = 6.335 µm.

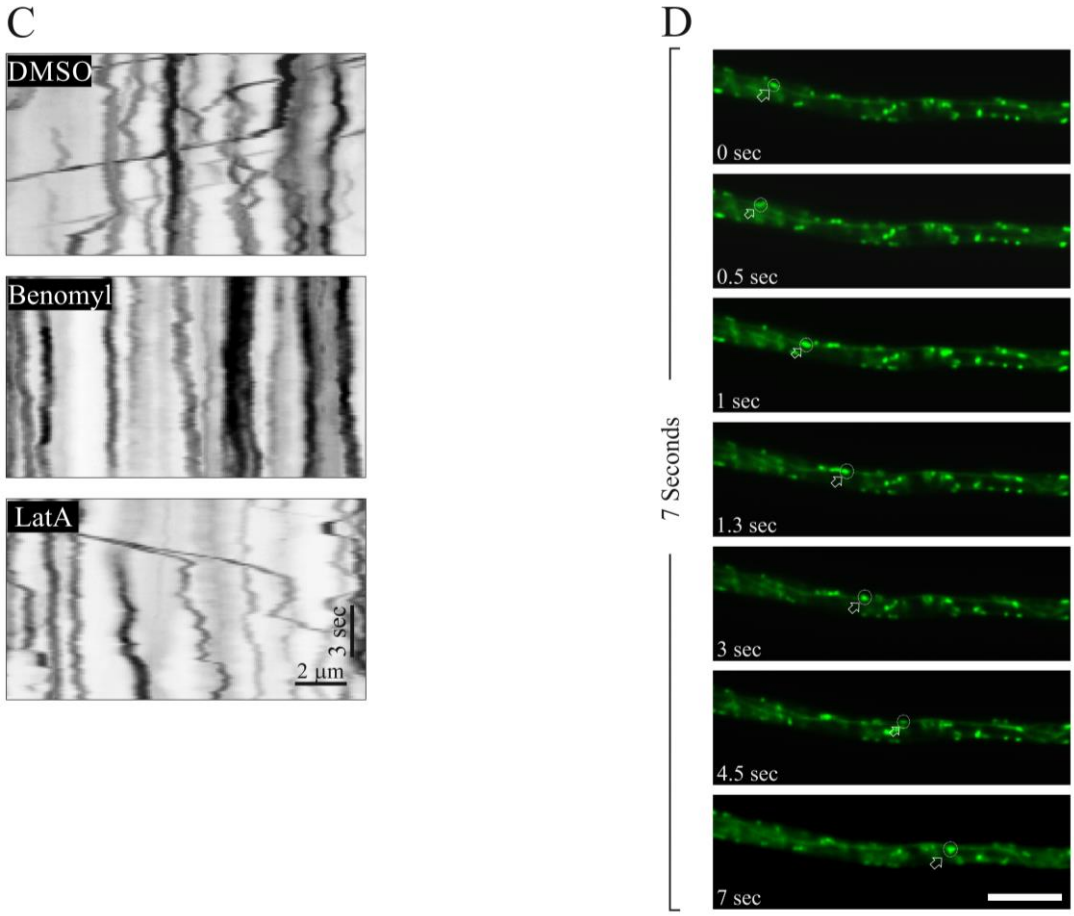

Figure 17 B - Characterization of peroxisome motility in *U. maydis* (continued). C) The AB33_GFP-SKL strain was incubated with the microtubule-depolymerizing drug benomyl, with the actin-depolymerising compound latrunculin A, or DMSO (control). A clear reduction in peroxisome motility was observed when the cells were treated with benomyl, whereas no effect was observed with latrunculin A or DMSO. Images were contrast inverted. Bars, 2 µm, 3 s. D) Motility of peroxisomes along microtubules was observed in AB33GFPTub1_GFP-SKL strain which expresses GFP-α-Tubulin (Tub1) and GFP-SKL. White arrows show the peroxisomal motion over 7 s an image series. Scale bar 5 µm.

5.3.2 Peroxisomal motility in *U. maydis* is regulated by Kinesin-3 and Dynein-2

Microtubule-based organelle transport is regulated by dyneins and kinesins. In *U. maydis* it is known that Kin1, Kin3 and Dyn2 are the key players in organelle long-distance transport (Wedlich-Soldner et al., 2002b; Schuchardt et al., 2005; Fink and Steinberg, 2006; Schuster et al., 2011b; Schuster et al., 2011c;). The *U. maydis* genome encodes 10 kinesins, however, so far only Kin1 and Kin3 are known to mediate microtubule-dependent motility. Whereas Kin5, Kin6 and Kin14 are thought to be implicated in mitosis, and Kin4, Kin7 (a and b), Kin8 and Kin9 are of unknown function. When expressing GFP-SKL in all the deletion mutants (except for Kin6) (data not shown), peroxisome motility was solely impaired in the Kin1 (data not shown) and Kin3 deletion mutants (Figures 18 A-B).

On the other hand, only one dynein (Dyn2) is present in the fungal genome. Dynein 2 deletion in *U. maydis* is not viable, thus, an alternative temperature sensitive mutant was generated (Wedlich-Soldner et al., 2002a). Briefly, a temperature-sensitive allele was integrated into the *dyn2* locus resulting in a strain that allows to shift from active (22ºC) to defective (32ºC) dynein expression. We integrated GFP-SKL in Dyn2^{ts} and found that peroxisome motility was significantly reduced (Figures 18 A-B). Thus, peroxisome motility in *U. maydis* depends on Kin3, Kin1 and Dyn2. *U. maydis* possesses a unipolar and an antipolar region, with the unipolar segment located at the 10-12 μm region behind the cell tip and septa (Lenz et al., 2006; Schuster et al., 2011b) (see Figure 8, Introduction). We have measured motility in the unipolar region for accounting anterograde (towards the plus end) and retrograde (towards the minus end) motility events. No differences in velocity (P=0.290), run length (P=0.3836) or frequency of motile events (P=0.7923) were observed (Figure 18 C). In conclusion, in hyphal cells peroxisome motility is regulated by Kin3 and Dyn2 in a cooperative fashion.

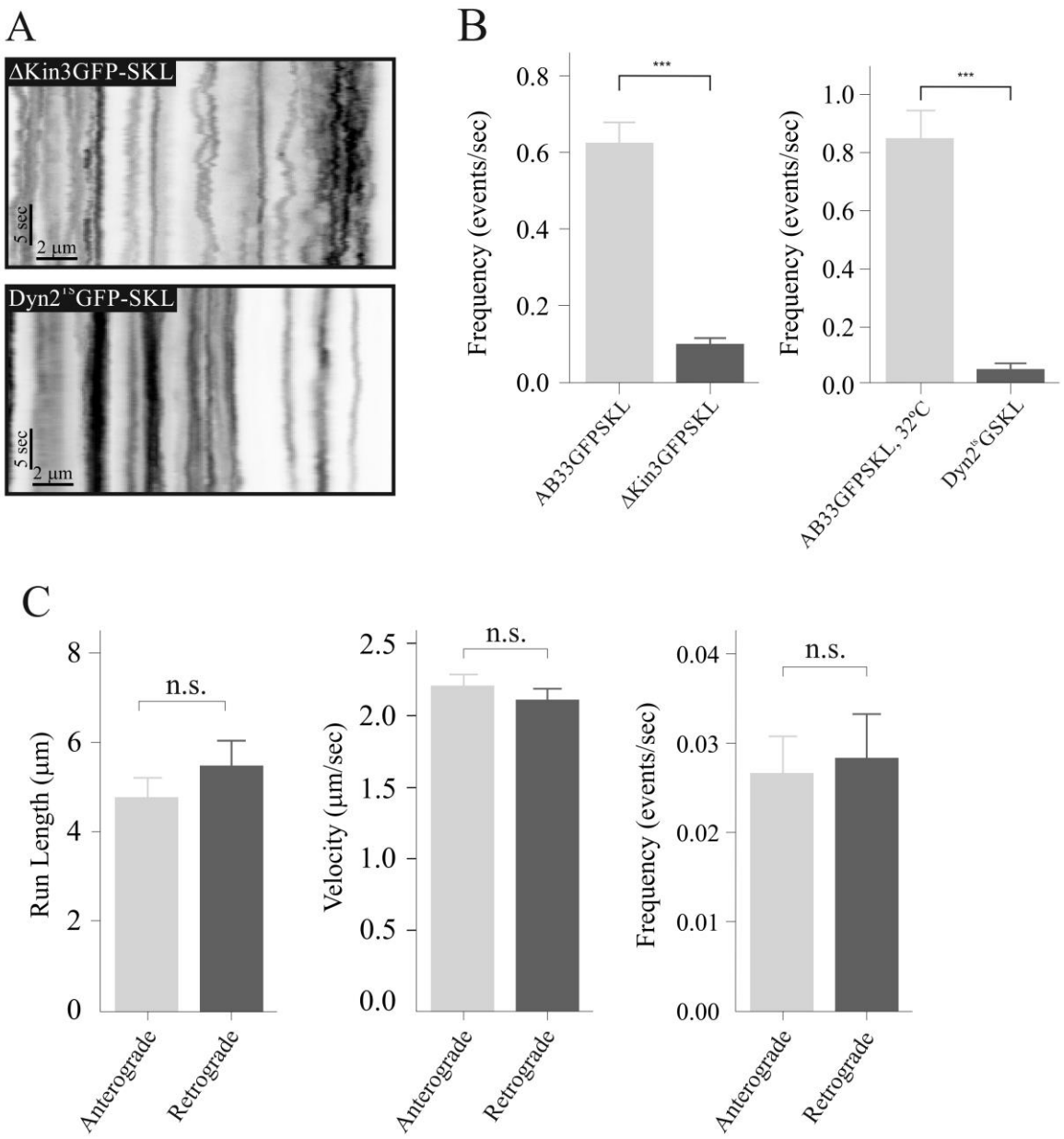

Figure 18 - Peroxisomal motility is regulated by Kin3 and Dyn2 molecular motors.A) Kymograph showing the utterly reduction of peroxisomal motion in *Kin3*-null mutant (Δkin3GSKL) (upper panel) and Dyn2^{ts}_GFP-SKL strain at a restrictive temperature (32ºC) (lower panel). Images were contrast inverted. Bars 5 s, 2 µm. B) Graph showing that peroxisome motility frequency in Δkin3GSKL and Dyn2^{ts}_GFP-SKL is reduced when compared to the control. C) Anterograde and retrograde motility was analysed in a control strain, AB33_GFP-SKL, regarding velocity, run length and motility frequency. No significant differences were observed. Parameters were only analysed in the unipolar region (10-12 µm behind the tip). All bars are given as mean ± SEM (from at least two different experiments. 40 cells for each experiment were analysed. ***, significant difference to control with $P < 0.0001$, n.s., non-significant when compared to the control, using a Student's t test.

5.3.3. Peroxisomes in *U. maydis* hitchhike on early endosomes

To understand in more detail how peroxisomes move with the molecular motor we co-localized Kin3-GFP with the peroxisomal marker mCherry-SKL. Indeed, the two signals travel together (Figure 19 A). However, Kin3 does not localize at the peroxisomes, instead is leading peroxisome motion (Figure 19 A). In *U. maydis*, early endosomes are highly bound to kinesin-3 (Schuster et al., 2011c) and only transiently bind to dynein. Rab5a is a small GTPase that specifically binds to early endosomes (Chavrier et al., 1990), and is widely used as an early endosome marker in *U. maydis* in several studies (Schuster et al., 2011a Bielska et al., 2014a; Bielska et al., 2014b; Higuchi et al., 2014). Work performed in collaboration with Gulay Dagdas in *U. maydis* yeast-like cells showed co-migration peroxisomes with early endosomes (Dagdas, 2015) However, in yeast-like cells directed/long-range motility is not present. Therefore, we have tested if in the hyphal cells, where a long-range motility and unipolar microtubule organization is present, peroxisomes co-migrate with early endosomes. mCherry-SKL was integrated into an AB33_GFP-Rab5 strain and it was observed that early endosomes co-migrate with peroxisomes, however early endosomes lead the peroxisomal motion (Figure 19 B).

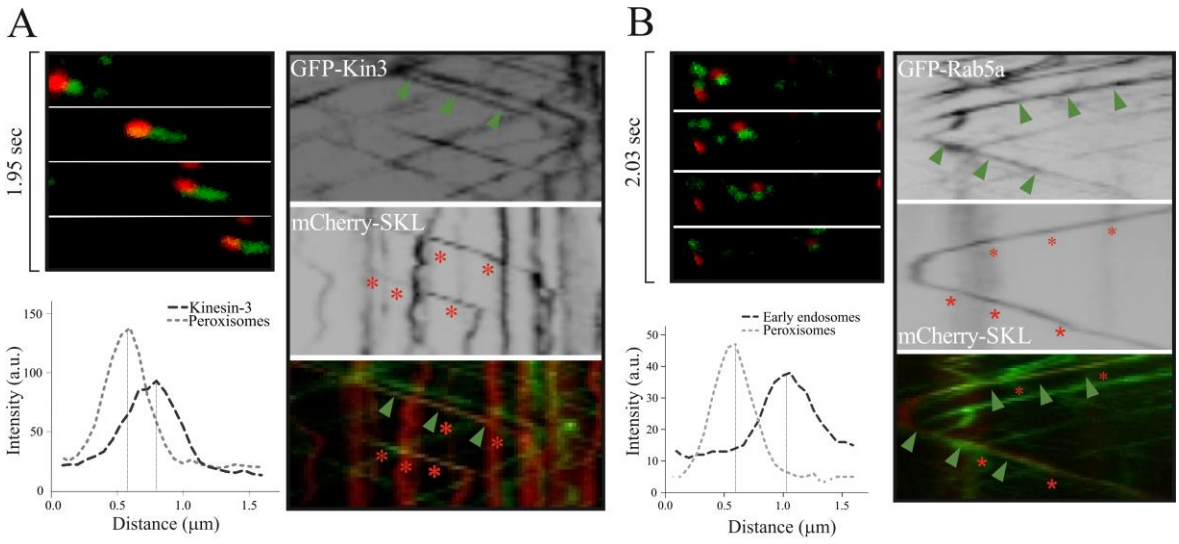

Figure 19 - Early endosomes drive peroxisome motility. A) *Left panel* - Co-motility of a peroxisome (mCherry-SKL, red) with GFP-Kin3 (green). Kin3 leads peroxisomal movement. Image series covers 1.95 s. Linescan over a co-motility shows that Kin3 leads the movement. *Right panel* - Kymographs showing bi-directional co-motility of Kin3 (GFP-Kin3) and peroxisomes (mCherry-SKL). B) *Left panel* - GFP-Rab5a (green) and mCherry-SKL (red) move together but do not overlap. Image series covers 2.03 s. Linescan shows early endosomes pulling the peroxisome *Right panel* - Bi-directional co-motility of early endosomes (GFP-Rab5a, green) and a peroxisomes (mCherry-SKL, red). Kymograph shows a peroxisome being dragged by an early endosome, pauses, and captured by another early endosome moving in the opposite direction. Linescan over a co-motility shows that early endosomes are leading the peroxisomal motility. All images were adjusted in brightness, contrast and gamma settings.

To confirm that peroxisomal motility was early endosome-dependent, we introduced mCherry-SKL into a *Rab5a*-null mutant, which abolishes early endosome motility (Bielska et al., 2014a) and causes a growth defect (short hyphae). Yup1, a t-SNARE protein found at early endosomes, was previously shown to be part of the endocytic pathway (Wedlich-Soldner et al., 2000). In the absence of Rab5, Yup1 (Yup1-GFP) clusters at the cell tip, therefore it was used as an internal control to confirm that early endosomes are immotile. In the *Rab5*-null mutant, AB33ΔRab5-Yup1GFP- mCherry-SKL, peroxisome motility was highly diminished when compared to the control (AB33-mCherry-SKL) (Figure 20 A-B). Yup1 is located at the early endosome membrane and is thought to cause fusion defects. Inactivation of Yup1 leads to a diminishment in early endosome number and motility. We have expressed GFP-SKL in AB33_Yup1^{ts}, a temperature sensitive mutant in which the *yup1* allele is inactivated after 5 hours at 34ºC (Higuchi et al., 2014). We incubated the AB33Yup1^{ts}-GFP-SKL over 5 hours at 34ºC and observed that early endosome and peroxisomal motility was reduced (Figure 20 C-D). Controls were performed at 34ºC for 5-6 hours, both for AB33_GFP-SKL and AB33_Yup1^{ts}_GFP-Rab5. AB33_GFP-SKL was used as a control for peroxisome motility at higher temperatures, and AB33_Yup1^{ts}_GFP-Rab5 to confirm that the *yup1* allele was inactive after 5 hours with subsequently diminishing early endosome motility. The peroxisomal control at higher temperatures showed an increase of events when compared to experiments performed at 28ºC (usual protocol). This enhancement could be explained by a stress response, in this case to higher temperatures. Increased motility in response to oxidative stress was previously described in *A. thaliana* (Rodriguez-Serrano et al., 2009). We can conclude that peroxisome motility is diminished when: 1) early endosome motility is abolished: *i)* in *Rab5a* null mutants and ii) in a ΔKin3 mutant; and 2) early endosome motility is reduced in *yup1^{ts}* mutants, with reduced numbers of early endosomes due to membrane fusion defects. Together these results reinforce the conclusion that early endosomes support long-distance transport of peroxisomes.

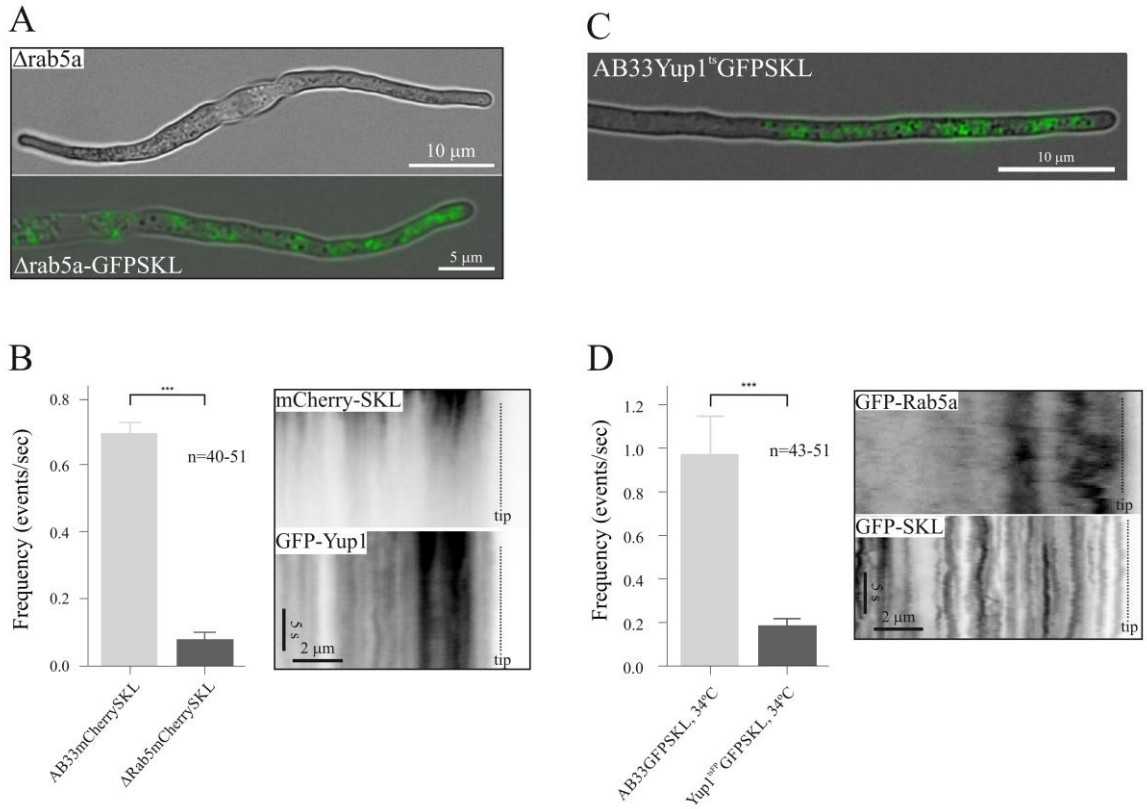

Figure 20 - Peroxisome motility is early endosome-dependent. A) *Upper panel:* Brightfield image of AB33ΔRab5a morphological defects with formation of bipolar short hyphae, where early endosome motility is impaired. Scale bar, 10 µm. *Lower panel:* Peroxisome (GFP-SKL) distribution in *Rab5* null strains. Peroxisomes cluster at the plus end. Scale bar 5 µm. B) *Left panel:* Frequency of peroxisome motility is significantly reduced in AB33ΔRab5a_GFP-Yup1-mCherrySKL (ΔRab5mCherrySKL) when compared to the control (AB33GFP-Yup1-mCherrySKL). *Right panel:* Kymographs show peroxisome motility (mCherry-SKL) is highly reduced in the Δrab5 strain. Early endosomes labelled with GFP-Yup1 are immotile. Bars, 5 µm, 2 s. Images were contrast inverted. Bars 5 s, 2 µm C) Peroxisome distribution in the endosomal t-SNARE Yup1 (AB33Yup1^{ts}) strain, after 5-6 h at restrictive temperature (34°C). Peroxisomes shift towards the hyphal tip. Scale bar, 10 µm D) *Left panel:* Frequency of peroxisome motility in control cells and temperature-sensitive mutants. Peroxisome motility is significantly reduced when compared to the control. *Right panel.* Kymograph shows that early endosome motility is highly reduced, as well the peroxisomal, in Yup1^{ts} background. Image was contrast inverted. All images were adjusted in brightness, contrast and gamma settings. All bars are given as mean ± SEM (error bars) from at least two different experiments. Sample size is indicated. ***, significant difference to control at $P < 0.0001$ using a Student's t test. Scale bar, 10 µm.

5.3.4Targeting of truncated Hok1 proteins restores peroxisomes motility

Hok1 is a protein that was first discovered in an early endosome motility screening (Bielska et al., 2014b). Impaired growth of *U. maydis* has been linked to an early endosome motility defect. Fast and polarized tip growth requires: synthesis and extension of the cell wall; delivery of secretory vesicles; and endocytosis, specifically, recycling of membrane proteins and lipids. Therefore, when early endosomes are disrupted, hyphal growth is affected. Hence, in ΔRab5a and ΔKin3 strains, where early endosome motility is highly impaired,

hyphal growth is deficient, resulting in a bipolar hyphae. Hok1 was identified as an adaptor protein for Dyn2 and Kin3 at early endosomes. In *Hok1* null cells, early endosomes accumulate at the cell tip, similar to what occurs when dynein is inactivated, where dynein cannot travel towards the microtubule minus end. It was shown that Hok1 does not affect dynein motility, but instead the binding of dynein to early endosomes, and therefore disables minus end-directed transport. Recently, Zhang et al. (2014) showed that in *A. nidulans* deletion of Hok1 homologue (HookA) alters peroxisomal distributions. Hence we hypothesised that Hok1 in *U. maydis* would link peroxisomes to Kin3. We have inserted GFP-SKL into a *Hok1* null strain and observed that peroxisome motility was abolished. In concordance with the previous observations in *A. nidulans*, peroxisomes cluster at the cell apex (Figure 21 C). Co-migration studies of peroxisomes (mCherry-SKL) and Hok1 (GFP-Hok1) revealed that peroxisomes and Hok1 travel together, although Hok1 leads the movement (Figure 21 A-B).

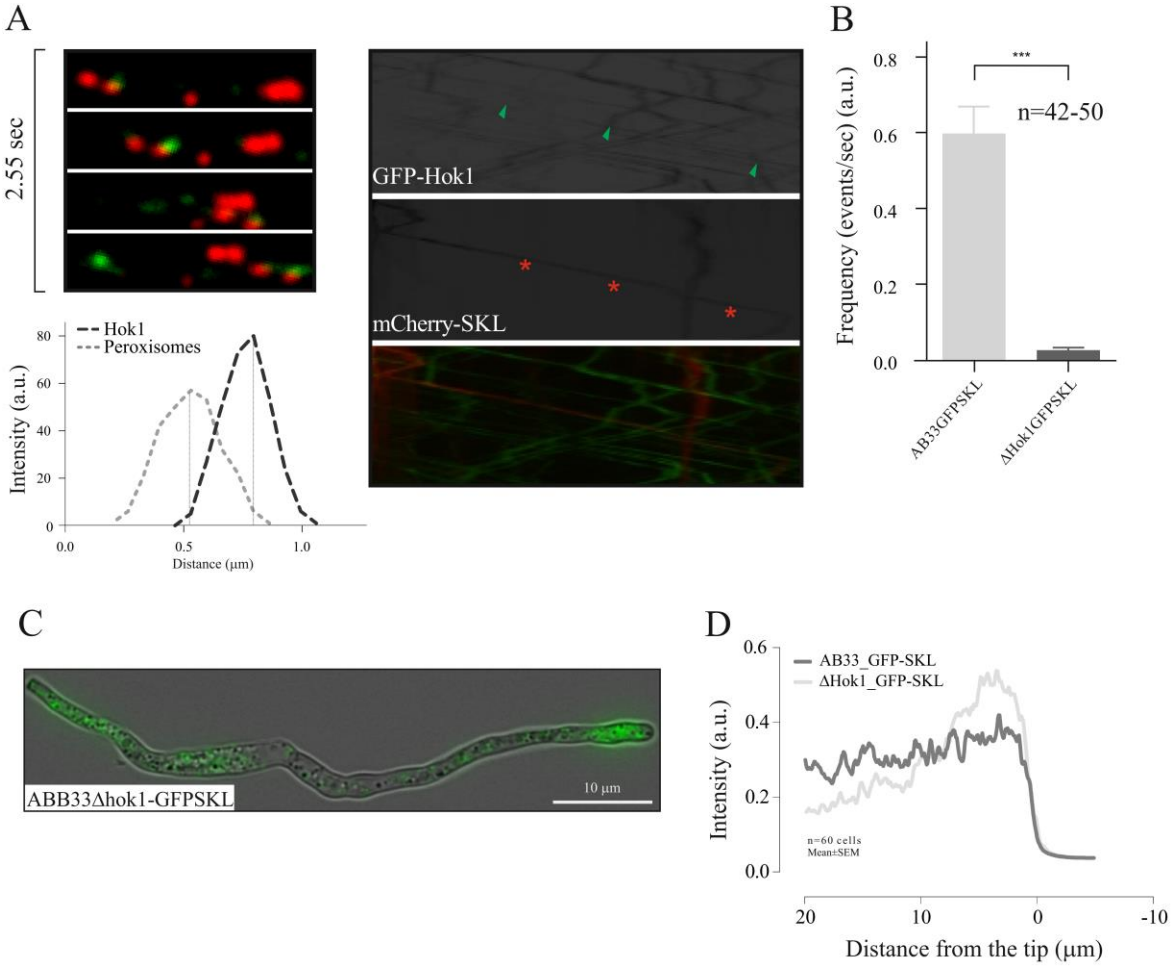

Figure 21 - Peroxisome motility is impaired in a *Hok1* null mutant. A) *Left panel* - GFP-Hok1 motor adaptor protein travels together with peroxisomes. Image series covers 2.55 s. Linescan confirms that Hok1

leads the movement. *Right panel* – Co-motility of GFP-Hok1 with a peroxisome (mCherry-SKL). B) Frequency of peroxisome motility in control cells (AB33-GFP-SKL) and AB33ΔHok1_GFPSKL. A dramatic decrease in peroxisome motility was observed. C) Deletion of Hok1 leads to bipolar hyphae with clustering of peroxisomes at the cell tip. D) Intensity profiles, over a length of 20 µm behind the tip and 5 µm outside of the hyphal cell, show that peroxisomes cluster in ΔHok1 cells. Profiles are given in mean. Sample size of 60 cells of three independent experiments.

Bielska et al. (2014b) determined that the N-terminal region of Hok1 is crucial for microtubule binding, whereas the C-terminal attaches to the early endosomes. Hence, by using a plasmid deleted in the C-term region, in a *Hoκ1* depleted background [ΔHok1_Hok1ΔC_GFP-Rab5_mChSKL (ΔHok1-ΔC)] we clearly observed a reduction in peroxisomal and early endosomes flux (Figure 22 A-B). Early endosomes are enriched in the lipid phosphatidylinositol 3-phosphate (PtdINs(3)P) (Gilooly 2000). The Phox (PX) domain binds to PtdINs(3)P-enriched membranes. The Rab5a-carrying organelles bind to the Yup1PX domain, which suggests that they are enriched in PtdINs(3)P. Therefore, the PX domain was fused to the plasmid Hok1ΔC (Hok1ΔC-PX) and integrated in ΔHok1_GFP-Rab5_mChSKL, resulting in ΔHok1_Hok1ΔC-PX_GFP-Rab5_mChSKL (ΔHok1-ΔC-PX). In this mutant, early endosome motility and hyphal growth were partially restored, overcoming bipolar growth (Bielska et al., 2014b) (Figure 22 A-C). In concordance, peroxisome motility was also re-established (Figure 22 A and C). Moreover, alterations in peroxisomal distribution were also re-established with the introduction of ΔHok1-ΔC-PX (Figure 22 B).

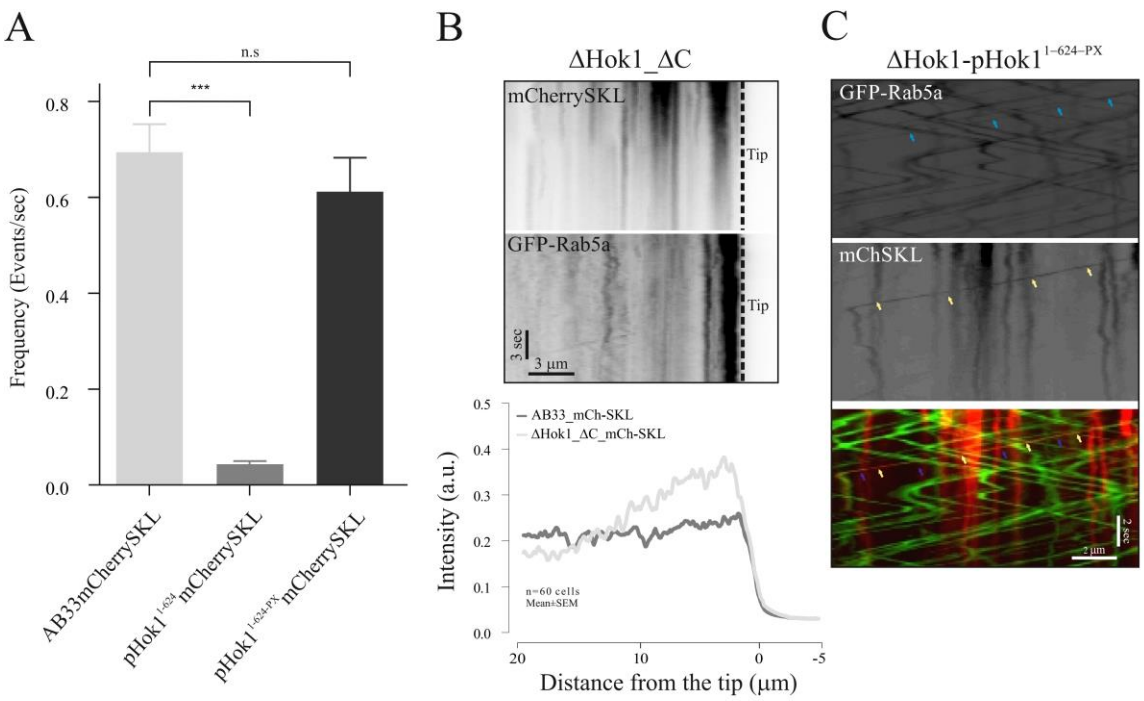

Figure 22 - Targeting truncated Hok1 protein to early endosome-specific lipids restored peroxisome motility. A) Peroxisome motility is highly reduced in a ΔHok1-ΔC when compared to the control (***). When cells express phox domain (ΔHok1-ΔC-PX) peroxisome motility is recovered. B) Kymographs show absence of motility of early endosomes (GFP-Rab5a) and peroxisomes (mCherry-SKL) in ΔHok1-ΔC mutants. In the lower panel, a linescan shows that peroxisomes cluster at the cell tip, as visualized in ΔHok1. C) By adding a phox domain to Hok1ΔC (Hok1ΔC-PX) early endosome and peroxisome motility were restored. Images were contrast inverted. All images were adjusted in brightness, contrast and gamma settings. All bars are given as mean ± SEM (error bars) from three different experiments. Sample size is indicated. ***, significant difference to control at $P < 0.001$; n.s., non-significant when compared to the control, using a Student's t test.

Thus far, it has become clear that peroxisomes transiently bind to moving early endosomes. Previous work has described a similar mechanism for poly-ribosomes in *U. maydis* (Higuchi et al., 2014), in which an RNA-binding protein, Rrm4, anchors the poly-ribosomes to the motile early endosomes. In *Rrm4* null mutants, early endosome motility is not altered, however poly-ribosome are immotile. We have integrated mCherry-SKL into AB33ΔRrm4-GFP-Rab5a and found that peroxisomes still move (Figure 23 A-B), thus Rrm4 does not seem to be the linker between peroxisomes and early endosomes. Furthermore, the *Rrm4* null strain also shows bipolar growth, morphological defected observed in ΔKin3, ΔHok1 and ΔRab5a strains. So, by observing that peroxisome motility was unaffected, we can exclude the possibility that impaired peroxisome motility is an artefact of bipolar hyphal growth. In summary, peroxisome motility is diminished in ΔHok1 strains, however, when early endosome motility is re-established (Hok1ΔC-PX), the peroxisomal motility is

recovered. Furthermore, neither Rrm4 nor Hok1 seem to be the linkers between peroxisomes and early endosomes.

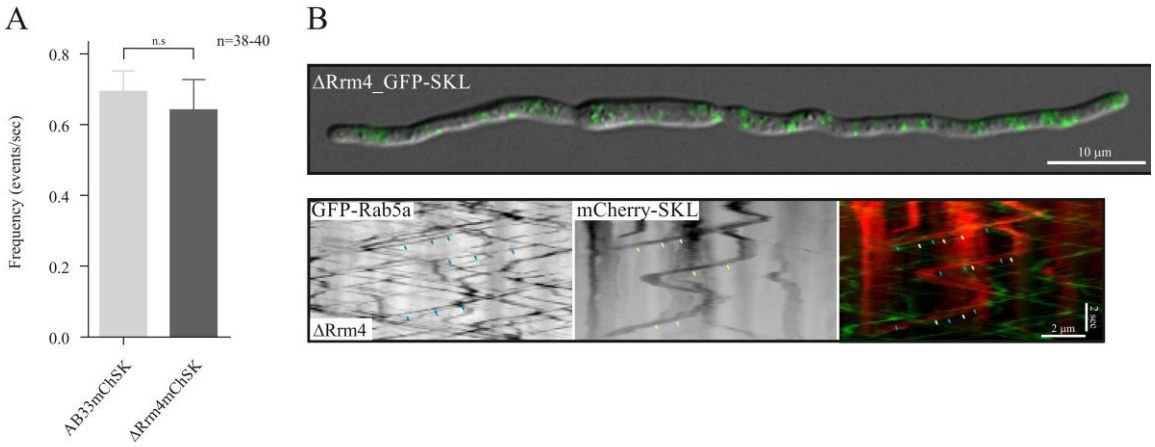

Figure 23 - Peroxisome motility in ΔRrm4 mutants. A) ΔRrm4GFP-Rab5_mCherrySKL shows no significant difference in peroxisome motility when compared to the control. B) *Upper panel.* Rrm4 deletion results in bipolar growth with short hyphae. Scale bar, 10 µm. *Lower panel.* Co-motility of early endosomes (GFP-Rab5a) and peroxisomes (mCherry-SKL) is observed. Bars, 2µm, 2 s. All bars are given as mean ± SEM (error bars) from at least two different experiments. All images were adjusted in brightness, contrast and gamma settings. Sample size is indicated. n.s., non-significant when compared to the control, using a Student's t test.

5.2.4 Lipid droplets and ER, but not mitochondria, hitchhike on early endosomes

We next asked if early endosome-mediated motility supports organelles other than peroxisomes. We set out to study lipid droplet dynamics in *U. maydis.* Labelling of lipid droplets was previously established in our lab using the Erg6 protein. Erg6 is a Δ24 sterol methyltransferase which is established as a lipid droplet marker in fungi (Leber et al., 1994) We have used GFP-labelled Erg6 to visualize lipid droplets in *U. maydis* by integrating it into the AB33 strain. The organelles were scattered throughout the cell and exhibited different phenotypes, ranging from clusters – honey comb-like – to punctuated structures (Figure 24 A). Most of the lipid droplets showed short range motility, where 8.1% ± 1.1 (n=40 cells) showed long-range bi-directional motility (Figure 24 C), which was blocked when the cells were treated with benomyl (Figure 24 B-C). To investigate the existence of a similar motility mechanism of peroxisomes, we have integrated GFP-Erg6 in an AB33ΔHok1 strain. We observed a reduction of lipid droplets motility when compared to the control. Moreover, cluster formation at the cell apex was observed, as it occurred with peroxisomes (Figure 24 D). Previous work from our laboratory suggested that lipid droplets are exclusively hitchhiking on early endosomes. Nonetheless, motility analysis in ΔHok1

strains revealed a different mechanism, since lipid droplets motility was not fully abolished. In order to gain more insight, co-localization experiments with GFP-Erg6 and mCherry-Rab5a were performed and showed that the two organelles co-migrate. Though, not all lipid droplets move together with early endosomes (72 % ± 0.7, n=30 cells). We can conclude that while the majority of lipid droplets move on motile early endosomes, a different mechanism might be involved.

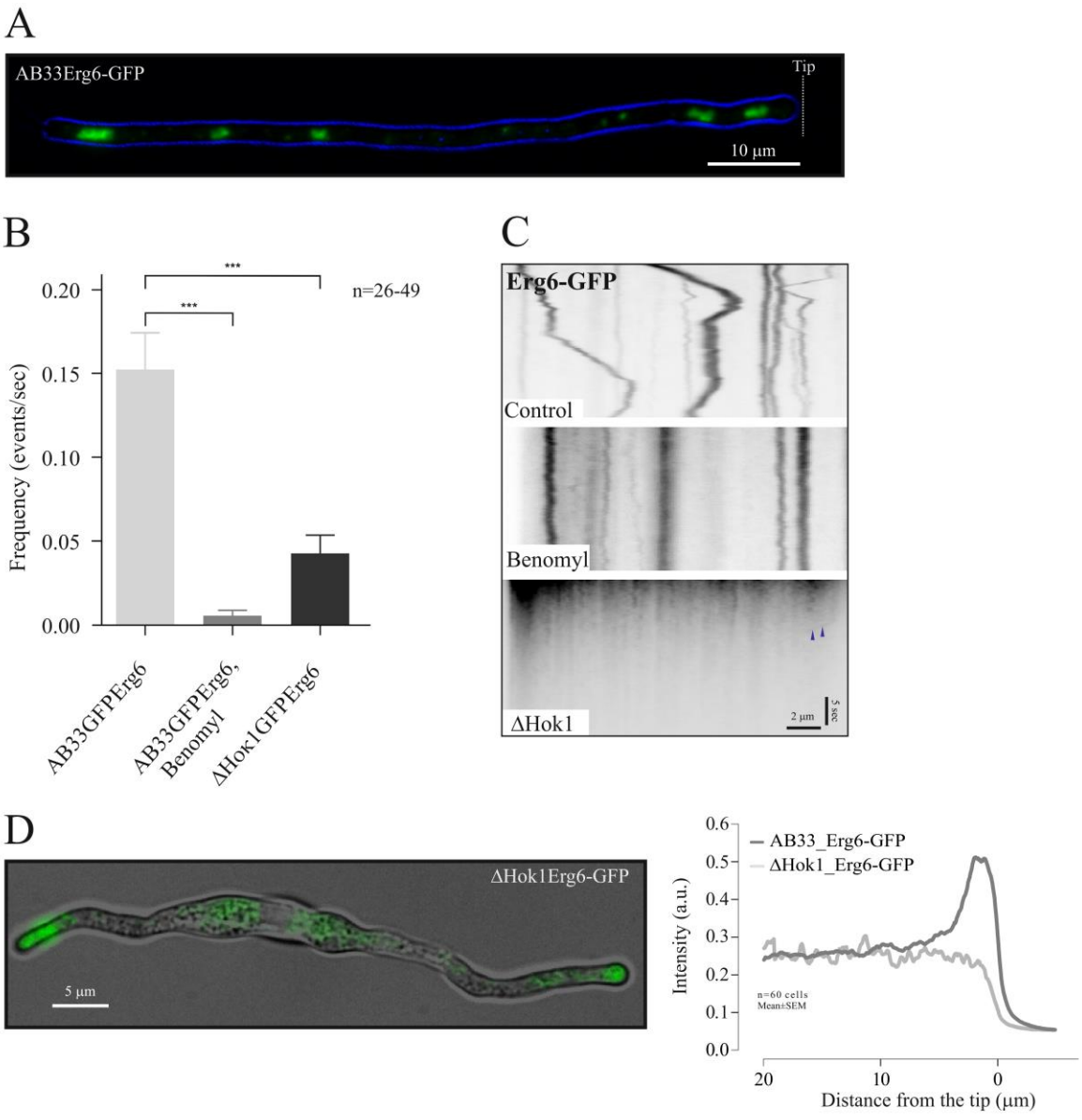

Figure 24 A - Lipid droplets motility is early endosome assisted. A) Lipid droplet distribution throughout the cell, labelled with Erg6-GFP. Cell edge indicated in blue. Scale bar, 10 µm B) Graphs showing the significant decrease of frequency of moving lipid droplets under microtubule-depolymerizing conditions and in a *hok1* null mutant. C) Kymographs show the dynamic behaviour of lipid droplets. *Upper panel*: shows lipid

droplet motility in wild type conditions (AB33-Erg6-GFP); *middle panel* when treated with benomyl and lower panel in AB33ΔHok1-Erg6-GFP. Note that lipid droplet mobility is reduced in a *Hok1* null mutant, although with few events occurring (purple arrowheads). D) *Left:* Lipid droplet distribution in control and ΔHok1 mutant, overlay image. Scale bar, 5 µm. *Right:* Intensity profile 20 µm behind the tip shows that lipid droplets cluster at the plus-end.

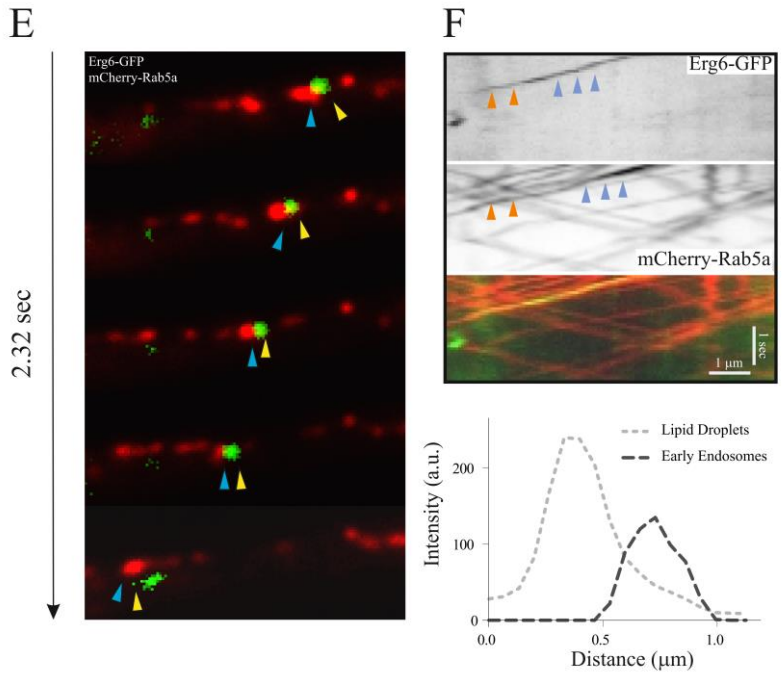

Figure 24.B - Lipid droplets motility is early endosome assisted (continued) E) Image series covers 2.32 s showing Erg6-GFP (yellow arrowhead) dragged by an early endosome (mCherry-Rab5a) (blue arrowhead. F) Co-motility of early endosomes (mCherry-Rab5a) and lipid droplets (Erg6-GFP). Linescan over one event clearly shows that lipid droplets are moved by the early endosome, as observed for peroxisomes. Kymographs were contrast inverted. All images were adjusted in brightness, contrast and gamma settings. All bars are given as mean ± SEM (error bars) from at least two different experiments. Sample size is indicated. ***, significant difference to control at $P < 0.0001$ using a Student's t test.

We next set to determine if mitochondria share the same type of mechanism as observed for peroxisomes in *U. maydis*. We labelled the mitochondrial protein Lga2 (Bortfeld et al., 2004) with GFP and observed that mitochondria are distributed along the length of the cell (Figure 25 A). However, in contrast to mammalian cells, where they can be highly motile, mitochondria in *U. maydis* show short-range, but not frequent directed motility (Figure 25 B), which when present, was of short length. The AB33-Lga2-GFP strain, when treated with benomyl, showed no difference in the scarce motile events. However, to further confirm that mitochondria behaves differently from peroxisomes and lipid droplets, Lga2-GFP was introduced into a ΔHok1 strain. Expectedly, no significant alteration on mitochondrial flux was registered. Interestingly, the distribution seems to be slightly altered, with a cluster forming at the nuclear region. In co-localization experiments with Rab5a (AB33Lga2-GFP_mCherry-Rab5a), co-migration events were not visualised, though, close interactions

between the two organelles occurred (Figure 25 E-F). Altogether, our data suggest that mitochondrial motility in *U. maydis* is early endosomes-independent.

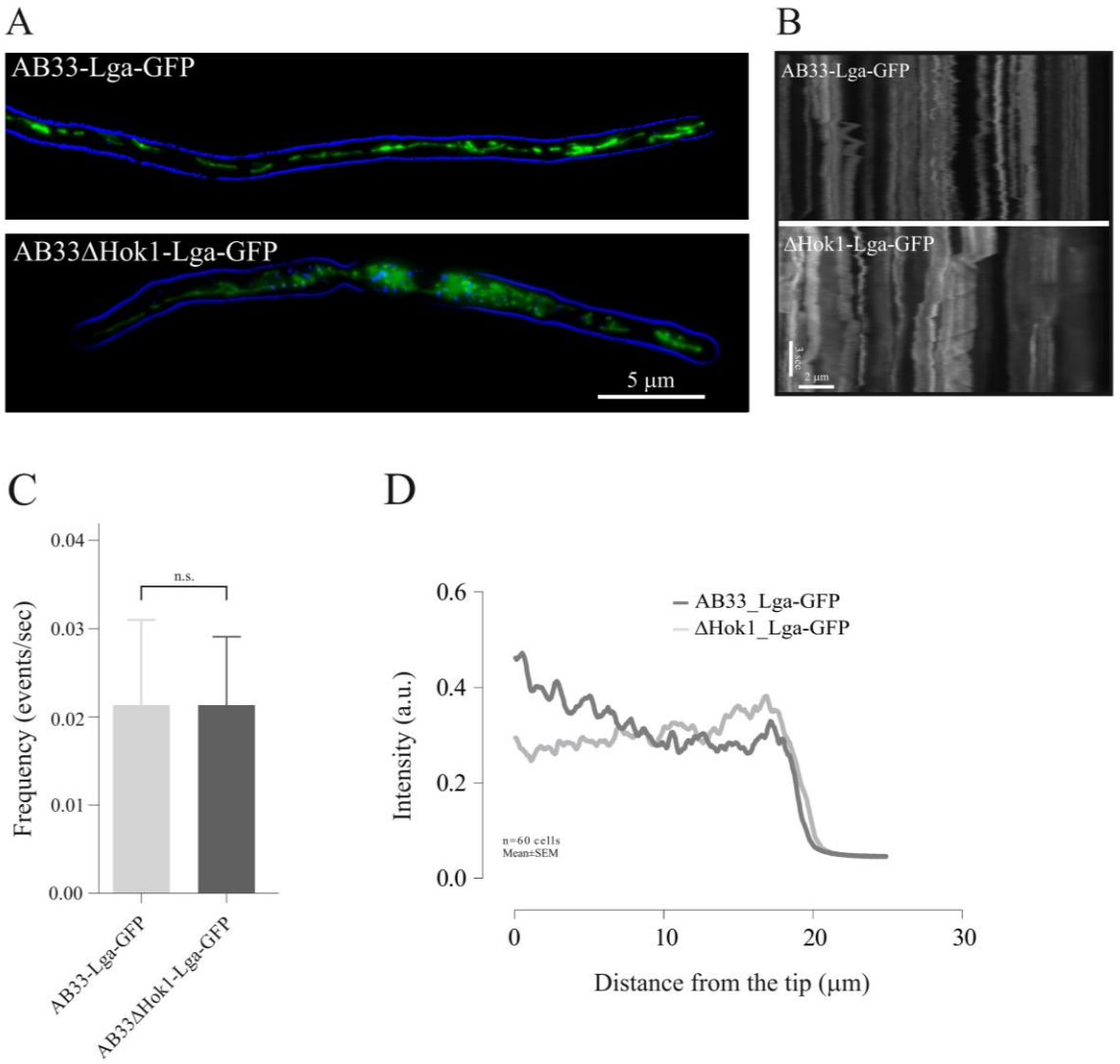

Figure 25 - Mitochondrial motility dynamics in *U. maydis.* A) *Upper panel:* Distribution of mitochondria, labelled with Lga2-GFP, in *U. maydis*. Mitochondria are evenly distributed throughout the cytoplasm. *Lower panel:* Mitochondria distribution in ΔHok1 shows that mitochondria do not cluster at the cell tip but slight clustering at the minus end is observed. Cell edge indicated in blue. Scale bar, 5 µm B) Kymographs show low frequency of motile events of mitochondria which is comparable to wild type cells and *Hok1* null cells. C) Mitochondria motility frequency is low and is not altered between the control and *Hok1* null mutant. D) Intensity profiles of mitochondria in control and ΔHok1. E) Image series of mitochondria (Lga2-GFP) and early endosomes (mCherry-Rab5) show that mitochondrial motility is independent of early endosomes. In fact, the two organelles travel in opposite direction E) Kymograph shows that early endosomes (blue asterisk) and mitochondria have independent motion although there are interactions between the two organelles (dashed line). All images were adjusted in brightness, contrast and gamma settings. Sample size is indicated. n.s, no significant difference to control using a Student's t test.

Lastly, we studied the ER as it is known to interact with lipid droplets and peroxisomes during biogenesis lipid metabolism (Barbosa et al., 2015; Shai et al., 2016). Furthermore, it was recently shown that the ER interacts with early endosomes during their maturation (Friedman et al., 2013). Therefore, the ER could potentially mediate peroxisome and lipid droplet motility driven by the early endosomes. The ER in *U. maydis* presents as a reticular and tubular structure evenly distributed throughout the cell (Figure 26 A). It is a highly dynamic compartment with constant tubular-reticular motion and tubular extensions. We have used HDEL, an ER targeting sequence, fused to GFP to observe the ER dynamics in *U. maydis* (Wedlich-Söldner et al., 2002a). We expressed HDEL-GFP in a *Hok1* null mutant. The frequency of the ER motile events was highly reduced, which implies early endosome-dependent transport. To confirm it, we co-localized early endosomes (mCherry-Rab5a) with the HDEL-GFP revealing that the majority of the ER tubules were pulled by the early endosomes (90.2%±0.68, n=30 cells). However, the ER distribution was slightly affected in ΔHok1 cells as clustering near the nucleus was observed. In conclusion, we have shown that in *U. maydis* peroxisomes, lipid droplets and the ER share a common mobility mechanism.

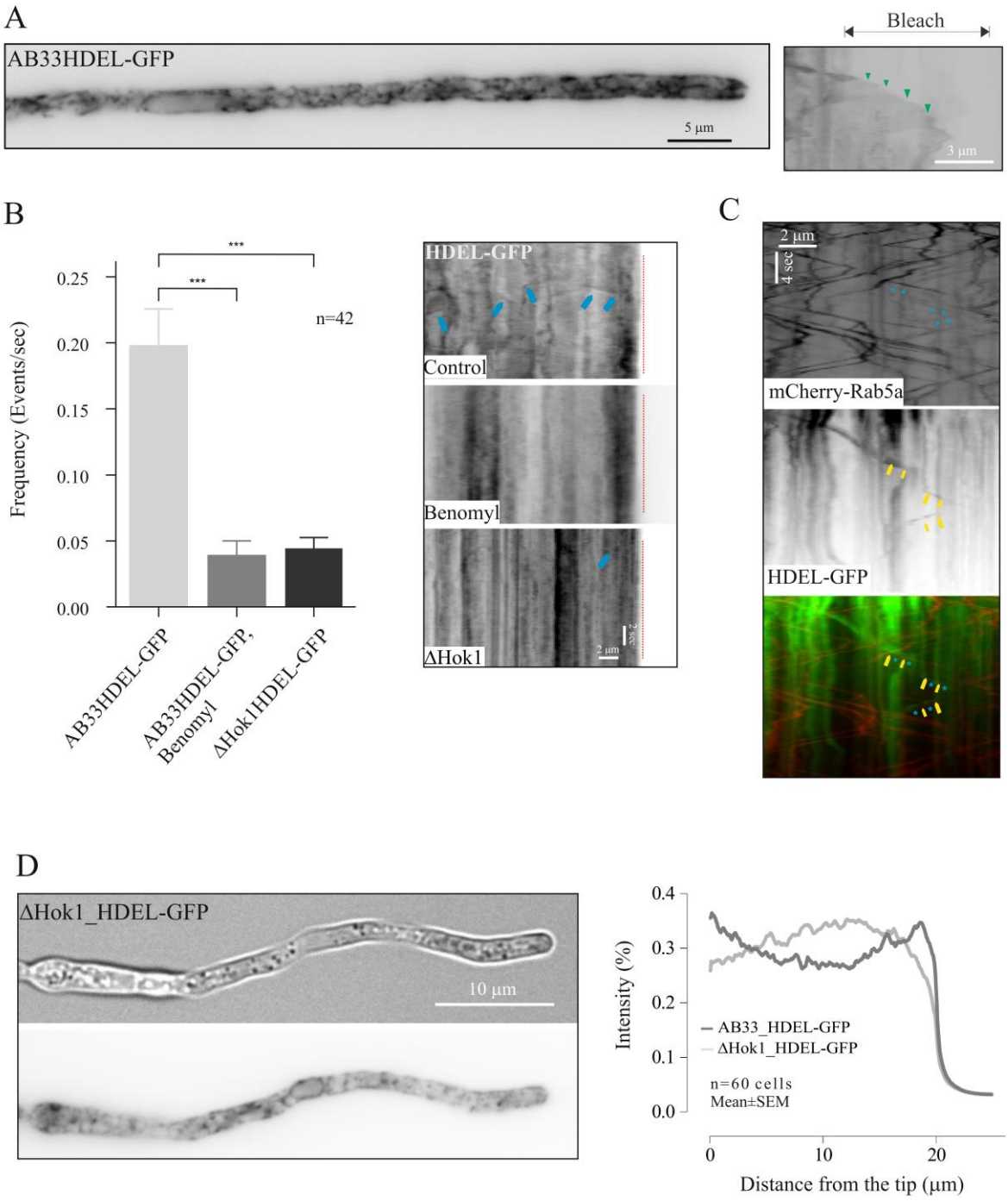

Figure 26 - ER motility depends on early endosome. A) HDEL, an ER targeting signal, tagged with eGFP (HDEL-GFP) shows the reticular structure of the ER in *U. maydis.* Bar, 10 µm. Here, due to highly dynamic behaviour, we bleached 5 µm of the cell and observed the recovery of the ER. Image was contrast inverted. Bar 3 µm. B) Frequency of motility events shown under control conditions (DMSO), microtubule-depolymerization (benomyl) and in a *Hok1* null mutant (ΔHok1). Kymograph shows that motility under depolymerizing conditions (benomyl, middle panel) and in a *Hok1* null mutant (lower panel) are diminished when compared to the control (upper panel). C) Co-motility of early endosomes (mCherryRab5) with the ER (HDEL-GFP).Early endosome pull the ER tubule. D) The ER distribution is not highly affected when Hok1 is deleted. Intensity profiles show a slight difference in the distribution, however this is not statistically significant. All bars are given as mean ± SEM (error bars) from at least two different experiments. Sample size is indicated. ***, significant difference to control at $P < 0.0001$ using a Student's t test.

It has been well described that the ER form contact sites with organelles such as peroxisomes, mitochondria, and endosomes (English and Voeltz, 2013; Phillips and Voeltz, 2016). Therefore, we wanted to exclude the possibility that the ER is linking early endosome motility to other organelles. Thus, co-motility experiments were perform. We co-labelled the ER and either lipid droplets or peroxisomes. By analysing the co-motile events, we observed that peroxisomes move mostly independently of the ER (87.5% ± 2.06, 64 events, 30 cells). However, lipid droplets showed that while a majority of events occurred independently (63.4% ± 2.4, 93 events, 30 cells), still a moderate number (36.6 ± 1.01, 93 events, 30 cells) was dependent on the ER. This likely accounts for the number of lipid droplets that move independently of the early endosomes. Suggesting that lipid droplets motility is mediated both by early endosomes and the ER. Due to their functional proximity, we hypothesised that the ER could mediate the transport of both lipid droplets and peroxisomes. However, the lack of an appropriate third fluorescent marker only allowed us to verify solely peroxisomal and lipid droplets co-motility. By labelling both organelles (Erg6-GFP and mCherry-SKL) we verified that peroxisomes and lipid droplets, although interacting, do not travel together (99.6% ± 0.39, 30 cells) (Figure 27 B, left panel). In summary, peroxisomes and lipid droplet motility is mostly mediated by early endosomes. However, the ER seems to account for the early endosome-independent motility events of the lipid droplets and peroxisomes.

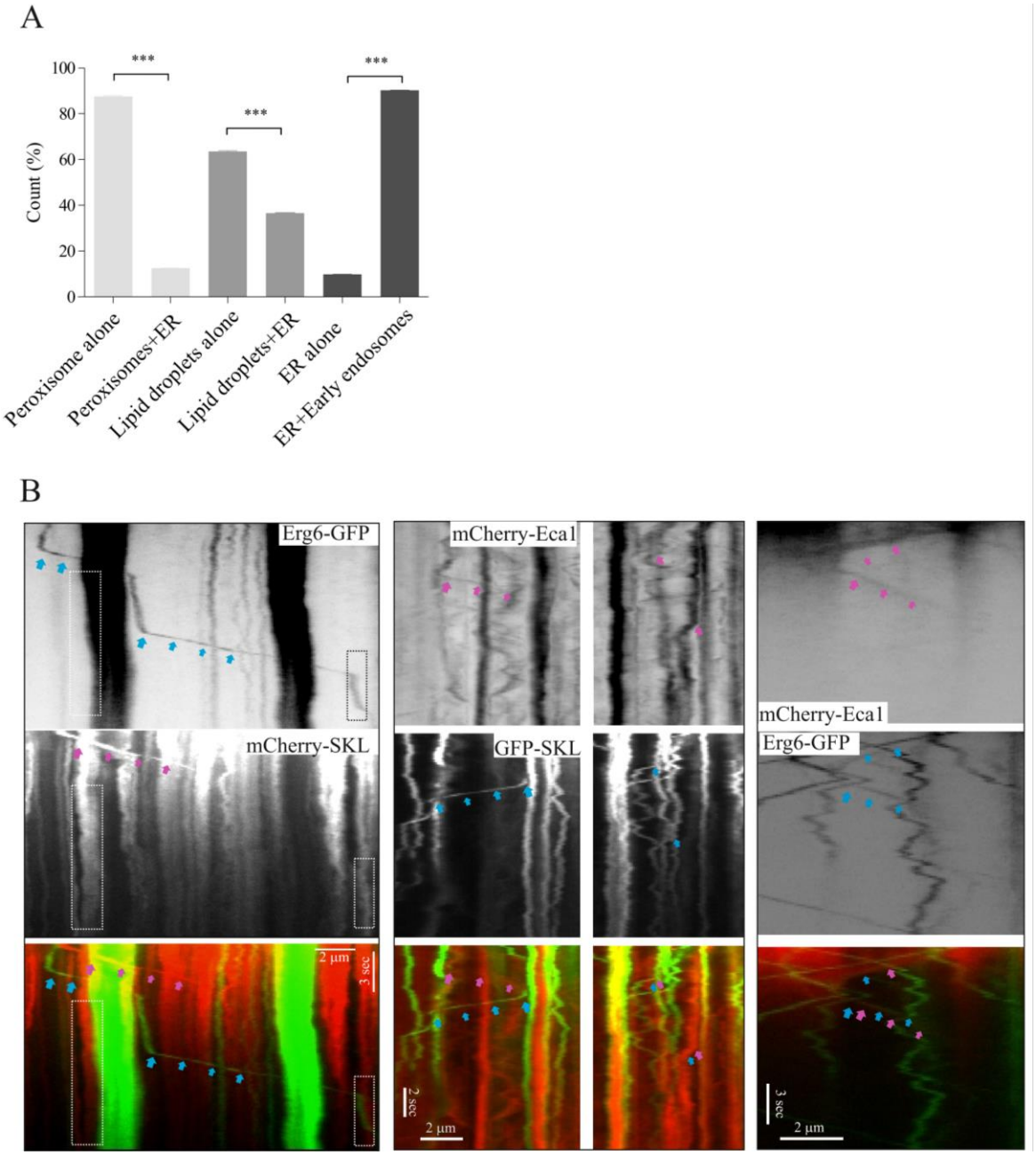

Figure 27 - The ER accounts for the peroxisome and lipid droplets-independent motility A) Graph shows that peroxisomes and lipid droplets are partially driven by the ER. Moreover, a small portion of the ER moves independently of the early endosomes, possibly accounting for the early endosomes-independent peroxisome and lipid droplet movements. 30 cells from three different experiments were analysed. ***, significant difference to control at $P < 0.0001$ using a Student's t test. B) *Left panel:* Kymographs show that peroxisomes (pink arrow) and lipid droplets (blue arrow) do not travel together, however frequent interactions are present (dashed light grey box). *Centre panel:* Within the same cell we can visualise ER (pink arrow) and peroxisomes (blue arrowhead)-dependent and -independent motions. Bar 2 s, 2 µm. *Right panel*: Lipid droplets (blue arrows) moved by the ER (pink arrows). Bars, 2 µm, 3 s.

5.3 Discussion

Organelle motility remains a challenge to unravel, as much is still a mystery. One of the core issues is to extrapolate from *in vitro* assays, where we have single motors, to *in vivo* experiments where multiple motors carry one single cargo. In this regard, the use of a simple organism, yet close to the mammalian system would be pivotal. We have used *U. maydis* as it is a filamentous fungus that constitutes a suitable cellular and molecular biology model. Although not phylogenetically close to *H. sapiens*, its complete genome sequencing has revealed that *U. maydis* shares more predicted proteins with *H. sapiens* than with the budding yeast, *S. cerevisiae*. Furthermore, contrarily to other yeasts and fungi, it possesses open mitosis, microtubule organization, microtubule-based long distance organelle transport and DNA repair mechanisms similar to mammals (Steinberg and Perez-Martin, 2008). These similarities together with the available and specific molecular and cell biology tools and live-cell imaging techniques reinforce its use as a model organism. We set to study peroxisomal motility in *U. maydis* as it presents interesting similarities with the mammalian model. Moreover, the comparisons between the hyphal cell and neurons might be of crucial importance to understand neurological diseases caused by axonal transport impairments. In *U. maydis* hyphal cells we observed, *in vivo*, three types of peroxisomal motilities: long-distance motility; short range/oscillatory; and resting, which is in concordance with other systems such as mammals (Ishikawa et al., 2001; Schrader et al., 1996), plants (Mathur et al., 2002), *D. melanogaster* (Kim et al., 2007) and fission yeast, *S. pombe (Jourdain et al., 2008)*. Previously, microtubules were shown to mediate long-distance transport of peroxisomes in mammals (Schrader et al., 1996; Huber et al., 1997; Schrader et al., 2000; Thiemann et al., 2000; Schrader and Gould, 2005), filamentous fungi (Egan et al., 2012b) and *D. melanogaster* (Kural et al., 2005), whereas in yeast cells and plants, actin filaments are involved (Mathur et al., 2002). In *U. maydis* we have observed that ≈12% of the peroxisomes show long-range motility dependent on microtubules but independent of F-actin. This is confirmed by: 1) microtubule-depolymerising drugs, 2) co-localization studies between microtubules and peroxisomes showing that peroxisomes move rapidly along microtubules and 3) transport dependent on microtubule-dependent molecular motors (kinesin-1, kinesin-3 and dynein). Taken together, microtubule-dependent peroxisome motility in *U. maydis* is reminiscent of animal cells, but different from budding yeast and plants.

Although Kin3 co-migrates with peroxisomes in *U. maydis*, it was visualized that Kin3 was in front of the organelle. In *U. maydis*, early endosome motility is mediated by Kin3 and Dyn2 (Wedlich-Soldner et al., 2002b; Schuster et al., 2011b; Steinberg, 2014). Thus, we performed co-visualization studies of early endosomes and peroxisomes and indeed, early endosomes were leading in the vast majority. To confirm that peroxisome transport is early endosome-dependent we have shown that peroxisome motility was reduced when 1) early endosome motility was abolished in *hok1* and *rab5a* null mutants and 2) in a *yup1*^{ts} mutant with reduced early endosome motility. Recently, Hok1 was shown to be an adaptor protein for molecular motors on early endosomes, being the C-terminal domain fundamental for the interaction with early endosomes. We have shown that in Hok1ΔC mutants peroxisomal motility is abolish but restored when Hok1ΔC is fused to PX. The Phox domain (PX) is known to target to phosphatidylinositol 3-phosphate-enriched early endosomes (Lemmon, 2003). This, in agreement with the previous results, clearly confirms that peroxisome motility is early endosome-dependent. Furthermore, in *Kin3*, *Rab5a* and *Hok1* null mutant peroxisomes clustered at the cell tip, which implies that early endosomes may play a role in peroxisomal distribution in the cell. In fact, in *A. nidulans* peroxisome clusters were also observed when Kin3 (Egan et al., 2012b) or HookA (Zhang et al., 2014) were absent.

Peroxisomes piggy bag on moving early endosomes to be transported to different locations. Previously, a similar mechanism was observed for poly-ribosomes, where Rrm4 binds the poly-ribosome to early endosomes via Rrm4 (Becht et al., 2006). Therefore, we have tested Rrm4 as a potential adaptor for peroxisomes. However, no differences were observe in *Rrm4* null mutants, neither in peroxisome motility nor in co-migration with early endosomes. Implying that Rrm4 is not linking early endosomes and peroxisomes. In some organisms, piggy backing of organelles to other organelles/cell components has been reported. As such, the ER was shown to move the Golgi complex (Sparkes et al., 2009), polysomes were moved by early endosomes (Higuchi et al., 2014) and mitochondria transported peroxisomes (Jourdain et al., 2008). We have thus considered the possibility that other organelles might hitchhike on early endosomes. Peroxisomes interact with several organelles for biogenesis and metabolic purposes. Therefore, we have studied lipid droplets, the ER and mitochondrial motility in *U. maydis*. Lipid droplets were labelled with the sterol 24-C methyltransferase, Erg6. They exhibit a motile and dynamic behaviour by oscillating from short range to long-

distance directed transport. As in mammals, lipid droplets in *U. maydis* were shown to move along microtubules. Moreover, around 60% of the lipid droplets showed an early endosome-dependent motility, which was confirmed by labelling lipid droplets in a ΔHok1 mutant. It should be noted that that reduction in lipid droplets motility is not as severe as when microtubules are absent. However, lipid droplets exhibit a subpopulation that moves via the ER. As observed for peroxisomes, early endosomes lead the motility event of lipid droplets which is probably due to an unknown binding protein. Interestingly, lipid droplets show cluster formation at the tip when Hok1 is abolished, which suggests that early endosomes might play a role in distributing the organelles throughout the hyphal cell.

The ER is characterized by its unique tubular structure distributed along the hyphal cell. Microtubule dependent motility of the ER was shown in in mammals (Lippincott-Schwartz et al., 1990) and in *U. maydis* (Wedlich-Soldner et al., 2002a). The ER drastically reduced its dynamic behaviour when cells were treated with microtubule-depolymerizing drugs. In ΔHok1 background their motile events were significantly reduced. This scenario was further confirmed by co-visualizing the ER and the early endosomes, where the ER tubules are pushed by the early endosomes. However, alterations in the distribution were subtle, presenting minor clusters near the nuclear region. Previously, in neurons, the ER was shown to retract when kinesin-1 is impaired (Feiguin et al., 1994). In summary, these data suggest that although the ER is moving with early endosomes, the organization machinery is more complex and multifactorial.

Lastly, mitochondria were taken into account, however, in contradiction with observations in other organisms, mitochondria motility was highly restricted in *U. maydis*. Most cells showed no mitochondrial motility, whereas others exhibited a low percentage of moving organelles. It is possible that mitochondria move only under specific conditions, such as oxidative stress or during the *U. maydis* growth phase. In fact, in neurons the number of mitochondria that shows motility varies considerably depending on the localization of the growth cone and growth cone state. In a growing axon, there are 25% of motile mitochondria, whereas away from the growth cone the motility increased to 75% (Morris and Hollenbeck, 1993). Mitochondrial motility and distribution was visualized in a *Hok1* null mutant,

although alterations in mitochondrial distribution and morphology were observed, the underlying mechanisms are still elusive.

In conclusion, we observed that the motility of peroxisomes, lipid droplets and the ER depends on a continuous shuttling of early endosomes and a certain stickiness of the early endosomes to other organelles. We propose a model which we call “underground traffic”. Basically, the underground (=early endosomes) travel from A to Z where they pick up different passengers (= lipid droplets, peroxisomes and the ER) and drop them off at different points. Peroxisomes, lipid droplets and ER are transiently taken by early endosomes and transported to different locations. Interestingly, the ER seems to play a part in peroxisome and lipid droplet motility. Peroxisomes, lipid droplets and the ER overlap in different functions. Therefore, it might be that the ER motility-dependent events account for specific organelle-organelle interactions. Overall, we show that early endosomes can move different organelles and act as master organizers of the hyphal cell.

6. ACTIVE DIFFUSION AND DIRECTED TRANSPORT OPPOSE ACTIN DRIFT TO SPATIALLY ORGANIZE FUNGAL AND MAMMALIAN PEROXISOMES

6.1. Introduction

Spatial organization of the cell is thought to serve several functions including cell polarization (Bornens, 2008), intracellular signalling (Al-Mehdi et al., 2012), and cell survival and apoptosis (Mellman and Nelson, 2008). In mammalian and fungal cells, organelles are transported towards their final location via microtubule-based processes and actin dynamics. However, the exact mechanisms governing organelle distribution are still obscure. Across species, peroxisomes are uniformly distributed throughout the cytoplasm, which might be fundamental to fulfil their different functions. Peroxisomes interact with different organelles for lipid metabolism, metabolite exchange and signalling (Kohlwein et al., 2013; Schrader et al., 2015b). They can undergo directed long-range motility (see Chapter 5) or short/diffusive motion. Diffusion was firstly defined by Brown through observations of pollen grains. In his observations he noted that the pollen grains moved irregularly, with no defined trajectory and independently of one another. Moreover, the diffusional behaviour would alter with temperature and viscosity. Later, Brownian motion was defined as motion of small particles due to thermal agitation. This erratic particle agitation is essential as a transport mechanism in prokaryotic cells (Armitage, 1999). In the eukaryotic cell, however, Brownian motion is restricted. Instead, diffusive motion of organelles is enhanced by ATP-dependent activity and cytoskeleton dynamics. This random motion dependent on biological processes is denominated “active diffusion” (Brangwynne et al., 2008; Brangwynne et al., 2009; Almonacid et al., 2015).

In *U. maydis* and *A. nidulans*, peroxisomes behave in a similar manner as in mammalian cells. A small population of peroxisomes undergoes directed transport along microtubules (Egan et al., 2012b; Guimaraes et al., 2015a; Salogiannis et al., 2016) whereas the vast majority shows oscillatory movement scattered throughout the cell. In *A. nidulans* and *U. maydis* peroxisomes hitchhike on early endosomes. Therefore, depletion of plus-end motors

(Kinesin-3) and a motor adapter (Hook1) blocks peroxisome motility (see Chapter 5). Unexpectedly, in these deletion mutants, peroxisomes cluster at the cell tip (plus-end) (chapter 5) (Egan et al., 2012b; Guimaraes et al., 2015a; Salogiannis et al., 2016; Zhang et al., 2014), however, this unexpected phenotype is not yet understood.

We have used the filamentous fungus *U. maydis* to comprehend the mechanism by which peroxisomes are distributed along the hyphal cell. We show that F-actin and myosin-5exerts a propelling force that moves peroxisomes to the growing apex that is counteracted by microtubule-dependent processes. Furthermore, we observed that peroxisome diffusion is mediated by the constant flow of organelles, specifically early endosomes, and by the dynamic behaviour of microtubules. We defined that peroxisome distribution in the hyphal cell relays on directed transport, active diffusion and polar drift. We further combined biological results with mathematical modelling to unravel the impact of the different forces on peroxisomal distribution and motility. Lastly, we show that mammalian cells appear to follow the same principle for peroxisome distribution.

6.2 Materials and methods

6.2.1 *U. maydis* strains and plasmids

All the strains and plasmids are decribed bellow (Table 10). To be noted that strains AB33paGFP2, AB33_GFP-SKL, AB33ΔKin3_GFP-SKL, AB33ΔHok1_GFP-SKL, AB33GFP$_3$-Myo5 and AB33Lifeact-GFP, AB33GFP-Tubulin1, AB33GFP-Tub1_GFP-SKL were described previously (chapter 5; Schuster et al., 2011a; Schuster et al., 2012). The primers used in the course of this chapter are described in Table 11.

Table 10: Strains and plasmids used in Chapter 6.

Strain name	Genotype	Reference
AB33_GFP-SKL	*a*2 P*narb*W2 P*narb*E1, *ble*^{R} /po^{C}GSKL	(Guimaraes et al., 2015b)
AB33Δkin3_kin3^{ts}_paGFP-SKL	a2 P*narb*W2 P*narb*E1, *ble*^{R}, Δ*kin3*, *nat*^{R} /pKin3^{ts} /po^{C}paGSKL	This study
AB33GFP-Rab5a	*a2 PnarbW2 PnarbE1*, *ble*^{R} /poGRab5a	(Schuster et al., 2011a)
AB33Δkin3_kin3^{ts}_GFP-SKL	*a2* P*narb*W2 P*narb*E1, *ble*^{R}, Δ*kin3*, *nat*^{R} /pKin3^{ts} /po^{C}GSKL	This study
AB33Lifeact-GFP	*a2* P*narb*W2 P*narb*E1, *ble*^{R}/ po^{C}LifeactG	(Schuster et al., 2012)
AB33GFP$_3$-Myo5	*a2* P*narb*W2 P*narb*E1, *ble*^{R}, P*myo5*-3*egfp-myo5*, *hyg*^{R}	(Schuster et al., 2012)
AB33GFP-Tub1_GFP-SKL	*a2* P*narb*W2 P*narb*E1, *ble*^{R} / poGTub1^C /po^{H}GSKL	(Guimaraes et al., 2015)
AB33ΔHok1_GFP-SKL	*a*2 P*narb*W2 P*narb*E1, *ble*^{R}, Δ*hok1*, *nat*^{R} /po^{C}GSKL	(Guimaraes et al., 2015b)
AB33ΔKin3_GFP-SKL	*a*2 P*narb*W2 P*narb*E1, *ble*^{R}, Δ*kin3*, *nat*^{R} / po^{H}GSKL	(Guimaraes et al., 2015b)
AB33GFP-Tub1	*a2* P*narb*W2 P*narb*E1, *ble*^{R} /poGTub1^C	(Schuster et al., 2011a)
poGRab5a	P*otef-egfp-rab5a*, *nat*^{R}	(Schuster et al., 2011a)
po^{C}GSKL	P*otef-egfp*- SKL, *cbx*^{R}	(Steinberg and Schuster, 2011)
po^{H}GSKL	P*otef-egfp*- SKL, *hyg*^{R}	(Guimaraes et al., 2015b)
pKin3^{ts}	P*kin3-kin3^{ts}*, *hyg*^{R}	(Schuster et al., 2011b)
po^{C}paGSKL	P*otef-paegfp-SKL*, *cbx*^{R}	This study
po^{C}LifeActG	P*otef-LifeAct-egfp*, *cbx*^{R}	(Schuster et al., 2012)
poGTub1^C	P*otef-egfp-tub1*, *cbx*^{R}	(Steinberg et al., 2001)

a, *b*: mating type loci; P: promoter; -: fusion; Δ: deletion; *hyg*^{R}: hygromycin resistance; *ble*^{R}: phleomycin resistance; *nat*^{R}: nourseothricin resistance; *cbx*^{R}: carboxin resistance; *otef*: constitutive promoter; /: ectopically integrated; *E1*, *W2*: genes of the *b* mating type loci; *egfp*: enhanced green fluorescent protein; NLS, nuclear localization signal of the GAL-4 DNA binding domain from pC-ACT1 (Clontech); nup107, nucleoporin; rab5a, small endosomal Rab5-like GTPase *kin3*: kinesin-3; *hok:* hook motor adapter; *Tub1*: α tubulin; SKL, peroxisomal targeting sequence; ^{ts}, temperature-sensitive allele; *pagfp*,photo-activatable GFP; LifeAct:: 17 amino acid peptide that binds F-actin

Plasmid paGFP-SKL (carboxin)

AB33_paGFP-SKL was generated by fusing the peroxisome targeting signal 1 (SKL= serine-lysine-leucine) to C-term of paGFP (Schuster et al., 2011a) using primers gd112 and gd113 (Table 11). The carboxin resistance cassette was amplified from paGFP-Rab5a, using primers gd110 and gd111 (Table 11). The above plasmid was linearized with *Eco*RV and ectopically integrated in AB33 strain. AB33ΔKin3-Kin3^{ts} was obtained by digestion of plasmid pKin3ts with *Bsr*GI, followed by ectopic integration into a *Kin3* null mutant stain. Successful integration was confirmed by studying the rescue of the morphological phenotype of AB33ΔKin3_Kin3ts at permissive (22ºC) and restrictive (32ºC) temperature. This was followed by ectopic integration of plasmid popa^{C}GFP-SKL, digested with *Eco*RV.

Plasmid GFP-SKL (carboxin)

Kin3^{ts} plasmid (Schuster et al., 2011b) was linearised with *Bsr*GI and integrated ectopically into ΔKin3 cells (Higuchi et al., 2014) to generate AB33ΔKin3_Kin3^{ts}. po^{C}GSKL plasmid was linearised with *Bgl*I and ectopically integrated into AB33ΔKin3_Kin3^{ts}, resulting in AB33ΔKin3_Kin3^{ts}_paGFP-SKL

6.2.2 Growth conditions

U. maydis. Liquid cultures were grown at 28ºC, shacking at 200rpm, for 8-12h in complete medium (CM), supplemented with 1% glucose. Hyphal growth was induced by transferring the yeast-like cells to nitrate minimal medium, supplemented with 1% glucose (NM-Glu), following published procedures (Schuster et al., 2011a). Microscopic observation was started after additional 8-14h growth at 28ºC, 200 rpm in NM-Glu. Temperature sensitive mutant strain AB33Kin3ts_paGSKL and AB33Kin3^{ts}GFPSKL were grown in CM-Glu for 8-12 h. Hyphal growth was induced by shifting into nitrate minimal medium, supplemented with 1% glucose, and subsequent incubation at a permissive temperature (22ºC) for 8-14h. To inactivate Kin3, liquid cultures were transferred to restrictive temperature (32ºC). AB33Kin3ts_paGSKL was incubated for 2-5 hours with hourly observations.

Mammalian COS-7 cells. COS-7 (ECACC 87021302) and COS-7-GFP-SKL cells, which stably express GFP-SKL fusion protein 45, were maintained in Dulbecco's modified Eagle medium (DMEM) high glucose (4.5 g/L) (Life Technology, Paisley, UK) supplemented with

10% FBS (Life Technology, Paisley, UK), 100 U/ml penicillin and 100 µg/ml streptomycin (Life Technology, Paisley, UK), at 37ºC in a 5 % CO2-humidified incubator (Thermo Fischer Scientific, Waltham,US)

6.2.3 Live cell imaging

U. maydis microscopy was performed as previously described (chapter 5). In brief, cells were placed on a 2% agarose cushion and observed using a motorized inverted microscope (IX81; Olympus, Hamburg, Germany), using a Plan-Apochromat 100×/1.45 NA total internal reflection fluorescence oil objective or UPlan-SApochromat 60×/1.35 NA oil objective (Olympus, Hamburg, Germany). Fluorescent proteins were excited by 70-mW solid-state lasers, at 488 and 561 nm, which were controlled by a VS-LMS4 Laser Merge System (Visitron Systems, Munich, Germany). Photo-bleaching experiments were performed using a 405-nm/60-mW diode laser, dimmed to 15-mW output power, which was controlled by a UGA-40 unit (Rapp OptoElectronic, Hamburg, Germany) and VisiFRAP-2D FRAP control software for Meta Series 7.5.x (Molecular Devices, Downingtown, PA). Simultaneous observation of mCherry and eGFP fluorescence was performed using a Dual-View Micro Imager (Photometrics/Roper Scientific, Ottobrunn, Germany), equipped with a dual-line beam splitter (z491/561; Chroma Technology Corp., Olching, Germany), an emission beam splitter (565 DCXR; Chroma Technology Corp. Olching, Germany), an ET-Band pass 525/50 (Chroma Technology Corp. Olching, Germany), and a single band pass filter (BrightLine HC 617/73; Semrock Rochester, USA). Images were acquired using a cooled charge-coupled device camera (CoolSNAP HQ2; Photometrics/Roper Scientific, Ottobrunn, Germany). The microscopic system was under the control of the software package MetaMorph 7.5.x (Molecular Devices, Downingtown, PA).For temperature-dependent experiments, the objective lenses were cooled or heated using a metal hull connected to a water bath (Huber). All image processing and quantitative analysis was done using MetaMorph 7.5.x (Molecular Devices, Downingtown, PA).

Mammalian COS-7 cells were observed using an Olympus IX81 microscope (Olympus Optical, Hamburg, Germany), equipped with a PlanApo 100x/1.40 oil objective and eGFP filter sets equipped with a 470/40 ET Bandpass, Beamsplitter T 495 LPXR and a 525/50 ET Bandpass filter (Chroma Technology Corp. Olching, Germany) and a TxRed HC filter set

equipped with a 562/40 BrightLine HC, HC Beamsplitter BS 593 and a 624/40 BrightLine HC (Semrock Rochester, USA). Cells were kept in a closed chamber in glass bottom 35 mm petri dishes with 20 mm bottom well (Greiner Bio-One, Frickenhausen, Germany). Temperature was kept at 37°C, using a temperature control system and an objective heater (Visitron Systems, Munich, Germany). Image acquisition was performed as described above.

6.2.4 Drug treatments

For disruption of microtubules or F-actin cytoskeleton in *U. maydis*, 500µl of the cell culture was supplemented with 30µM benomyl (Stock: 30 mM in DMSO; Fluka; Sigma-Aldrich) 20 µM latrunculin A (stock: 20mM in DMSO, Life Technologies, Paisley, UK) or 100µM of CCCP, Carbonyl cyanide 3-chlorophenylhydrazone (Sigma-Aldrich, Gillingham, UK) and incubated for 30 minutes in 2 ml Eppendorf tube at 28ºC at 200rpm. Control cells were incubated under identical conditions with 0.5 µl of DMSO. Cells were placed on 2% agarose cushions, supplemented with 30µM benomyl, 20 µM latrunculin A or DMSO, respectively. Image series of 100 frames at 150ms were acquired. The effective depolymerisation of microtubules or F-actin was tested in control experiments, using GFP-αtubulin expressing strain AB33_GFP-Tubulin and Lifeact-GFP expressing strain AB33_Lifeact-GFP. Reversibility of CCCP treatment was confirmed by washing cells with CM-medium, followed by 15-30 min incubation in fresh media and monitoring the reappearance of peroxisome movements. For longer incubations, cells were placed in glass tubes to allow oxygen exchanges. 2-5 ml cultures with cytoskeleton inhibitors (30 µM benomyl, 20 µM latrunculin A or a combination of both) were incubated at 28ºC, 200 rpm, for 4 hours. Distribution analysis was then performed as described below (see 6.2.6).

To investigate the effect of cytoskeletal drugs or CCCP on mammalian peroxisomes motility, GFP-SKL expressing COS-7 cells were grown in glass bottom dishes (Greiner Bio-One, Frickenhausen, Germany). 10 µM nocodazole (stock: 33.2 mM), 300 nM (long-term incubation) or 20 µM latrunculin A (short-term incubation; stock: 20mM) or a combination of both, or CCCP (1mM), was added to the culture medium for 30 min, followed by microscopic analysis in DMEM without phenol red (DMEM 1x, Gibco, Life Technology, Paisley, UK) at 37ºC, for no longer than 1 hour. To observe alterations on peroxisome

distribution, unlabelled COS-7 cells were grown on glass coverslips and were treated with 10 µM nocodazole, 300 nM latrunculin A or both drugs simultaneously for 6h, followed by fixation in 4% para-formaldehyde in phosphate buffered saline, pH 7.4. Cells were permeabilised with 0.2 % Triton X-100, blocked with 1 % bovine serum albumin and incubated with rabbit polyclonal anti-Pex14 antibodies (kindly provided by D. Crane, Griffith University, Brisbane, Australia), followed by incubation with goat-anti-rabbit IgG conjugated to Alexa 488 (Life Technology, Paisley, UK). Effective disruption of microtubules and F-actin was tested in parallel experiments, staining F-actin with Phalloidine-A594 (Life Technologies, Paisley, UK) and MTs with anti-α tubulin (Sigma-Aldrich, Gillingham, UK).

6.2.5 Analysis of directed organelle and Myo5 motility

Directed motility and run-length of POs was analysed in image series and in movies, taken from strain AB33_GSKL. Directed motility was defined as rapid and continuous motility that lasted > 1.2µm. The percentage of motility was determined in a 15s time interval. To measure the flux of GFP_3-Myo5, image series of 150 frames were acquired, using strain AB33_GFP_3Myo5, 150ms exposure time and a 488nm laser at 90% output power. Kymographs were generated from these image stacks using MetaMorph 7.5.x, and anterograde and retrograde flux were measured.

6.2.6 Analysis of peroxisomal distribution

Peroxisomal distribution in hyphal cells of control, *Kin3, Myo5* and *Hok1* null mutants (strains AB33_GSKL, AB33ΔKin3_GFP-SKL, AB33ΔHok1_GFP-SKL, AB33ΔMyo5_GFP-SKL and AB33Kin3^{ts}_GFP-SKL), z-axis image stacks were acquired at an exposure time of 150 ms and 200nm steps in z-direction. From these stacks, maximum projections were generated using MetaMorph 7.5.x and the average fluorescent intensity over the 30 µm behind the tip region and 5 µm outside the cell was measured using the linescan function in MetaMorph 7.5.x (Molecular Devices, Downingtown, PA). The effect of inactivation of kinesin-3 on peroxisome distribution was investigated in strain AB33Kin3^{ts}_paGFPSKL. Peroxisomes in hyphal cells were bulk photo-activated in a custom-built glass chamber, containing a cover-slip, inside which the cell suspension was placed, covered by on a liquid reservoir to prevent cells from drying out, using a 10x

objective (Olympus, Hamburg, Germany) and a 405nm laser at 100% output power successful photo-activation was confirmed by epi-fluorescent microscopy, using the 488nm observation laser at 20% output power. Cells in the custom-built glass chamber were transferred into a 32°C incubator for 5h. Z-axis image stacks were acquired at an exposure time of 150 ms and 200nm steps in z-direction and analysed as described above.

6.2.7 Mean square displacement (MSD) analysis and diffusion coefficient estimation

To analyse the random motions of peroxisomes, the mean square displacement was calculated according to published methods (Otten et al., 2012). Image series of GFP-SKL expressing *U. maydis* and COS-7 cells were recorded at 150 ms interval and covering 15-45 s observation time Random motions of peroxisomes were automatically detected using tracking software that determined the peroxisome centre after Gaussian filtering. Trajectory plots were drawn in MATLAB R2011b (MathWorks, Cambridge, United Kingdom), using trajectories that record 10 s of random motions. MSD calculations were done using MATLAB R2011b and curve fitting analysis was done in Prism 5.03. Diffusion coefficients *D*PO were calculated from MSD of individual trajectories, using MATLAB R2011b, or derived from fitted curves, using Prism 5.03. Unpaired Student's T-testing was performed in Prism 5.03. To calculate that axial and radial diffusion rates, the axis of *U. maydis* hyphal cells was determined using the image moments of the live cell imaging data after applying a median threshold. Subsequently, individual trajectories were oriented according to this spatial information and *D* for random movements along the axis (axial) and 90° to the axis (radial) was calculated as described. Nonlinear curve regression and F-tests for *D* comparison were performed using the software GraphPad Prism 5.03.

Table 11: Primers used in current study

Primer	Sequence 5' → 3'
gd110	TAAGCTGTCAAACATGAGAATTCATCGATGGCGGCCGCACGGGGATCTTC
gd111	CTTAATTAAGGATCCGGCGCGCCGCGGCCGCACGCTAAGTGGAGTTGTCC
gd112	TATTTGAGAAGATGCGGCCAGCAAAACTAACTGAAGCTTGCATGCCTGCA
gd113	TGCAGCCGGGCGGCCGCTTTAAAGCTTCGACTTGTACAGCTCGTCCATGC

6. 3 Results

6.3.1 Peroxisomes in *U. maydis* cluster at the plus-end of the hyphal cell when Kin3 or Hok1 are impaired.

As shown in Chapter 5, peroxisomal motility in *U. maydis* is early endosome-dependent, which is consequently associated to Kin-3 and Dyn2 to move along the microtubule array. We have determined that peroxisomal motility is highly impaired in mutants such as ΔKin3 and ΔHok1 (adaptor protein) (Figure 28 A-B). Interestingly, when peroxisomal distribution was analysed in *Kin3* and *Hok1* null cells, an intriguing peroxisomal accumulation at the plus-end was observed (Figure 28A-C). Clustering at the cell tip is highly unexpected as the plus-end motor in abolished. In fact, one would assume a clustering at the minus-end, since the peroxisomes would not be able to travel towards the tip. Comparable observations in *A. nidulans* showed peroxisomes clusters at the cell apex in a HookA (Hok1 homologue) (Zhang et al., 2014) and Kin3 (Egan et al., 2012b) deleted strains. In *P. chrysogenum* peroxisomes were suggested to form apically due to accumulation at the hyphal tip in a Dynamin-like protein (Dnm1) mutant (Meijer et al., 2010).

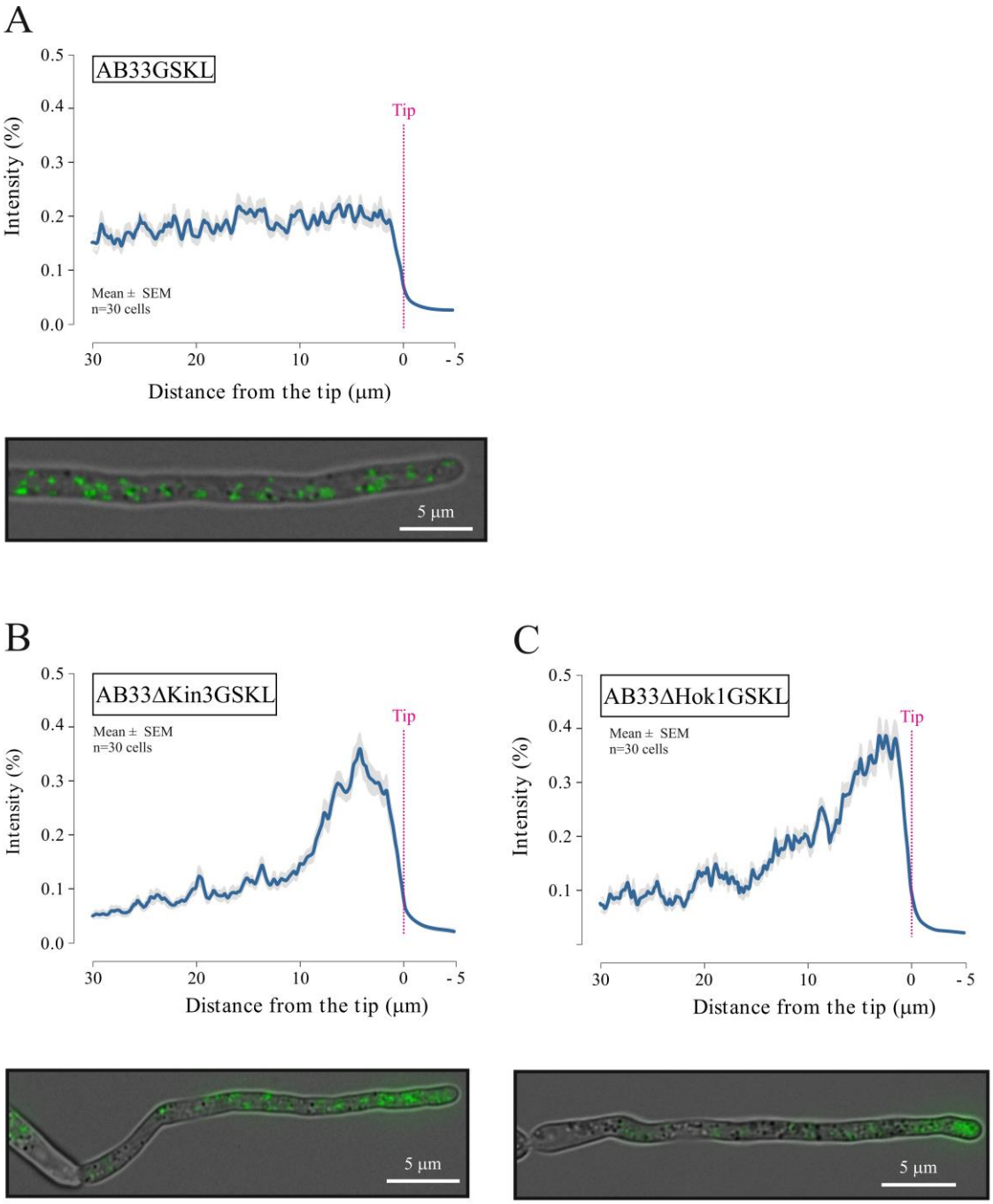

Figure 28 - Peroxisomes cluster at the tip when Kin3 and Hok1 are deleted. Peroxisomal morphology can be observed in brightfield images overlay with fluorescent pictures of GFP-SKL.A) Fluorescent intensity profile of AB33-GFP-SKL (control) shows an even distribution of peroxisomes. B+C) In *Kin3* and *Hok1* null mutants, linescans clearly show cluster formation 10 µm behind the cell tip. Fluorescence intensity profiles were performed over a distance of 30 µm behind the hyphal tip plus 5 µm outside the cell, to eliminate background interference. Each data point represents mean ± SEM, n=30 cells from at least two independent experiments. Scale bar, 5 µm.

Taking this into account, we questioned if peroxisomes in *U. maydis* were formed at the hyphal tip. To address it we used a photoactivatable GFP reporter (paGFP) fused to the

tripeptide SKL (paGFP-SKL). Correct targeting of the paGFP-SKL was confirmed by integration into an AB33mCherry-SKL strain. Activation of paGFP-SKL (405 nm laser) allowed the visualisation of peroxisomes, which also co-localised with a red peroxisomal marker (mCherry-SKL) (Figure 29 A). Kin3 temperature sensitive allele (Schuster et al., 2011b) was introduced in a Δkin3 background (AB33Kin3^{ts}). The *Kin3^{ts}* allele allows the "switch off" Kin3 activity after 5 minutes incubation at 32ºC, the restrictive temperature. At permissive temperature (22ºC), Kin3 is fully functional, which can be determined by the presence of organelle bidirectional motility; for reference we have used early endosomes (data not shown). We introduced paGFP-SKL into AB33Kin3^{ts}, the rationale behind this approach was to follow newly activated peroxisomes with impaired plus-end microtubule-based transport. In a hand-made dish we add a small amount of the culture and exposed the entire dish to the laser 405 nm, which activates the fluorophore paGFP. The photoactivation was performed at 22ºC and proper activation was confirmed by the appearance of fluorescent peroxisomes. paGFP-SKL was not further exposed to the 405 nm radiation during the course of the experiment. Afterwards, the dish was incubated at 32ºC. Images were acquired every hour over the course of 5 h. We observed the formation of peroxisomal clusters at the cell tip after 3 hours (Figure 29 A). To confirm if the cluster was significantly different from the control, a t-test showed that the slope in the linear fitting is significant different,$P < 0.0001$ (R^2= 0.12 for T=0h; R^2=0.69 for T= 3h) (Figure 29 B). After 5 hours, the distribution phenotype was similar to 3 hours. Thus, in *U. maydis* cluster formation at the polar region is not related to newly formed peroxisomes.

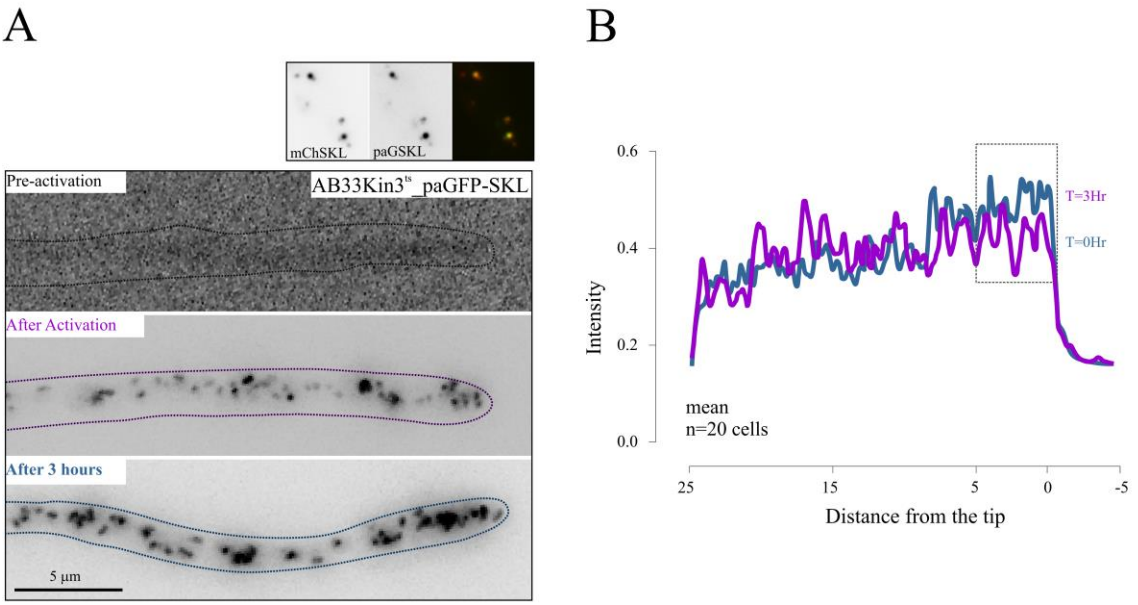

Figure 29 - Peroxisomes move towards the cell tip in a Kin3 independent manner.A) paGFP-SKL colocalization with mCherry-SKL. AB33Kin3^{ts}_paGFP-SKL shows no peroxisome fluorescent signals before activation (upper panel). Activation with the 405-nm laser was performed at 22ºC. Peroxisomes are evenly distributed throughout the cell (Middle panel). After 3 hours at 32ºC peroxisomal clustering is visible (lower panel). Images were contrast inverted. Bar, 5 µm. B) Fluorescent intensity profile shows clustering after 3 hours when compared to T=0 hours. Linescan over 20 µm behind the cell tip and 5 µm outside the cell to eliminate background interference. Each data point represents mean, n=20 cells from at least two experiments. Scale bar, 5µm.

6.3.2 Peroxisomal accumulation at the plus-end is actin dependent

U. maydis trafficking relays on two different cytoskeleton components, microtubules and actin. To investigate, if actin could play a role in peroxisome accumulation at the cell tip, we integrated GFP-SKL into the AB33Kin3^{ts} strain to reason if depletion of microtubule-based motility and F-actin would alter peroxisomal distribution. Hyphal cells were treated with DMSO (control) or latrunculin A, over 2 hours at a restrictive temperature (32ºC). In AB33Kin3^{ts} it requires only 5 minutes to inactivate Kin3. We have performed our observations so alterations of the distribution could be tracked. AB33GFP-SKL was used as a control for drug treatment and temperature. After 2 hours, AB33Kin3^{ts}GFP-SKL treated with latrunculin A showed no clear peroxisomal accumulation at the cell tip, however, when treated solely with DMSO, the accumulation was perceptible. Control cells showed no clustering, and interestingly, when actin was depolymerized, diminishment in peroxisome number at the cell tip was observed (Figure 30 A-D).

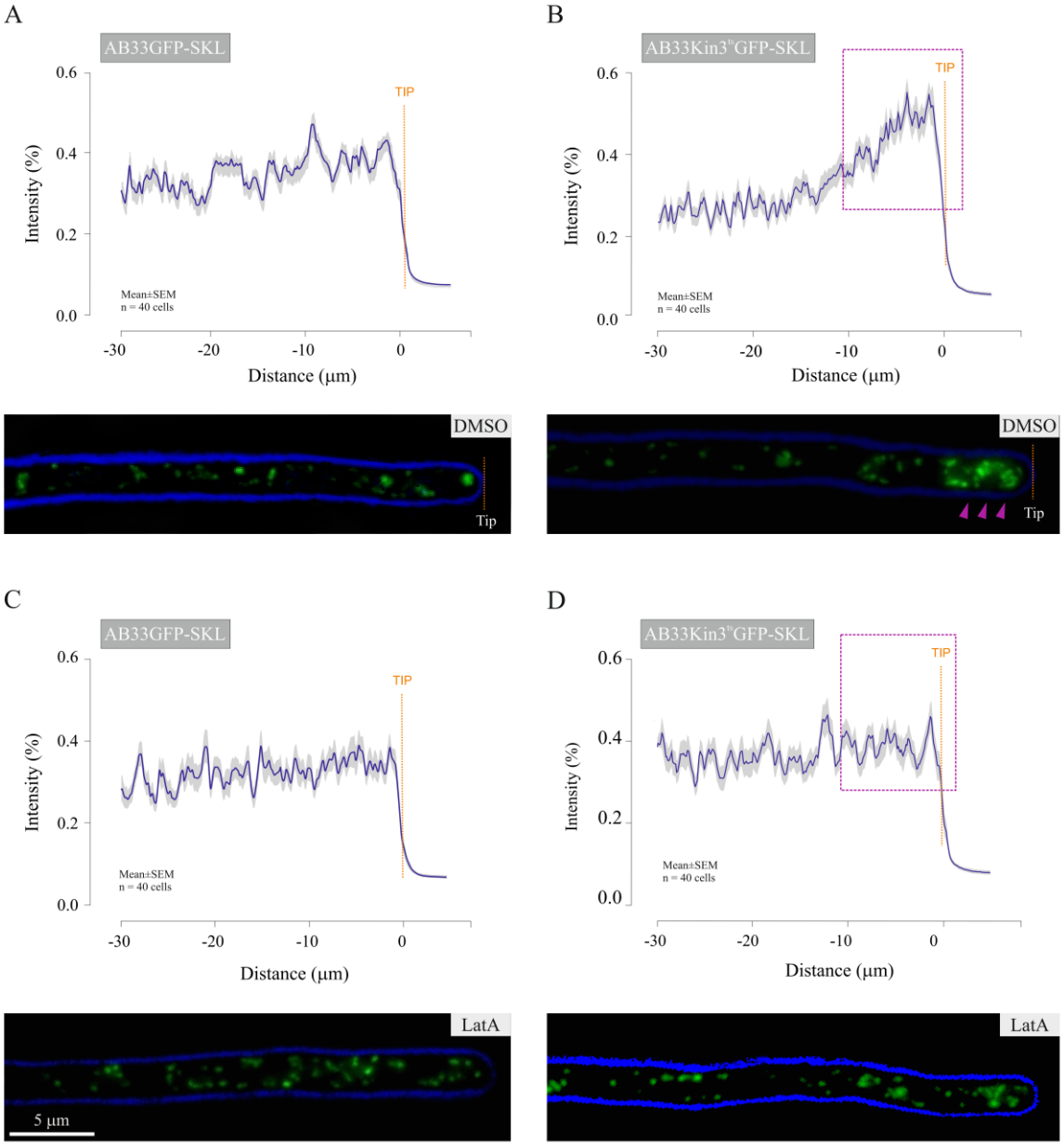

Figure 30 - Clustering at the cell apex is actin dependent AB33Kin3^{ts}GFPSKL allows to shift from active to an inactive state of Kin3. Peroxisomal positioning was observed under different conditions. AB33GFP-SKL or AB33Kin3^{ts}GFP-SKL strain were treated for 2 hours with DMSO or latrunculin A at 32ºC. A) AB33GSKL treated with DMSO showed only a slight clustering. B) AB33Kin3^{ts}GSKL treated with DMSO exhibited an accumulation of peroxisomes at the cell tip after 2 hours. C) After latrunculin A treatment, control cells showed no peroxisomal cluster and even a shift away from the tip. D) Clustering in AB33Kin3^{ts}GSKL is overcome when cells are incubated with latrunculin A (LatA). Linescan over 30 µm behind the cell tip and 5 µm outside the cell to eliminate background interference. Each data point represents mean ± SEM, n=40 cells from at least two experiments.

This observation suggests that clustering at the plus-end, is F-actin-dependent. Transport along F-actin is mediated by myosin class V motors. Myosin-5 motors are essential for polarized growth of *U .maydis* (Weber et al., 2003; Schuchardt et al., 2005), with these

motors mainly moving towards the growth region (86.5% ± 1.9, n=23 cells) (Figure 31 A). It was shown, previously, that F-actin and Myo5 fully co-localize (Schuster et al., 2012). One can envisage that, the constant flow of Myo5 towards the hyphal tip provides polar drift current that might enable peroxisome flux. To further strengthen our hypothesis, GFP-SKL was integrated into a ΔMyo5 strain. Peroxisome were constrained at the cell tips and no clustering was visible (Figure 31 A-C), even though peroxisomes could directed motility could still be observed. This transport is likely to be mediated by microtubules. Weber et al. (2003) showed that F-actin is clustered at the cell periphery in ΔMyo5 cells, supporting the notion that peroxisomes cluster at the tip is likely related to actomyosin pole-ward forces.

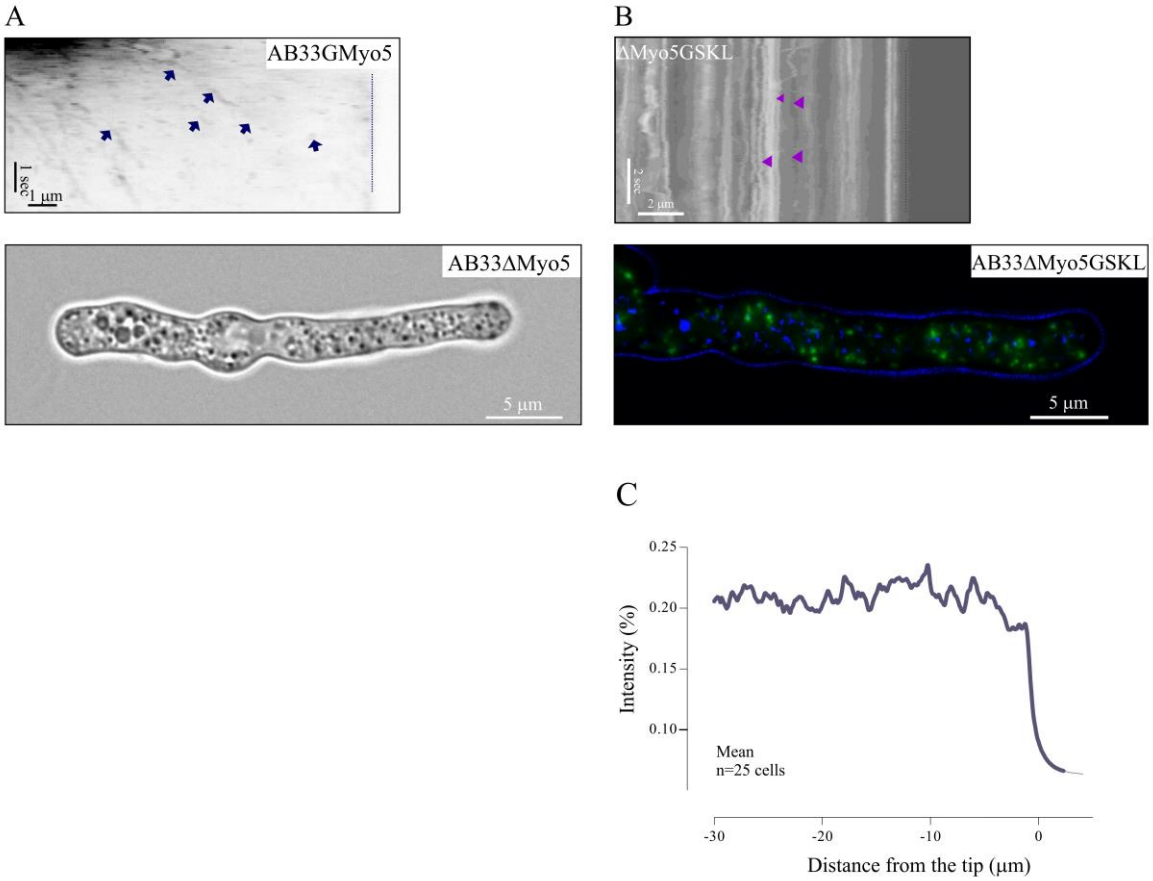

Figure 31 - Peroxisomes are stationary at the apical region in *Myo5* null mutant.A) *Upper panel:* Kymograph show myosin 5 motion in with 87% moving towards the hyphal tip (blue arrows) Bars, 1 s, 1 µm. *Lower panel*: Growth defects of *Myo5* null cells. Bar 5 µm. B) Peroxisome motility and distribution in ΔMyo5 strain. Reduced motility at the tip region (upper panel). *Lower panel:* kymographs shows that peroxisomes are less abundant at the tip. C) Intensity profile of peroxisomes in AB33ΔMyo5 shows no cluster at the polar region.

Lastly, we have analysed the effect of benomyl and latrunculin A over longer period (4 hours). DMSO, latrunculin A, benomyl, and latrunculin A plus benomyl treatment was

performed. Peroxisome accumulation at the cell apex was observed after incubation with the microtubule-depolymerising agent (benomyl). In contrast, when actin and microtubules were disturbed, a minor accumulation was detected (Figure 32). Interestingly, peroxisomes were retracted when treated with Latrunculin (Figure 30 C and Figure 32), as observed when Myo5 is deleted (Figure 31 C). These scenarios imply that without F-actin peroxisomes are unable to reach the tip region (Figure 32). This data shows that the motion towards the hyphal apex is due to an F-actin-based process.

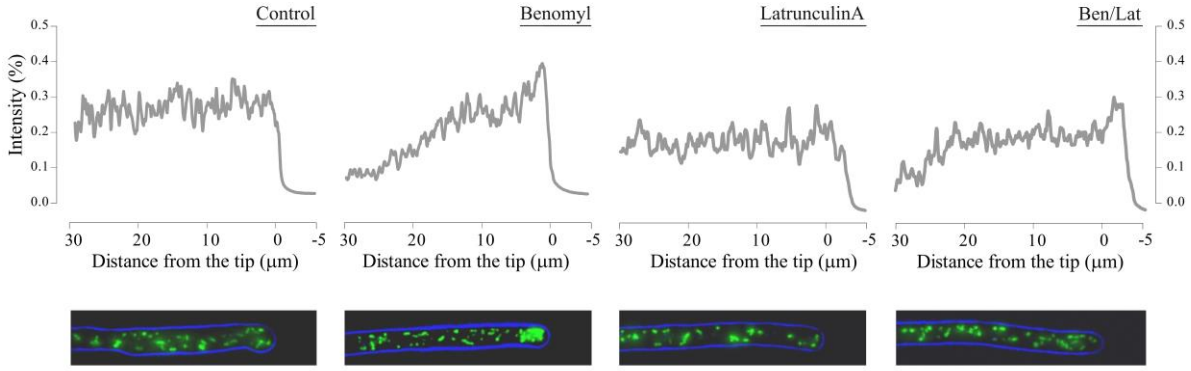

Figure 32 - Peroxisomes move pole-ward without microtubules. Intensity profiles and phenotype of AB33GFP-SKL treated with DMSO, benomyl, latrunculin, and benomyl plus Latrunculin for 4 hours.

6.3.3 Peroxisomal diffusion is ATP and microtubule dependent

It is now clear that the polar drift is due to actomyosin pole ward forces. However, the reason is still elusive. About 12% of peroxisomes show long-distance motility in *U. maydis*, though the vast majority of peroxisomes show random motion. Peroxisomes switch from random motion to directed transport and *vice-versa*. To further comprehend the peroxisome diffusion behaviour, e.g. the polar drift, we used different drug treatments to analyse the peroxisomal diffusion rates in different conditions. Cells were treated for 30 minutes with benomyl, benomyl plus latrunculin A or CCCP (carbonyl cyanide m-chlorophenylhydrazone). CCCP inhibits cell respiration and rapidly depletes the ATP from the cytosol (Azarkina and Kosntantinov 2002). DMSO was used as a solvent control. Following the treatments, movies of 15 s were acquired. Arbitrarily, sections of the hyphal cell were selected and analysed. Diffusional events for the first 10 s of each region were analysed and their trajectories were projected onto the 2-dimensional space with origin at the centre for each trajectory (Dr. Jeremy Metz, Biomedical informatics Hub, University of Exeter). Plots summarise the

random events of 70 trajectories resulting from the analysis (Figure 34 A). Peroxisome diffusional behaviour is highly restricted when ATP is depleted, showing that random motion depends on biological processes. In living cells, Brownian motion is constrained, so, diffusional behaviour relays on cytoplasmic activity such as organelle and/or motor movements. Brangwynne and co-workers (2009) have described this processes in the living system, a highly dependent ATP- induced biological processes, and denominated as "active diffusion". We have shown that in *U. maydis* indeed peroxisome diffusion is ATP-dependent and not due to Brownian motion.

Mean square displacement (MSD) is a computational analysis that measures the square distance of a particle deviation that travels from an initial location to and end location, over time. The obtained curve of MSD againt τ can be fit to τ^{α}. The dynamic behaviour is given by the exponential value, α which defines the type of motion. $\alpha < 1$ the particle is subdiffusional; $\alpha = 1$ the partical is diffusional, $\alpha > 1$, the particle performs superdiffusion with the limiting ballistic behaviour of $\alpha=2$ (Figure 33). MSD provides three core outcomes: 1) how far a particle travels; 2) dynamical behaviour of the particle (active diffusion, active transport or constriction; 3) the amount of time and space a particle can move (diffusive constant). Therefore, depending on the slope MSD determines which type of motility is present. A straight line illustrates diffusion behaviour, if it curves up this is indicative of directed motility, if curves down, this represents superdiffusion, and if it reaches a plateau shows that the particle is constricted (Figure 33).

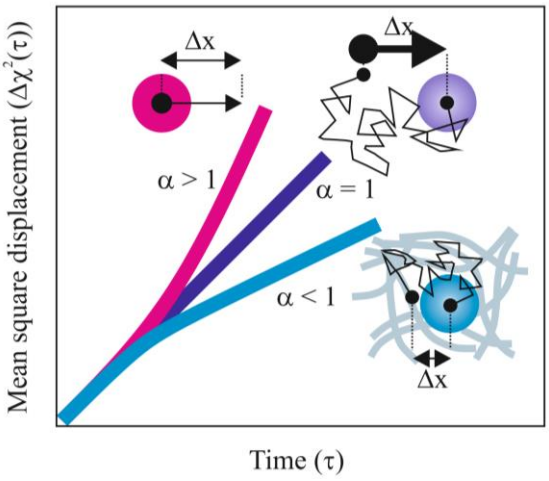

Figure 33 - Representation of a mean square displacement in the different types of motion. Mean square displacement characterizes the displacement of a particles over a time interval τ. Superdiffusion is defined by a ballistic behaviour with $\alpha>1$ (pink line). When $\alpha=1$, the particle exhibits a diffusive behaviour (dark blue line). Particles constrained by the viscoelastic network exhibit a subdiffusive behaviour with $\alpha<1$ (light blue line). *Adapted from* Brangwynne et al.,2008.

In our model, under control conditions, peroxisomes showed α=1.11, which indicates a diffusional dynamic. When microtubules were depolymerized, α decreased (α=1. 01), representing a more restricted behaviour. This was even more perceptible when F-actin was disassembled (α=0.90) (Figure 34 B). These results show that indeed peroxisome motion is diffusive and random. To dissect the motion behaviour, we have analysed the MSD after treating with CCCP. In this scenario, MSD reached a plateau, which is in line with the highly restricted mobility (Figure 34 B).

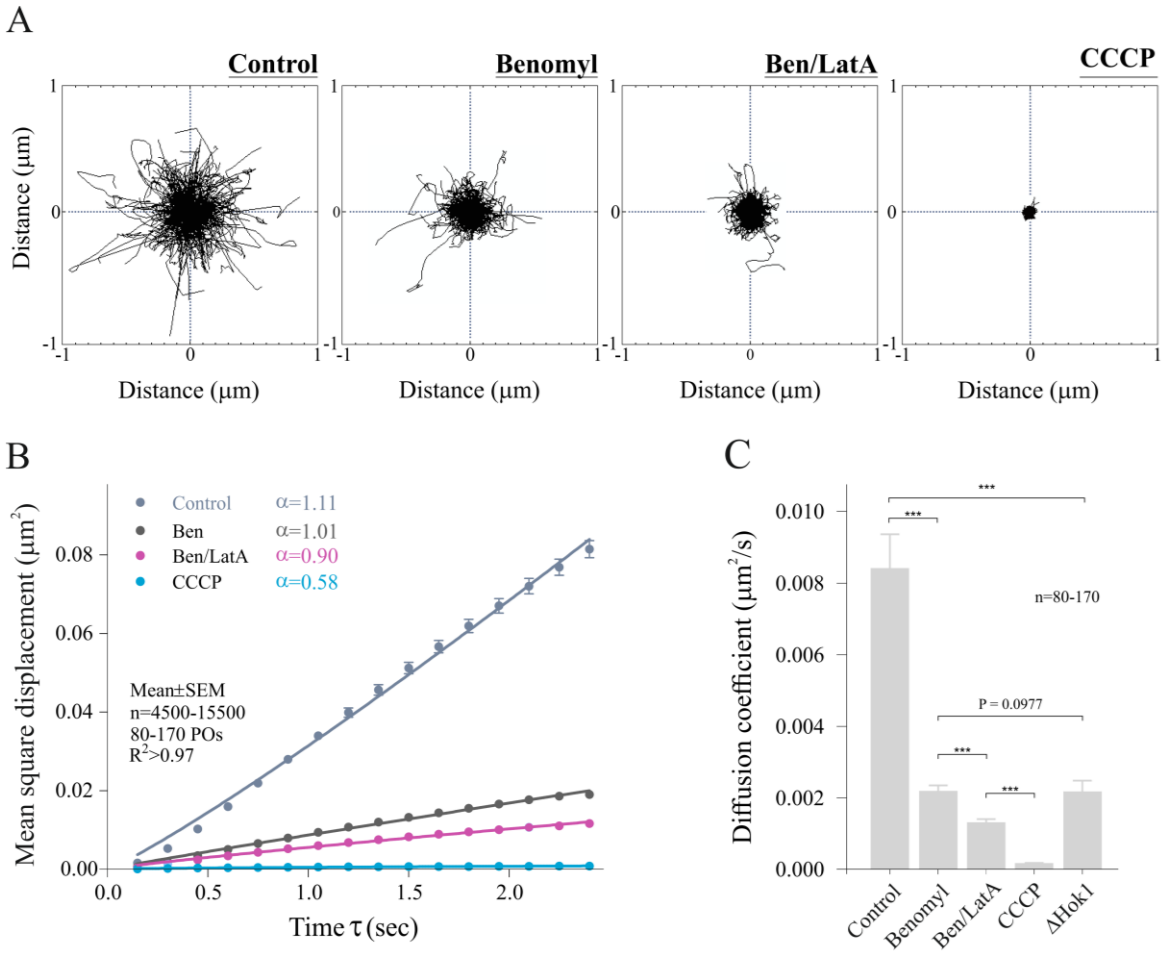

Figure 34 - Peroxisome diffusion in *U. maydis*.A) Plot analysis of peroxisomal trajectories in *U. maydis* treated with DMSO, benomyl, benomyl plus latrunculin A and CCCP. In all cases there is a decrease in diffusion. B) Mean square displacement shows a decrease in the diffusion behaviour, the higher the slope, the higher the passive behaviour. POs – Peroxisomes. Mean ± SEM is shown based on 4500-15500 measurements of 80-170 POs. C) Diffusion coefficient determined in control, benomyl, benomyl plus latrunculin A, CCCP and ΔHok1. Sample size is indicated. ***, significant difference to control at P < 0.0001; n.s., non-significant when compared to the control, using a Student's t test

To fully grasp which cytoskeleton component has an impact on peroxisomal oscillation we determine the diffusion coefficient, *D*, which corresponds to the mean diffusion per unit of

time. Basically, it illustrates how fast, on average, the particles move along their trajectories, which essentially allows defining the average diffusion rate of a given particle. Curiously, it showed that microtubules had the highest impact in active diffusion when compared to the control. It is well described that early endosomes constantly move along microtubule tracks in *U. maydis,* in a bidirectional fashion. This constant flow of early endosomes enhances the active diffusion due to constant collisions with organelles such as peroxisomes. Therefore, we have analysed peroxisomal oscillatory dynamics in the ΔHok1 mutant, where early endosomes are immobile. We determined a diminished peroxisomal diffusion rate. In fact, the diffusion rate was similar to the conditions where microtubules were depolymerized. This observation imply that microtubule-based motility is fundamental for peroxisome diffusion.

Previously, it was shown that microtubule bending enhances peroxisomal motility (Kulic et al., 2005). It has been described, in *U. maydis,* that microtubules have a dynamic behaviour performing constant motor-driven bending which most probably increases the likelihood of interacting with different organelles. In your model, we have co-labelled tubulin (GFP-α-Tubulin) and peroxisomes (GFP-SKL) which showed that peroxisomes close to the microtubules oscillate in axial motions. Moreover, in rare occasions, we could observe that microtubule lateral bending occurs near a peroxisome, propelling its motility (Figure 36 B). This oscillatory behaviour was shown to be axial oriented by plot analysis, suggesting that organelle trafficking along microtubules could enhance peroxisome diffusion (Figure 35 A-B). Moreover, this behaviour was reduced in ΔHok1 cells (Figure 35 A-B). These scenarios: 1) diffusion coefficient is equally diminished when microtubules are depolymerized and the early endosomes are immotile; 2) the axial motions are reduced when microtubules are depolymerized and early endosomes motility is impaired; suggest that the constant flow of early endosomes enhances organelle diffusion, namely peroxisomes.

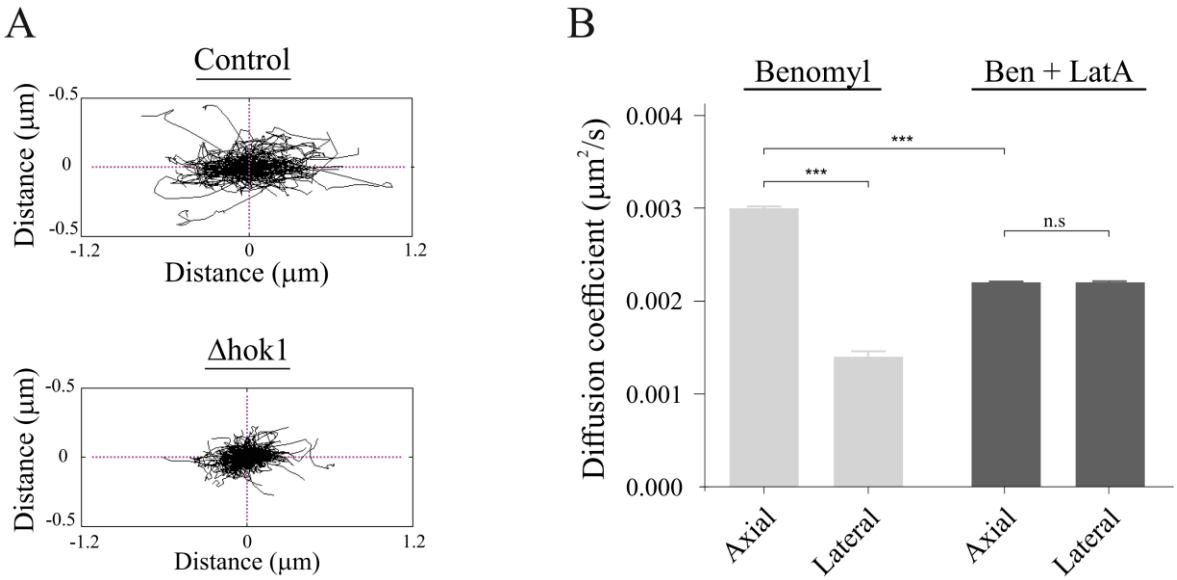

Figure 35 - Axial diffusion of peroxisomes in *U. maydis*. A) Trajectory overview of axial motility over lateral. Axial motility is prevalent in basal conditions when compared to ΔHok1 background. B) Diffusion coefficient rate (D*cyto*).shows that depolymerisation of microtubules results in significantly higher axial diffusion when compared to lateral diffusion. However, no significant difference is obtained when actin polymerization is also blocked. Sample size is indicated. ***, significant difference to control at $P < 0.0001$; n.s., non-significant when compared to the control, using a Student's t test.

6.3.4 Mathematical modelling of peroxisomal positioning in *U. maydis*

Our data suggest that in *U. maydis* peroxisome displacement is a result of multifactorial components of peroxisome motility, diffusion and positioning. We have shown thus far that actin-based polar drift opposed to microtubule-associated processes. Moreover, the constant flow of early endosome bi-directional motility enhances active diffusion (Figure 36 B). Interestingly, early endosomes are involved in both peroxisome directed transport (see chapter 4) and active diffusion. To understand the different variables and their impact on peroxisome distribution, we have created a mathematical model.

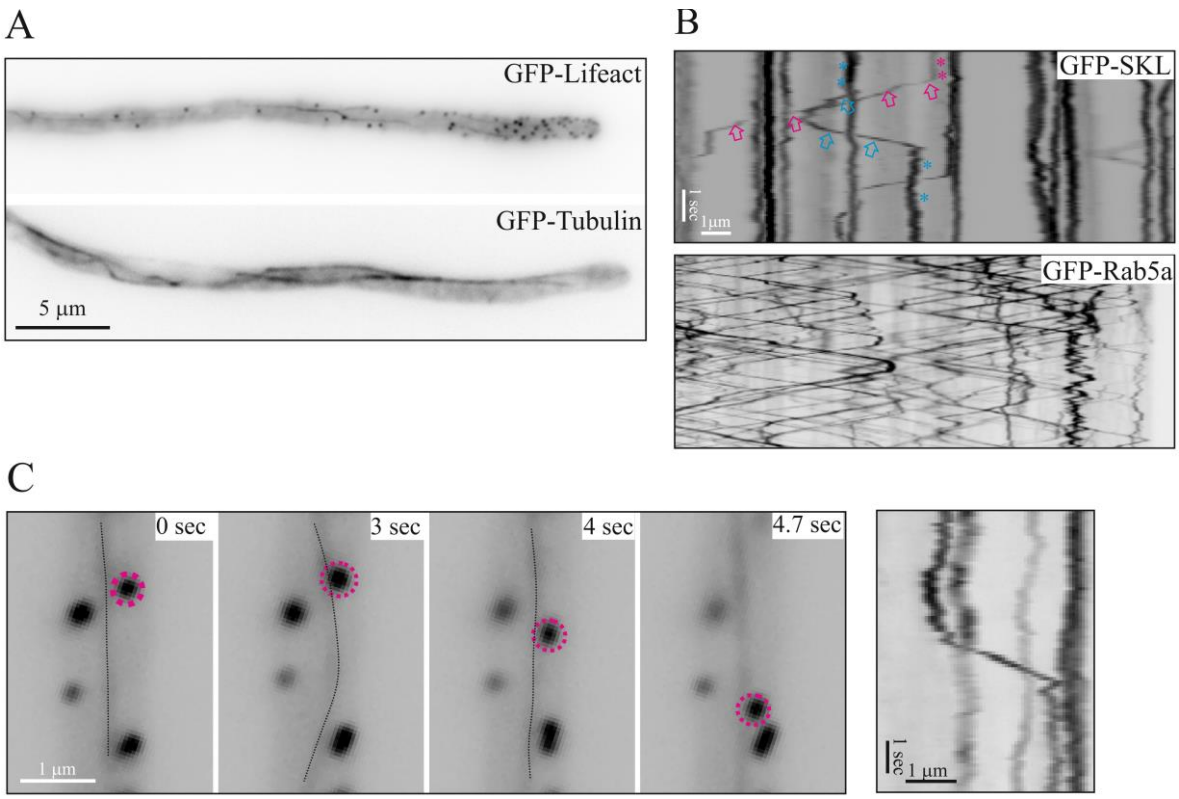

Figure 36 - Parameters for the hypothetical hyphal model. A) *Upper panel:* Actin cables and patches labelled with Lifeact, a peptide that labels actin. The patches are predominantly in a 5 µm region behind the tip but also at the cell cortex, more frequently at the cell periphery. *Lower panel:* Microtubule phenotype after labelling with GFP-tubulin where the bundles and flexible morphology is visible. Scale bar, 5 µm. B) *Upper panel:* Kymographs represent the dynamic behaviour of peroxisomes (GFP-SKL). The capacity of peroxisomes to switch from a stationary/diffusional state (asterisk) to a directed transport (arrows) is highlighted. *Lower panel*: Kymograph that exhibits the continuous and constant flow of early endosomes in the hyphal cell. Bars, 1 s, 1 µm. C) *Left panel:* Frames over 4.7 s of microtubule bending and peroxisome motility. Microtubule bends and grasps a peroxisome allowing its motility. Pink dashed circle over a moving peroxisome and dashed line delineates microtubule bending. *Right panel*: Kymograph of the left panel peroxisomal motion. Bars 1 s, 1 µm.

The model, generated in collaboration with Dr Congping Lin and Dr Peter Ashwin (Department of Mathematics, University of Exeter), describes the peroxisomal distribution along the cell. First, we considered the architecture of the hyphal cell. We combined all the available measurements and published data and a virtual cross section of the cell was generated. We considered that microtubules are in the middle of the cell, and actin cables are present at the cell periphery (Figure 36 A). Peroxisomes in close proximity with microtubules can either move by active diffusion or directed motility. To generate a virtual cell we analysed a set of parameters including: 1) hyphal diameter (2.03±0.03 µm, n=58); 2) peroxisome diameter (237.01±8.68 nm, n=45, measured in immuno-gold labelled electron micrographs) 3) early endosome size 187.35±11.4 nm (n= 56; determined from electron micrographs, derived from immuno-labelling experiments). We also estimated the area

around a microtubule and assumed, based on experimental data and previous studies: 1) two microtubule bundles (≈17 nm), 2) the diameter of a microtubule bundle (≈ 50 nm); 3) distance of the organelle to the microtubule (25nm). The same was performed to actin bundles where it was assumed that each hyphal cell comprises around 4.5 actin cables and that Myo5 (60 nm), F-actin (20 nm) and the secretory vesicles (40 nm) comprise 120 nm area.

After generating a hypothetical hyphal cell, it was presumed that three populations of peroxisomes contribute to their distribution: i) peroxisomes that bind to early endosomes and move anterograde; ii) peroxisomes that bind to early endosomes that undergo retrograde movements; iii) peroxisomes that undergo active diffusion and slow pole-ward drift. Peroxisomes can exchange between the three different states, from random motion to directed transport, as visible in image sequences (Figure 36 B). The turning point was calculated using the diffusion coefficient from experimental data. Moreover, the microtubule bending was also considered as it exerts a constant dynamic behaviour in the cell, and therefore enabling peroxisome- and/or other organelles' motility (Figure 36 C). To confirm the accuracy of the model, peroxisome distribution predictions were modelled in a region of 30 µm of the hyphal cell. Comparing experimental data to the model prediction accurately confirmed the distribution patterns, both in the control and in ΔHok1 cells (Figure 37 A), hence validating our model.

6.3.5 Modelling suggests that microtubule-dependent processes cooperate for peroxisome distribution

By creating a mathematical model that predicts the experimental outcome, we are able to dissect the impact of each independent mechanism, or combination, in peroxisomal mixing and distribution (Figure 38 B). We assume three essential contributions: 1) active diffusion enhanced by early endosome motility (active diffusion); 2) actin-based polar drift (polar drift); and 3) directed transport of peroxisomes along microtubules (directed transport). Peroxisome distribution is characterized by an even distribution with slight clustering at the cell tip (Control). Interestingly, by removing actin drift from the model, no clustering was predicted, which is in agreement with the experimental data where the peroxisomes are

unable to reach the tip. However, when active diffusion was removed, a slight accumulation at the apical region was predicted. The peroxisomal drift becomes even more pronounced when directed transport is abolished, reaching the highest degree of clustering when both microtubule-dependent processes were absent (active diffusion and directed transport). The latter exhibits a similar phenotype to ΔKin3. Curiously, when all three processes are abolished, peroxisomes evenly distribute throughout the cell, likely due to the lack of counteracting forces. In summary, we can conclude that: i) peroxisome distribution is governed by three major processes: active diffusion, actin drift and directed transport; ii) active diffusion and directed transport counteract the polar actin-based drift.

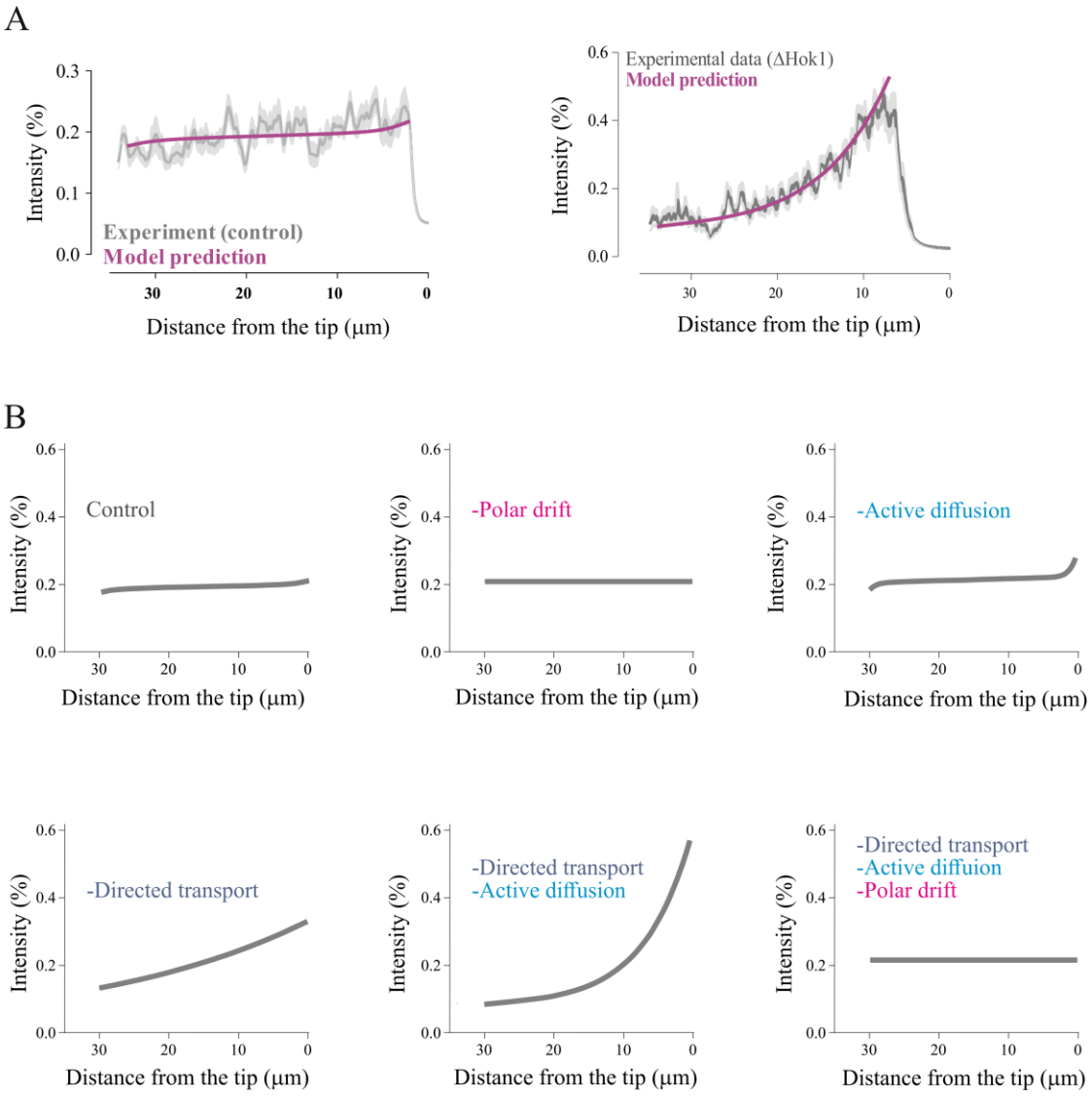

Figure 37 - Mathematical modelling simulation. A) Fitting of simulation (purple curve) to experimental data in the control and in Δhok1 cells. B) Simulation of different scenarios: control, polar drift, active diffusion and directed transport which are studied separately or in combination.

6.3.6 *U. maydis* and COS-7 cells share the same peroxisome distribution mechanism

In *U. maydis* microtubules and actin seem to act in an orchestrated manner to determine peroxisomal positioning. Previous studies in mammalian cells showed that peroxisomes move long distances in a microtubule-dependent manner and that actin might be implicated in short range motions (Schollenberger et al., 2010). *U. maydis* and COS-7 cells possess distinct cytoskeleton organization, however in both models peroxisomes are uniformly distributed throughout the cell (Figure 38 A). We have used COS-7 cells stably transfected with GFP-SKL for live cell imaging. We confirmed that in COS-7 cells, peroxisomes display the three types of motions: directed transport, oscillatory and stationary (Figure 38 B). The percentage of moving peroxisomes was approximately 12% (n=1793 peroxisomes) in *U. maydis*. In COS-7 cells about 6 % (n=4180 peroxisomes) move over long distances. Percentages were determined from 45 s movies and the total number of moving peroxisomes accounted.

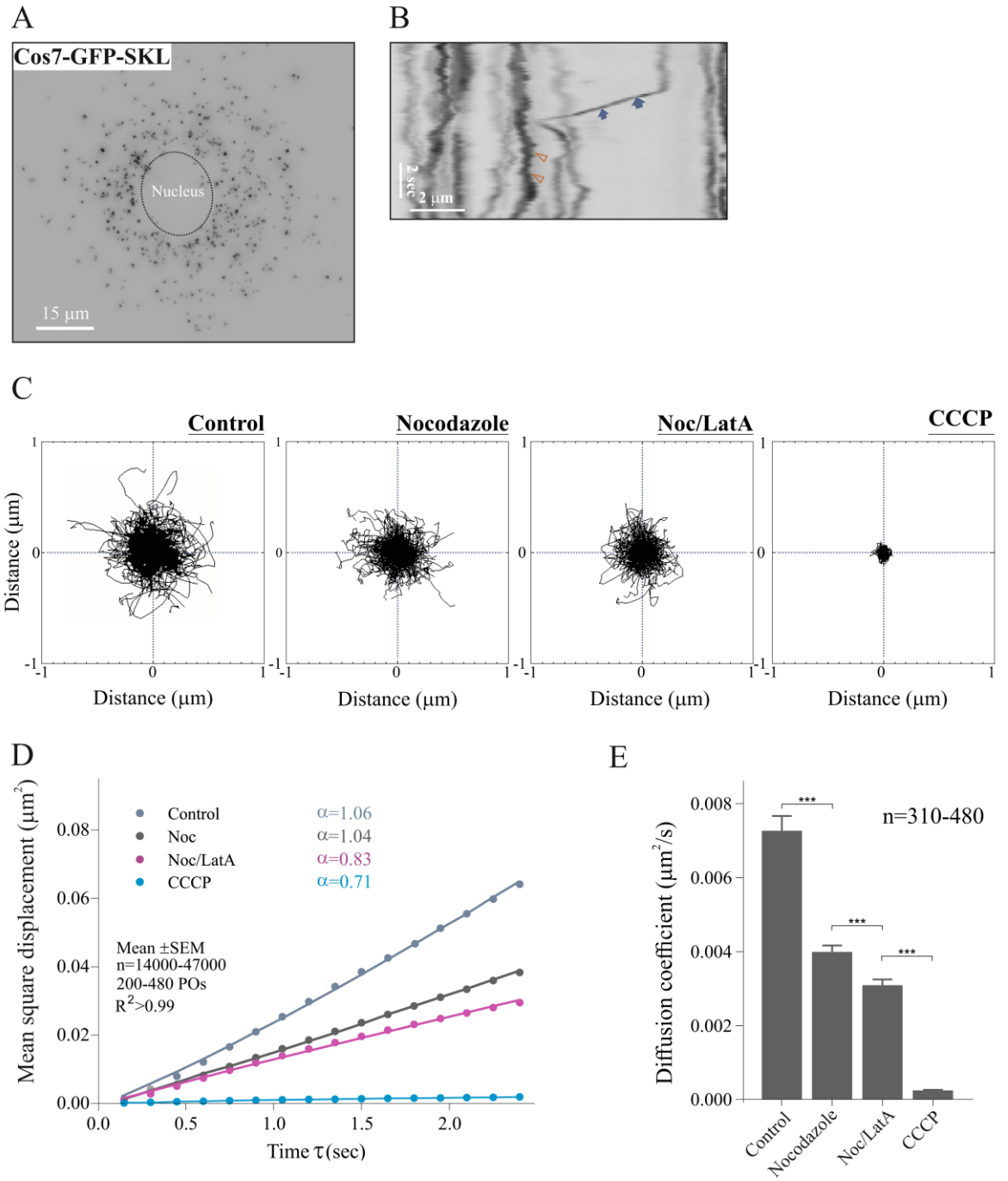

Figure 38 - Peroxisome distribution and motility in mammalian cells A) Peroxisome distribution in COS-GFP, GFP-SKL stably transfected in COS-7 cells. Image was contrast inverted. Brightness, contrast and gamma settings were adjusted. Scale bar, 15 µm. B) Kymograph shows directed (blue arrows) and oscillatory motility (orange arrowhead).Bars 2 s, 2 µm C) Qualitative plot analysis of peroxisomal trajectories in COS-7 cells when treated with DMSO, nocodazole, nocodazole plus latrunculin A and CCCP. D) MSD shows a decrease in the diffusion- Mean ± SEM is shown based on 14000-47000 measurements of 200-480 peroxisomes. E) Diffusion coefficient determined in the control, and cells treated with nocodazole, nocodazole plus latrunculin A, and CCCP. Sample size is indicated. ***, significant difference to control at $P < 0.0001$; n.s., non-significant when compared to the control, using a Student's t test.

Like in *U. maydis* the majority of peroxisomes showed oscillatory motion behaviour. We have treated COS-7 cells with nocodazole (microtubule depolymerisation agent), nocodazole plus latrunculin A and with CCCP. The cells were exposed to the different drugs for 30 min after which live-cell imaging was performed. As in *U. maydis*, peroxisome long-distance transport was highly compromised when cells were incubated with nocodazole. By plot analysis we could clearly observe that peroxisome diffusional behaviour was reduced when compared to the control (Figure 39 C). Moreover, when actin filaments were depolymerised, peroxisomal diffusional behaviour was additionally impaired. As observed in *U. maydis* by depleting ATP (CCCP), peroxisome motion was almost completely abolished. MSD analysis revealed that indeed peroxisomes present a diffusional behaviour (α= 1.06, control). By analysing the diffusion coefficient *D* it was confirmed that microtubule-dependent processes have a higher impact on peroxisomal diffusion behaviour. Together we show that peroxisome short-range motion in mammalian cells is: i) diffusional; ii) ATP-dependent; and iii) supported by microtubules and actin dynamic behaviour.

Schrader et al. (2000) have shown that depolymerisation of microtubules induces peroxisomal clustering in HepG2 cells, supporting the earlier observations in *U. maydis* (Figure 33 – benomyl). We have therefore treated COS-7 cells with 10 μM nocodazole over 6 hours, after which immunofluorescence against peroxisomal membrane protein (Pex14), αTubulin and phalloidin (actin marker). Indeed, cluster formation occurs when compared to control cells (DMSO) (Figure 39 A and C). To confirm a similar behaviour to the hyphal cells we combined latrunculin (300 nM) and nocodazole (10 μM) and treated for 6 hours. Remarkably, we observed a clear reduction in the number and fluorescent intensity of the peroxisomal clusters in the cell. In conclusion, peroxisome diffusional behaviour in mammalian cells acts in a similar manner than in the fungal system (Figure 39 A and B).

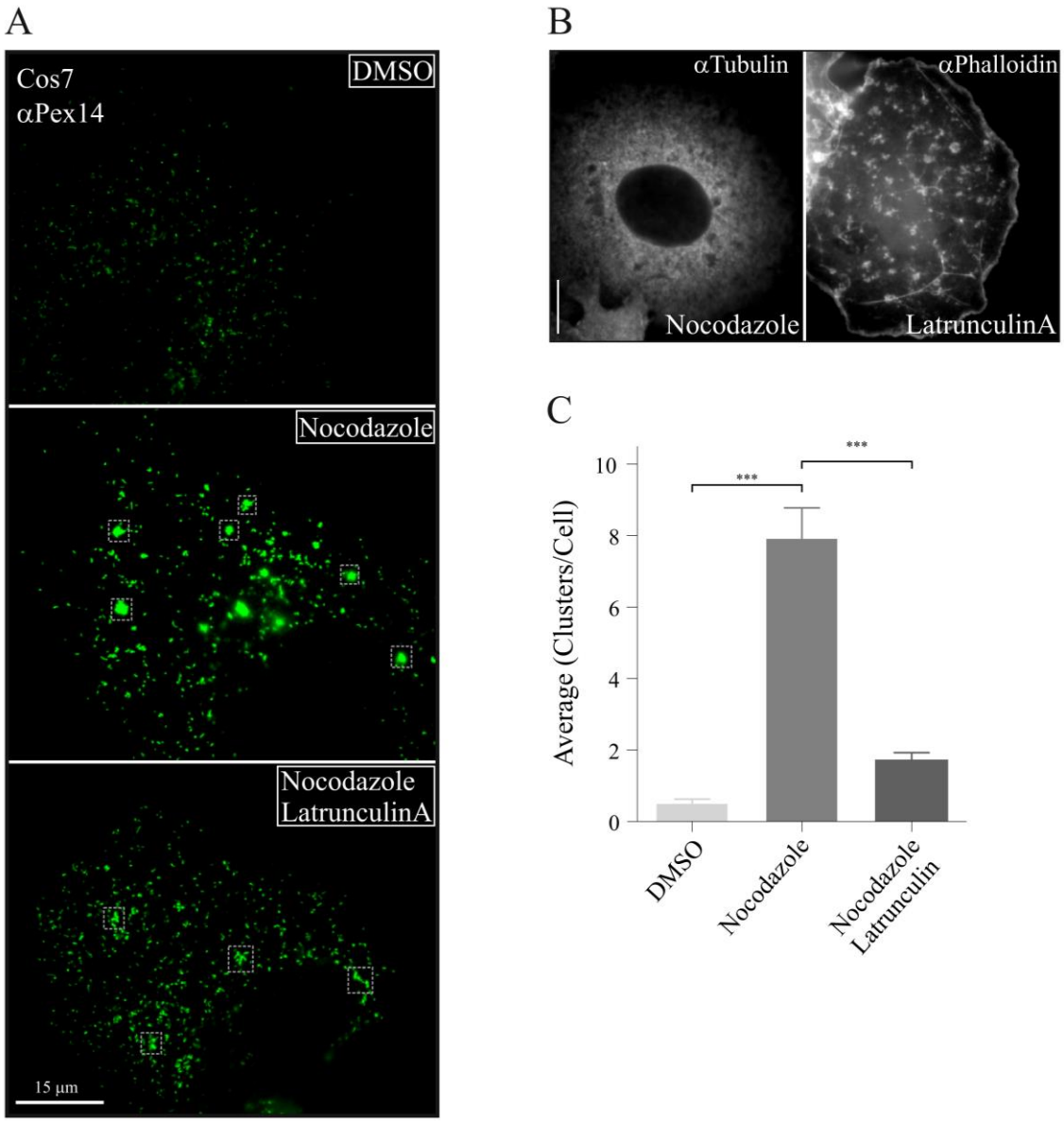

Figure 39 - Microtubule- and F-actin-based forces distribute peroxisomes in COS-7 cells. A) COS-7 cells were incubated with DMSO, nocodazole and LatA/nocodazole for 6 hours. Control cells show no peroxisomal clusters (left panel), nocodazole treatment resulted in high numbers of clusters (middle panel) and the combination of nocodazole and latrunculin A showed less clustering (right panel). Immunofluorescence was performed using antibody αPex14. Scale bar, 15 µm. B) Drug efficiency was analysed by immunofluorescence, α-tubulin/Alexa 488 staining confirmed microtubule depolymerisation, and Phalloidine-A594 staining confirmed actin dissociation. Scale bar 10 µm. C) Bar chart showing a decrease in the number of peroxisome clusters in DMSO and Nocodazole/LatA when compared to Nocodazole treatment. All bars are given as mean ± SEM (error bars) from at least 3 experiments. Sample size =219 cells.

6.4 Discussion

Organelle positioning within a cell is a mysterious process that is not yet fully understood. In mammals and filamentous fungi, peroxisomes show an even distribution throughout the cell. It is hypothesized that peroxisome distribution enables organelle-organelle interaction, lipid homeostasis, membrane and secondary metabolite synthesis, signalling and detoxification. It is known that peroxisome directed transport in *U. maydis* is mediated by microtubules and early endosomes. We have observed that in the absence of microtubules or early endosome motility, peroxisomes cluster at the polar region. A similar scenario was previously observed in *A. nidulans* in *HookA* and *Kin3* null mutants (Egan et al., 2012b; Zhang et al., 2014). Previous studies in *P. chrysogenum* suggested that peroxisomes accumulate at the hyphal tip due to biogenesis at the apical region (Meijer et al., 2010). We confirmed that in *U. maydis* that is not the case. Fungal hyphae are polar structures that extend by tip growth. This is due to constant delivery of secretory vesicles to the apical region, which will fuse with the plasma membrane and support cell elongation. Little is known about the underlying mechanism; however, myosin-5 plays a central role in polarized growth, which is conserved in the yeast *S. cerevisiae* (Govindan et al., 1995), *S. pombe* (Motegi et al., 2001) and the filamentous fungi *C. albicans* (Woo et al., 2003), *U. maydis* (Schuchardt et al., 2005; Weber et al., 2003) and *A. nidulans* (Taheri-Talesh et al., 2012; Zhang et al., 2011). Myosin 5, an actin motor, shows mainly anterograde short-range motility. We showed several lines of evidence that peroxisomes are moved by F-actin based polar drift. We have observed that when actin disassembled there was no formation of peroxisomal clusters, neither in the control nor in strain AB33Kin3^{ts}GFP-SKL. Also, by depleting Myo5, peroxisomes showed reduced motion at the cell tip. Although there were frequent motility events at the cell cortex, at the polar region the motility was diminished. It is known that F-actin is clustered at the cell apex (Weber et al., 2003) in the *U. maydis* ΔMyo5 strain, which corroborates our observations by disabling pole-ward flow. Moreover, peroxisomes at the cell tip were stationary which would imply the lack of a polar diffusional behaviour. To fully confirm the existence of a polar drift, we have analysed cells treated with latrunculin and benomyl for a longer period. With benomyl we could observe peroxisomal cluster similar to AB33ΔKin3, and in latrunculin treated cells, no peroxisomal cluster was present. Curiously, when cells were treated with benomyl, besides the formation of

peroxisomal clusters, we could also observe elongated peroxisomes, which have been described in mammalian cells (Schrader, 2001). We have determined that actin pole-ward flow transports peroxisomes to the tip when not counteracted by microtubules.

Short range oscillatory behaviour of peroxisomes has been suggested to be due to Brownian motion (Mathur et al., 2002). Brownian motion is characterized by stochastic diffusion of particles in a given space filled with other particles and physical barriers. Those particles can range from small molecules to entire organelles. However, it is suggested that the eukaryotic cell, Brownian motion is restricted. Instead, of thermal diffusional behaviour, active diffusion is essential. Active diffusion is dependent energy-driven movement such as the activity of molecular motors that by moving organelles along the cytoskeleton or rearrangement of the microtubules will enable a cytoplasmic mobility/fluidity. Using MSD analysis, we could confirm that peroxisomes underwent active diffusion and not Brownian motion in both mammalian cells and filamentous fungi. We further showed that active diffusion is a by-product of a chaotic microtubule based processes, namely, constant bidirectional motility of organelles and motor proteins, and due to microtubule dynamic behaviour (e.g. lateral bending).

By creating a mathematical model we were able to understand in more detail the effect of different parameters on peroxisomal motility and distribution. Peroxisomal directed motility mediated by microtubules is sporadic in *U. maydis* and COS-7 cells. However, we show here that it is essential for peroxisome distribution along the cell length. In our model we were able to observe that directed transport is essential for peroxisomal even distribution. Active diffusion does not alone disturb peroxisome positioning. Nevertheless, in the absence of directed transport and active diffusion, the actin-based flow is predominant and hence induces clustering of peroxisomes at the cell tip. Interestingly, in the absence of directed transport, active diffusion and polar drift, peroxisomes do not form any cluster which is thought to be due to the absence of counteracting forces. It is likely that active diffusion may be essential for organelle-organelle communication and therefore, alone, is not expected to exert a drastic impact on peroxisome distribution.

Lastly, we have shown that peroxisome random motion in mammalian cells, behaves in a similar manner to *U. maydis*. Both organisms show active random motion. Cluster formation when microtubules were depolymerized was overcome by disassembling the actin filament. Therefore, actin forces may counteract microtubules-related forces. Also, actin polymerization occurs mainly at the cell rim, thus leading to actin treadmilling towards the cell centre. This dynamic process might explain the accumulation of peroxisomes when microtubules are depolymerized. Nonetheless, the mechanism underpinning organelle distribution are yet to be fully elucidated. Our results show that, a similar balance of cytoskeleton forces for peroxisome distribution and positioning seems to be conserved from fungi to mammals.

7. GENERAL DISCUSSION AND FUTURE PERSPECTIVES

Peroxisomes are remarkable organelles that display diverse phenotypes and play different fundamental functions within the cell. They can vary in shape and protein content within the same cell and also between different species, even possessing specialized structures in some organisms (reviewed in 1.1.2). Their importance has been emphasized over the last decades due to their multiple roles in: the biosynthesis of bile acids, purines, antibiotics (penicillin), hormonal signalling molecules; the degradation of prostaglandins, amino acids, polyamines; signalling in viral immune defence; H_2O_2 signalling in hypothalamic neurons; amongst others (*reviewed in* Smith and Aitchison, 2013). Not surprisingly, impairment in single enzymes or proteins localized to these organelles in humans leads to severe pathologies (*reviewed in* De Munter et al., 2015). In the plant pathogenic fungi, peroxisomes have also been shown to play a key role in plant infection. In different fungal species it was shown that the deletion of certain peroxins or peroxisomal enzymes drastically reduces the fungal infection capacity of the host plant. In particular in the pathogenic fungus *U. maydis* recent studies have highlighted the importance of peroxisomes for fungal growth and pathogenicity (Klose and Kronstad, 2006; Kretschmer et al., 2012). *U. maydis* is a filamentous fungus that is known to infect maize resulting in tumours that ultimately might lead to a decrease in crop yield. On the other hand, it is, potentially, a new organism to study eukaryotic cell biology. *In silico* studies have shown that *H. sapiens* and *S. cerevisiae* share 514 proteins, whereas *H. sapiens* and *U. maydis* share 777 (Munsterkotter and Steinberg, 2007). In fact, *U. maydis* exhibits several features that are common to mammalian cells, but are absent in the widely used model *S. cerevisiae* (reviewed in 1.2.2). Another advantage of *U. maydis* is its easy handling together with its well established tools for genetic manipulation. Therefore, *U. maydis* has been suggested to be a reliable and valuable organism for new breakthroughs in the study of fundamental biological questions in the mammalian system. In this study, we were able to validate that *U. maydis* as a suitable model for peroxisomal biology. Firstly, in a combination of molecular and cell biology, bioinformatics and phylogenetic analyses we report a comprehensive inventory of peroxisomal proteins and pathways (Chapter 4 - Camoes et al., 2015). In addition, we have used *U. maydis* to study the mechanism of microtubule-based peroxisome motility, a process shared with mammalian cells but not yeast or plant cells (Chapter 5 - Guimaraes et al., 2015a). Moreover, in an interdisciplinary

approach, biological and mathematical methods, a model was developed for the understanding of peroxisome distribution and positioning, which revealed to be similar to the mammalian cells (Chapter 6 - Lin et al., 2016).

U. maydis β-oxidation is shared by peroxisomes and mitochondria

Different *in silico* studies have shown that in fungi most species possess a shared β-oxidation pathway between the mitochondria and peroxisomes. However, depending on the species in study the number of common functions differs (Camoes et al., 2015; Shen and Burger, 2009). In *U. maydis* a complete enzymatic set of mitochondrial and peroxisomal β-oxidation pathways was found (see 4.3.1). Furthermore, we provided evidence that ACADs are *bona fide* peroxisomal proteins in fungi and mammals and together with ACOXs belong to the basic enzymatic repertoire of peroxisomes. ACAD11 orthologues are present in all organisms analysed including other fungi but are completely absent in *S. cerevisiae* (Ochman et al., 2005). These findings highlight the understanding of the evolution and function of the complex interrelationship between peroxisomes and mitochondria. In addition, indicate that *U. maydis* is a suitable model to study organelle interplay and cooperation. Studies with a peroxisome-deficient ΔPex3 mutant revealed the existence of parallel and complex, cooperative β-oxidation pathways in peroxisomes and mitochondria, mimicking the situation in mammals (Figure 15). We could verify that in concordance with *in silico* data (Klose and Kronstad, 2006; Kretschmer et al., 2012), peroxisomes and mitochondria share fatty acid β-oxidation. Apparently, short- and medium-chain fatty acids are primarily metabolized in the mitochondria, whereas saturated and unsaturated long- and very long- chain fatty acids are substrates for peroxisomal β-oxidation followed by degradation in the mitochondria. The bioinformatics screen also showed that *U. maydis* possesses an incomplete enzymatic set for peroxisomal α-oxidation of C-3 branched-chain fatty acids (Figure 15). Mitochondria do not have the repertoire of enzymes required for α-oxidation. Alternatively to peroxisomes, C-3 branched-chain fatty acids may be degraded via ω-oxidation in the ER in mammals (Wanders et al., 2011b). As with the remaining fatty acids, our observations in *U. maydis* imply that α-oxidation relays on the same alternative pathways as well. With this study, we were able to open new routes to the understanding of the metabolic functions of peroxisomes in *U. maydis.* More importantly, we were able to highlight the similarities between β-

oxidation in *U. maydis* and *H. sapiens. U. maydis* genetic accessibility allows an easy manipulation of different genes. Therefore, it presents a useful model to study organelle interplay and cooperation.

Peroxisomes hitchhike on motile early endosomes in U. maydis

To date, little is known about the mechanism(s) of microtubule-dependent peroxisomal motility in different organisms; even less is available on the physiological importance of peroxisome motility and distribution in the cells. However, it is well established that peroxisomal motility in the mammalian and fungal system is highly regulated by kinesins and dyneins that travel on the microtubule array (Rapp et al., 1996). Contrary, in yeast and plants peroxisomal motility relies on actin filaments and myosins (Hoepfner et al., 2001; Jedd and Chua, 2002). *U. maydis* has been proven a suitable model for microtubule-based transport due to its highly polarized hyphal growth. In *U. maydis* microtubules are unipolar oriented near both cell poles but antipolar in the central region (Figure 40).

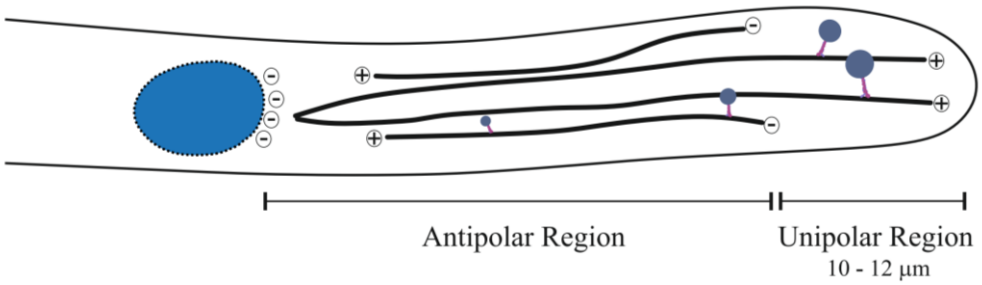

Figure 40 - Microtubule orientation in *U. maydis* Schematic representation of a hyphal cells shows unipolar region at 10-12 µm from the tip, whereas the central region is antipolar.

We could determine that peroxisome motility displays three different types of motilities, which are also found in mammalian cells: long-range, short-range and resting (Figure 17). We first characterized long-distance transport, which is mediated by dynein, kinesin-1 and -3. We showed that peroxisome motion is mediated by moving early endosomes (Figure 19). This was confirmed by reduction of peroxisome motion when early endosome motility was abolish or highly reduced (Figure 20). Recently, it was shown that in *U. maydis* and *A. nidulans*, dynein and kinesin-3 are bound to the protein-adaptor, Hok1 (Bielska, et al., 2014; Zhang et al., 2014). It was previously determined that early endosome motility is regulated by Hok1, with the C-terminus of Hok1 being the adaptor for early endosomes. Therefore, deletion of Hok1 abolished early endosome motility. Though, early endosomes motility was

re-established by expressing a Yup1 PX (ΔC-PX) domain that is known to bind to Rab5a-positive structures enriched in PtdINs(3)P (Gillooly et al., 2000; Lemmon, 2003). Hence, peroxisome motility was abolished in the Hok1ΔC mutant, and re-established in ΔC-PX (Figure 22). In addition, we have shown that peroxisomes hitchhike on constantly moving early endosomes. However, the linker between the two organelles is not known. Very recently, our observations were confirmed in *A. nidulans* , where peroxisome travel on early endosomes in a similar manner to *U. maydis*. Salogiannis et al. (2016) showed that the early-endosome associated protein PxdA acts as a linker protein between the early endosome and the peroxisome. In a short bioinformatics analysis, we found that PdxA has no homologues in *U. maydis* and in fact, is Ascomycota-specific. Although we now know how peroxisomes move in *U. maydis,* there are still questions to be addressed. Namely, the identification of the linker protein to the early endosomes, and the physiological relevance for peroxisome motility in *U. maydis* and other organisms. To search for the early endosome-peroxisome linker protein in *U. maydis*, screening approaches [e.g. UV (Bielska et al., 2014), mutagenesis drug-induced (Tan et al., 2014)] for peroxisomal misdistribution or impaired motility could be performed.

In mammals, a receptor/adaptor protein which links the microtubule-dependent motor proteins to peroxisomes has long been elusive. However, our laboratory has evidence that Miro1 is involved in the recruitment of kinesin to peroxisomes in mammalian cells (unpublished data). It will be essential to elucidate, if peroxisomes in mammalian cells can also hitchhike on other organelles under certain conditions or bind directly to the microtubule tracks.

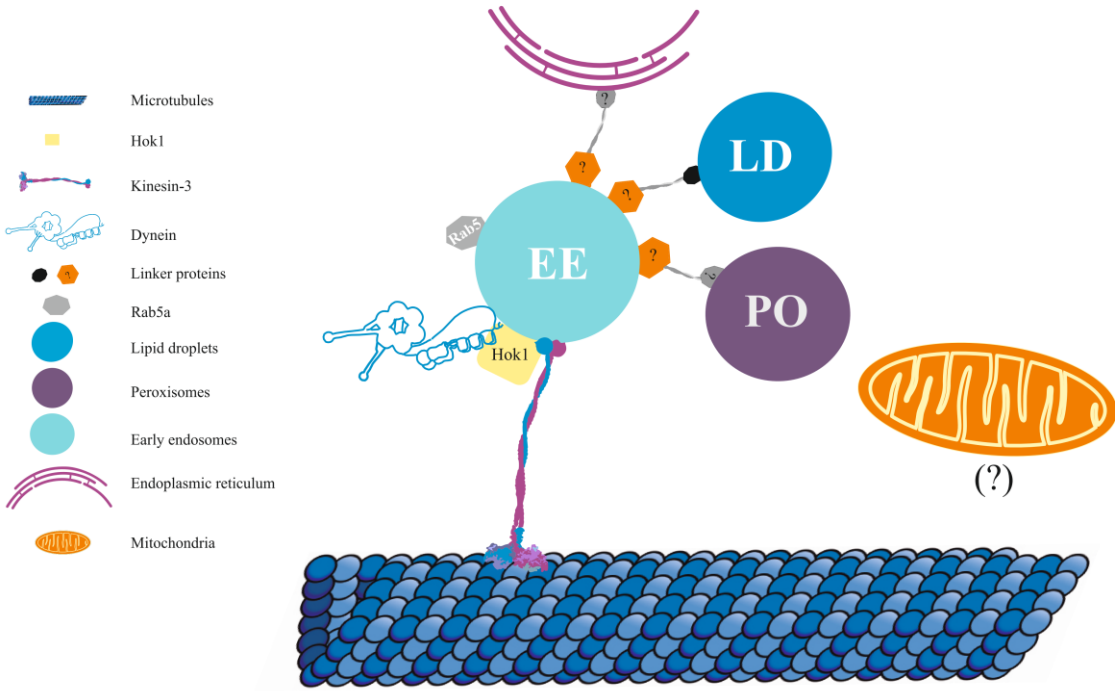

Figure 41 - Organelles hitchhike on early endosomes. Schematic view of the early-endosome regulated motility. Peroxisomes, lipid droplets and the endoplasmic reticulum bind to the fast moving early endosome and move over long distances. Mitochondria motility is not fully elucidated.

Cross-talk of peroxisomes with other organelles has long been described, so we addressed if in *U. maydis* the motility of organelles such as lipid droplets, mitochondria or the ER motility were in any way influenced by the early endosomes. We found that lipid droplets and endoplasmic reticulum move with the early endosomes (Figure 24,26 and 41). However, mitochondrial movement was independent (Figure 25). Nevertheless, mitochondria cluster at the nuclear region in the absence of early endosome motility. Interestingly, in hippocampal neurons, overexpression of Kif5 cargo-binding domain disrupts mitochondrial adaptor proteins and consequently impairs anterograde transport (Cai et al., 2005), suggesting that in the absence of Hok1 the mitochondria cargo-binding mechanism might be altered.

Moreover, we observed that motility of peroxisomes, lipid droplets and the ER was not exclusively mediated by the early endosomes. In fact, a small population of peroxisomes and the ER moved independently; this was even more prominent for lipid droplets (Figure 27). We found that the endoplasmic reticulum appears to account for the independent movements of the peroxisomes and the lipid droplets. One can reason that the different types of motility account for inter-organelle crosstalk. Recently, it was shown that peroxisomes are in close contact with the ERMES complex and lysosomes (Cohen et al., 2014; Chu et al., 2015).

Therefore, the ER-dependent motion might be fundamental for exchanging metabolites and regulation of lipid homeostasis. We hypothesise that different motility events are triggered by different signals to account for different functions. In mammals, it has been described that Pex14 binds to microtubules exclusively to targeted peroxisomes for degradation (Bharti et al., 2011, Jiang et al. 2015). This may suggest that different regulatory motility mechanisms are also present in the mammalian and fungal system. To date, it is not completely understood why peroxisomes, lipid droplets and the endoplasmic reticulum move, however we speculate that it is essential for fatty acid degradation, hydrogen peroxide detoxification and autophagy. *U. maydis* with its robustness and excellent accessibility to molecular genetics is a suitable model to study different stimuli and their impact on the motility and interaction of organelles. In fact, in our observations, interactions between different cellular compartments were frequently visualised which strengthen the use of *U. maydis* towards the understanding of organelle-organelle interplay and cooperation.

In conclusion, we identified early endosomes as a key regulator for the motility and distribution of peroxisomes, lipid droplets and the endoplasmic reticulum. This piggyback mechanism is not exclusive for *U. maydis* (Jourdain et al., 2008; Sparkes et al., 2009; Salogiannis et al., 2016). If similar piggyback mechanisms are shared with higher eukaryotes has to be elucidated.

Peroxisomal spatial organization in fungal and mammalian cells is dependent on opposing cytoskeletal forces

The distribution of organelles throughout the cell is key for cellular function and homeostasis. We have found that peroxisomes in *U. maydis* cluster at the tip region of the hyphae when the plus-end motor (Kin3) is deleted (Figure 28). First, we determined that this accumulation is not due to the formation of new peroxisomes at the tip (Figure 29). Instead, results from propelling forces of the actin cytoskeleton that mediated the drift of the peroxisomes towards the microtubule-plus-end (Figure 30-32). *U. maydis* fungal hyphae are polarized structures that constantly expand by tip growth (*reviewed in* Steinberg, 2007). This polar expansion is mediated by constant delivery of secretory vesicles to the plasma membrane at the cell tip (*reviewed in* Steinberg, 2007). Although our knowledge on vesicle delivery is still scarce it is well defined that myosin-5 is essential for polar growth in different fungi e.g., *U.* maydis, and in neurons. Moreover, one can say that the polymerization

processes of actin and microtubules might account for the polar drift of peroxisomes. In *U. maydis* microtubule polymerization occurs in antipolar bundles that extend to the polar regions (Schuster et al., 2011b). Hence is highly unlikely that microtubule polymerization enables accumulation at the cell poles. The high incidence of anterograde motility of myosin-5 (≈90%), suggest that the actin array is unipolar with the plus-end at the hyphal tip. Therefore, actin treadmilling will generate an opposing retrograde flow. In fact, this scenario has been observed in mammalian stereocilia (Naoz et al., 2008). Thus, it unexpected that the actin polymerization dynamics would cause the polar drift. Overall, is unforeseen that actin and/or microtubules polymerization regulate peroxisomal shift towards the cell apex. We thus assumed that this constant flow, when not counteracted by other forces (e.g., microtubule-mediated transport), allows the drift of peroxisomes towards the polar region.

We set out to understand this diffusional mechanism in more detail. In our system we have defined three types of motions: directed transport; active diffusion, and polar drift. Directed transport is mediated by the microtubules binding motors and target the peroxisomes over long distances in a ballistic motion. Active diffusion is defined as a random and diffusive motion however does not follows the principles of Brownian/thermal motion, e.g. the erratic movements are governed by temperature or size of particle. Brownian motion is rarely observed in cells. In fact, thermal equilibrium would lead to small-amplitude movements and stiffness of the microtubules, which is not present in the living system (Brangwynne et al., 2009). Active diffusion is a result of the cytoskeleton polymerization dynamics and the constant flow of molecular motor along those filaments. Polar drift is the consequence of the constant flow of myosin motors along the actin filaments at the cell periphery. Myosin, *in vitro*, was shown to induce internal tension leading to augmented stiffness of actin mesh (Mizuno et al., 2007; Koenderink et al., 2009). Interestingly, in such scenario random agitations are enhances, which might result from the forces exerted by the myosin motors to actin network (MacKintosh and Levine, 2008). For a comprehensive study on effect of each motion in peroxisomal distribution we have generated a mathematical modelling. To this end, a hypothetical hyphal cross section was hypothesized with actin bundles positioned at the cell periphery (Figure 42 - dark grey area) and 2 microtubule bundles at the cell centre (Figure 42 - two light grey regions). It was considered that areas surrounding actin and microtubules fibres enhance the collision probability. This “collision zones” enable the

likelihood of an organelle to collide with another organelle or motor protein, thus causing diffusion.

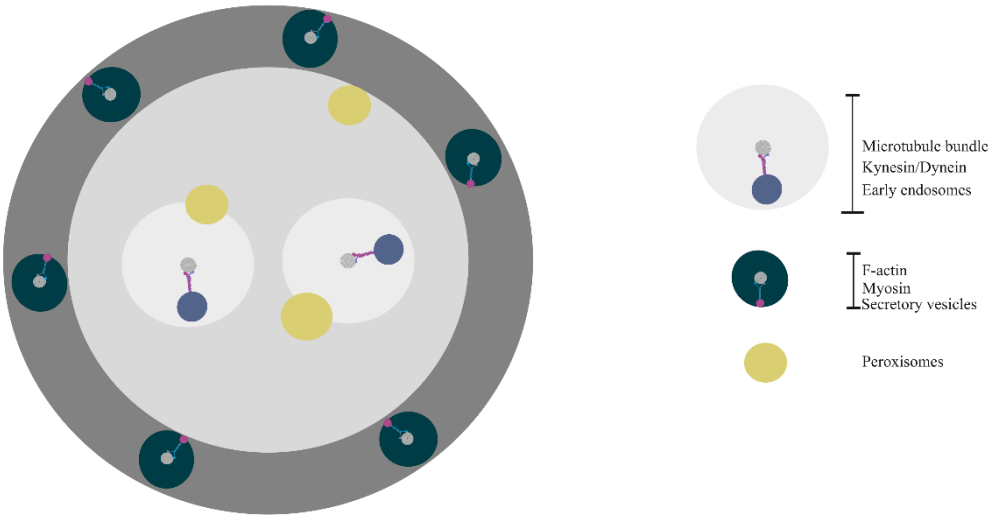

Figure 42 - Schematic view of the hypothetical cross section of a hyphal cell. Section of the hyphal cell with two microtubules at the cell centre. Motors are constantly moving on microtubules, enabling a constant contact with peroxisomes in the area surrounding the movement, the collision zones. Moreover, pole-ward forces are present at the periphery, where the myosin travels along the actin cables and therefore creating a propelling actomyosin forces when in contact with organelles.

By combining the hypothetical hyphae and the different motilities of peroxisomes: directed transport (anterograde and retrograde), active diffusion and polar drift it was able fit the experimental curves (control and ΔHok1). Therefore we could use this system to understand the distribution mechanism of peroxisomes in the hyphal cell. We conclude that directed transport and active diffusion counteract with polar drift. Diffusional behaviour is highly enhanced by organelles trafficking along the microtubules, in our study, early endosomes were shown to be fundamental for active diffusion. Reduction of early endosome motility causes a diminishment of peroxisomal diffusional behaviour. With this model it was shown that directed transport is essential to counteract with the polar drift. Interestingly, with both microtubule-based processes (active diffusion and directed transport) the cluster formation is even more prominent than without directed transport alone. However, if no active diffusion is available, peroxisomes distribution is very similar to the control. The reason is elusive, although one could hypothesise that the active diffusion is fundamental for organelle-organelle interaction and not essential for distribution alone, but likely to provide strength to directed transport. This cooperation between cytoskeleton forces has been

described in other organisms: melanocytes, where actin and microtubules regulate clustering (perinuclear region) and dispersion (cell periphery) of melanosomes in melanocyte dendrites (Evans et al., 2014); in *Xenopus* melanophores (Gross et al., 2002); and in mouse oocytes (Almonacid et al., 2015) implying a conserved mechanims across species. In fact, the use of COS-7 cells showed that peroxisomes positioning seem to be regulated by an actin and microtubule-based process. Moreover, the diffusional behaviour of peroxisomes was shown to be ATP-dependent and not Brownian motion. Our observation showed that both in *U. maydis* and COS-7 cells long periods of depolymerisation of microtubules result in the formation of peroxisomes aggregates, which are partially overcome by depletion of actin (Figure 39). Together, our observations show that despite the fact that *U. maydis* and COS-7 cells are different in their cytoskeleton organization, similar mechanisms cooperatively mediate the uniform distribution of peroxisomes. Although we were able to comprehend how peroxisomes cluster, to the date no information is there on the impact on peroxisomal functions. Curiously, it was shown that, in neurons, mitochondria accumulate where the need for ATP is higher (Morris and Hollenbeck, 1993). One could say that peroxisomes drift towards the tip to mediate cell survival, that might redistribute according to metabolic demands such as fatty acid degradation or ROS metabolism and signalling. Moreover, in different peroxisomal diseases and impairment in peroxisomal division proteins leads to large peroxisomes that display altered distribution in neurons and axons (Ishihara et al., 2009; Wakabayashi et al., 2009; Waterham et al., 2007). Therefore, *U. maydis* might be of key importance to understand disorders associated with impaired distribution of peroxisomes. In conclusion, we characterized peroxisome motility in *U. maydis* hyphal cell and developed a model to understand peroxisome distribution in fungi and mammals. This work not only emphasized *U. maydis* as a suitable model for molecular and metabolic studies on peroxisomes, but also as a tool for studies on peroxisomal disorders and therapeutics.

8. BIBLIOGRAPHY

Agrawal, G., S. Joshi, and S. Subramani. 2011. Cell-free sorting of peroxisomal membrane proteins from the endoplasmic reticulum. *Proc Natl Acad Sci U S A*. 108:9113-9118.

Al-Mehdi, A.B., V.M. Pastukh, B.M. Swiger, D.J. Reed, M.R. Patel, G.C. Bardwell, V.V. Pastukh, M.F. Alexeyev, and M.N. Gillespie. 2012. Perinuclear mitochondrial clustering creates an oxidant-rich nuclear domain required for hypoxia-induced transcription. *Sci Signal*. 5:ra47.

Alberts, B. 2014. Molecular biology of the cell. Vol. 2014. Garland Science, New York.

Alexander, A., J. Kim, and C.L. Walker. 2010. ATM engages the TSC2/mTORC1 signaling node to regulate autophagy. *Autophagy*. 6:672-673.

Ally, S., A.G. Larson, K. Barlan, S.E. Rice, and V.I. Gelfand. 2009. Opposite-polarity motors activate one another to trigger cargo transport in live cells. *J Cell Biol*. 187:1071-1082.

Almonacid, M., W.W. Ahmed, M. Bussonnier, P. Mailly, T. Betz, R. Voituriez, N.S. Gov, and M.H. Verlhac. 2015. Active diffusion positions the nucleus in mouse oocytes. *Nat Cell Biol*. 17:470-479.

Angermuller, S., G. Bruder, A. Volkl, H. Wesch, and H.D. Fahimi. 1987. Localization of xanthine oxidase in crystalline cores of peroxisomes. A cytochemical and biochemical study. *Eur J Cell Biol*. 45:137-144.

Antonenkov, V.D., S. Grunau, S. Ohlmeier, and J.K. Hiltunen. 2010. Peroxisomes are oxidative organelles. *Antioxid Redox Signal*. 13:525-537.

Antonenkov, V.D., and J.K. Hiltunen. 2012b. Transfer of metabolites across the peroxisomal membrane. *Biochim Biophys Acta*. 1822:1374-1386.

Armitage, J.P. 1999. Bacterial tactic responses. *Adv Microb Physiol*. 41:229-289.

Asakura, M., K. Yoshino, A.M. Hill, Y. Kubo, Y. Sakai, and Y. Takano. 2012. Primary and secondary metabolism regulates lipolysis in appressoria of Colletotrichum orbiculare. *Fungal Genet Biol*. 49:967-975.

Ayscough, K.R., J. Stryker, N. Pokala, M. Sanders, P. Crews, and D.G. Drubin. 1997. High rates of actin filament turnover in budding yeast and roles for actin in establishment and maintenance of cell polarity revealed using the actin inhibitor latrunculin-A. *J Cell Biol*. 137:399-416.

Baerends, R.J., S.W. Rasmussen, R.E. Hilbrands, M. van der Heide, K.N. Faber, P.T. Reuvekamp, J.A. Kiel, J.M. Cregg, I.J. van der Klei, and M. Veenhuis. 1996. The Hansenula polymorpha PER9 gene encodes a peroxisomal membrane protein essential for peroxisome assembly and integrity. *J Biol Chem*. 271:8887-8894.

Baker A, G.I. 2002. Plant Peroxisomes. Biochemistry, Cell Biology and Biotechnological Applications. Kluwer Academic Publishers, Dordrecht, The Netherlands.

Banuett, F. 1995. Genetics of Ustilago maydis, a fungal pathogen that induces tumors in maize. *Annu Rev Genet*. 29:179-208.

Banuett, F., and I. Herskowitz. 1989. Different a alleles of Ustilago maydis are necessary for maintenance of filamentous growth but not for meiosis. *Proc Natl Acad Sci U S A*. 86:5878-5882.

Banuett, F., and I. Herskowitz. 1994. Identification of fuz7, a Ustilago maydis MEK/MAPKK homolog required for a-locus-dependent and -independent steps in the fungal life cycle. *Genes Dev*. 8:1367-1378.

Barbosa, A.D., D.B. Savage, and S. Siniossoglou. 2015. Lipid droplet-organelle interactions: emerging roles in lipid metabolism. *Curr Opin Cell Biol*. 35:91-97.

Barnett, P., H.F. Tabak, and E.H. Hettema. 2000. Nuclear receptors arose from pre-existing protein modules during evolution. *Trends Biochem Sci*. 25:227-228.

Bartnicki-Garcia, S., D.D. Bartnicki, G. Gierz, R. Lopez-Franco, and C.E. Bracker. 1995. Evidence that Spitzenkorper behavior determines the shape of a fungal hypha: a test of the hyphoid model. *Exp Mycol*. 19:153-159.

Bartoszewska, M., L. Opalinski, M. Veenhuis, and I.J. van der Klei. 2011. The significance of peroxisomes in secondary metabolite biosynthesis in filamentous fungi. *Biotechnol Lett*. 33:1921-1931.

Bauer, S., J.C. Morris, and M.T. Morris. 2013. Environmentally regulated glycosome protein composition in the African trypanosome. *Eukaryot Cell*. 12:1072-1079.

Baumann, S., J. Konig, J. Koepke, and M. Feldbrugge. 2014. Endosomal transport of septin mRNA and protein indicates local translation on endosomes and is required for correct septin filamentation. *EMBO Rep*. 15:94-102.

Becht, P., J. Konig, and M. Feldbrugge. 2006. The RNA-binding protein Rrm4 is essential for polarity in Ustilago maydis and shuttles along microtubules. *J Cell Sci*. 119:4964-4973.

Bharti, P., W. Schliebs, T. Schievelbusch, A. Neuhaus, C. David, K. Kock, C. Herrmann, H.E. Meyer, S. Wiese, B. Warscheid, C. Theiss, and R. Erdmann. 2011. PEX14 is required for microtubule-based peroxisome motility in human cells. *J Cell Sci*. 124:1759-1768.

Bhetariya, P.J., T. Madan, S.F. Basir, A. Varma, and S.P. Usha. 2011. Allergens/Antigens, toxins and polyketides of important Aspergillus species. *Indian J Clin Biochem*. 26:104-119.

Bielska, E., Y. Higuchi, M. Schuster, N. Steinberg, S. Kilaru, N.J. Talbot, and G. Steinberg. 2014a. Long-distance endosome trafficking drives fungal effector production during plant infection. *Nat Commun*. 5:5097.

Bielska, E., M. Schuster, Y. Roger, A. Berepiki, D.M. Soanes, N.J. Talbot, and G. Steinberg. 2014b. Hook is an adapter that coordinates kinesin-3 and dynein cargo attachment on early endosomes. *J Cell Biol*. 204:989-1007.

Binns, D., T. Januszewski, Y. Chen, J. Hill, V.S. Markin, Y. Zhao, C. Gilpin, K.D. Chapman, R.G. Anderson, and J.M. Goodman. 2006. An intimate collaboration between peroxisomes and lipid bodies. *J Cell Biol*. 173:719-731.

Bolker, M. 2001. Ustilago maydis--a valuable model system for the study of fungal dimorphism and virulence. *Microbiology*. 147:1395-1401.

Bolker, M., H.U. Bohnert, K.H. Braun, J. Gorl, and R. Kahmann. 1995. Tagging pathogenicity genes in Ustilago maydis by restriction enzyme-mediated integration (REMI). *Mol Gen Genet*. 248:547-552.

Bonekamp, N.A., A. Volkl, H.D. Fahimi, and M. Schrader. 2009. Reactive oxygen species and peroxisomes: struggling for balance. *Biofactors*. 35:346-355.

Borgese, N., and E. Fasana. 2011. Targeting pathways of C-tail-anchored proteins. *Biochim Biophys Acta*. 1808:937-946.

Bornens, M. 2008. Organelle positioning and cell polarity. *Nat Rev Mol Cell Biol*. 9:874-886.

Bortfeld, M., K. Auffarth, R. Kahmann, and C.W. Basse. 2004. The Ustilago maydis a2 mating-type locus genes lga2 and rga2 compromise pathogenicity in the absence of the mitochondrial p32 family protein Mrb1. *Plant Cell*. 16:2233-2248.

Boyle, J.S., and A.M. Lew. 1995. An inexpensive alternative to glassmilk for DNA purification. *Trends Genet*. 11:8.

Brangwynne, C.P., G.H. Koenderink, F.C. MacKintosh, and D.A. Weitz. 2008. Cytoplasmic diffusion: molecular motors mix it up. *J Cell Biol*. 183:583-587.

Brangwynne, C.P., G.H. Koenderink, F.C. MacKintosh, and D.A. Weitz. 2009. Intracellular transport by active diffusion. *Trends Cell Biol*. 19:423-427.

Braverman, N.E., M.D. D'Agostino, and G.E. Maclean. 2013. Peroxisome biogenesis disorders: Biological, clinical and pathophysiological perspectives. *Dev Disabil Res Rev*. 17:187-196.

Brefeld, O. 1883. Botanische Untersuchunen ubreHefen pilze. *Die Bradpilze (Ustilagineen) Verlag V. A. Leipzig*.

Brocard, C., and A. Hartig. 2006. Peroxisome targeting signal 1: is it really a simple tripeptide? *Biochim Biophys Acta*. 1763:1565-1573.

Brocard, C.B., K.K. Boucher, C. Jedeszko, P.K. Kim, and P.A. Walton. 2005. Requirement for microtubules and dynein motors in the earliest stages of peroxisome biogenesis. *Traffic*. 6:386-395.

Broniec, A., R. Klosinski, A. Pawlak, M. Wrona-Krol, D. Thompson, and T. Sarna. 2011. Interactions of plasmalogens and their diacyl analogs with singlet oxygen in selected model systems. *Free Radic Biol Med*. 50:892-898.

Brown, L.A., and A. Baker. 2003. Peroxisome biogenesis and the role of protein import. *J.Cell Mol.Med.* 7:388-400.

Brunswik, H. 1924. Untersuchungen über Geschlechts- und Kernverhältnisse bei der Hymenomycetengattung Coprinus. *Bot. Abh*. 5:152.

Cai, Q., C. Gerwin, and Z.H. Sheng. 2005. Syntabulin-mediated anterograde transport of mitochondria along neuronal processes. *J Cell Biol*. 170:959-969.

Camoes, F., N.A. Bonekamp, H.K. Delille, and M. Schrader. 2009. Organelle dynamics and dysfunction: A closer link between peroxisomes and mitochondria. *J Inherit Metab Dis*. 32:163-180.

Camoes, F., M. Islinger, S.C. Guimaraes, S. Kilaru, M. Schuster, L.F. Godinho, G. Steinberg, and M. Schrader. 2015. New insights into the peroxisomal protein inventory: Acyl-CoA oxidases and -dehydrogenases are an ancient feature of peroxisomes. *Biochim Biophys Acta*. 1853:111-125.

Castillo-Lluva, S., I. Alvarez-Tabares, I. Weber, G. Steinberg, and J. Perez-Martin. 2007. Sustained cell polarity and virulence in the phytopathogenic fungus Ustilago maydis depends on an essential cyclin-dependent kinase from the Cdk5/Pho85 family. *J Cell Sci*. 120:1584-1595.

Chang, J., A. Fagarasanu, and R.A. Rachubinski. 2007. Peroxisomal peripheral membrane protein YlInp1p is required for peroxisome inheritance and influences the dimorphic transition in the yeast Yarrowia lipolytica. *Eukaryot Cell*. 6:1528-1537.

Chang, J., F.D. Mast, A. Fagarasanu, D.A. Rachubinski, G.A. Eitzen, J.B. Dacks, and R.A. Rachubinski. 2009. Pex3 peroxisome biogenesis proteins function in peroxisome inheritance as class V myosin receptors. *J Cell Biol*. 187:233-246.

Chapman, K.D., J.M. Dyer, and R.T. Mullen. 2012. Biogenesis and functions of lipid droplets in plants: Thematic Review Series: Lipid Droplet Synthesis and Metabolism: from Yeast to Man. *J Lipid Res*. 53:215-226.

Chavrier, P., R.G. Parton, H.P. Hauri, K. Simons, and M. Zerial. 1990. Localization of low molecular weight GTP binding proteins to exocytic and endocytic compartments. *Cell*. 62:317-329.

Chen, Y., L. Pieuchot, R.A. Loh, J. Yang, T.M. Kari, J.Y. Wong, and G. Jedd. 2014. Hydrophobic handoff for direct delivery of peroxisome tail-anchored proteins. *Nat Commun*. 5:5790.

Chu, B.B., Y.C. Liao, W. Qi, C. Xie, X. Du, J. Wang, H. Yang, H.H. Miao, B.L. Li, and B.L. Song. 2015. Cholesterol transport through lysosome-peroxisome membrane contacts. *Cell*. 161:291-306.

Cohen, Y., Y.A. Klug, L. Dimitrov, Z. Erez, S.G. Chuartzman, D. Elinger, I. Yofe, K. Soliman, J. Gartner, S. Thoms, R. Schekman, Y. Elbaz-Alon, E. Zalckvar, and M. Schuldiner. 2014. Peroxisomes are juxtaposed to strategic sites on mitochondria. *Mol Biosyst*. 10:1742-1748.

Corpas, F.J., J.B. Barroso, and L.A. del Rio. 2001. Peroxisomes as a source of reactive oxygen species and nitric oxide signal molecules in plant cells. *Trends Plant Sci*. 6:145-150.

Dagdas, G. Studies on Peroxisome Motility in the Model Fungal System Ustilago maydis (Doctoral dissertation). Retrieved from Open Research Exeter

Davidse, L.C., and W. Flach. 1977. Differential binding of methyl benzimidazol-2-yl carbamate to fungal tubulin as a mechanism of resistance to this antimitotic agent in mutant strains of Aspergillus nidulans. *J Cell Biol*. 72:174-193.

Day, P.R., S.L. Anagnostakis, and J.E. Puhalla. 1971. Pathogenicity resulting from mutation at the b locus of Ustilago maydis. *Proc Natl Acad Sci U S A*. 68:533-535.

De Munter, S., S. Verheijden, L. Regal, and M. Baes. 2015. Peroxisomal Disorders: A Review on Cerebellar Pathologies. *Brain Pathol*. 25:663-678.

Dean, R., J.A. Van Kan, Z.A. Pretorius, K.E. Hammond-Kosack, A. Di Pietro, P.D. Spanu, J.J. Rudd, M. Dickman, R. Kahmann, J. Ellis, and G.D. Foster. 2012. The Top 10 fungal pathogens in molecular plant pathology. *Mol Plant Pathol*. 13:414-430.

del Rio, L.A., L.M. Sandalio, F.J. Corpas, J.M. Palma, and J.B. Barroso. 2006. Reactive oxygen species and reactive nitrogen species in peroxisomes. Production, scavenging, and role in cell signaling. *Plant Physiol*. 141:330-335.

Delille, H.K., R. Alves, and M. Schrader. 2009. Biogenesis of peroxisomes and mitochondria: linked by division. *Histochem Cell Biol*. 131:441-446.

Delmaghani, S., J. Defourny, A. Aghaie, M. Beurg, D. Dulon, N. Thelen, I. Perfettini, T. Zelles, M. Aller, A. Meyer, A. Emptoz, F. Giraudet, M. Leibovici, S. Dartevelle, G. Soubigou, M. Thiry, E.S. Vizi, S. Safieddine, J.P. Hardelin, P. Avan, and C. Petit. 2015. Hypervulnerability to Sound Exposure through Impaired Adaptive Proliferation of Peroxisomes. *Cell*. 163:894-906.

Dias, A.F., T. Francisco, T.A. Rodrigues, C.P. Grou, and J.E. Azevedo. 2016. The first minutes in the life of a peroxisomal matrix protein. Biochim Biophys Acta. 1863:814-820.

Dietrich, D., F. Seiler, F. Essmann, and G. Dodt. 2013. Identification of the kinesin KifC3 as a new player for positioning of peroxisomes and other organelles in mammalian cells. *Biochim Biophys Acta*. 1833:3013-3024.

Dirkx, R., I. Vanhorebeek, K. Martens, A. Schad, M. Grabenbauer, D. Fahimi, P. Declercq, P.P. Van Veldhoven, and M. Baes. 2005. Absence of peroxisomes in mouse hepatocytes causes mitochondrial and ER abnormalities. *Hepatology*. 41:868-878.

Dixit, E., S. Boulant, Y. Zhang, A.S. Lee, C. Odendall, B. Shum, N. Hacohen, Z.J. Chen, S.P. Whelan, M. Fransen, M.L. Nibert, G. Superti-Furga, and J.C. Kagan. 2010. Peroxisomes are signaling platforms for antiviral innate immunity. *Cell*. 141:668-681.

Egan, M.J., M.A. McClintock, and S.L. Reck-Peterson. 2012a. Microtubule-based transport in filamentous fungi. *Curr Opin Microbiol*. 15:637-645.

Egan, M.J., K. Tan, and S.L. Reck-Peterson. 2012b. Lis1 is an initiation factor for dynein-driven organelle transport. *J Cell Biol*. 197:971-982.

Eitzen, G.A., R.K. Szilard, and R.A. Rachubinski. 1997. Enlarged peroxisomes are present in oleic acid-grown Yarrowia lipolytica overexpressing the PEX16 gene encoding an intraperoxisomal peripheral membrane peroxin. *J Cell Biol*. 137:1265-1278.

English, A.R., and G.K. Voeltz. 2013. Endoplasmic reticulum structure and interconnections with other organelles. *Cold Spring Harb Perspect Biol*. 5:a013227.

Erdmann, R., M. Veenhuis, D. Mertens, and W.H. Kunau. 1989. Isolation of peroxisome-deficient mutants of Saccharomyces cerevisiae. *Proc Natl Acad Sci U S A*. 86:5419-5423.

Evans, R.D., C. Robinson, D.A. Briggs, D.J. Tooth, J.S. Ramalho, M. Cantero, L. Montoliu, S. Patel, E.V. Sviderskaya, and A.N. Hume. 2014. Myosin-Va and dynamic actin oppose microtubules to drive long-range organelle transport. *Curr Biol*. 24:1743-1750.

Fagarasanu, A., M. Fagarasanu, G.A. Eitzen, J.D. Aitchison, and R.A. Rachubinski. 2006. The Peroxisomal Membrane Protein Inp2p Is the Peroxisome-Specific Receptor for the Myosin V Motor Myo2p of Saccharomyces cerevisiae. *Dev Cell*. 10:587-600.

Fagarasanu, M., A. Fagarasanu, Y.Y. Tam, J.D. Aitchison, and R.A. Rachubinski. 2005. Inp1p is a peroxisomal membrane protein required for peroxisome inheritance in Saccharomyces cerevisiae. *J Cell Biol*. 169:765-775.

Fang, Y., J.C. Morrell, J.M. Jones, and S.J. Gould. 2004. PEX3 functions as a PEX19 docking factor in the import of class I peroxisomal membrane proteins. *J Cell Biol*. 164:863-875. Epub 2004 Mar 2008.

Feiguin, F., A. Ferreira, K.S. Kosik, and A. Caceres. 1994. Kinesin-mediated organelle translocation revealed by specific cellular manipulations. *J Cell Biol*. 127:1021-1039.

Feldbrugge, M., J. Kamper, G. Steinberg, and R. Kahmann. 2004. Regulation of mating and pathogenic development in Ustilago maydis. *Curr Opin Microbiol*. 7:666-672.

Fink, G., and G. Steinberg. 2006. Dynein-dependent motility of microtubules and nucleation sites supports polarization of the tubulin array in the fungus Ustilago maydis. *Mol Biol Cell*. 17:3242-3253.

Fransen, M., M. Nordgren, B. Wang, and O. Apanasets. 2012. Role of peroxisomes in ROS/RNS-metabolism: Implications for human disease. *Biochim Biophys Acta*. 1822:1363-1373.

Fransen, M., M. Nordgren, B. Wang, O. Apanasets, and P.P. Van Veldhoven. 2013. Aging, age-related diseases and peroxisomes. *Subcell Biochem*. 69:45-65.

Fransen, M., I. Vastiau, C. Brees, V. Brys, G.P. Mannaerts, and P.P. Van Veldhoven. 2004. Potential role for Pex19p in assembly of PTS-receptor docking complexes. *J.Biol.Chem.* 279:12615-12624.

Fransen, M., I. Vastiau, C. Brees, V. Brys, G.P. Mannaerts, and P.P. Van Veldhoven. 2005. Analysis of human Pex19p's domain structure by pentapeptide scanning mutagenesis. *J.Mol.Biol.* 346:1275-1286.

Fransen, M., T. Wylin, C. Brees, G.P. Mannaerts, and P.P. Van Veldhoven. 2001. Human pex19p binds peroxisomal integral membrane proteins at regions distinct from their sorting sequences. *Mol.Cell Biol.* 21:4413-4424.

Freitag, J., J. Ast, and M. Bolker. 2012. Cryptic peroxisomal targeting via alternative splicing and stop codon read-through in fungi. *Nature*. 485:522-525.

Friedman, J.R., J.R. Dibenedetto, M. West, A.A. Rowland, and G.K. Voeltz. 2013. Endoplasmic reticulum-endosome contact increases as endosomes traffic and mature. *Mol Biol Cell*. 24:1030-1040.

Friedman, J.R., L.L. Lackner, M. West, J.R. DiBenedetto, J. Nunnari, and G.K. Voeltz. 2011. ER tubules mark sites of mitochondrial division. *Science*. 334:358-362.

Friedman, J.R., and G.K. Voeltz. 2011. The ER in 3D: a multifunctional dynamic membrane network. *Trends Cell Biol*. 21:709-717.

Froeliger, E.H., and S.A. Leong. 1991. The a mating-type alleles of Ustilago maydis are idiomorphs. *Gene*. 100:113-122.

Fuchs, U., G. Hause, I. Schuchardt, and G. Steinberg. 2006. Endocytosis is essential for pathogenic development in the corn smut fungus Ustilago maydis. *Plant Cell*. 18:2066-2081.

Fuchs, U., I. Manns, and G. Steinberg. 2005. Microtubules are dispensable for the initial pathogenic development but required for long-distance hyphal growth in the corn smut fungus Ustilago maydis. *Mol Biol Cell*. 16:2746-2758.

Fujiki, Y., K. Okumoto, S. Mukai, M. Honsho, and S. Tamura. 2014. Peroxisome biogenesis in mammalian cells. *Front Physiol*. 5:307.

Gandre-Babbe, S., and A.M. van der Bliek. 2008. The Novel Tail-anchored Membrane Protein Mff Controls Mitochondrial and Peroxisomal Fission in Mammalian Cells. Mol Biol Cell. 19:2402-2412.

Gao, Q., and J.M. Goodman. 2015. The lipid droplet-a well-connected organelle. *Front Cell Dev Biol*. 3:49.

Garcia-Muse, T., G. Steinberg, and J. Perez-Martin. 2003. Pheromone-induced G2 arrest in the phytopathogenic fungus Ustilago maydis. *Eukaryot Cell*. 2:494-500.

Gatto, G.J., Jr., B.V. Geisbrecht, S.J. Gould, and J.M. Berg. 2000. Peroxisomal targeting signal-1 recognition by the TPR domains of human PEX5. *Nat.Struct.Biol.* 7:1091-1095.

Geuze, H.J., J.L. Murk, A.K. Stroobants, J.M. Griffith, M.J. Kleijmeer, A.J. Koster, A.J. Verkleij, B. Distel, and H.F. Tabak. 2003. Involvement of the endoplasmic reticulum in peroxisome formation. *Mol Biol Cell*. 14:2900-2907.

Gillooly, D.J., I.C. Morrow, M. Lindsay, R. Gould, N.J. Bryant, J.M. Gaullier, R.G. Parton, and H. Stenmark. 2000. Localization of phosphatidylinositol 3-phosphate in yeast and mammalian cells. *EMBO J*. 19:4577-4588.

Girbardt, M. 1969. Die Ultrastruktur der Apikalregion von Pilzhyphen. *Protoplasma*. 67:413-441.

Gomes, L.C., and L. Scorrano. 2013. Mitochondrial morphology in mitophagy and macroautophagy. *Biochim Biophys Acta*. 1833:205-212.

Gould, G.W., and J. Lippincott-Schwartz. 2009. New roles for endosomes: from vesicular carriers to multi-purpose platforms. *Nat Rev Mol Cell Biol*. 10:287-292.

Gould, S.J., G.A. Keller, N. Hosken, J. Wilkinson, and S. Subramani. 1989. A conserved tripeptide sorts proteins to peroxisomes. *J.Cell Biol.* 108:1657-1664.

Govindan, B., R. Bowser, and P. Novick. 1995. The role of Myo2, a yeast class V myosin, in vesicular transport. *J Cell Biol*. 128:1055-1068.

Gross, S.P., M.C. Tuma, S.W. Deacon, A.S. Serpinskaya, A.R. Reilein, and V.I. Gelfand. 2002. Interactions and regulation of molecular motors in Xenopus melanophores. *J Cell Biol*. 156:855-865.

Guimaraes, S.C., M. Schuster, E. Bielska, G. Dagdas, S. Kilaru, B.R. Meadows, M. Schrader, and G. Steinberg. 2015a. Peroxisomes, lipid droplets, and endoplasmic reticulum "hitchhike" on motile early endosomes. *J Cell Biol*. 211:945-954.

Hanahan, D. 1985. in DNA Cloning: A Practical Approach. Glover, D. M. (ed.), Vol. 1, p. 109, IRL Press, McLean, Virginia.

Hara-Kuge, S., and Y. Fujiki. 2008. The peroxin Pex14p is involved in LC3-dependent degradation of mammalian peroxisomes. *Exp Cell Res*. 314:3531-3541.

Helle, S.C., G. Kanfer, K. Kolar, A. Lang, A.H. Michel, and B. Kornmann. 2013. Organization and function of membrane contact sites. *Biochim Biophys Acta*. 1833:2526-2541.

Herms, A., M. Bosch, N. Ariotti, B.J. Reddy, A. Fajardo, A. Fernandez-Vidal, A. Alvarez-Guaita, M.A. Fernandez-Rojo, C. Rentero, F. Tebar, C. Enrich, M.I. Geli, R.G. Parton, S.P. Gross, and A. Pol. 2013. Cell-to-cell heterogeneity in lipid droplets suggests a mechanism to reduce lipotoxicity. *Curr Biol*. 23:1489-1496.

Herrmann, L., C. Wiegmann, A. Arsalan-Werner, I. Hilbrich, C. Jager, K. Flach, A. Suttkus, I. Lachmann, T. Arendt, and M. Holzer. 2015. Hook proteins: association with Alzheimer pathology and regulatory role of hook3 in amyloid beta generation. *PLoS One*. 10:e0119423.

Hettema, E.H., W. Girzalsky, M. van Den Berg, R. Erdmann, and B. Distel. 2000. Saccharomyces cerevisiae pex3p and pex19p are required for proper localization and stability of peroxisomal membrane proteins. *Embo J*. 19:223-233.

Higuchi, Y., P. Ashwin, Y. Roger, and G. Steinberg. 2014. Early endosome motility spatially organizes polysome distribution. *J Cell Biol*. 204:343-357.

Hirokawa, N., and R. Takemura. 2005. Molecular motors and mechanisms of directional transport in neurons. *Nat Rev Neurosci*. 6:201-214.

Hirokawa, N., and Y. Tanaka. 2015. Kinesin superfamily proteins (KIFs): Various functions and their relevance for important phenomena in life and diseases. *Exp Cell Res*. 334:16-25.

Hoepfner, D., D. Schildknegt, I. Braakman, P. Philippsen, and H.F. Tabak. 2005. Contribution of the endoplasmic reticulum to peroxisome formation. *Cell*. 122:85-95.

Hoepfner, D., M. van den Berg, P. Philippsen, H.F. Tabak, and E.H. Hettema. 2001. A role for Vps1p, actin, and the Myo2p motor in peroxisome abundance and inheritance in Saccharomyces cerevisiae. *J Cell Biol*. 155:979-990.

Hoffman, C.S., and F. Winston. 1987. A ten-minute DNA preparation from yeast efficiently releases autonomous plasmids for transformation of Escherichia coli. *Gene*. 57:267-272.

Hoftberger, R., M. Kunze, T. Voigtlander, U. Unterberger, G. Regelsberger, J. Bauer, F. Aboul-Enein, F. Garzuly, S. Forss-Petter, H. Bernheimer, J. Berger, and H. Budka. 2010. Peroxisomal localization of the proopiomelanocortin-derived peptides beta-lipotropin and beta-endorphin. *Endocrinology*. 151:4801-4810.

Hohfeld, J., M. Veenhuis, and W.H. Kunau. 1991. PAS3, a Saccharomyces cerevisiae gene encoding a peroxisomal integral membrane protein essential for peroxisome biogenesis. *J Cell Biol*. 114:1167-1178.

Holliday, R. 1974. *Ustilago maydis* Handbook of Genetics. RC King, New York, Plenum 231-248 pp.

Hoogenraad, C.C., A. Akhmanova, F. Grosveld, C.I. De Zeeuw, and N. Galjart. 2000. Functional analysis of CLIP-115 and its binding to microtubules. *J Cell Sci*. 113:2285-2297.

Horner, S.M., H.M. Liu, H.S. Park, J. Briley, and M. Gale, Jr. 2011. Mitochondrial-associated endoplasmic reticulum membranes (MAM) form innate immune synapses and are targeted by hepatitis C virus. *Proc Natl Acad Sci U S A*. 108:14590-14595.

Horner, S.M., C. Wilkins, S. Badil, J. Iskarpatyoti, and M. Gale, Jr. 2015. Proteomic analysis of mitochondrial-associated ER membranes (MAM) during RNA virus infection reveals dynamic changes in protein and organelle trafficking. *PLoS One*. 10:e0117963.

Howard, R.J. 1981. Ultrastructural analysis of hyphal tip cell growth in fungi: Spitzenkorper, cytoskeleton and endomembranes after freeze-substitution. *J Cell Sci*. 48:89-103.

Hsu, V.W., and R. Prekeris. 2010. Transport at the recycling endosome. *Curr Opin Cell Biol*. 22:528-534.

Hu, J., A. Baker, B. Bartel, N. Linka, R.T. Mullen, S. Reumann, and B.K. Zolman. 2012. Plant Peroxisomes: Biogenesis and Function. *Plant Cell*. 24:2279-2303.

Huber, C., R. Saffrich, M. Anton, M. Passreiter, W. Ansorge, K. Gorgas, and W. Just. 1997. A heterotrimeric G protein-phospholipase A2 signaling cascade is involved in the regulation of peroxisomal motility in CHO cells. *J Cell Sci*. 110:2955-2968.

Huber, C.M., R. Saffrich, W. Ansorge, and W.W. Just. 1999. Receptor-mediated regulation of peroxisomal motility in CHO and endothelial cells. *Embo J*. 18:5476-5485.

Huotari, J., and A. Helenius. 2011. Endosome maturation. *EMBO J*. 30:3481-3500.

Hynes, M.J., S.L. Murray, G.S. Khew, and M.A. Davis. 2008. Genetic analysis of the role of peroxisomes in the utilization of acetate and fatty acids in Aspergillus nidulans. *Genetics*. 178:1355-1369.

Imazaki, A., A. Tanaka, Y. Harimoto, M. Yamamoto, K. Akimitsu, P. Park, and T. Tsuge. 2010. Contribution of peroxisomes to secondary metabolism and pathogenicity in the fungal plant pathogen Alternaria alternata. *Eukaryot Cell*. 9:682-694.

Ishihara, N., M. Nomura, A. Jofuku, H. Kato, S.O. Suzuki, K. Masuda, H. Otera, Y. Nakanishi, I. Nonaka, Y. Goto, N. Taguchi, H. Morinaga, M. Maeda, R. Takayanagi, S. Yokota, and K. Mihara. 2009. Mitochondrial fission factor Drp1 is essential for embryonic development and synapse formation in mice. *Nat Cell Biol*. 11:958-966.

Ishikawa, T., C. Kawai, M. Sano, and Y. Minatogawa. 2001. Peroxisomes exist in growth cones and move anterogradely and retrogradely in neurites of PC12D cells. *Exp Cell Res*. 266:260-269.

Islinger, M., S. Grille, H.D. Fahimi, and M. Schrader. 2012. The peroxisome: an update on mysteries. *Histochem Cell Biol*. 137:547-574.

Islinger, M., K.W. Li, J. Seitz, A. Volkl, and G.H. Luers. 2009. Hitchhiking of Cu/Zn superoxide dismutase to peroxisomes--evidence for a natural piggyback import mechanism in mammals. *Traffic*. 10:1711-1721.

Issemann, I., and S. Green. 1990. Activation of a member of the steroid hormone receptor superfamily by peroxisome proliferators. *Nature.* 347:645-650.

Jansen, G.A., S.J. Mihalik, P.A. Watkins, H.W. Moser, C. Jakobs, H.S. Heijmans, and R.J. Wanders. 1997. Phytanoyl-CoA hydroxylase is not only deficient in classical Refsum disease but also in rhizomelic chondrodysplasia punctata. *J Inherit Metab Dis*. 20:444-446.

Jansen, R.P., D. Niessing, S. Baumann, and M. Feldbrugge. 2014. mRNA transport meets membrane traffic. *Trends Genet*. 30:408-417.

Jean, S., and A.A. Kiger. 2012. Coordination between RAB GTPase and phosphoinositide regulation and functions. *Nat Rev Mol Cell Biol*. 13:463-470.

Jedd, G., and N.H. Chua. 2000. A new self-assembled peroxisomal vesicle required for efficient resealing of the plasma membrane. *Nat.Cell Biol.* 2:226-231.

Jedd, G., and N.H. Chua. 2002. Visualization of peroxisomes in living plant cells reveals acto-myosin-dependent cytoplasmic streaming and peroxisome budding. *Plant Cell Physiol.* 43:384-392.

Jiang, L., S. Hara-Kuge, S. Yamashita, and Y. Fujiki. 2015. Peroxin Pex14p is the key component for coordinated autophagic degradation of mammalian peroxisomes by direct binding to LC3-II. *Genes Cells*. 20:36-49.

Jones, J.M., J.C. Morrell, and S.J. Gould. 2004. PEX19 is a predominantly cytosolic chaperone and import receptor for class 1 peroxisomal membrane proteins. *J Cell Biol*. 164:57-67.

Jourdain, I., D. Sontam, C. Johnson, C. Dillies, and J.S. Hyams. 2008. Dynamin-dependent biogenesis, cell cycle regulation and mitochondrial association of peroxisomes in fission yeast. *Traffic*. 9:353-365.

Jovic, M., M. Sharma, J. Rahajeng, and S. Caplan. 2010. The early endosome: a busy sorting station for proteins at the crossroads. *Histol Histopathol*. 25:99-112.

Jung, M.K., I.B. Wilder, and B.R. Oakley. 1992. Amino acid alterations in the benA (beta-tubulin) gene of Aspergillus nidulans that confer benomyl resistance. *Cell Motil Cytoskeleton*. 22:170-174.

Kamper, J., R. Kahmann, M. Bolker, L.J. Ma, T. Brefort, B.J. Saville, F. Banuett, J.W. Kronstad, S.E. Gold, O. Muller, M.H. Perlin, H.A. Wosten, R. de Vries, J. Ruiz-Herrera, C.G. Reynaga-Pena, K. Snetselaar, M. McCann, J. Perez-Martin, M. Feldbrugge, C.W. Basse, G. Steinberg, J.I. Ibeas, W. Holloman, P. Guzman, M. Farman, J.E. Stajich, R. Sentandreu, J.M. Gonzalez-Prieto, J.C. Kennell, L. Molina, J. Schirawski, A. Mendoza-Mendoza, D. Greilinger, K. Munch, N. Rossel, M. Scherer, M. Vranes, O. Ladendorf, V. Vincon, U. Fuchs, B. Sandrock, S. Meng, E.C. Ho, M.J. Cahill, K.J. Boyce, J. Klose, S.J. Klosterman, H.J. Deelstra, L. Ortiz-Castellanos, W. Li, P. Sanchez-Alonso, P.H. Schreier, I. Hauser-Hahn, M. Vaupel, E. Koopmann, G. Friedrich, H. Voss, T. Schluter, J. Margolis, D. Platt, C. Swimmer, A. Gnirke, F. Chen, V. Vysotskaia, G. Mannhaupt, U. Guldener, M. Munsterkotter, D. Haase, M. Oesterheld, H.W. Mewes, E.W. Mauceli, D. DeCaprio, C.M. Wade, J. Butler, S. Young, D.B. Jaffe, S. Calvo, C. Nusbaum, J. Galagan, and B.W. Birren. 2006. Insights from the genome of the biotrophic fungal plant pathogen Ustilago maydis. *Nature*. 444:97-101.

Kapitein, L.C., M.A. Schlager, W.A. van der Zwan, P.S. Wulf, N. Keijzer, and C.C. Hoogenraad. 2010. Probing intracellular motor protein activity using an inducible cargo trafficking assay. *Biophys J*. 99:2143-2152.

Karpichev, I.V., Y. Luo, R.C. Marians, and G.M. Small. 1997. A complex containing two transcription factors regulates peroxisome proliferation and the coordinate induction of beta-oxidation enzymes in Saccharomyces cerevisiae. *Mol Cell Biol*. 17:69-80.

Kikuchi, M., N. Hatano, S. Yokota, N. Shimozawa, T. Imanaka, and H. Taniguchi. 2004. Proteomic analysis of rat liver peroxisome: presence of peroxisome-specific isozyme of Lon protease. *J Biol Chem*. 279:421-428.

Kim, H., S.C. Ling, G.C. Rogers, C. Kural, P.R. Selvin, S.L. Rogers, and V.I. Gelfand. 2007. Microtubule binding by dynactin is required for microtubule organization but not cargo transport. *J Cell Biol*. 176:641-651.

Kim, P.K., and E.H. Hettema. 2015. Multiple pathways for protein transport to peroxisomes. *J Mol Biol*. 427:1176-1190.

Kleff, S., S. Sander, G. Mielke, and R. Eising. 1997. The predominant protein in peroxisomal cores of sunflower cotyledons is a catalase that differs in primary structure from the catalase in the peroxisomal matrix. *Eur J Biochem*. 245:402-410.

Klose, J., and J.W. Kronstad. 2006. The multifunctional beta-oxidation enzyme is required for full symptom development by the biotrophic maize pathogen Ustilago maydis. *Eukaryot Cell*. 5:2047-2061.

Knoblach, B., X. Sun, N. Coquelle, A. Fagarasanu, R.L. Poirier, and R.A. Rachubinski. 2013. An ER-peroxisome tether exerts peroxisome population control in yeast. *EMBO J*. 32:2439-2453.

Koch, A., M. Thiemann, M. Grabenbauer, Y. Yoon, M.A. McNiven, and M. Schrader. 2003. Dynamin-like protein 1 is involved in peroxisomal fission. *J Biol Chem*. 278:8597-8605.

Koch, A., Y. Yoon, N.A. Bonekamp, M.A. McNiven, and M. Schrader. 2005. A role for fis1 in both mitochondrial and peroxisomal fission in Mammalian cells. *Mol Biol Cell*. 16:5077-5086.

Koch, J., and C. Brocard. 2011. Membrane elongation factors in organelle maintenance: the case of peroxisome proliferation. *BioMol Concepts*. 2:353-364.

Koch, J., K. Pranjic, A. Huber, A. Ellinger, A. Hartig, F. Kragler, and C. Brocard. 2010. PEX11 family members are membrane elongation factors that coordinate peroxisome proliferation and maintenance. *J Cell Sci*. 123:3389-3400.

Koenderink, G.H., Z. Dogic, F. Nakamura, P.M. Bendix, F.C. MacKintosh, J.H. Hartwig, T.P. Stossel, and D.A. Weitz. 2009. An active biopolymer network controlled by molecular motors. *Proc Natl Acad Sci U S A*. 106:15192-15197.

Kohlwein, S.D., M. Veenhuis, and I.J. van der Klei. 2013. Lipid droplets and peroxisomes: key players in cellular lipid homeostasis or a matter of fat--store 'em up or burn 'em down. *Genetics*. 193:1-50.

Kojic, M., C.F. Kostrub, A.R. Buchman, and W.K. Holloman. 2002. BRCA2 homolog required for proficiency in DNA repair, recombination, and genome stability in Ustilago maydis. *Mol Cell*. 10:683-691.

Kornmann, B., E. Currie, S.R. Collins, M. Schuldiner, J. Nunnari, J.S. Weissman, and P. Walter. 2009. An ER-mitochondria tethering complex revealed by a synthetic biology screen. *Science*. 325:477-481.

Kou, J., G.G. Kovacs, R. Hoftberger, W. Kulik, A. Brodde, S. Forss-Petter, S. Honigschnabl, A. Gleiss, B. Brugger, R. Wanders, W. Just, H. Budka, S. Jungwirth, P. Fischer, and J. Berger. 2011. Peroxisomal alterations in Alzheimer's disease. *Acta Neuropathol*. 122:271-283.

Kragt, A., T. Voorn-Brouwer, M. van den Berg, and B. Distel. 2005. Endoplasmic reticulum-directed Pex3p Routes to peroxisomes and restores peroxisome formation in a Saccharomyces cerevisiae pex3Delta strain. *J Biol Chem*. 280:34350-34357.

Kretschmer, M., J. Klose, and J.W. Kronstad. 2012. Defects in mitochondrial and peroxisomal beta-oxidation influence virulence in the maize pathogen Ustilago maydis. *Eukaryot Cell*. 11:1055-1066.

Kronstad, J.W., and S.A. Leong. 1990. The b mating-type locus of Ustilago maydis contains variable and constant regions. *Genes Dev*. 4:1384-1395.

Kulic, I.M., A.E. Brown, H. Kim, C. Kural, B. Blehm, P.R. Selvin, P.C. Nelson, and V.I. Gelfand. 2008. The role of microtubule movement in bidirectional organelle transport. *Proc Natl Acad Sci U S A*. 105:10011-10016.

Kunze, M., N. Malkani, S. Maurer-Stroh, C. Wiesinger, J.A. Schmid, and J. Berger. 2015. Mechanistic insights into PTS2-mediated peroxisomal protein import: the co-receptor PEX5L drastically increases the interaction strength between the cargo protein and the receptor PEX7. *J Biol Chem*. 290:4928-4940.

Kural, C., H. Kim, S. Syed, G. Goshima, V.I. Gelfand, and P.R. Selvin. 2005. Kinesin and dynein move a peroxisome in vivo: a tug-of-war or coordinated movement? *Science*. 308:1469-1472.

Lanver, D., A. Mendoza-Mendoza, A. Brachmann, and R. Kahmann. 2010. Sho1 and Msb2-related proteins regulate appressorium development in the smut fungus Ustilago maydis. *Plant Cell*. 22:2085-2101.

Lazarow, P.B. 1987. The role of peroxisomes in mammalian cellular metabolism. *J Inherit Metab Dis*. 10:11-22.

Lazarow, P.B., and Y. Fujiki. 1985. Biogenesis of peroxisomes. *Annu Rev Cell Biol*. 1:489-530.

Leber, R., E. Zinser, G. Zellnig, F. Paltauf, and G. Daum. 1994. Characterization of lipid particles of the yeast, Saccharomyces cerevisiae. *Yeast*. 10:1421-1428.

Lemberger, T., B. Desvergne, and W. Wahli. 1996. Peroxisome proliferator-activated receptors: a nuclear receptor signaling pathway in lipid physiology. *Annu Rev Cell Dev Biol*. 12:335-363.

Lemmon, M.A. 2003. Phosphoinositide recognition domains. *Traffic*. 4:201-213.

Lenz, J.H., I. Schuchardt, A. Straube, and G. Steinberg. 2006. A dynein loading zone for retrograde endosome motility at microtubule plus-ends. *EMBO J*. 25:2275-2286.

Lin, C; Schuster M ; Guimaraes SC, Ashwin P.; Schrader, M.; Metz J; Hacker, C., Gurr, S.J. and Steinberg G. Active diffusion and microtubule-based transport oppose myosin forces to position organelles in cells *Nature commun* (*in press*).

Lippincott-Schwartz, J., J.G. Donaldson, A. Schweizer, E.G. Berger, H.P. Hauri, L.C. Yuan, and R.D. Klausner. 1990. Microtubule-dependent retrograde transport of proteins into the ER in the presence of brefeldin A suggests an ER recycling pathway. *Cell*. 60:821-836.

Lismont, C., M. Nordgren, P.P. Van Veldhoven, and M. Fransen. 2015. Redox interplay between mitochondria and peroxisomes. *Front Cell Dev Biol*. 3:35.

Liu, F., Y. Lu, L. Pieuchot, T. Dhavale, and G. Jedd. 2011. Import oligomers induce positive feedback to promote peroxisome differentiation and control organelle abundance. *Dev Cell*. 21:457-468.

Lockshon, D., L.E. Surface, E.O. Kerr, M. Kaeberlein, and B.K. Kennedy. 2007. The sensitivity of yeast mutants to oleic acid implicates the peroxisome and other processes in membrane function. *Genetics*. 175:77-91.

Lodhi, I.J., and C.F. Semenkovich. 2014. Peroxisomes: a nexus for lipid metabolism and cellular signaling. *Cell Metab*. 19:380-392.

Ma, H., S. Kunes, P.J. Schatz, and D. Botstein. 1987. Plasmid construction by homologous recombination in yeast. *Gene*. 58:201-216.

MacKintosh, F.C., and A.J. Levine. 2008. Nonequilibrium mechanics and dynamics of motor-activated gels. *Phys Rev Lett*. 100:018104.

Mak, H.Y. 2012. Lipid droplets as fat storage organelles in Caenorhabditis elegans: Thematic Review Series: Lipid Droplet Synthesis and Metabolism: from Yeast to Man. *J Lipid Res*. 53:28-33.

Maldonado-Baez, L., N.B. Cole, H. Kramer, and J.G. Donaldson. 2013. Microtubule-dependent endosomal sorting of clathrin-independent cargo by Hook1. *J Cell Biol*. 201:233-247.

Manivannan, S., C.Q. Scheckhuber, M. Veenhuis, and I.J. van der Klei. 2012. The impact of peroxisomes on cellular aging and death. *Front Oncol*. 2:50.

Mao, K., X. Liu, Y. Feng, and D.J. Klionsky. 2014. The progression of peroxisomal degradation through autophagy requires peroxisomal division. *Autophagy*. 10:652-661.

Mariappan, M., A. Mateja, M. Dobosz, E. Bove, R.S. Hegde, and R.J. Keenan. 2011. The mechanism of membrane-associated steps in tail-anchored protein insertion. *Nature*. 477:61-66.

Martin, J.F., R.V. Ullan, and C. Garcia-Estrada. 2010. Regulation and compartmentalization of beta-lactam biosynthesis. *Microb Biotechnol*. 3:285-299.

Martin, S., and R.G. Parton. 2006. Lipid droplets: a unified view of a dynamic organelle. *Nat Rev Mol Cell Biol*. 7:373-378.

Masterson, C., and C. Wood. 2001. Mitochondrial and peroxisomal beta-oxidation capacities of organs from a non-oilseed plant. *Proc Biol Sci*. 268:1949-1953.

Masterson, C., and C. Wood. 2009. Influence of mitochondrial beta-oxidation on early pea seedling development. *New Phytol*. 181:832-842.

Mathur, J., N. Mathur, and M. Hulskamp. 2002. Simultaneous visualization of peroxisomes and cytoskeletal elements reveals actin and not microtubule-based peroxisome motility in plants. *Plant Physiol*. 128:1031-1045.

Matsuzono, Y., N. Kinoshita, S. Tamura, N. Shimozawa, M. Hamasaki, K. Ghaedi, R.J. Wanders, Y. Suzuki, N. Kondo, and Y. Fujiki. 1999. Human PEX19: cDNA cloning by functional complementation, mutation analysis in a patient with Zellweger syndrome, and potential role in peroxisomal membrane assembly. *Proc Natl Acad Sci U S A*. 96:2116-2121.

Matsuzono, Y., T. Matsuzaki, and Y. Fujiki. 2006. Functional domain mapping of peroxin Pex19p: interaction with Pex3p is essential for function and translocation. *J Cell Sci*. 119:3539-3550.

Mattiazzi Usaj, M., M. Brloznik, P. Kaferle, M. Zitnik, H. Wolinski, F. Leitner, S.D. Kohlwein, B. Zupan, and U. Petrovic. 2015. Genome-Wide Localization Study of Yeast Pex11 Identifies Peroxisome-Mitochondria Interactions through the ERMES Complex. *J Mol Biol*. 427:2072-2087.

McNew, J.A., and J.M. Goodman. 1994. An oligomeric protein is imported into peroxisomes in vivo. *J Cell Biol*. 127:1245-1257.

Meijer, W.H., L. Gidijala, S. Fekken, J.A. Kiel, M.A. van den Berg, R. Lascaris, R.A. Bovenberg, and I.J. van der Klei. 2010. Peroxisomes are required for efficient penicillin biosynthesis in Penicillium chrysogenum. *Appl Environ Microbiol*. 76:5702-5709.

Mellman, I., and W.J. Nelson. 2008. Coordinated protein sorting, targeting and distribution in polarized cells. *Nat Rev Mol Cell Biol*. 9:833-845.

Menon, S., C.C. Dibble, G. Talbott, G. Hoxhaj, A.J. Valvezan, H. Takahashi, L.C. Cantley, and B.D. Manning. 2014. Spatial control of the TSC complex integrates insulin and nutrient regulation of mTORC1 at the lysosome. Cell. 156:771-785

Michels, P.A., F. Bringaud, M. Herman, and V. Hannaert. 2006. Metabolic functions of glycosomes in trypanosomatids. *Biochim Biophys Acta*. 24:24.

Mihalik, S.J., J.C. Morrell, D. Kim, K.A. Sacksteder, P.A. Watkins, and S.J. Gould. 1997. Identification of PAHX, a Refsum disease gene. *Nat Genet*. 17:185-189.

Mindthoff, S., S. Grunau, L.L. Steinfort, W. Girzalsky, J.K. Hiltunen, R. Erdmann, and V.D. Antonenkov. 2016. Peroxisomal Pex11 is a pore-forming protein homologous to TRPM channels. *Biochim Biophys Acta*. 1863:271-283.

Mizuno, D., C. Tardin, C.F. Schmidt, and F.C. Mackintosh. 2007. Nonequilibrium mechanics of active cytoskeletal networks. *Science*. 315:370-373.

Morris, N.R., V.P. Efimov, and X. Xiang. 1998. Nuclear migration, nucleokinesis and lissencephaly. *Trends Cell Biol*. 8:467-470.

Morris, R.L., and P.J. Hollenbeck. 1993. The regulation of bidirectional mitochondrial transport is coordinated with axonal outgrowth. *J Cell Sci*. 104 (Pt 3):917-927.

Morris, R.L., and P.J. Hollenbeck. 1995. Axonal transport of mitochondria along microtubules and F-actin in living vertebrate neurons. *J Cell Biol*. 131:1315-1326.

Motegi, F., R. Arai, and I. Mabuchi. 2001. Identification of two type V myosins in fission yeast, one of which functions in polarized cell growth and moves rapidly in the cell. *Mol Biol Cell*. 12:1367-1380.

Motley, A.M., and E.H. Hettema. 2007. Yeast peroxisomes multiply by growth and division. *J Cell Biol*. 178:399-410.

Muench, D.G., and R.T. Mullen. 2003. Peroxisome dynamics in plant cells: a role for the cytoskeleton. *Plant Science*. 164:307-315.

Munsterkotter, M., and G. Steinberg. 2007. The fungus Ustilago maydis and humans share disease-related proteins that are not found in Saccharomyces cerevisiae. *BMC Genomics*. 8:473.

Muntau, A.C., A.A. Roscher, W.H. Kunau, and G. Dodt. 2003. The interaction between human PEX3 and PEX19 characterized by fluorescence resonance energy transfer (FRET) analysis. *Eur J Cell Biol*. 82:333-342.

Murphy, D.J. 2001. The biogenesis and functions of lipid bodies in animals, plants and microorganisms. *Prog Lipid Res*. 40:325-438.

Murphy, D.J., and J. Vance. 1999. Mechanisms of lipid-body formation. *Trends Biochem Sci*. 24:109-115.

Naoz, M., U. Manor, H. Sakaguchi, B. Kachar, and N.S. Gov. 2008. Protein localization by actin treadmilling and molecular motors regulates stereocilia shape and treadmilling rate. *Biophys J*. 95:5706-5718.

Neuberger, G., S. Maurer-Stroh, B. Eisenhaber, A. Hartig, and F. Eisenhaber. 2003. Motif refinement of the peroxisomal targeting signal 1 and evaluation of taxon-specific differences. J Mol Biol. 328:567-579.

Neuhaus, A., C. Eggeling, R. Erdmann, and W. Schliebs. 2016. Why do peroxisomes associate with the cytoskeleton? Biochim Biophys Acta. 1863:1019-1026.

Neuspiel, M., A.C. Schauss, E. Braschi, R. Zunino, P. Rippstein, R.A. Rachubinski, M.A. Andrade-Navarro, and H.M. McBride. 2008. Cargo-selected transport from the mitochondria to peroxisomes is mediated by vesicular carriers. *Current Biology*. 18:102-108.

Nguyen, T., J. Bjorkman, B.C. Paton, and D.I. Crane. 2006. Failure of microtubule-mediated peroxisome division and trafficking in disorders with reduced peroxisome abundance. *J Cell Sci*. 119:636-645.

Nielsen, E., F. Severin, J.M. Backer, A.A. Hyman, and M. Zerial. 1999. Rab5 regulates motility of early endosomes on microtubules. *Nat Cell Biol*. 1:376-382.

Nordgren, M., and M. Fransen. 2014. Peroxisomal metabolism and oxidative stress. *Biochimie*. 98:56-62.

Novikoff, A.B., and W.Y. Shin. 1964. The endoplasmic reticulum in the Golgi zone and its relations to microbodies, Golgi apparatus, and autophagic vacuoles in rat liver cells. *J Microscopy* 3:187-206.

Novikoff, P.M., and A.B. Novikoff. 1972. Peroxisomes in absorptive cells of mammalian small intestine. *J Cell Biol.* 53:532-560.

Nyathi, Y., and A. Baker. 2006. Plant peroxisomes as a source of signalling molecules. *Biochim Biophys Acta*. 1763:1478-1495.

Ochman, H., V. Daubin, and E. Lerat. 2005. A bunch of fun-guys: the whole-genome view of yeast evolution. *Trends Genet*. 21:1-3.

Odendall, C., E. Dixit, F. Stavru, H. Bierne, K.M. Franz, A.F. Durbin, S. Boulant, L. Gehrke, P. Cossart, and J.C. Kagan. 2014. Diverse intracellular pathogens activate type III interferon expression from peroxisomes. *Nat Immunol*. 15:717-726.

Ohsaki, Y., J. Cheng, M. Suzuki, Y. Shinohara, A. Fujita, and T. Fujimoto. 2009. Biogenesis of cytoplasmic lipid droplets: from the lipid ester globule in the membrane to the visible structure. *Biochim Biophys Acta*. 1791:399-407.

Ono, K., M. Kondo, T. Osafune, K. Miyatake, H. Inui, S. Kitaoka, M. Nishimura, and Y. Nakano. 2003. Presence of glyoxylate cycle enzymes in the mitochondria of Euglena gracilis. J Eukaryot Microbiol. 50:92-96.

Opalinski, L., M. Bartoszewska, S. Fekken, H. Liu, R. de Boer, I. van der Klei, M. Veenhuis, and J.A. Kiel. 2012. De novo peroxisome biogenesis in Penicillium chrysogenum is not dependent on the Pex11 family members or Pex16. *PLoS One*. 7:e35490.

Opalinski, L., J.A. Kiel, C. Williams, M. Veenhuis, and I.J. van der Klei. 2011. Membrane curvature during peroxisome fission requires Pex11. *EMBO J*. 30:5-16.

Otera, H., C. Wang, M.M. Cleland, K. Setoguchi, S. Yokota, R.J. Youle, and K. Mihara. 2010. Mff is an essential factor for mitochondrial recruitment of Drp1 during mitochondrial fission in mammalian cells. J Cell Biol. 191:1141-1158.

Otten, M., A. Nandi, D. Arcizet, M. Gorelashvili, B. Lindner, and D. Heinrich. 2012. Local motion analysis reveals impact of the dynamic cytoskeleton on intracellular subdiffusion. Biophys J. 102:758-767.

Otzen, M., R. Rucktaschel, S. Thoms, K. Emmrich, A.M. Krikken, R. Erdmann, and I.J. van der Klei. 2012. Pex19p contributes to peroxisome inheritance in the association of peroxisomes to myo2p. *Traffic*. 13:947-959.

Pacher, P., J.S. Beckman, and L. Liaudet. 2007. Nitric oxide and peroxynitrite in health and disease. *Physiol Rev*. 87:315-424.

Peeters, A., P. Fraisl, S. van den Berg, E. Ver Loren van Themaat, A. Van Kampen, M.H. Rider, H. Takemori, K.W. van Dijk, P.P. Van Veldhoven, P. Carmeliet, and M. Baes. 2011. Carbohydrate metabolism is perturbed in peroxisome-deficient hepatocytes due to mitochondrial dysfunction, AMP-activated protein kinase (AMPK) activation, and peroxisome proliferator-activated receptor gamma coactivator 1alpha (PGC-1alpha) suppression. *J Biol Chem*. 286:42162-42179.

Peeters, A., A.B. Shinde, R. Dirkx, J. Smet, K. De Bock, M. Espeel, I. Vanhorebeek, A. Vanlander, R. Van Coster, P. Carmeliet, M. Fransen, P.P. Van Veldhoven, and M. Baes. 2015. Mitochondria in peroxisome-deficient hepatocytes exhibit impaired respiration, depleted DNA, and PGC-1alpha independent proliferation. *Biochim Biophys Acta*. 1853:285-298.

Peraza-Reyes, L., and V. Berteaux-Lecellier. 2013. Peroxisomes and sexual development in fungi. *Front Physiol*. 4:244.

Phillips, M.J., and G.K. Voeltz. 2016. Structure and function of ER membrane contact sites with other organelles. *Nat Rev Mol Cell Biol*. 17:69-82.

Pinto, M.P., C.P. Grou, I.S. Alencastre, M.E. Oliveira, C. Sa-Miranda, M. Fransen, and J.E. Azevedo. 2006. The import competence of a peroxisomal membrane protein is determined by Pex19p before the docking step. *J Biol Chem*. 281:34492-34502.

Ploegh, H.L. 2007. A lipid-based model for the creation of an escape hatch from the endoplasmic reticulum. *Nature*. 448:435-438.

Poirier, Y., V.D. Antonenkov, T. Glumoff, and J.K. Hiltunen. 2006. Peroxisomal beta-oxidation--a metabolic pathway with multiple functions. *Biochim Biophys Acta*. 1763:1413-1426.

Pol, A., S.P. Gross, and R.G. Parton. 2014. Review: biogenesis of the multifunctional lipid droplet: lipids, proteins, and sites. *J Cell Biol*. 204:635-646.

Powers, S.K., and M.J. Jackson. 2008. Exercise-induced oxidative stress: cellular mechanisms and impact on muscle force production. *Physiol Rev*. 88:1243-1276.

Praefcke, G.J., and H.T. McMahon. 2004. The dynamin superfamily: universal membrane tubulation and fission molecules? *Nat Rev Mol Cell Biol*. 5:133-147.

Prinz, W.A. 2014. Bridging the gap: membrane contact sites in signaling, metabolism, and organelle dynamics. *J Cell Biol*. 205:759-769.

Pu, J., C.W. Ha, S. Zhang, J.P. Jung, W.K. Huh, and P. Liu. 2011. Interactomic study on interaction between lipid droplets and mitochondria. *Protein Cell*. 2:487-496.

Rapp, S., R. Saffrich, M. Anton, U. Jakle, W. Ansorge, K. Gorgas, and W.W. Just. 1996. Microtubule-based peroxisome movement. *J Cell Sci*. 109:837-849.

Raymond, C.K., T.A. Pownder, and S.L. Sexson. 1999. General method for plasmid construction using homologous recombination. *Biotechniques*. 26:134-138, 140-131.

Reddy, J., and D. Svoboda. 1973. Further evidence to suggest that microbodies do not exist as individual entities. *Am J Pathol*. 70:421-438.

Ribeiro, D., I. Castro, D. Fahimi, and M. Schrader. 2012. Peroxisome morphology in pathology. *Histol Histopathol - Cellular and Molecular Biology*. 27, 661-67.

Richard, V.R., A. Beach, A. Piano, A. Leonov, R. Feldman, M.T. Burstein, P. Kyryakov, A. Gomez-Perez, A. Arlia-Ciommo, S. Baptista, C. Campbell, D. Goncharov, S. Pannu, D. Patrinos, B. Sadri, V. Svistkova, A. Victor, and V.I. Titorenko. 2014. Mechanism of liponecrosis, a distinct mode of programmed cell death. *Cell Cycle*. 13:3707-3726.

Rida, P.C., A. Nishikawa, G.Y. Won, and N. Dean. 2006. Yeast-to-hyphal transition triggers formin-dependent Golgi localization to the growing tip in Candida albicans. *Mol Biol Cell*. 17:4364-4378.

Rodriguez-Serrano, M., M.C. Romero-Puertas, I. Sparkes, C. Hawes, L.A. del Rio, and L.M. Sandalio. 2009. Peroxisome dynamics in Arabidopsis plants under oxidative stress induced by cadmium. *Free Radic Biol Med*. 47:1632-1639.

Rokka, A., V.D. Antonenkov, R. Soininen, H.L. Immonen, P.L. Pirila, U. Bergmann, R.T. Sormunen, M. Weckstrom, R. Benz, and J.K. Hiltunen. 2009. Pxmp2 is a channel-forming protein in Mammalian peroxisomal membrane. *PLoS One*. 4:e5090.

Rowell, J.B. 1955. Segregation of Sex Factors in a Diploid Line of Ustilago zeae Induced by Alpha Radiation. *Science*. 121:304-306.

Sacksteder, K.A., and S.J. Gould. 2000. The genetics of peroxisome biogenesis. *Annu Rev Genet*. 34:623-652.

Saikia, S., and B. Scott. 2009. Functional analysis and subcellular localization of two geranylgeranyl diphosphate synthases from Penicillium paxilli. *Mol Genet Genomics*. 282:257-271.

Salogiannis, J., M.J. Egan, and S.L. Reck-Peterson. 2016. Peroxisomes move by hitchhiking on early endosomes using the novel linker protein PxdA. *J Cell Biol*. 212:289-296.

Sambrook, J. 2001. Molecular cloning : a laboratory manual. Cold Spring Harbor, N.Y.

Santos, M.J., T. Imanaka, H. Shio, G.M. Small, and P.B. Lazarow. 1988. Peroxisomal membrane ghosts in Zellweger syndrome--aberrant organelle assembly. *Science*. 239:1536-1538.

Schirawski, J., B. Heinze, M. Wagenknecht, and R. Kahmann. 2005. Mating type loci of Sporisorium reilianum: novel pattern with three a and multiple b specificities. *Eukaryot Cell*. 4:1317-1327.

Schliebs, W., and W.H. Kunau. 2006. PTS2 co-receptors: diverse proteins with common features. *Biochim Biophys Acta*. 1763:1605-1612.

Schollenberger, L., T. Gronemeyer, C.M. Huber, D. Lay, S. Wiese, H.E. Meyer, B. Warscheid, R. Saffrich, J. Peranen, K. Gorgas, and W.W. Just. 2010. RhoA regulates peroxisome association to microtubules and the actin cytoskeleton. *PLoS One*. 5:e13886.

Schrader, M. 2001. Tubulo-reticular clusters of peroxisomes in living COS-7 cells: dynamic behavior and association with lipid droplets. *J Histochem Cytochem*. 49:1421-1429.

Schrader, M., N.A. Bonekamp, and M. Islinger. 2012. Fission and proliferation of peroxisomes. *Biochim Biophys Acta*. 822:1343-1357.

Schrader, M., J.K. Burkhardt, E. Baumgart, G. Luers, H. Spring, A. Volkl, and H.D. Fahimi. 1996. Interaction of microtubules with peroxisomes. Tubular and spherical peroxisomes in HepG2 cells and their alterations induced by microtubule-active drugs. *Eur J Cell Biol*. 69:24-35.

Schrader, M., J. Costello, L.F. Godinho, and M. Islinger. 2015a. Peroxisome-mitochondria interplay and disease. *J Inherit Metab Dis*. 38:681-702.

Schrader, M., J.L. Costello, L.F. Godinho, A.S. Azadi, and M. Islinger. 2016. Proliferation and fission of peroxisomes - An update. *Biochim Biophys Acta*. 1863:971-983.

Schrader, M., and H.D. Fahimi. 2006. Peroxisomes and oxidative stress. *Biochim Biophys Acta*. 1763:1755-1766.

Schrader, M., and H.D. Fahimi. 2008. The peroxisome: still a mysterious organelle. *Histochem Cell Biol*. 129:421-440.

Schrader, M., L.F. Godinho, J.L. Costello, and M. Islinger. 2015b. The different facets of organelle interplay-an overview of organelle interactions. *Front Cell Dev Biol*. 3:56.

Schrader, M., and S.J. Gould. 2005. Assay and functional analysis of dynamin-like protein 1 in peroxisome division. *Methods Enzymol*. 404:586-597.

Schrader, M., S.J. King, T.A. Stroh, and T.A. Schroer. 2000. Real time imaging reveals a peroxisomal reticulum in living cells. *J Cell Sci*. 113:3663-3671.

Schrader, M., B.E. Reuber, J.C. Morrell, G. Jimenez-Sanchez, C. Obie, T.A. Stroh, D. Valle, T.A. Schroer, and S.J. Gould. 1998. Expression of PEX11beta mediates peroxisome proliferation in the absence of extracellular stimuli. *J Biol Chem*. 273:29607-29614.

Schrader, M., and Y. Yoon. 2007. Mitochondria and peroxisomes: are the 'big brother' and the 'little sister' closer than assumed? *Bioessays*. 29:1105-1114.

Schuchardt, I., D. Assmann, E. Thines, C. Schuberth, and G. Steinberg. 2005. Myosin-V, Kinesin-1, and Kinesin-3 cooperate in hyphal growth of the fungus Ustilago maydis. *Mol Biol Cell*. 16:5191-5201.

Schulz, B., F. Banuett, M. Dahl, R. Schlesinger, W. Schafer, T. Martin, I. Herskowitz, and R. Kahmann. 1990. The b alleles of U. maydis, whose combinations program pathogenic development, code for polypeptides containing a homeodomain-related motif. *Cell*. 60:295-306.

Schuster, M., S. Kilaru, P. Ashwin, C. Lin, N.J. Severs, and G. Steinberg. 2011a. Controlled and stochastic retention concentrates dynein at microtubule ends to keep endosomes on track. *EMBO J*. 30:652-664.

Schuster, M., S. Kilaru, G. Fink, J. Collemare, Y. Roger, and G. Steinberg. 2011b. Kinesin-3 and dynein cooperate in long-range retrograde endosome motility along a nonuniform microtubule array. *Mol Biol Cell*. 22:3645-3657.

Schuster, M., R. Lipowsky, M.A. Assmann, P. Lenz, and G. Steinberg. 2011c. Transient binding of dynein controls bidirectional long-range motility of early endosomes. *Proc Natl Acad Sci U S A*. 108:3618-3623.

Schuster, M., S. Treitschke, S. Kilaru, J. Molloy, N.J. Harmer, and G. Steinberg. 2012. Myosin-5, kinesin-1 and myosin-17 cooperate in secretion of fungal chitin synthase. *EMBO J*. 31:214-227.

Shai, N., M. Schuldiner, and E. Zalckvar. 2016. No peroxisome is an island - Peroxisome contact sites. *Biochim Biophys Acta*. 1863:1061-1069.

Shamseldin, H.E., M. Alshammari, T. Al-Sheddi, M.A. Salih, H. Alkhalidi, A. Kentab, G.M. Repetto, M. Hashem, and F.S. Alkuraya. 2012. Genomic analysis of mitochondrial diseases in a consanguineous population reveals novel candidate disease genes. *J Med Genet*. 49:234-241.

Sheibani, S., V.R. Richard, A. Beach, A. Leonov, R. Feldman, S. Mattie, L. Khelghatybana, A. Piano, M. Greenwood, H. Vali, and V.I. Titorenko. 2014. Macromitophagy, neutral lipids synthesis, and peroxisomal fatty acid oxidation protect yeast from "liponecrosis", a previously unknown form of programmed cell death. *Cell Cycle*. 13:138-147.

Shen, Y.Q., and G. Burger. 2009a. Plasticity of a key metabolic pathway in fungi. *Funct Integr Genomics*. 9:145-151.

Shen, Y.Q., B.F. Lang, and G. Burger. 2009b. Diversity and dispersal of a ubiquitous protein family: acyl-CoA dehydrogenases. Nucleic Acids Res. 37:5619-5631.

Shibata, H., Y. Kashiwayama, T. Imanaka, and H. Kato. 2004. Domain architecture and activity of human Pex19p, a chaperone-like protein for intracellular trafficking of peroxisomal membrane proteins. *J.Biol.Chem.* 279:38486-38494.

Sindelar, P.J., Z. Guan, G. Dallner, and L. Ernster. 1999. The protective role of plasmalogens in iron-induced lipid peroxidation. *Free Radic Biol Med*. 26:318-324.

Smith, J.J., and J.D. Aitchison. 2013. Peroxisomes take shape. *Nat Rev Mol Cell Biol*. 14:803-817.

Snetselaar, K.a.M., C. 1992. Sporidial fusion and infection of maize seedlings by the smut fungus Ustilago maydis. *Mycologia*. 84 (2):193-203.

Snetselaar, K.M., M. Bolker, and R. Kahmann. 1996. Ustilago maydis Mating Hyphae Orient Their Growth toward Pheromone Sources. *Fungal Genet Biol*. 20:299-312.

Sparkes, I.A., T. Ketelaar, N.C. de Ruijter, and C. Hawes. 2009. Grab a Golgi: laser trapping of Golgi bodies reveals in vivo interactions with the endoplasmic reticulum. *Traffic*. 10:567-571.

Spector, I., N.R. Shochet, Y. Kashman, and A. Groweiss. 1983. Latrunculins: novel marine toxins that disrupt microfilament organization in cultured cells. *Science*. 219:493-495.

Speijer, D. 2011. Oxygen radicals shaping evolution: why fatty acid catabolism leads to peroxisomes while neurons do without it: FADH(2)/NADH flux ratios determining mitochondrial radical formation were crucial for the eukaryotic invention of peroxisomes and catabolic tissue differentiation. Bioessays. 33:88-94.

Spellig, T., M. Bolker, F. Lottspeich, R.W. Frank, and R. Kahmann. 1994a. Pheromones trigger filamentous growth in Ustilago maydis. *EMBO J*. 13:1620-1627.

Spellig, T., E. Regenfelder, M. Reichmann, F. Schauwecker, R. Bohlmann, M. Urban, M. Bolker, J. Kamper, and R. Kahmann. 1994b. Control of mating and development in Ustilago maydis. *Antonie Van Leeuwenhoek*. 65:191-197.

Stamer, K., R. Vogel, E. Thies, E. Mandelkow, and E.M. Mandelkow. 2002. Tau blocks traffic of organelles, neurofilaments, and APP vesicles in neurons and enhances oxidative stress. *J Cell Biol.* 156:1051-1063. Epub 2002 Mar 1018.

Steinberg, G. 2007. Hyphal growth: a tale of motors, lipids, and the Spitzenkorper. *Eukaryot Cell*. 6:351-360.

Steinberg, G. 2014. Endocytosis and early endosome motility in filamentous fungi. *Curr Opin Microbiol*. 20:10-18.

Steinberg, G., and J. Perez-Martin. 2008. Ustilago maydis, a new fungal model system for cell biology. *Trends Cell Biol*. 18:61-67.

Steinberg, G., M. Schliwa, C. Lehmler, M. Bolker, R. Kahmann, and J.R. McIntosh. 1998. Kinesin from the plant pathogenic fungus Ustilago maydis is involved in vacuole formation and cytoplasmic migration. *J Cell Sci*. 111 (Pt 15):2235-2246.

Steinberg, G., and M. Schuster. 2011. The dynamic fungal cell. *Fungal Biol. Rev.* 25:14-37.

Steinberg, G., R. Wedlich-Soldner, M. Brill, and I. Schulz. 2001. Microtubules in the fungal pathogen Ustilago maydis are highly dynamic and determine cell polarity. *J Cell Sci*. 114:609-622.

Stenmark, H. 2009. Rab GTPases as coordinators of vesicle traffic. *Nat Rev Mol Cell Biol*. 10:513-525.

Stolz, D.B., R. Zamora, Y. Vodovotz, P.A. Loughran, T.R. Billiar, Y.M. Kim, R.L. Simmons, and S.C. Watkins. 2002. Peroxisomal localization of inducible nitric oxide synthase in hepatocytes. *Hepatology*. 36:81-93.

Straube, A., I. Weber, and G. Steinberg. 2005. A novel mechanism of nuclear envelope break-down in a fungus: nuclear migration strips off the envelope. *EMBO J*. 24:1674-1685.

Sugiura, A., G.L. McLelland, E.A. Fon, and H.M. McBride. 2014. A new pathway for mitochondrial quality control: mitochondrial-derived vesicles. *EMBO J*. 33:2142-2156.

Swinkels, B.W., S.J. Gould, A.G. Bodnar, R.A. Rachubinski, and S. Subramani. 1991. A novel, cleavable peroxisomal targeting signal at the amino-terminus of the rat 3-ketoacyl-CoA thiolase. *Embo J.* 10:3255-3262.

Szabo, Z., M. Tonnis, H. Kessler, and M. Feldbrugge. 2002. Structure-function analysis of lipopeptide pheromones from the plant pathogen Ustilago maydis. *Mol Genet Genomics*. 268:362-370.

Tabak, H.F., D. Hoepfner, A. Zand, H.J. Geuze, I. Braakman, and M.A. Huynen. 2006. Formation of peroxisomes: present and past. *Biochim Biophys Acta*. 1763:1647-1654.

Tabak, H.F., J.L. Murk, I. Braakman, and H.J. Geuze. 2003. Peroxisomes start their life in the endoplasmic reticulum. *Traffic*. 4:512-518.

Tabak, H.F., A. van der Zand, and I. Braakman. 2008. Peroxisomes: minted by the ER. *Curr Opin Cell Biol*. 20:393-400.

Taheri-Talesh, N., Y. Xiong, and B.R. Oakley. 2012. The functions of myosin II and myosin V homologs in tip growth and septation in Aspergillus nidulans. *PloS one*. 7:e31218.

Takeuchi, O., and S. Akira. 2009. Innate immunity to virus infection. *Immunol Rev*. 227:75-86.

Tan, K., A.J. Roberts, M. Chonofsky, M.J. Egan, and S.L. Reck-Peterson. 2014. A microscopy-based screen employing multiplex genome sequencing identifies cargo-specific requirements for dynein velocity. *Mol Biol Cell*. 25:669-678.

Thiemann, M., M. Schrader, A. Volkl, E. Baumgart, and H.D. Fahimi. 2000. Interaction of peroxisomes with microtubules. In vitro studies using a novel peroxisome-microtubule binding assay. *Eur J Biochem*. 267:6264-6275.

Thoms, S., and R. Erdmann. 2005. Dynamin-related proteins and Pex11 proteins in peroxisome division and proliferation. *Febs J*. 272:5169-5181.

Thoms, S., S. Gronborg, and J. Gartner. 2009. Organelle interplay in peroxisomal disorders. *Trends Mol Med*. 15:293-302.

Titorenko, V.I., and R.A. Rachubinski. 2001. Dynamics of peroxisome assembly and function. *Trends Cell Biol*. 11:22-29.

Treitschke, S., G. Doehlemann, M. Schuster, and G. Steinberg. 2010. The myosin motor domain of fungal chitin synthase V is dispensable for vesicle motility but required for virulence of the maize pathogen Ustilago maydis. *Plant Cell*. 22:2476-2494.

Tripathi, D.N., R. Chowdhury, L.J. Trudel, A.R. Tee, R.S. Slack, C.L. Walker, and G.N. Wogan. 2013. Reactive nitrogen species regulate autophagy through ATM-AMPK-TSC2-mediated suppression of mTORC1. *Proc Natl Acad Sci U S A*. 110:E2950-2957.

Vale, R.D. 2003. The molecular motor toolbox for intracellular transport. *Cell*. 112:467-480.

Van Ael, E., and M. Fransen. 2006. Targeting signals in peroxisomal membrane proteins. *Biochim Biophys Acta*. 1763:1629-1638.

van der Klei, I.J. and M. Veenhuis. 2013. The versatility of peroxisome function in filamentous fungi. *In* Peroxisomes and their Key Role in Cellular Signaling and Metabolism. *Subcellular Biochemistry*. 69:135-152.

van der Klei, I.J., and M. Veenhuis. 2006. PTS1-independent sorting of peroxisomal matrix proteins by Pex5p. *Biochim Biophys Acta*. 1763:1794-1800.

van der Zand, A., I. Braakman, H.J. Geuze, and H.F. Tabak. 2006. The return of the peroxisome. *J Cell Sci*. 119:989-994.

van der Zand, A., I. Braakman, and H.F. Tabak. 2010. Peroxisomal membrane proteins insert into the endoplasmic reticulum. *Mol Biol Cell*. 21:2057-2065.

van der Zand, A., J. Gent, I. Braakman, and H.F. Tabak. 2012. Biochemically distinct vesicles from the endoplasmic reticulum fuse to form peroxisomes. *Cell*. 149:397-409.

van Roermund, C.W., E.H. Hettema, M. van den Berg, H.F. Tabak, and R.J. Wanders. 1999. Molecular characterization of carnitine-dependent transport of acetyl-CoA from peroxisomes to mitochondria in Saccharomyces cerevisiae and identification of a plasma membrane carnitine transporter, Agp2p. *EMBO J*. 18:5843-5852.

Van Veldhoven, P.P. 2010. Biochemistry and genetics of inherited disorders of peroxisomal fatty acid metabolism. *J Lipid Res*. 51:2863-2895.

Veenhuis, M., W. Harder, J.P. van Dijken, and F. Mayer. 1981. Substructure of crystalline peroxisomes in methanol-grown Hansenula polymorpha: evidence for an in vivo crystal of alcohol oxidase. *Mol Cell Biol*. 1:949-957.

Vizeacoumar, F.J., J.C. Torres-Guzman, Y.Y. Tam, J.D. Aitchison, and R.A. Rachubinski. 2003. YHR150w and YDR479c encode peroxisomal integral membrane proteins involved in the regulation of peroxisome number, size, and distribution in Saccharomyces cerevisiae. *J Cell Biol.* 161:321-332.

Volkl, A., E. Baumgart, and H.D. Fahimi. 1988. Localization of urate oxidase in the crystalline cores of rat liver peroxisomes by immunocytochemistry and immunoblotting. *J Histochem Cytochem*. 36:329-336.

Wakabayashi, J., Z. Zhang, N. Wakabayashi, Y. Tamura, M. Fukaya, T.W. Kensler, M. Iijima, and H. Sesaki. 2009. The dynamin-related GTPase Drp1 is required for embryonic and brain development in mice. *J Cell Biol*. 186:805-816.

Wallner, S., and G. Schmitz. 2011. Plasmalogens the neglected regulatory and scavenging lipid species. *Chem Phys Lipids*. 164:573-589.

Walther, T.C., and R.V. Farese, Jr. 2012. Lipid droplets and cellular lipid metabolism. *Annu Rev Biochem*. 81:687-714.

Wanders, R.J., J. Komen, and S. Ferdinandusse. 2011a. Phytanic acid metabolism in health and disease. *Biochim Biophys Acta*. 1811:498-507.

Wanders, R.J., J. Komen, and S. Kemp. 2011b. Fatty acid omega-oxidation as a rescue pathway for fatty acid oxidation disorders in humans. *FEBS J*. 278:182-194.

Wanders, R.J., P. Vreken, S. Ferdinandusse, G.A. Jansen, H.R. Waterham, C.W. van Roermund, and E.G. Van Grunsven. 2001. Peroxisomal fatty acid alpha- and beta-oxidation in humans: enzymology, peroxisomal metabolite transporters and peroxisomal diseases. *Biochem Soc Trans*. 29:250-267.

Wanders, R.J., and H.R. Waterham. 2006a. Peroxisomal disorders: the single peroxisomal enzyme deficiencies. *Biochim Biophys Acta*. 1763:1707-1720.

Wanders, R.J., H.R. Waterham, and S. Ferdinandusse. 2015. Metabolic Interplay between Peroxisomes and Other Subcellular Organelles Including Mitochondria and the Endoplasmic Reticulum. *Front Cell Dev Biol*. 3:83.

Wanders, R.J.A., and H.R. Waterham. 2006b. Biochemistry of mammalian peroxisomes revisited. *Annu. Rev. Biochem.* 75:295-332.

Waterham, H.R., and M.S. Ebberink. 2012. Genetics and molecular basis of human peroxisome biogenesis disorders. *Biochim Biophys Acta*. 1822:1430-1441.

Waterham, H.R., S. Ferdinandusse, and R.J. Wanders. 2016. Human disorders of peroxisome metabolism and biogenesis. *Biochim Biophys Acta*. 1863:922-933.

Waterham, H.R., J. Koster, C.W. van Roermund, P.A. Mooyer, R.J. Wanders, and J.V. Leonard. 2007. A lethal defect of mitochondrial and peroxisomal fission. *N Engl J Med*. 356:1736-1741.

Watters, D., P. Kedar, K. Spring, J. Bjorkman, P. Chen, M. Gatei, G. Birrell, B. Garrone, P. Srinivasa, D.I. Crane, and M.F. Lavin. 1999. Localization of a portion of extranuclear ATM to peroxisomes. *J Biol Chem*. 274:34277-34282.

Weber, I., C. Gruber, and G. Steinberg. 2003. A class-V myosin required for mating, hyphal growth, and pathogenicity in the dimorphic plant pathogen Ustilago maydis. *Plant Cell*. 15:2826-2842.

Wedlich-Soldner, R., M. Bolker, R. Kahmann, and G. Steinberg. 2000. A putative endosomal t-SNARE links exo- and endocytosis in the phytopathogenic fungus Ustilago maydis. *EMBO J*. 19:1974-1986.

Wedlich-Soldner, R., I. Schulz, A. Straube, and G. Steinberg. 2002a. Dynein supports motility of endoplasmic reticulum in the fungus Ustilago maydis. *Mol Biol Cell*. 13:965-977.

Wedlich-Soldner, R., A. Straube, M.W. Friedrich, and G. Steinberg. 2002b. A balance of KIF1A-like kinesin and dynein organizes early endosomes in the fungus Ustilago maydis. *EMBO J*. 21:2946-2957.

Whittaker, R.H. 1969. New concepts of kingdoms or organisms. Evolutionary relations are better represented by new classifications than by the traditional two kingdoms. *Science*. 163:150-160.

Wiemer, E.A., T. Wenzel, T.J. Deerinck, M.H. Ellisman, and S. Subramani. 1997. Visualization of the peroxisomal compartment in living mammalian cells: dynamic behavior and association with microtubules. *J Cell Biol*. 136:71-80.

Wilfling, F., J.T. Haas, T.C. Walther, and R.V. Farese, Jr. 2014. Lipid droplet biogenesis. *Curr Opin Cell Biol*. 29:39-45.

Williams, C., L. Opalinski, C. Landgraf, J. Costello, M. Schrader, A.M. Krikken, K. Knoops, A.M. Kram, R. Volkmer, and I.J. van der Klei. 2015. The membrane remodeling protein Pex11p activates the GTPase Dnm1p during peroxisomal fission. Proc Natl Acad Sci U S A. 112:6377-6382.

Woo, M., K. Lee, and K. Song. 2003. MYO2 is not essential for viability, but is required for polarized growth and dimorphic switches in Candida albicans. *FEMS Microbiol Lett*. 218:195-202.

Yoon, Y., E.W. Krueger, B.J. Oswald, and M.A. McNiven. 2003. The mitochondrial protein hFis1 regulates mitochondrial fission in mammalian cells through an interaction with the dynamin-like protein DLP1. *Mol Cell Biol*. 23:5409-5420.

Yoshida, Y., H. Niwa, M. Honsho, A. Itoyama, and Y. Fujiki. 2015. Pex11mediates peroxisomal proliferation by promoting deformation of the lipid membrane. Biol Open. 4:710-721.

Yuan, W., M. Veenhuis, and I.J. van der Klei. 2016. The birth of yeast peroxisomes. *Biochim Biophys Acta*. 1863:902-910.

Zerial, M., and H. McBride. 2001. Rab proteins as membrane organizers. *Nat Rev Mol Cell Biol*. 2:107-117.

Zhang, J., J. Kim, A. Alexander, S. Cai, D.N. Tripathi, R. Dere, A.R. Tee, J. Tait-Mulder, A. Di Nardo, J.M. Han, E. Kwiatkowski, E.A. Dunlop, K.M. Dodd, R.D. Folkerth, P.L. Faust, M.B. Kastan, M. Sahin, and C.L. Walker. 2013. A tuberous sclerosis complex signalling node at the peroxisome regulates mTORC1 and autophagy in response to ROS. *Nat Cell Biol*. 15:1186-1196.

Zhang, J., R. Qiu, H.N. Arst, Jr., M.A. Penalva, and X. Xiang. 2014. HookA is a novel dynein-early endosome linker critical for cargo movement in vivo. *J Cell Biol*. 204:1009-1026.

Zhang, J., K. Tan, X. Wu, G. Chen, J. Sun, S.L. Reck-Peterson, J.A. Hammer, 3rd, and X. Xiang. 2011. Aspergillus myosin-V supports polarized growth in the absence of microtubule-based transport. *PloS one*. 6:e28575.

Zhang, J., D.N. Tripathi, J. Jing, A. Alexander, J. Kim, R.T. Powell, R. Dere, J. Tait-Mulder, J.H. Lee, T.T. Paull, R.K. Pandita, V.K. Charaka, T.K. Pandita, M.B. Kastan, and C.L. Walker. 2015. ATM functions at the peroxisome to induce pexophagy in response to ROS. *Nat Cell Biol*. 17:1259-1269.

Zhang, S.O., R. Trimble, F. Guo, and H.Y. Mak. 2010. Lipid droplets as ubiquitous fat storage organelles in C. elegans. *BMC Cell Biol*. 11:96.

APPENDIX

Supplemntary methods (from Lin et al., 2016)

Mean square displacement analysis and diffusion coefficient estimation

To analyze the spatial-temporal spreading of peroxisomes, the mean square displacement MSD(t) =<⟦|x(t'+t)-x(t')|⟧^2> was calculated, where |⋯| represents Euclidean distance, <⋯> represents an ensemble average, and x(t)=(x(t),y(t)) is the time-dependent trajectory position of the centre of an organelle. The local behaviour of a peroxisome in Figure 34 and Figure 38 was classified by calculating the MSD(t) using an ensemble average with a rolling window (t-5s,t+5s) and fitting the MSD(t) to a power law of the form At^α in the time interval 0-3s. To classify the behaviour, for α>1.6 the motion was classified as directed, while for α<1.6 it was classified as diffusive. The MSD(t) curves were calculated using an ensemble average over the entire trajectories of all tracked diffusive organelles and the exponents α were obtained by fitting the MSD(t) to the form At^α in a time interval 0-2.5 s (Figure 34 and 38).

The diffusion coefficients *D* were estimated by fitting MSD(t) to a linear function 4*D*t in a time interval 0-1.8s for each tracked diffusive-like peroxisome (Fig. 34) in *U. maydis* hyphal cells and in a time interval 0-3s for each tracked diffusive peroxisome in COS-7 cells (Figure 38). Mean and standard errors were calculated for the diffusion rates and student-t tests were performed to detect significant differences between experiments. For the axial and radial diffusion coefficients in Figure 34, as well as for the control experiments used in the mathematical modelling, the cell axis was determined through an automatic imaging process (described in the method part) and each trajectory *x*(t) was rotated so that its first and second components correspond to axial and radial directions; the MSD(t) in the axial (respectively radial) direction was calculated using an ensemble average of tracked diffusive peroxisome for the first (respectively second) component of *x*(t). These 1-dimensional MSD(t) were fitted to a linear function 2*D*t in a time interval 0-3s to get the best fit for the diffusion rate *D*. An F-test was performed for the significant difference between the best fitting diffusion coefficients in axial and radial direction (Figure 35). Nonlinear curve regression and F tests

for diffusion coefficient comparison were performed using the software Prism 5.03 (GraphPad Software, San Diego, USA).

Modelling the distribution of peroxisomes in mutant Δkin3

The situation for the mutant Δkin3 is simpler than the wild type – there appears to be no fast long-range directed motion of early endosomes. We took a simple drift diffusion model with no flux at the ends:

$$\frac{\partial \rho}{\partial t} = v\frac{\partial \rho}{\partial x} + D\frac{\partial^2 \rho}{\partial x^2} \text{ for } x_0 \le x \le x_L, \quad v\rho(x,t) + D\frac{\partial \rho(x,t)}{\partial x} = 0 \text{ at } x = x_0, x_L. \quad \text{(S0)}$$

Here $x=x_0$ represents the cell tip, $x=x_L$ represents the other end of the region of interest and t represents time in seconds. Although the diffusion rate was estimated from the mean square displacement to be D=0.0049±0.00004 μm^2/s, a reliable and direct measurement of the slow drift velocity v was not possible with the current time and spatial resolution. The model (S0) predicted a steady profile that is exponential of the form $\rho(x) = A\exp\left(\frac{-v}{D}x\right)$. We used this model to infer a value for this drift: we experimentally measured the average intensity profile in steady state in the Δkin3 mutant and fitted this intensity for profile to $7 \le x \le 34$ μm using nonlinear regression implemented in GraphPad Prism 5.03; parameter B concerns the background intensity in the experimental data. The best fit v/D=0.09 ± 0.005 1/um was used to give v =0.00044 μm/s. $\rho(x) = A\exp\left(\frac{-v}{D}x\right) + B$

Modelling the distribution of peroxisomes in the wild type cells

In order to understand the coordination between the mechanisms that are transporting peroxisomes within the wild type cells, we construct an extension of the dynamical model (S0) for the distribution of peroxisomes along a portion of the cell $x_0 \le x \le x_L$. We postulate that peroxisomes move between three populations: $\rho_{1(2)}(x,t)$ is the density of peroxisomes that are propagating actively and rapidly away from the tip (to the tip) carried by early endosomes while $\rho_3(x,t)$ is the density of peroxisomes within the cytoplasm and that is undergoing both diffusion with rate D and a slow but deterministic drift with velocity v towards the tip. We assume that the propagation of the direct-transported peroxisomes is at velocity u in the respective direction and changes direction with a rate w; we assume peroxisomes in directed transport unbind from early endosomes at a rate w_d and those in cytoplasm bind to early endosomes and move in directly along microtubules with a rate w_a.

Thus the dynamics of the three populations is modelled by the following system of coupled partial differential equations:

$$\frac{\partial \rho_1}{\partial t} = -u\frac{\partial \rho_1}{\partial x} + \frac{w_a}{2}\rho_3 + w\rho_2 - (w_d + w)\rho_1 \qquad \text{(S1)}$$

$$\frac{\partial \rho_2}{\partial t} = u\frac{\partial \rho_2}{\partial x} + \frac{w_a}{2}\rho_3 + w\rho_1 - (w_d + w)\rho_2 \qquad \text{(S2)}$$

$$\frac{\partial \rho_3}{\partial t} = v\frac{\partial \rho_3}{\partial x} + D\frac{\partial^2 \rho_3}{\partial x^2} - w_a\rho_3 + w_d(\rho_1 + \rho_2) \qquad \text{(S3)}$$

Note that directed motion of peroxisomes is driven by early endosomes motion and consequently, the behavior of peroxisomes at the ends reflects that of early endosomes. It has been shown in *U mayis* hyphal cells that early endosomes do not typically fall off the track, nor form clusters at the cell tip. Instead, they rapidly move away from the tip due to dynein activity. Therefore, at the ends of the domain, we assume that the directly-transported peroxisomes are recycled: a peroxisome reaching the ends of the domain is assumed to immediately change direction and return. For the cytoplasmic peroxisomes we assume that there is no net flux at the ends of the domain. These correspond to applying boundary conditions on the fluxes *at* $x=x_0,x_L$

$$J_1=-J_2 \text{ and } J_3=0 \qquad \text{(S4)}$$

where the fluxes are $J_1=u\rho_1, J_2=-u\rho_2$ and $J_3=-v\rho_3(x,t)-D(\partial\rho_3(x,t))/\partial x$. Steady solutions for (S1-S3) can be found by superposition of eigenmodes of the form $\rho_i(x) = B_{ij}e^{\lambda_j x}$ where $B_{ij}, \lambda_j\ (i = 1,2,3;\ j = 1,2,3,4)$ are eigenvectors and eigenvalues for the corresponding linear problem. Note there is a uniform solution $\lambda_1=0$ but this does not satisfy (S4) except for the special case where there is no drift (v=0). For typical parameters we can only satisfy (S4) for a specific combination of the eigenmodes.

We next estimated the parameters in (S1-S3) and used these and boundary conditions (S4) to predict the steady distribution of peroxisomes in the wild type. We note that measurements of the MSD(t) reveals more structure in the data if we align the cells to measure the axial and radial diffusion rates separately and if we restrict to certain populations of peroxisomes within the cell. However, the microtubules dynamics enhances lateral interaction of peroxisomes with moving early endosomes and this presumably has an effect both on axial diffusion and on the binding rate to moving early endosomes. We therefore estimated the

axial diffusion coefficients and binding rate from randomly chosen peroxisomes (regardless of relative distance to the microtubules). To estimate the binding rate w_a, we counted at every 4.5 s the number of peroxisomes that have switched from random to directed transport as well as the total number of peroxisomes observed, and determined the binding rate by fitting the proportion of first binding events as a function of time duration, to a one phase association $1-e^{-w_a t}$ with binding rate w_a. The diffusion rate was estimated from MSD(t) using an ensemble average over randomly selected diffusive peroxisomes. Other parameters in the model (S1-S3) were estimated directly from experimental data (Supplementary Table S2). Using estimated parameters our model (S1-S4) predicted a distribution (shown in Figure 37) which well agrees with the measured distribution of peroxisomess for the wild type cells. Numerical calculations of the predicted distributions from the model were performed in Maple 17 (Maplesoft Europe Ltd., Cambridge, UK). We remark here that over long time scale and sufficiently long space, the bi-directed random motion of peroxisomes can be viewed as another diffusion process; and the effective diffusion rate of this process reads as u2/(2w)=15 μm2/s using the velocity and the turning rate in Supplementary Table S2.

Model validation for mutant cells (Δhok1)

For the Δhok1 mutant cells, we measured the axial diffusion rate as D=0.0034±0.00002/s from MSD(t) analysis. Using the drift velocity shown in Supplementary Table S2 and measured axial diffusion rate, and assuming the same background intensity as in Δkin3 mutant, the model (S0) predicted the intensity profile for peroxisomes in the Δhok1 mutant cells as shown in Figure 37.

Hypothetical scenarios: model predictions

We used the model to explore the hypothetical scenarios shown in Supplementary Table S3 some of which were currently unable to be explored experimentally. The model allows us to examine the importance of the various processes in achieving an even distribution of peroxisomes along the cell as well as the speed of mixing for these scenarios. The speed of mixing was characterized using the first arrival time of a peroxisome to a distance distal from the hyphal tip. This was estimated using simulations of peroxisomes motility starting at the hyphal tip, averaged over a number of simulations (n=100-2000); random motility of individual peroxisomes along cell axis was simulated according to the parameters in

Supplementary Table S3 for each scenario. To visualize the mixing process in a virtual hyphal-like cell (a cylinder of 10 μm length and 2 μm diameter), we extend the model describing the motility of peroxisomes with the inclusion of homogeneous lateral diffusion in the cell cross section and visualize the motility in the longitudinal projection.

Tracking of peroxisomes in *U. maydis* and COS-7 cells

Image series of GFP-SKL expressing *U. maydis* and COS-7 cells, covering 15-45s observation time were used to automatically record peroxisomes oscillations over time using a hosted image processing platform (https://apollo.ex.ac.uk/impi; for access to this platform contact J. Metz@exeter.ac.uk). Each image was filtered using a scale-space Laplace of Gaussian filtering approaching1 over scales corresponding to the size range of peroxismes. After filtering, a threshold was determined using the median absolute deviation as a robust estimator of the background level and applied to the filter response to determine peroxisome positions. Once detected, peroxisomes were tracked using the Jonker-Volgenant algorithm on object positions to assign identities in successive frames. Results from this method were manually verified for accuracy.

Supplementary Table S1: The values for the axial diffusion rate and binding rate in the model for the wild type cell**.**

Quantity	Value
D: axial diffusion rate (μm^2/s)	0.0137±0.0001
w_a: binding rate (1/s)	0.0034±0.00006

Supplementary Table S2: The measured and inferred rates in the model (S1-S3) for the wild type cell.

Quantity	Value	Estimate used
v: net drift velocity in cytoplasm (μm/s)	0.00044	See caption
M: run length (μm)	*6.5±0.61 (n=60)*	direct measurement
u: long-range transport velocity (μm/s)	*1.9±0.05 (n=60)*	direct measurement
P_{turn}: Proportion of turning in directed transport (%)	*41*±1.45 (n=*279*)	direct measurement
w: turning rate (1/s)	0.12	$(uP_{turn})/M$
w_d: unbinding rate (1/s)	0.17	$u/M - w$

The net drift velocity v was estimated via fitting density profile from the model (S0) to experimental measured intensity for Δ*kin3* mutant cells.

Supplementary Table S3: The parameters used for hypothetical scenarios.

Quantity	control	no actin drift	no active diffusion	no directed transport	no directed transport and no active diffusion	no directed transport and no active diffusion and no actin drift
D: (μm²/s)	*0.0137*	√	*0.0030*	√	*0.0030*	*0.0030*
u: (μm/s)	*1.9*	√	√	*n/a*	*n/a*	*n/a*
w_a: (1/s)	*0.0034*	√	√	*0*	*0*	√
w_d: (1/s)	*0.17*	√	√	∞	∞	∞
v*: *(μm/s)	*0.00044*	*0*	√	√	√	*0*
w*: *(1/s)	*0.12*	√	√	*n/a*	*n/a*	*n/a*

'√': indicates the value from the control data and its specific values are in Supplementary Table S1 and Supplementary Table S2